Effects of K_{ATP} channel mutations on neurological function

A Thesis submitted to the University of Oxford for the degree of Doctor of Philosophy

Carolina Lahmann Gutiérrez

University College

Trinity 2013

Abstract

Effects of K_{ATP} channel mutations on neurological function

Carolina Lahmann Gutiérrez, University College, University of Oxford

Submitted for the degree of DPhil, Trinity 2013

Activating mutations in the ATP-sensitive potassium (K_{ATP}) channel cause neonatal diabetes mellitus (ND). In some patients, ND is accompanied by neurological symptoms including developmental delay, muscle hypotonia, balance and coordination problems, and hyperactivity- a condition known as iDEND syndrome. The majority of ND patients successfully manage their diabetes with sulphonylureas, which are selective blockers of the K_{ATP} channel. In the case of iDEND, it was hoped that sulphonylureas would also restore neurological function. However, the extent to which these drugs ameliorate these symptoms is not clear.

In this thesis, I used mice hemizygously expressing the most common iDEND mutation (Kir6.2-V59M) selectively in neurones (nV59M mice) to assess the extent to which sulphonylureas modulate neuronal function *in vivo*. Interestingly, nV59M mice displayed reduced sensitivity to isoflurane anaesthesia, taking longer to lose their righting and withdrawal reflexes (LORR and LOWR, respectively). Systemic delivery of glibenclamide (a sulphonylurea) had no effect on the LORR (central nervous system mediated) although partially restored the LOWR (peripheral-reflex arc). Consistent with the idea that glibenclamide poorly modulates central nervous system activity *in vivo*, very low levels of glibenclamide were detected in the cerebrospinal fluid and brain of rats after systemic administration of the drug, despite high drug plasma levels. Furthermore, direct brain delivery of glibenclamide results in rapid transport out of the brain and into the blood. Taken together, the results presented in this thesis suggest that the inability of sulphonylureas to fully restore neurological function in iDEND patients is due to the failure of the drugs to accumulate in the brain at high enough concentrations.

Contents

Acknowledgements

My greatest thanks go to Prof. Frances Ashcroft, my supervisor, who has been enthusiastic, supportive, and a fantastic source of ideas throughout my studies. I would also like to thank Prof. Patrik Rorsman for his encouragement and guidance. I am greatly indebted to all members of the Ashcroft group, past and present, as well as Dr. Holger Kramer and Dr. Louise Upton, who have been a great source of inspiration, support and help. I would also like to thank the Biomedical Services staff for all their help. I am grateful to the Bannerman and Roeper groups, particularly to Amy Taylor and Annabelle Zimmermann, for teaching me some of the techniques used for this thesis. I also thank my family for their ever-present love, encouragement and support. Finally, I thank Benjamin Stagg for his love, understanding and patience.

Declaration

The work in this thesis is my own, with the following exceptions. Miss Michaela Iberl provided valuable technical assistance by genotyping most of the mice that were used in Chapters 3, 4, 5 and 6. Dr. Holger Kramer developed the LC-MS method described in Chapter 7 and conducted the LC-MS runs for the data presented in that chapter. RNA integrity for the RT-qPCR experiments, presented in Chapters 3 and 6, was assessed by Ms. Sheena Lee.

Abbreviations

ABC protein	ATP-binding cassette protein
aCSF	Artificial cerebrospinal fluid
ADP	Adenosine diphosphate
ANOVA	Analysis of variance
ATP	Adenosine triphosphate
BBB	Blood-brain barrier
BSA	Bovine serum albumin
CAG	Chicken β-actin promoter with cytomegalovirus enhancer
Ca^{2+}	Calcium ion
cAMP	Cyclic adenosine monophosphate
CHI	Congenital hyperinsulinism of infancy
CNS	Central nervous system
CP	Choroid plexus
CSF	Cerebrospinal fluid
d_{11}*-glibenclamide*	Deutrated glibenclamide
DEND	Developmental delay, Epilepsy and Neonatal Diabetes
DM	Diabetes mellitus
DMSO	Dimethyl sulfoxide
DNA	Deoxyribonucleic acid
ENU	*N*-ethyl-*N*-nitrosourea
ER	Oestrogen receptor
ESI	Electrospray ionisation
GFP	Green fluorescent protein
HPLC	High-pressure liquid chromatography
IC_{50}	Half maximal inhibitory concentration
ICV	Intracranioventricular
iDEND	Intermediate DEND syndrome
IP	Intraperitoneal
IQ	Intelligence quotient

IRES	Internal ribosome entry site
IS	Internal standard
K^+	Potassium ion
K_{ATP}	ATP-sensitive potassium channel
Kir	Inwardly-rectifying potassium channel
LC-MS	Liquid chromatography tandem mass spectrometry
LORR	Loss of righting reflex
LOWR	Loss of withdrawal reflex
MAC	Minimum alveolar concentration
Mg^{2+}	Magnesium ion
MS	Mass spectrometry
mRNA	Messenger ribonucleic acid
mV59M	Myocyte creatine kinase driven Kir6.2-V59M
Na^{2+}	Sodium ion
ND	Neonatal diabetes
NMDA	N-methyl D-aspartate
nV59M	Nestin driven Kir6.2-V59M
PB	Phosphate buffer (no sodium chloride present)
PBS	Phosphate-buffered saline
PCR	Polymerase chain reaction
P-gp	P-glycoprotein
PIP_2	Phosphatidylinositol 4,5-bisphosphate
PNS	Peripheral nervous system
QC	Quality control
RT-qPCR	Real time quantitative PCR
SEM	Standard error of the mean
SPE	Solid phase extraction
SPECT	Single-photon emission computer tomography
SRM	Selected reaction monitoring
SUR	Sulphonylurea receptor
T1DM	Type 1 diabetes mellitus
T2DM	Type 2 diabetes mellitus

TNDM	Transient neonatal diabetes mellitus
Ubi-ROSA	Ubiquitin driven ROSA-Kir6.2-V59M
Ubi-ROSA-CAGS	Ubiquitin driven ROSA-CAG-Kir6.2-V59M
Ubi-ROSA-DN	Ubiquitin driven ROSA-CAG-Kir6.2-[ΔN30, K185Q]
v/w	Volume to weight
WT	Wild type

Chapter 1: Introduction

Potassium channels are key regulators of excitation in most tissues, opening or closing in response to depolarization or binding of channel regulators in order to hasten membrane repolarization and dampen electrical activity. Although all members of this ion channel superfamily share this membrane hyperpolarizing property, many potassium channels are specialized for specific functions. A unique member of this family is the ATP-sensitive potassium (K_{ATP}) channel, which couples membrane excitability to the metabolic state of the cell [1-3]. These channels are hence involved in many physiological functions including regulation of neuronal, cardiac and endocrine excitability, glucose uptake by skeletal muscle, control of smooth muscle tone, and insulin secretion from pancreatic β-cells.

Recently, the physiological importance of the K_{ATP} channel has been highlighted by the discovery that activating mutations in this channel are associated with a variety of metabolic syndromes, ranging from neonatal diabetes (ND) [4] to intermediate DEND (iDEND) and DEND (**d**evelopmental delay, **e**pilepsy and **n**eonatal **d**iabetes) syndromes [5]. For the majority of patients, this discovery has allowed them to successfully manage their diabetes with sulphonylureas, which are selective blockers of the K_{ATP} channel, instead of insulin [6]. However, mixed results have been obtained with the management of neurological symptoms in iDEND and DEND patients. Furthermore, due to the rarity of this disease, no thorough clinical studies

have been carried out to assess the extent to which sulphonylureas ameliorate iDEND and DEND syndromes. This thesis will focus on sulphonylurea therapy for iDEND/DEND syndrome and will provide novel insights into the ability of sulphonylurea drugs to reverse the neurological symptoms associated with gain-of-function mutations in the K_{ATP} channel.

1.1. The K_{ATP} channel

The K_{ATP} channel was first discovered in cardiac myocytes by Noma and colleagues, who described a potassium current which appeared in response to hypoxia and was inhibited by intracellular injection of ATP in the millimolar range [7]. This was shortly followed by description of the K_{ATP} channel in pancreatic β-cells [8-10], skeletal muscle [11], smooth muscle [12] and neurones [13], which established its role as the key linker of metabolism and cellular excitability in most tissues. It achieves this by sensing changes in adenosine nucleotide concentrations [2,3]. At low levels of metabolic activity, K_{ATP} channels are open, allowing the efflux of potassium ions, and thus maintaining the membrane potential at a hyperpolarized level and reducing electrical activity. By contrast, increased metabolic activity triggers the closure of K_{ATP} channels, leading to membrane depolarization, increased electrical activity, and stimulation of cellular responses such as insulin exocytosis or neurotransmitter release [2,3].

1.1.1. Structure of the K_{ATP} channel

The K_{ATP} channel is formed by the association of four Kir6.x subunits with four sulphonylurea receptor (SUR) subunits [14-16]. A low-resolution structure of the purified complex revealed that the channel is a hetero-octameric complex, in which the Kir6.x subunits assemble to form a potassium-selective central pore that is surrounded by the SUR subunits (Fig. 1.1) [17].

Kir6.x is a member of the inwardly rectifying potassium (Kir) channel family [14,18]. Inward rectifiers preferentially conduct K^+ ions into the cell at negative voltages as their pore gets blocked by positively-charged intracellular polyamines and Mg^{2+} ions, which are forced into the channel under depolarizing conditions and thus significantly reduce channel conductance at positive potentials [19,20]. In the case of Kir2.1, a strong inward rectifier, these endogenous blockers interact with an aspartate residue at the second transmembrane segment of the channel [21]. This residue is an asparagine in Kir6.x channels, which explains why they show very weak rectification [14,18]. Physiologically, the preferential high conductance at negative potentials allows inward rectifiers to stabilise the cell's resting potential and to avoid short-circuiting action potentials in certain tissues (e.g. by elongating the plateau of the cardiac action potential) [22].

There are two isoforms of Kir6.x: Kir6.2 and Kir6.1. Kir6.2, which is encoded by the gene *KCNJ11*, is the main pore-forming subtype and is found in pancreatic β-cells, neurones, skeletal and cardiac myocytes [14]. Kir6.1 is encoded by the gene *KCNJ8* and is expressed in vascular smooth muscle and glial cells and a subset of neurones [18,23].

The sulphonylurea receptor is an atypical member of the ATP-binding Cassette (ABC) superfamily of proteins [24] because it serves as an ion channel regulator rather than a transporter. It belongs to the ABCC subfamily, which also includes the multidrug resistance-related proteins (MRP) and the cystic fibrosis transmembrane conductance receptor (CFTR) [25].

Three main SUR isoforms exist: SUR1 (encoded by *ABCC8*) is expressed in atrial myocytes, neurones, and endocrine tissues including pancreatic alpha- and beta-cells [14,24,26-28]; SUR2A is found in ventricular and skeletal myocytes [14,28]; and SUR2B is expressed in smooth muscle as well as a small population of neurones [27,29]. SUR2A and SUR2B are splice variants of the same gene, *ABCC9*. Association of Kir6.2 with different SUR subtypes endows the channel with different sensitivities to modulation by metabolism and pharmacological agents.

Unlike all other members of the inward rectifiers, Kir6.x is unable to express functional channels in the absence of SUR [14,18,30]. This is because both Kir6.x

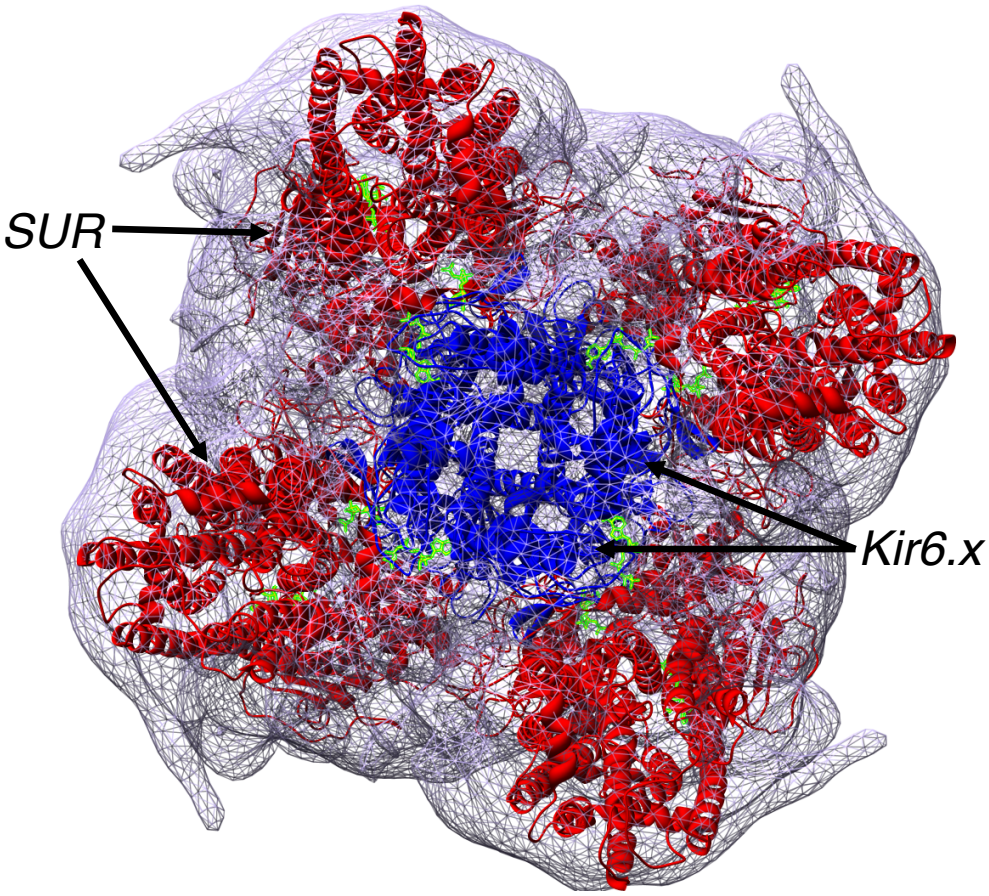

Figure 1.1: K_{ATP} channel structure

Top view of the K_{ATP} channel's electron microscopy density with models of Kir6.2 (blue) and SUR1 without TMD0 (red) [17]. ATP molecules are shown in green.

and SUR possess an endoplasmic reticulum (ER) retention motif, which is only masked by the association of the two subunits, preventing them from reaching the plasma membrane in the absence of their partner [31]. Thus, only fully assembled K_{ATP} channels are transported to the cell membrane.

1.1.2. Molecular structure of the K_{ATP} channel

Presently, the only available structure of the K_{ATP} channel is a single-particle electron microscopy map of the purified fusion protein complex at a resolution of 18Å (Fig. 1.1) [17,32]. In this map, the protein appears to have a compact structure with maximal dimensions of 18nm in diameter and 13nm in height. As was mentioned previously, the channel assembles as a tetrameric Kir6.2 pore with each subunit associated with a SUR1 subunit [17]. However, a higher resolution structure is required to gain further details on the allosteric interaction between Kir6.2 and SUR as well as on the location of ligand-binding sites.

To date, the structure of Kir6.2 has not been determined. Nonetheless, the 3D structures of other members of the Kir channel family have revealed that these channels are tetramers of identical subunits, with each subunit having two transmembrane domains (TM1 and TM2) linked by a pore loop that re-enters the membrane to form the selectivity filter [21,33-36]. The N-terminus, which is linked to TM1, and the C-terminus, linked to TM2, form the

cytoplasmic domain. The transmembrane domain is thought to be mainly responsible for ion selectivity whilst the cytoplasmic domain is thought to regulate gating.

These 3D structures have also enabled the construction of a molecular model of the Kir6.2 tetramer (Fig. 1.2) [37,38]. This homology model allowed the identification of a putative ATP-binding site, which is formed by five basic or uncharged residues located at the interface of the N- and C-termini. Furthermore, this model suggests that movement of the slide helix along the membrane interface plays a crucial role in channel gating. Due to the amphipatic nature of the slide helix, it is thought that no substantial rotational movement is involved in the sliding of the helix during channel opening [37].

SUR is a member of the ABC protein superfamily. All of these proteins share a similar primary structure, which consists of two transmembrane domains (TMD1-2) of varying length and two cytosolic nucleotide-binding domains (NBD1-2). SUR is unusual in that, in addition to its two TMDs (each composed of 6 α-helices), it also has a TMD with 5 α-helices near the N-terminus (Fig. 1.3). This section is known as TMD0 and is connected to TMD1 by a cytosolic loop known as the CL3-linker, which is thought to contribute to the sulphonylurea-binding site [39] and also to modulation of Kir6.2 gating [40,41].

The cytosolic loop between TMD1 and TMD2 and the one following TMD2 form the NBDs (Fig. 1.3). These domains cooperate in the binding and

hydrolysis of nucleotides [42]. The NBDs of most ABC proteins show a number of highly conserved structural motifs, which include the Walker A and B motifs and the ABC signature motif (Fig. 1.3).

As with Kir6.2, there are currently no high-resolution structures of SUR. Furthermore, in the absence of high-resolution structures of any members of the ABCC subfamily, it has been impossible to generate a homology model of the entire protein. Nonetheless, as the crystal structures of various isolated NBDs have been determined, several models of the SUR NBDs have been created [43,44]. The NBDs are thought to associate in a head-to-tail arrangement and form two nucleotide-binding sites (NBS1-2) by interaction of the Walker A and B motifs of one NBD and the signature motif of the other NBD [45].

Molecular models of SUR1 lacking TMD0 and the CL3 linker have also been generated [46,47]. These are based on the crystal structure of three prokaryotic ABC proteins: BtuCD, MsbA and Sav1866 [48-51].

1.1.3. Metabolic regulation of the K_{ATP} channel

K_{ATP} channels are regulated by a variety of different intracellular factors. Their gating is determined by changes in the intracellular concentrations of adenosine nucleotides, namely ATP and MgADP. Furthermore, their activity is modulated by intracellular pH[52] as well as lipids, including phosphatidylinositol 4,5-bisphosphate (PIP_2) [53,54] and long-chain acyl CoAs [55,56].

Metabolic regulation of the K_{ATP} channel is mediated by both Kir6.2 and SUR subunits. Binding of ATP to Kir6.2 closes the channel pore while the interaction between MgADP and SUR opens it [56-59]. MgATP can also stimulate the channel by interacting with SUR [56], although it must first be hydrolysed to MgADP [60].

Intracellular pH, long-chain acyl CoAs, and PIP_2 significantly increase the IC_{50} of ATP, resulting in a reduction in the ATP sensitivity of the K_{ATP} channel [52,61]. In the case of acyl CoAs and PIP_2, this effect is thought to be mediated by interaction with the Kir6.2 subunit [56,61]. Interestingly, while acyl CoAs and PIP_2 are capable of increasing the open probability of the channel, increasing the proton concentration reduces channel opening [52].

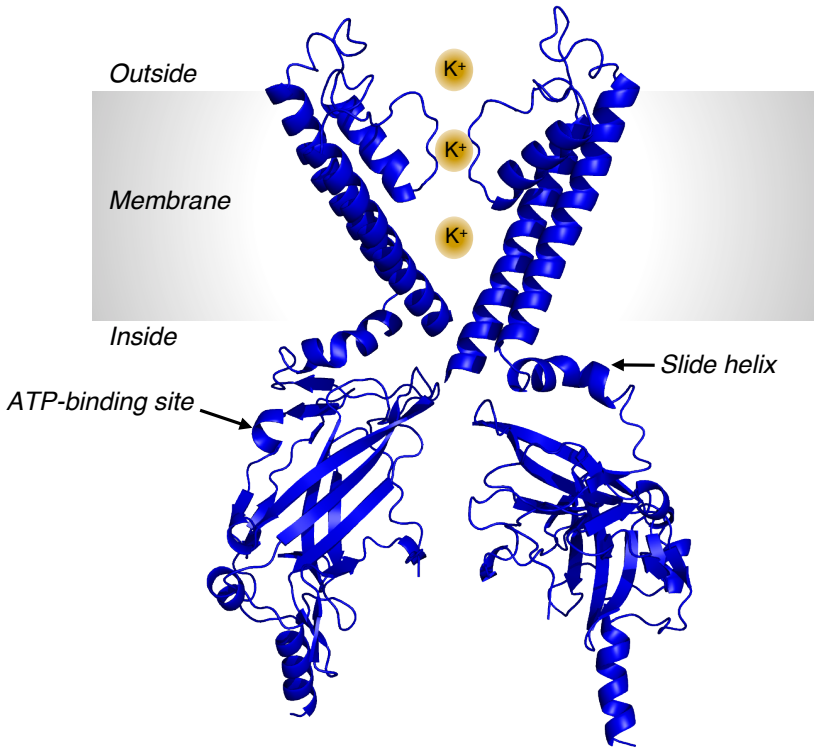

Figure 1.2: Kir6.2 homology model

Homology model of Kir6.2 viewed from the side [38]. For clarity, only two transmembrane domains and two separate cytosolic domains are shown.

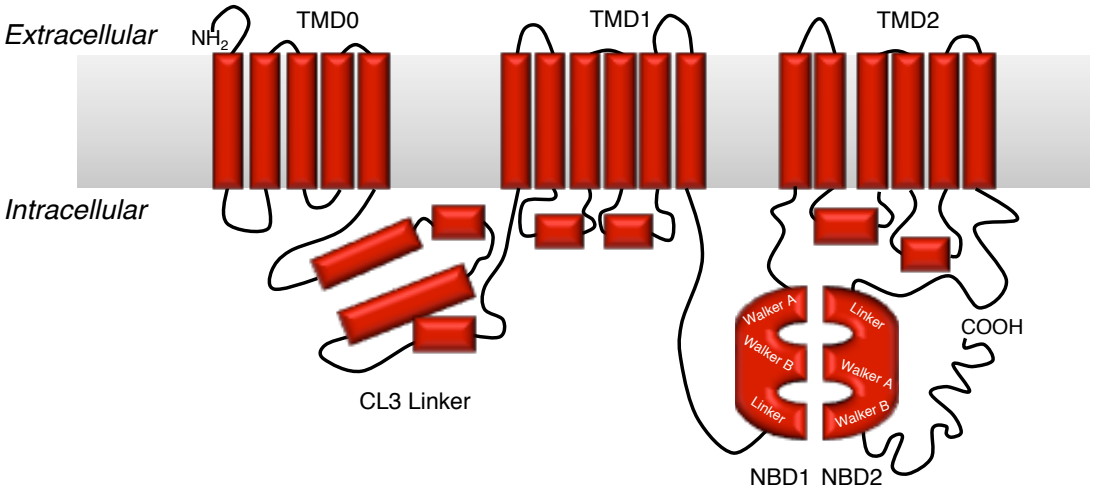

Figure 1.3: The sulphonylurea receptor

Membrane topology of the sulphonylurea receptor. Some of the nucleotide binding domain (NBD) motifs involved in ATP-binding and hydrolysis have been labelled (Walker A, Walker B, linker “signature sequence”).

Association of Kir6.2 with the different SUR subtypes results in K_{ATP} channels with different sensitivities to metabolic modulation. When Kir6.2/SUR1 channels are expressed heterologously, large currents are observed in response to metabolic inhibition. By contrast, metabolic inhibition has little or no effect on Kir6.2/SUR2A channels [62]. Furthermore, unlike SUR1-containing channels, MgADP does not shift the MgATP sensitivity of Kir6.2/SUR2A channels [62]. In the case of SUR2B, this subunit tends to associate with Kir6.1 to form functional channels. These channels are considerably insensitive to ATP and are activated by nucleoside diphosphates [63].

1.2. Physiology of the K_{ATP} channel

K_{ATP} channels are key players in many physiological functions including regulation of neuronal, cardiac and endocrine excitability, glucose uptake by skeletal muscle, control of smooth muscle tone, and insulin secretion from pancreatic β-cells. Although the physiological role of the K_{ATP} channel in skeletal and cardiac myocytes is of great importance, for this introduction, I will focus on the physiological roles of the K_{ATP} channel in the pancreatic β-cell and the nervous system.

1.2.1. Pancreatic β-cell

The physiological function of K_{ATP} channels has been best characterised in the pancreatic β-cell, where channel activity is at the heart of insulin secretion. In the early 1980s, it was well known that glucose stimulates insulin secretion. However, the molecular entities responsible for this phenomenon were unknown. In 1984, Cook and Hales described a potassium current in pancreatic β-cells which was blocked by elevation of intracellular ATP [8]. Simultaneously, Ashcroft and colleagues described a potassium current in pancreatic β-cells, which was active at the resting potential of the β-cell and was inhibited by increases in glucose metabolism [9]. Work by Rorsman and Trube showed these two potassium currents were identical, providing a model by which glucose alters the β-cell membrane potential and triggers insulin secretion [10].

Further work showed that the β-cell membrane potential is mainly determined by K_{ATP} channel activity [64]. Thus, when K_{ATP} channels are shut, the membrane resistance is high and very small changes in K_{ATP} conductance have significant effects on insulin secretion [65].

These discoveries provided a model for glucose-stimulated insulin secretion (Fig. 1.4). At low concentrations of plasma glucose, K_{ATP} channels remain open, allowing efflux of K^+ ions from the β-cell, which maintains it in a

hyperpolarized (non-secreting) state (Fig. 1.4A). When plasma glucose levels rise, there is a concomitant increase in β-cell metabolism, which results in the closure of K_{ATP} channels, depolarization of the plasma membrane, and subsequent activation of voltage-gated Ca^{2+} channels. The consequent Ca^{2+} influx stimulates exocytosis of insulin granules (Fig. 1.4B).

In addition to glucose-dependent insulin secretion, it has been reported that Epac2, a member of the cAMP-regulated guanine nucleotide exchange factor family, mediated cAMP-dependent insulin secretion from pancreatic β-cells via a mechanism involving the closure of K_{ATP} channels as it seems to interact with the NBDs of the SUR subunits of the K_{ATP} channel [66,67].

1.2.2. Central nervous system

1.2.2.1. Distribution of the neuronal K_{ATP} channel

Sulphonylurea binding studies as well as *in situ* hybridization and immunohistochemical experiments have demonstrated that K_{ATP} channels are widely expressed throughout the brain [26,68-70]. Functional studies have corroborated the wide distribution of the K_{ATP} channel in the brain, with activity being detected in the hippocampus [71-74], hypothalamus [13,75,76], basal ganglia [27,77-79], neocortex [80], and brainstem [81].

Interestingly, all known K_{ATP} channel subunits have been found in different neuronal populations [23,82], which would allow for the formation of K_{ATP} channels with different metabolic and pharmacological properties. Although the exact contribution of each of these channels to neuronal function is not currently known, significant advancements have been made in pinpointing the locations of these different subunits.

Kir6.2 appears to be the main pore-forming subunit of the neuronal K_{ATP} channel. Kir6.2 expression has been described in most brain regions including the hypothalamus, cerebellum, basal ganglia, hippocampus, neocortex, thalamus, and somatosensory and motor nuclei [26,69]. Its expression appears to be confined to neurones, with glial cells expressing little or no Kir6.2 [83,84]. Interestingly, Kir6.2 expression is not restricted to a specific functional class of neurones as it has been shown to co-express with a variety of different proteins, including glutamic acid decarboxylase 65 (a marker of GABAergic neurones) and tyrosine hydroxylase (a marker of dopaminergic neurones) [69].

The expression levels of Kir6.1 in neurones are relatively low. However, moderate levels of expression have been observed in the striatum and hypothalamus [84]. Furthermore, Kir6.1 appears to be the main pore-forming subunit of the glial K_{ATP} channel, with its expression being found in astrocytes, Bergman glial cells and tanycytes in various regions of the brain [84,85].

It is thought that SUR1 is the main regulatory subunit of the neuronal K_{ATP}

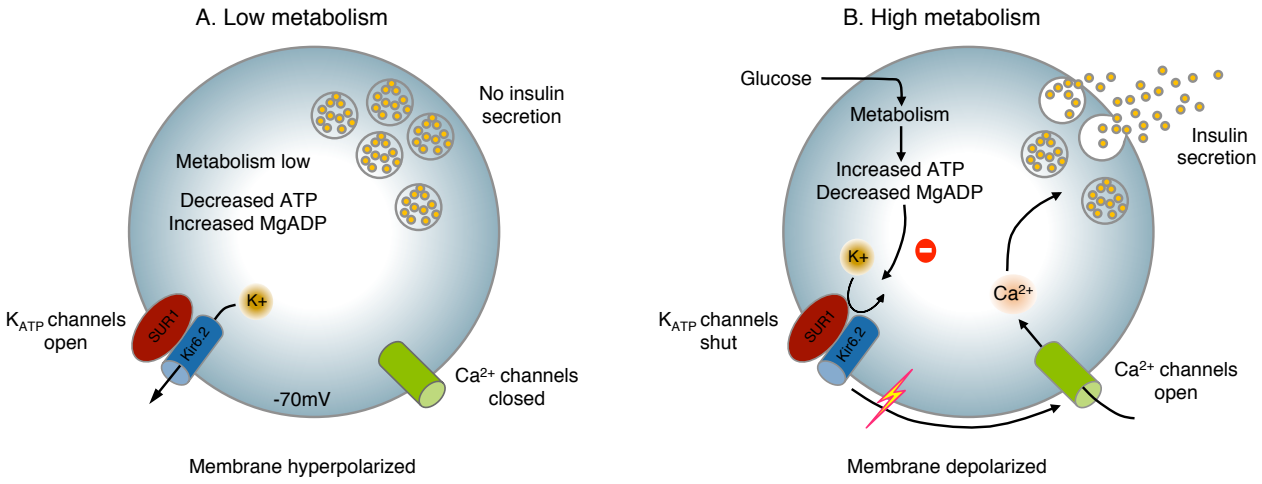

Figure 1.4: Metabolic regulation of K_{ATP} channels

Schematic representation of the metabolic regulation of K_{ATP} channels in pancreatic β-cells. (**A**) Under low plasma glucose conditions, K_{ATP} channels are open and maintain the membrane potential hyperpolarized. (**B**) When plasma glucose levels increase, the metabolism of β-cells increases causing an increase in the intracellular ATP and a decrease in MgADP. This leads to K_{ATP} channel closure, membrane depolarization, opening of voltage-gated calcium channels, Ca^{2+} influx and insulin release.

channel as its distribution closely overlaps with Kir6.2 [26,68,83]. For a long time it was thought that SUR2A was not expressed in the brain [82]. However, recent data has shown that SUR2A is expressed in several brain regions, including cerebral cortex, hippocampus and cerebellum. It also appears to be expressed in oligodendrocytes [23]. The other SUR2 isoform, SUR2B, is mainly located in glial cells, both astrocytes and oligodendrocytes, in various regions of the brain, including the anterior commissure, the corpus callosum, and the cerebellar white matter [23].

Although a variety of techniques have been used for assessing expression of the various K_{ATP} channel subunits in the brain, caution should be taking when interpreting the immunohistochemistry data as the specificity of the antibodies used has not been tested using Kir6.x or SUR knockout mice.

1.2.2.2. Glucose homeostasis

Neuronal K_{ATP} channels are key players in the central control of glucose homeostasis. In the ventromedial hypothalamus, opening of K_{ATP} channels in glucose-responsive neurones triggers the counter-regulatory response to hypoglycaemia [86]. This is mediated via brainstem nuclei and the autonomic nervous system, leading to the release of catecholamines, such as adrenaline, which are powerful triggers for glucagon release [86-88]. Furthermore, hypothalamic administration of diazoxide, a K_{ATP} channel

opener, significantly reduces hepatic glucose production. This is further supported by the observation that SUR1 knockout mice show a significant increase in the rate of gluconeogenesis [89]. Moreover, it has been demonstrated that oral administration of diazoxide suppresses hepatic glucose production in humans independently from pancreatic hormones [90].

1.2.2.3. Neuroprotection

A considerable body of work has shown that K_{ATP} channels also play an important role in preventing excitotoxicity linked to metabolic stress (e.g. ischemia, hypoglycaemia, hypoxia). *In vitro* and *in vivo* experiments indicate that most neuronal K_{ATP} channels are closed under normal conditions and open only in response to metabolic stress [82,91-94].

K_{ATP} channels are thought to act as "metabolic gatekeepers", with their activation acting as a negative feedback to ensure electrical signalling is matched to energy consumption [82,95]. For example, it has been demonstrated that increased Na^+/K^+ ATPase activity enhances neuronal K_{ATP} channel currents [93,96]. Furthermore, K_{ATP} channels contribute to the hypoxia-induced hyperpolarization of hippocampal neurones [72].

These *in vitro* observations correlate with subsequent *in vivo* experiments. Kir6.2 knockout mice have an increased susceptibility to generalized seizures

when exposed to hypoxia [97]. SUR1 knockout mice appear to also be hypersensitive to hypoxia-induced seizures [98]. This is supported by the fact that mice selectively over-expressing SUR1 in the forebrain are significantly less susceptible to kainate-induced seizures (a common animal model of epilepsy) [99].

Recent work by the Yellen group has suggested that K_{ATP} channel activity plays an important role in regulation of neuronal excitability under normal conditions [93]. They showed that modest action potential firing in hippocampal dentate granule neurones is sufficient to open single K_{ATP} channels via Na^+ influx and ATP depletion [93]. Moreover, they have shown that K_{ATP} activity in these neurones is further potentiated by ketone bodies, which hints at a cellular mechanism by which the ketogenic diet reduces seizure activity [93,94].

Interestingly, it has been demonstrated that activation of K_{ATP} channels in dopaminergic midbrain neurones for NMDA-mediated phasic burst firing in response to novel sensory cues, which is essential for context-dependent exploratory behaviour [100]. Thus, K_{ATP} channel opening under physiological conditions does not always result in reduced neuronal activity.

1.3. Pathophysiology of the K_{ATP} channel

In the last two decades, the physiological importance of the K_{ATP} channel has been highlighted by the discovery that mutations in Kir6.2 and SUR1 are associated with abnormal insulin secretion. Loss-of-function mutations, which result in permanent depolarization of the β-cell, have been linked to congenital hyperinsulinism of infancy (CHI). Conversely, gain-of-function mutations, resulting in permanent hyperpolarization of the β-cell, are associated with neonatal diabetes (ND).

1.3.1. Congenital hyperinsulinism of infancy

CHI is a rare disorder characterized by continuous and unregulated insulin release even at very low levels of plasma glucose, which presents during the first year of life [101-103]. If left untreated, CHI can have severe clinical consequences as the increased insulin secretion triggers hypoglycaemia and inappropriate suppression of lipolysis and ketogenesis, which, in turn, can result in permanent neurological damage [103,104].

To date, CHI has been associated with mutations in 7 different genes: SUR1 (*ABCC8*), Kir6.2 (*KCNJ11*), glutamate dehydrogenase (*GLUD1*), hepatocyte nuclear factor 4A (*HNF4A*), glucokinase (*GCK*), hydroxyacyl-coenzyme A

dehydrogenase (*HADH*), and mono-carboxylate transporter 1 (*SLC16A1)* [102,105-113]. Although in 45-55% of patients the genetic aetiology is currently unknown, mutations in the genes encoding for the K_{ATP} channel (*ABCC8, KCNJ11*) appear to be the most common cause of CHI, accounting for 40-45% of all cases [103,104].

Most K_{ATP} channel mutations associated with CHI are found in *ABCC8*, which encodes the SUR1 subunit. These mutations affect K_{ATP} channel function by either impairing the ability of MgADP to stimulate channel activity or by reducing channel expression at the plasma membrane [102,104,114,115]. This results in continuous depolarization of the β-cell membrane, over-activity of voltage-gated Ca^{2+} channels, and dysregulated insulin secretion (Fig. 1.5) [116].

Mutations can result in reduced channel surface expression due to abnormalities in gene expression, protein synthesis, maturation, assembly or trafficking [103,104,117-119]. These mutations tend to be distributed throughout the whole protein and result in a severe and drug-resistant form of CHI [103]. Mutations that affect MgADP stimulation tend to cluster around the NBDs of SUR1 and are thought to impair nucleotide binding/hydrolysis [120-123]. These mutations tend to result in a less severe phenotype, with some of the patients responding to diazoxide, a K_{ATP} channel opener used to treat some forms of CHI [103,122,124].

A few loss-of-function mutations in *KCNJ11* have been described, although they are a relatively rare cause of CHI [104,106,125,126]. These mutations result in ablation of K_{ATP} channel activity in the cell membrane.

CHI associated with mutations in *GLUD1, GCK, HNF4A* and *SLC16A1* can be managed by administration of diazoxide, which opens K_{ATP} channels and leads to β-cell hyperpolarization and reduced insulin secretion. However, in the case of *ABCC8* and *KCNJ11* mutations, subtotal pancreatectomy is required for alleviating the severe hyperinsulinaemia [103,104].

1.3.2. Neonatal diabetes (ND)

Neonatal diabetes is a very rare disorder with an incidence of approximately 1 in 100-200,000 live births [5,127,128]. It is characterized by severe hyperglycaemia, which presents itself within the first six months of life and can be either permanent (PNDM) or transient (TNDM) [5,127-129].

1.3.2.1. Transient neonatal diabetes mellitus

Approximately 50% of ND cases are transient, with patients usually being diagnosed in the first week of life and requiring insulin to maintain normoglycaemia [130]. Interestingly, their insulin requirements fall rapidly and

their diabetes usually goes into remission by 12 weeks of age [131]. However, a large number of TNDM patients tend to relapse and develop non-insulin dependent diabetes during pubescence [130,132]. The mechanism behind this remission and later relapse is currently unknown, although it has been suggested that it may be mediated by a transient increase in insulin sensitivity or increased β-cell function [133].

The genetic aetiology of TNDM is well defined, with approximately 70% of cases being caused by imprinting abnormalities affecting paternally expressed genes in the chromosome 6q24 region [132,134]. The remaining 30% of cases appear to be associated with gain-of-function mutations in either *KCNJ11* or *ABCC8* [135].

1.3.2.2. Permanent neonatal diabetes mellitus

Unlike TNDM, permanent neonatal diabetes requires life-long glycaemic control. Gain-of-function mutations in *KCNJ11* and *ABCC8* are the most common cause of PNDM, accounting for 30-50% of all cases [4,133,136,137]. Most of these mutations arise *de novo* in embryogenesis, although there are a few examples of familial transmission [4,133,137]. To date, more than 100 different *KCNJ11* and *ABCC8* mutations have been identified [127]. Most of the *KCNJ11* mutations are dominant, missense mutations, although one in-frame 15-nucleotide deletion has been reported [4,127,138]. *ABCC8* mutations are more

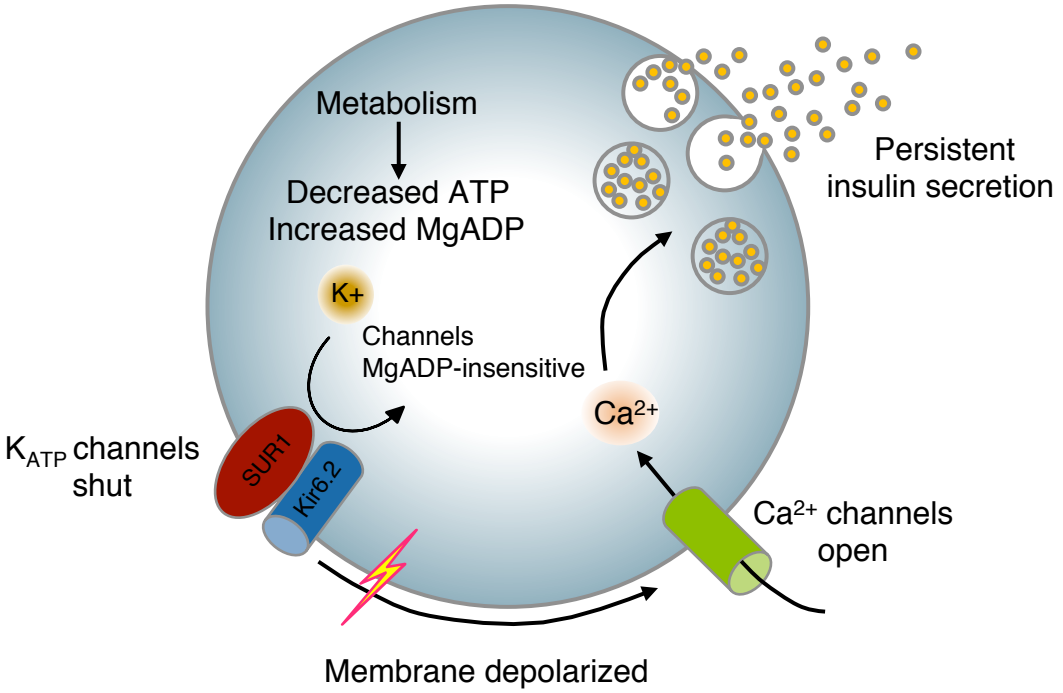

Figure 1.5: Congenital hyperinsulinism of infancy

Loss-of-function mutations in Kir6.2 or SUR1 lead to permanent K_{ATP} channel closure, regardless of cellular metabolism. Consequently, there is a constant depolarization of the plasma membrane, continuous calcium influx and persistent insulin secretion.

heterogeneous, with dominant, recessive, uniparental disomy, and compound heterozygocity being reported [127,128,139].

In addition to mutations in the genes encoding for the K_{ATP} channel, mutations in other key players of β-cell function have been described, including glucokinase, insulin, glucose transporter 2 (GLUT2), and insulin promoter factor 1 [140-144]. Furthermore, several rare autosomal recessive syndromes that feature PNDM exist, including Wolcott-Rallinson syndrome due to mutations in the *EIF2AK3* gene [145], pancreatic and cerebellar agenesis due to mutations in the *PTF1A* gene [146], X-linked diabetes mellitus due to mutations in the *FOXP3* gene [147], pancreatic agenesis due to mutations in the *Rfx6* gene [148], and ND with congenital hypothyrodism due to mutations in the *GLIS3* gene [149].

1.3.3. DEND syndrome

Although most patients with K_{ATP} mutations experience diabetes in isolation, approximately 25% also express extra-pancreatic symptoms [4,127]. About 5% of ND patients exhibit marked developmental delay (cognitive and motor), muscle hypotonia, epilepsy, and dysmorphic features (prominent metopic suture, bilateral ptosis, downturned mouth). This spectrum of symptoms is known as DEND syndrome (**d**elay, **e**pilepsy, and **n**eonatal **d**iabetes) [5]. The remaining 20% of patients with extra-pancreatic symptoms present with an intermediate condition (iDEND syndrome), which consists of neonatal

diabetes coupled with developmental delay (delayed speech and walking), muscle hypotonia and attention deficit [5]. Although it was originally thought that these patients did not suffer epilepsy, there is accumulating evidence that a small number of them may experience mild and isolated seizures [150-153].

1.3.4. Functional effects on the channel

All gain-of-function ND mutations in Kir6.2 exert their effect by "locking" the K_{ATP} channel in a permanently open state, even under hyperglycaemic conditions [65,133]. This leads to an increased whole-cell K_{ATP} current, membrane hyperpolarization and reduced electrical activity (Fig. 1.6). In all cases, the increased K_{ATP} channel activity is caused by a reduction in the sensitivity of the channel to ATP inhibition, which can be achieved directly or indirectly [4,154-157].

Mutations that cluster around the putative ATP-binding site of Kir6.2 are thought to impair ATP binding directly [158]. Some of these residues had been previously identified in biochemical and mutagenesis studies as being key players in ATP-binding [120,159,160].

Mutations that lie outside of the putative ATP-binding site of Kir6.2 act by increasing the channel's intrinsic open probability. This indirectly reduces ATP inhibition as ATP predominantly binds to the closed state of the channel and

thus any mutation that reduces the amount of time spent in the closed state secondarily decreases the channel's ATP sensitivity [154-156,161-163]. It is, however, not clear whether the increase in the open probability is mediated by changes in the gating of the channel or alterations in PIP_2 binding [164]. Interestingly, it has been shown that some Kir6.2 mutations are also able to enhance channel activation by Mg-ATP/ADP acting at the NBDs of SUR1 [155,165]. It has been suggested that this effect could be explained by conformational changes in Kir6.2 caused by the mutation producing secondary allosteric changes in SUR1 conformation to increase MgATP binding/hydrolysis at the NBDs [155]. However, in the absence of a high-resolution structure of the channel, it is difficult to demonstrate this.

Few ND mutations in SUR1 have been functionally characterized, but those mutations that have been studied also appear to impair the ability of ATP to inhibit the channel [136,139,166]. They do so by either increasing MgATP/ADP activation or by stabilizing the open state of the channel [47,162,167].

Electrophysiological studies have suggested that there is a marked correlation between the severity of the clinical phenotype and the ability of ATP to inhibit the whole-cell K_{ATP} current magnitude under resting conditions [4,155,158,164]. Thus, mutations causing a small reduction in ATP block produce a small increase in the resting K_{ATP} current and are associated with TNDM [158]. Larger reductions in ATP sensitivity result in PNDM [155]. In the case of iDEND and DEND mutations, a pedestal is observed at saturating ATP concentrations,

which would indicate that these channels cannot be completely shut even when all ATP-binding sites are occupied [155]. This suggests that under physiological conditions, mutant channels associated with iDEND and DEND syndromes will have significantly larger currents than wild-type channels.

To date, functional studies have shown that mutations in SUR1 have less pronounced effects on K_{ATP} currents than Kir6.2 mutations causing a similar phenotype [128]. This could explain why iDEND and DEND syndromes are more commonly associated with Kir6.2 mutations [127]. However, it should not be forgotten that Kir6.2 couples to SUR2 in some neurones [27], so that a greater population of cells might be affected by a Kir6.2 mutation than a SUR1 mutation.

Interestingly, phenotypic heterogeneity has been reported in ND in some families with multiple carriers of the same disease-causing mutation. In a family with the Kir6.2-C42R mutation, a range of phenotypes, including PNDM, gestational diabetes and T2DM, have been observed [168]. Similarly, in various families with SUR1 mutations, carriers are reported to be unaffected or suffer from T2DM or ND [135,136,169]. The reason for this phenotypic heterogeneity is currently unknown, but it indicates that the severity of the mutation may be modulated by additional genes or epigenetic factors.

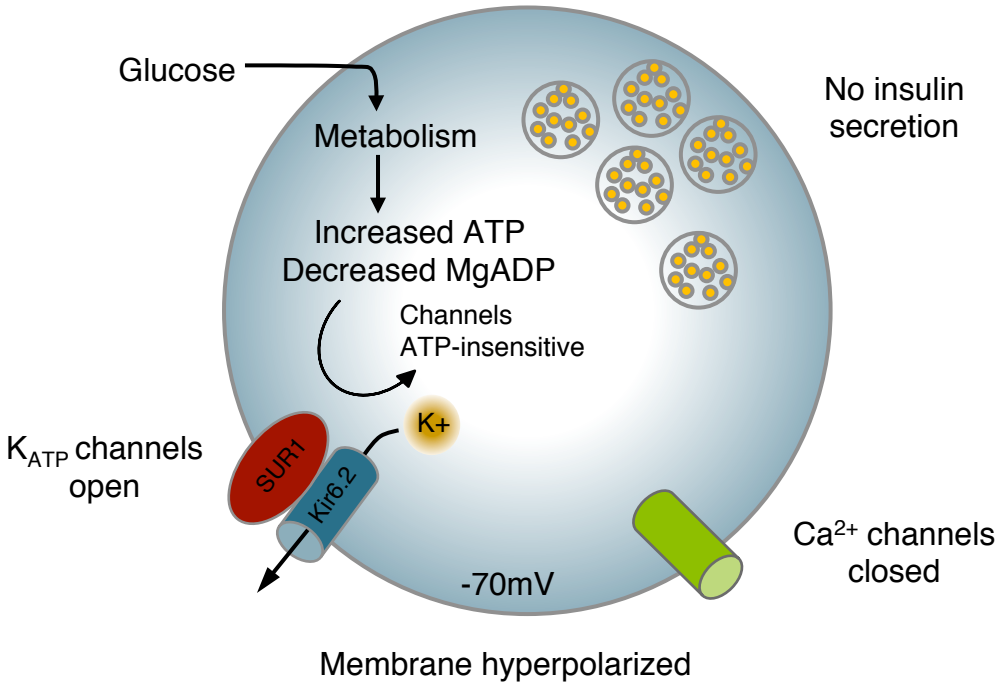

Figure 1.6: Neonatal diabetes

Gain-of-function mutations in Kir6.2 or SUR1 render the channel ATP-insensitive and hence prevent K_{ATP} channel closure when ATP levels rise in response to metabolism. Thus, the β-cell membrane remains hyperpolarised even when plasma glucose levels are elevated, preventing insulin secretion.

1.4. Mouse models of K_{ATP} dysfunction

Mouse models have been crucial tools for enhancing our understanding of human disease, particularly as they permit the study of cellular pathology and molecular mechanisms to an extent that is virtually impossible in human patients. Furthermore, *in vivo* pharmacological studies carried out using mouse models of human conditions are valuable for improving clinical management. For these reasons, a plethora of different murine models have been created to study diseases caused by K_{ATP} channel dysfunction.

1.4.1. Congenital hyperinsulinism of infancy

To date, various murine models of CHI caused by K_{ATP} mutations have been produced. Although none of these models fully recapitulate the human condition, they provide some insight into the effects of loss-of-function K_{ATP} mutations on pancreatic islets at the cellular level.

The first attempt to produce a CHI mouse model expressed a β-cell specific dominant-negative Kir6.2 mutation [170]. This mutation, G132S, alters the structure of the channel's selectivity filter, resulting in non-functional, or possibly slightly sodium permeable [171], K_{ATP} channels. At the cellular level, this resulted in a significant increase in the resting membrane potential as well as basal intracellular calcium levels in β-cells from Kir6.2-G132S mice.

At the whole organism level, expression of the G132S channel resulted in hypoglycaemia, increased insulin levels and unregulated insulin secretion during the neonatal period. However, by four weeks of age, Kir6.2-G132S mice had significantly higher blood glucose levels when compared to control and showed slight glucose intolerance as well as reduced glucose-stimulated insulin secretion. Histological studies demonstrated these phenotypical changes coincided with a significant reduction in the β-cell population and alterations to the morphological configuration of the islets. Furthermore, increased β-cell apoptosis was observed in adult mutant mice, leading Miki to suggest that the chronic depolarization of the β-cell and increased intracellular calcium load may promote apoptotic cell death and result in hyperglycaemia in adults [170].

This model was followed by the generation of whole body Kir6.2 ($Kir6.2^{-/-}$) or SUR1 knockout mice ($SUR1^{-/-}$) [97,172]. Knockout of each subunit individually resulted in complete abolition of K_{ATP} currents in β-cells as well as significantly higher resting membrane potential and elevated basal intracellular Ca^{2+} levels. Perifusion and batch incubation studies using islets from Kir6.2 or SUR1 knockout mice showed that insulin secretion was not regulated by ambient glucose concentrations, as would be expected in the absence of the K_{ATP} channel.

At the *in vivo* level, knockout of the individual subunits resulted in mild impairment of glucose tolerance [97,172]. Furthermore, in both groups of

knockout mice, plasma insulin levels barely increased following intraperitoneal glucose injection, reflecting the results obtained with the *in vitro* islet studies. Although both sets of knockout mice experienced transient hypoglycaemia during the first days after birth, this rapidly rectified and adult knockout mice had similar blood glucose levels to age-matched adult control mice. Interestingly, an increased sensitivity to insulin was observed in Kir6.2$^{-/-}$ mice, which the authors suggest explains why blood glucose levels were normal in these mice [97]. In the case of SUR1$^{-/-}$ mice, no increase in insulin sensitivity was observed.

Histology studies showed an increase in the number of α-cells found in the central region of islets from both Kir6.2$^{-/-}$ and SUR1$^{-/-}$ mice [97,172]. Interestingly, no difference in the levels of apoptosis was observed in the islets of these mice.

So far, only one mouse model with a human CHI mutation has been reported [173]. In this mouse, ENU (N-ethyl-N-nitrosourea) mutagenesis resulted in a single point mutation in the *KCNJ11* gene, which converted the tyrosine at residue 12 into a stop codon (Kir6.2-Y12STOP). This mutation has also been found homozygously in a patient with familial hyperinsulinaemia and had been shown to abolish K_{ATP} channel activity when expressed heterologously [125].

Adult Kir6.2-Y12STOP mice showed impaired glucose tolerance *in vivo* in response to both an intraperitoneal and an oral glucose bolus. This correlated

with *in vitro* studies, which showed decreased insulin secretion from isolated Kir6.2-Y12STOP islets. Interestingly, unlike the mouse models previously discussed, no changes to islet architecture and morphology were observed.

To date, the only mouse model with hyperinsulinaemia in adulthood is a transgenic mouse with dominant-negative mutations in the selectivity filter expressed only in β-cells [174]. In this mouse (Kir6.2[AAA]-GFP), residues 132-134 of Kir6.2, which are glycine-phenylalanine-glycine, were replaced with non-polar alanine residues. Additionally, the mutant Kir6.2 was C-terminally tagged with enhanced green fluorescent protein (EGFP).

Electrophysiological studies revealed that approximately 30% of β-cells from transgenic mice did not express EGFP and showed normal K_{ATP} currents, making this mouse a partial knockout. In the remaining 70% of β-cells, which expressed EGFP, no detectable K_{ATP} currents were observed [174]. Furthermore, the EGFP expressing β-cells had significantly depolarized resting membrane potentials and elevated cytosolic Ca^{2+} levels.

Unlike the mouse models discussed previously, this partial knockout of the K_{ATP} channel resulted in normoglycaemia and normoinsulinaemia during the neonatal period. However, significant increases in fed and fasted plasma insulin levels were observed in adult transgenic mice. Intraperitoneal glucose tolerance tests also revealed that adult Kir6.2[AAA]-GFP mice had a significantly lower increase in glucose excursion as well as a faster decrease

in glucose levels. This correlated with *in vitro* islet studies, which showed islets from adult Kir6.2[AAA]-GFP mice had increased insulin release at both stimulatory and non-stimulatory glucose concentrations. Histology studies on pancreatic sections from adult Kir6.2[AAA]-GFP mice showed no significant changes in islet architecture or morphology.

There are several reports of non-pancreatomized CHI patients developing diabetes in late life, which might correlate with the phenotype observed in CHI mouse models [109,115,175,176]. This is further supported by the fact that increased levels of β-cell apoptosis have been observed in histological samples from pancreatic tissues of CHI patients with K_{ATP} mutations [177]. It is possible that loss of K_{ATP} activity and concomitant long-term elevation of intracellular Ca^{2+} levels leads to increased rates of β-cell exhaustion and apoptosis and eventually results in diabetes. However, this hypothesis remains controversial[133].

1.4.2. Permanent neonatal diabetes mellitus

By contrast with CHI mouse models, all ND mouse models generated to date recapitulate the human disease [178-181]. These models express K_{ATP} channels with reduced ATP sensitivity selectively in pancreatic β-cells, which results in initial elevation of blood glucose levels shortly after birth (or induction of mutant gene) and overt diabetes within a few weeks.

The first gain-of-function mouse model was generated using a truncated version of Kir6.2 (Kir6.2ΔN30), which results in a 7-fold reduction in ATP sensitivity [182], under the control of the rat insulin promoter. Mice expressing the mutant channel developed severe diabetes, ketoacidosis and died shortly after birth [178]. Although it was not possible to carry out further experiments on glucose homeostasis in these mice, this mouse model provided the first *in vivo* evidence that overactivity of K_{ATP} channel can result in diabetes.

Interestingly, some of the transgenic lines generated by Koster and colleagues exhibited positive expression of the transgene, but did not show the severe neonatal phenotype [178,179]. These lines appeared to express the transgene in only 30-50% of their islets, which resulted in a milder phenotype consisting of lower glucose tolerance and a non-significant trend towards lower serum insulin levels and higher blood glucose values [179].

At the cellular level, islets from these mice showed normal morphology and normal glucose-stimulated insulin secretion (GSIS) except at high concentrations (16-23mM) where the amplifying effect of glucose was absent. Surprisingly, approximately 7% of the transgenic mice spontaneously developed diabetes post-weaning as well as complete loss of GSIS and altered islet morphology. The authors suggested the variability in the phenotype was caused by mosaic expression of the mutation, which is a common feature of transgenic mice [183,184]. The authors argue that although this would not normally occur in human patients, it is interesting that varying

degrees of K_{ATP} channel overactivity can affect glucose homeostasis to different degrees, which to a certain extent mirrors what is observed in humans, with Kir6.2 polymorphisms being risk factors in T2DM and gestational diabetes and single point mutations resulting in ND [179].

The first mouse model with a disease-causing activating K_{ATP} mutation was generated using Cre-lox technology to express the Kir6.2-V59M mutation, which is the most common cause of iDEND syndrome in humans, selectively in pancreatic β-cells [181]. These mice appear to express V59M-Kir6.2 mRNA at similar levels to WT-Kir6.2 in pancreatic islets, which argues for it being a reasonable model for the heterozygous state observed in human patients. The β-V59M mice had raised blood glucose levels within 3 days of birth, and developed severe diabetes by 5 weeks of age, with blood glucose concentrations higher than 30mM and undetectable plasma insulin levels.

At the cellular level, expression of the V59M mutation resulted in reduced glucose-stimulated insulin secretion and considerably smaller increases in intracellular calcium concentrations in response to glucose [181]. Furthermore, there was a reduction in the insulin content of these islets, which is thought to be caused by the lower transcription of the insulin gene observed by the authors. Histology of pancreatic sections from the β-V59M mice also showed a decrease in the β-cell mass of the islets as well as alterations in islet morphology.

The electrophysiological studies carried out on β-V59M β-cells showed a significant reduction in the channel's ATP and glucose sensitivity. Although the channel's sensitivity to inhibitors such as tolbutamide was reduced by the mutation, the drug was still able to block the majority of the channels at high concentrations. This observation went hand-in-hand with the fact that insulin secretion from β-V59M islets was stimulated by tolbutamide, indicating that the impaired insulin secretion results from the failure to close the K_{ATP} channel[181].

Simultaneously, another gain-of-function mouse model was generated using the Cre-lox approach [180]. This mouse expressed a Kir6.2 with an ATP-binding site mutation (K185Q) as well as an allosteric gating mutation (ΔN30), which resulted in a ~30-fold reduction in the channel's ATP sensitivity [180,182]. Selective expression of the mutation in β-cell was achieved by using a rat-insulin-promoter cre-line [185]. The resulting mice had a very similar phenotype to those described by Girard and colleagues: they developed diabetes within a few weeks of birth as well as reduced insulin content, β-cell mass, abnormal islet morphology, and impaired glucose-stimulated insulin secretion [180].

In addition to these mice, Remedi et al used a tamoxifen inducible Cre-line ($Pdx1^{PB}$ Cre-ER) [186] to generate a mouse where expression of the ATP-insensitive channel could be controlled temporally. These mice developed normally and showed normoglycaemia prior to tamoxifen injection. However, once the transgene was activated, the mice became severely diabetic and

developed the same severe secondary consequences as the neonatal constitutive models [180].

Remedi and colleagues used this model to study whether it was possible to prevent these secondary consequences by preserving normoglycaemia. They thus treated the mice with either islet transplantation or glibenclamide (a K_{ATP} channel blocker) pellet implantation prior to gene induction. These two treatments prevented diabetes and preserved islet architecture and β-cell mass, suggesting that the secondary consequences of transgene activation are due to untreated, systemic hyperglycaemia [180].

1.4.3. iDEND syndrome

When iDEND/DEND syndrome was first described in human patients with activating K_{ATP} channel mutations, it was not clear whether the extra-pancreatic symptoms, particularly the muscle hypotonia, were caused by expression of the mutant channel in nerve, muscle or a combination of both [5]. For this reason, Clark and colleagues developed two mouse models expressing the V59M-Kir6.2 mutation under the control of the nestin or the muscle creatine kinase promoters to selectively drive expression in either nerve or muscle, respectively [62].

Surprisingly, selective expression of the V59M-Kir6.2 mutation in muscle (mV59M) did not affect muscle strength or motor coordination. On the other hand, mice with selective neuronal expression of the mutation (nV59M) suffered from hypotonia, showing reduced performance in muscle strength and balance control tests [62]. Additionally, nV59M mice displayed hyperactivity, running for longer on free-running wheels and spontaneously moving around more frequently on activity threshold plates. Hyperactivity was not initially described as a trait of iDEND syndrome, particularly as many of the patients did not walk. However, there are now various reports of patients exhibiting hyperactivity once they start walking [187-189].

Clark and colleagues also carried out electrophysiological studies to determine whether the motor problems were caused by reduced excitability of central nervous system neurones or decreased activity at the neuromuscular junction. Recordings from isolated nerve-muscle preparations showed there were no differences in the amplitude or frequency of miniature endplate potentials or evoked endplate potentials as well as no differences in muscle resting potential, indicating that activity at the neuromuscular junction is normal.

By contrast, patch-clamp recordings from cerebellar Purkinje cells showed significantly lower action potential firing frequency as well as a significantly more hyperpolarized resting membrane potential. Interestingly, the action potential firing rate and the hyperpolarized resting membrane potential were

both restored by application of tolbutamide, a K_{ATP} channel blocker. K_{ATP} channels are highly expressed in various brain regions involved in movement and motor control, including the cortex and the cerebellum [26,68]. The authors thus concluded that an increased K_{ATP} current in Purkinje cells, and possibly in other neurones involved in movement, suppresses action potential firing leading to impaired motor function.

As both the mV59M and nV59M mice were normoglycaemic, these experiments also demonstrated that the extra-pancreatic symptoms of iDEND/DEND syndrome are not a secondary consequence of diabetes.

1.5. Sulphonylureas

Sulphonylureas are some of the most commonly used drugs for the management of non-insulin dependent diabetes. This family of drugs were developed after the serendipitous discovery that sulphonamides, which were being tested for the treatment of typhoid fever, cause hypoglycaemia in humans [190,191].

In the 1950's, Auguste Loubatières and colleagues were the first to explore the physiological mechanism of these drugs, by carrying a series of cross-circulation experiments in dogs. For these experiments, they connected the pancreatico-duodenal vein of a normal dog (donor) to the jugular vein of a

receiver dog that had previously undergone a pancreatectomy. Administration of compound 2254 RP, a sulphonamide, to the donor dog resulted in hypoglycaemia in the recipient. These results led Loubatières to postulate that sulphonamides elicit hypoglycaemia by directly stimulating insulin release from pancreatic β-cells [190-192].

Around the same time, Franke and Fuchs, who were working with a different sulphonamide (carbutamide) for the treatment of bacterial infections, noted that this drug also caused hypoglycaemia in normal subjects. Carbutamide differed from the compound tested by Loubatières in that the isopropylthiodiazol moiety had been substituted with an n-butylurea group (Fig. 1.7) [191]. This newer chemical structure formed the basis for the development of the sulphonylureas, which include tolbutamide, glibenclamide and gliclazide.

1.5.1. Mechanism of action

Although the experiments conducted by Loubatières and Franke & Fuchs indicated that sulphonamides/sulphonylureas acted on the pancreas to lower blood glucose, it was not until a decade later that their cellular mechanism was elucidated. Mehnert and colleagues were the first to demonstrate that carbutamide increases insulin release from isolated and perfused dog

pancreas [191,193]. These results were confirmed by subsequent experiments using perfused rat pancreata [194] and isolated rat islets [195].

Shortly after the initial description of the K_{ATP} channel in the 1980's, it was shown that sulphonylureas inhibit K_{ATP} channel activity in β-cells [196-198]. By the early 1990's it was clear that K_{ATP} channels were functionally linked to the sulphonylurea receptor [199-202], but it was not until the cloning of Kir6.2 that this association was shown experimentally [14,15,203-205].

A plethora of experiments conducted in the 1990's elucidated the molecular mechanism of action of the sulphonylureas. These drugs inhibit the K_{ATP} channel by binding to a high affinity and a low affinity site on the protein [206,207]. The high affinity site is located on the SUR subunit and is inhibited by clinically relevant concentrations, while the low-affinity site is located on Kir6.2 and is only activated by supra-pharmacological concentrations. Binding of sulphonylureas to SUR alters the single-channel kinetics of the K_{ATP} channel, reducing the open time and burst durations [208,209].

Interestingly, in excised patches, sulphonylureas only produce 50-70% current block even when drug binding is saturated [206,210,211]. It is thought that sulphonylureas prevent MgADP from stimulating channel opening as complete (>90%) inhibition of K_{ATP} channels is observed in intact cells as well as in excised patches when both MgADP and sulphonylureas are present [59,212]. Thus, sulphonylureas appear to block K_{ATP} channels by a combination

of direct and indirect inhibition. The latter involves abolition of the stimulatory effect of MgADP [213,214].

Mutagenesis and radioligand binding studies have shown that residues in the cytosolic loops between transmembrane helices 15 and 16 and between transmembrane helices 5 and 6 form the binding site for sulphonylureas [39,215,216]. However, in the absence of an atomic structure of the K_{ATP} channel, it is currently not possible to confirm the exact location of the sulphonylurea binding site or how binding of these drugs to the SUR subunit triggers closure of the Kir6.2 pore.

1.5.2. Management of neonatal diabetes with sulphonylureas

Since the 1960's, sulphonylureas have been one of the primary pharmacological treatments for the management of Type 2 diabetes mellitus. The discovery that many neonatal diabetes patients have K_{ATP} channel mutations led to the suggestion that sulphonylureas could be used for managing their diabetes. It was already known that sulphonylureas act by blocking open K_{ATP} channels, and electrophysiological studies had determined that activating mutations associated with ND lock the channel in an open

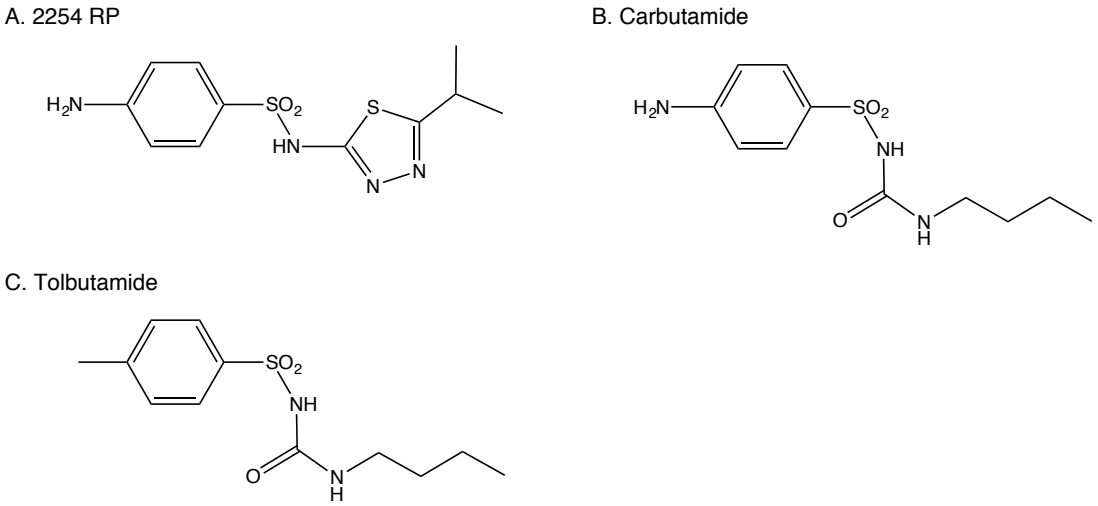

Figure 1.7: Sulphonamides and sulphonylureas

Chemical formulae of (**A**) compound 2254 RP, (**B**) carbutamide and (**C**) tolbutamide.

position [4,154,155,212]. Furthermore, experiments using heterologously expressed ND-mutant channels showed that it is possible to block these channels with sulphonylureas, which opened up the possibility of using these drugs for treating human patients [5,155].

To date, more than 90% of ND patients with K_{ATP} channel mutations have been successfully treated with sulphonylureas [6,217]. This therapy has resulted in significantly improved glycaemic control when compared to insulin treatment. A considerable decrease in glycated haemoglobin levels was observed as well as reductions in blood glucose fluctuations and hypoglycaemic episodes [6,217]. Prior to the discovery of the genetic aetiology of neonatal diabetes, ND patients were thought to suffer from very early-onset Type 1 diabetes mellitus, and were thus treated with insulin.

Increased insulin secretion in response to oral glucose administration was also observed in patients treated with sulphonylureas [6]. It has been suggested that this effect could be mediated by restoration of incretin-potentiated insulin secretion [6,218]. These hormones are secreted by the gut in response to food consumption and act on the β-cell to augment insulin secretion. Their stimulatory effect partially depends on a K_{ATP}-dependent elevation in intracellular calcium levels, which is absent in untreated ND. As closure of K_{ATP} channels by sulphonylureas leads to an increase in intracellular calcium concentrations, incretin-mediated insulin secretion is restored [218]. This may help explain the better glycaemic control observed in sulphonylurea-treated

ND patients, as their insulin secretion will be regulated by food consumption[218].

Although the vast majority of patients with gain-of-function K_{ATP} channel mutations successfully transferred to sulphonylurea treatment, a small percentage was unable to become insulin independent [6,157,217]. Six patients with *KCNJ11* mutations were reported to be unable to stop insulin treatment. Of these, five presented with additional neurological symptoms: three with iDEND syndrome (G53R, R201C and G334D mutations) and two with DEND syndrome (Q52R and I296L mutations) [6,157]. Electrophysiological studies have shown that sulphonylureas fail to block channels containing the latter two mutations [155,164,219]. In the case of patients with *ABCC8* mutations, four patients could not switch; two of the patients had neurological symptoms, including one with DEND syndrome [217].

Interestingly, two of the *KCNJ11* patients (G53R and R201C) who were unable to switch had children who successfully switched to sulphonylureas [6]. Furthermore, the *ABCC8* patients who failed to switch had been diagnosed with neonatal diabetes at a later stage than the patients who successfully switched (17 weeks versus 5 weeks) [217]. It is possible that some of these patients, particularly those with mutations that have been shown to respond to sulphonylureas, may be unable to transfer due to secondary consequences of diabetes. This is supported by the fact that mouse models of ND with untreated diabetes have altered islet morphology and a significant decrease in

β-cell mass [180]. Although most of these patients have been managed with insulin prior to the attempted sulphonylurea switch, it is possible they may have suffered from poor long-term blood glucose control [6,217,218].

There appears to be a good correlation between the efficacy of sulphonylureas at blocking whole-cell mutant K_{ATP} currents and the ability of patients with the same mutation to respond to sulphonylurea therapy [6,164]. For mutations where tolbutamide blocks <65% of current at saturating concentrations (0.5mM), patients fail to respond to sulphonylurea therapy (Fig. 1.8). By contrast, tolbutamide is able to block >75% of current through channels containing *KCNJ11* mutations of patients who successfully switched (Fig. 1.8) [6,164]. This suggests that mutations not only reduce ATP-sensitivity, but also affect sulphonylurea sensitivity [218].

1.5.3. Management of DEND/iDEND syndromes

Approximately 25% of patients with gain-of-function K_{ATP} channel mutations present with extra-pancreatic symptoms in addition to diabetes [4]. These symptoms are associated with mutations that cause considerable decrease in both the ATP and sulphonylurea sensitivity of the channel due to their effect on gating [218,219]. For this reason, most of the patients with severe DEND mutations have been unable to transfer to sulphonylurea treatment [6,217]. Nonetheless, a few DEND patients have successfully switched to

sulphonylureas, resulting in considerably better glycaemic control, both in terms of a reduction of blood glucose fluctuations and a decrease in glycated haemoglobin levels [220-224]. Most iDEND patients reported to date have switched to sulphonylurea treatment, with significant improvements in glycaemic control also reported [6,217].

There are some indications that sulphonylurea therapy improves neuronal function in both DEND and iDEND patients. Improved motor function (muscle tone, coordination and gait) has been reported for some iDEND patients [151,189,221,225,226]. In addition, a small number of patients display enhanced cognitive function after initiation of sulphonylurea therapy [188,189].

A significant reduction in epileptic seizures has also been reported in two DEND patients [221,223]. Although these reports are encouraging, for many iDEND and most DEND patients, sulphonylureas have been ineffective at improving cognitive deficits, developmental delay and seizure control, even when they successfully control their diabetes [157,220,222,224,227].

Interestingly, it has been reported that a few iDEND patients started experiencing seizures following therapy transfer. In one patient, absence seizures started developing two years after initiation of glibenclamide therapy[151]. This also occurred with two other iDEND patients (anecdotal evidence). Why this is the case is not clear, particularly as motor and

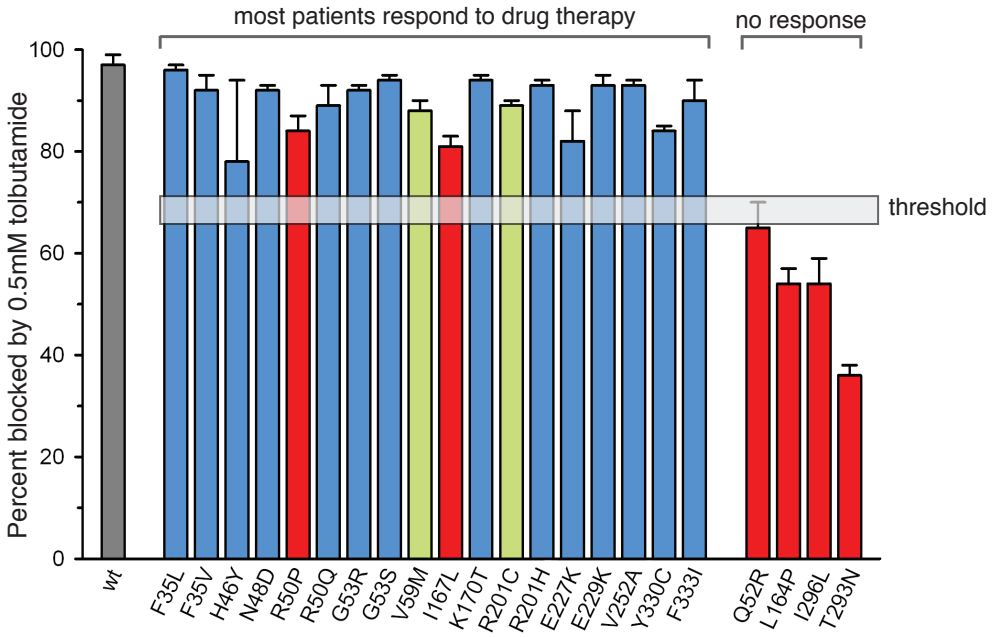

Figure 1.8: Tolbutamide sensitivity of mutant K_{ATP} channels

The correlation between the tolbutamide sensitivity of heterologously expressed mutant K_{ATP} channels and the ability of patients with the same mutation to transfer to sulphonylureas. Mean percent K_{ATP} current blocked by a saturating concentration of tolbutamide (0.5mM) for wild-type (wt) K_{ATP} channels and heteromeric K_{ATP} channels containing the indicated Kir6.2 mutations. Percent block was calculated by expressing the current in the presence of tolbutamide and 3mM azide (a metabolic inhibitor) as a percentage of the current in azide alone. Light grey bar indicated the threshold for successful transfer to sulphonylureas (65-72% block). Blue bars: neonatal diabetes in isolation. Green bars: iDEND syndrome. Red bars: DEND syndrome. Figure adapted from McTaggart *et al.*, 2010[164].

behavioural improvements were observed in these patients following transfer to sulphonylureas.

Even though these case studies suggest that sulphonylureas can improve neurological function, it was not restored to normal. It is not known whether this is due to irreversible neuronal damage as a consequence of poorly managed hyperglycaemia or if sulphonylureas are unable to penetrate the blood-brain barrier (BBB) and reach a high enough concentration in the cerebrospinal fluid (CSF) to close all overactive neuronal K_{ATP} channels.

Due to the rarity of the condition, and the fact that most patients are already given sulphonylureas, no thorough clinical studies have been carried out to assess the extent to which sulphonylureas ameliorate iDEND/DEND syndrome. The main aim of this thesis is to determine whether sulphonylureas are capable of reversing the neurological symptoms associated with gain-of-function mutations in the K_{ATP} channel by using the neuronal V59M-K_{ATP} mouse model.

Chapter 2: Materials and Methods

2.1. Animals

All work was conducted in accordance with the 1986 UK Animals (Scientific Procedures) Act and University of Oxford ethical guidelines. The care and use of mice and rats in this study were approved by the Ethics Committee of the University of Oxford.

2.1.1. Animal care

Animals were housed in same-sex littermate groups of 2-8 (mice) or 2-5 (rats), in a temperature and humidity controlled room on a 12h light-dark cycle (lights on at 7 am). Regular chow food was freely available. Animals had *ad libitum* access to water at all times.

2.1.2. Generation of mice

Mice heterozygous for the Kir6.2-V59M mutation were used in these studies. ROSA-V59M mice were generated by targeting the Kir6.2-V59M gene, preceded by a loxP-flanked STOP sequence and followed by a flippase

recombinase target (FRT)-flanked internal ribosome entry site (IRES) GFP cassette, to the ROSA26 locus [181]. Use of the endogenous ROSA26 locus ensured that a single copy of the mutant gene was expressed, from a known location. The endogenous and ubiquitously expressed [228] ROSA promoter was used to prevent excess gene expression.

In addition, a second mouse line in which the Kir6.2-V59M mutation was expressed under the control of the CAG (chicken beta-actin promoter with cytomegalovirus enhancer) promoter was used (ROSA-CAG-Kir6.2-V59M). The targeting strategy for the generation of these mice was the same as for the ROSA-Kir6.2-V59M line except that the CAG promoter was used to drive expression instead of the endogenous ROSA promoter. The CAG promoter is much stronger than the endogenous ROSA promoter.

Mice heterozygous for the Kir6.2-[K185Q, ΔN30] mutation were also used. These mice were generated by targeting the Kir6.2-[K185Q, ΔN30] gene, preceded by a loxP-flanked STOP sequence and followed by a flippase recombinase target (FRT)-flanked internal ribosome entry site (IRES) GFP cassette, to the endogenous ROSA26 locus under the control of the CAG promoter [180].

These ROSA mice were crossed with mice expressing Cre-recombinase under the control of different promoters to selectively express the Kir6.2 gain-of-function mutations in specific tissues: the nestin promoter (Nes-cre, stock

name Tg(Nes-cre) 1Kln/J #003771; Jackson Laboratory) [229] was used to drive expression in neurones, the muscle creatine kinase promoter (Mck-cre; kindly provided by Prof. Jens Bruning, Institute of Genetics, Cologne) was used for expression in skeletal and cardiac muscle, and the ubiquitin promoter (Ubi-cre-ER, stock name B6.Cg-Tg(UBC-cre/ERT2)1Ejb/J #008085; Jackson Laboratory) [230] was used to drive global expression. Male and female adult mice (11-20 weeks) were used for these studies. Littermates were used as controls.

2.1.3. Mouse genotyping

Genotypes were identified by PCR using genomic DNA isolated from ear biopsies (Maxwell® 16 Tissue DNA purification Kit, Promega). Transgenic sequences were amplified by PCR using specific primers (Table 2.1). PCR was carried out in 25µl reactions in a 2720 thermocycler (Applied Biosystems) using the DreamTaq Green PCR master mix (Fermentas) and 20ng of genomic DNA. PCR conditions were the following: 94°C for 3min followed by 45 cycles (94°C for 30s, 57°C for 45s, 72°C for 1min 30s) and a final extension at 72°C for 10min.

Table 2.1: Genotyping PCR primer information

Strain	*Sequence (5' to 3')*	*Amplicon size (bp)*
Nes-cre Ubi-cre-ER	fwd: ACGAGTGATGAGGTTCGCA rev: ATGTTTAGCTGGCCCAAATGT	~230
Mck-cre	P1: GTTCTTAAGTCTGAACCCGG P2: GTCTGGATGACATCGTCCAG P3: ATGTTTAGCTGGCCCAAATGT	~430
ROSA-Kir6.2-V59M	P1: AAAGTCGCTCTGAGTTGTTATC P2: GATATGAAGTACTGGGCTCTT P3: GCATCGCCTTCTATCGCCT	590 (ROSA-wt) 460 (ROSA-Kir6.2-V59M)
ROSA-CAG-Kir6.2-[K185Q, ΔN30] ROSA-CAG-Kir6.2-V59M	P1: GATATGAAGTACTGGGCTCTT P2: TGTCGCAAATTAACTGTGAATC P3: AAAGTCGCTCTGAGTTGTTATC	570 (ROSA-wt) 380 (ROSA-CAG)

2.2. Molecular biology

2.2.1. RNA extraction and cDNA synthesis

Mice were killed by cervical dislocation and tissues were quickly isolated, immersed in RNAlater solution (Qiagen), kept at 4°C overnight and later stored at -80°C until further processing.

Total RNA was extracted from 30mg of tissue using the RNeasy Mini Kit (Qiagen) with an on-column DNase digestion step to remove traces of genomic DNA. RNA concentration was determined in triplicate using a NanoDrop ND-1000 spectrophotometer (Thermo Scientific). One microgram of total RNA was reverse transcribed in a 20µl final volume using the High Capacity complementary DNA (cDNA) Reverse Transcription kit with RNAse inhibitor (Applied Biosystems). A separate microgram of total RNA was processed identically, but with no reverse transcriptase (Non-RT control). The reaction cycle consisted of 10min incubation at 25°C followed by a 30min incubation at 48°C.

2.2.2. Semi-quantitative PCR

Mouse Kir6.2 transcript was amplified by PCR using cDNA prepared from brain tissue of nV59M, Ubi-ROSA and control mice or from pancreatic tissue of Ubi-ROSA and control mice. The following primers were used:

Forward: 5'-ATGCTGTCCCGAAAGGGCATT-3'

Reverse: 5'-GGCGATGAGCCACCAGACCAT-3'

Each PCR reaction consisted of 20µl DreamTaq Green PCR master mix (Fermentas), 0.5µl of 10µM primers, 4µl of 25ng/µl cDNA, and 5µl nuclease-free water (total reaction volume was 30µl). The PCR conditions were the

following: 95°C for 2min followed by 40 cycles (95°C for 30s, 60°C for 30s, 72°C for 1min) and a final extension at 72°C for 10min.

The PCR products were digested with BtsCI restriction enzyme (New England Biolabs) for two hours at 50°C. Reactions consisted of 10µl PCR product, 2µl Buffer 4, 0.5µl BtsCI, and 7.5µl nuclease-free water. Digested PCR products were visualized in a 2% agarose gel with GelRed Nucleic Acid Stain (Biotium). The V59M mutation removes the unique BtsCI restriction site in the Kir6.2 transcript, allowing confirmation of the presence of the mutant Kir6.2 at the RNA level.

2.2.3. Real-time quantitative PCR

Real-time quantitative PCR was performed using an ABI Prism 7000 sequence detection system (Applied Biosystems) and SYBR green reagents (PowerSYBR green, Applied Biosystems). Each reaction consisted of 20ng cDNA, 12.5µl 2x PowerSYBR green master mix, 300nM primers (forward and reverse), and nuclease-free water up to a final volume of 25µl. The reaction cycle comprised an initial denaturation for 10min at 95°C, followed by 40 cycles of 95°C/15s, 60°C/60s. All reactions were performed in triplicate in a final volume of 25µl. Non-RT controls were included in each experiment to confirm the absence of genomic DNA contamination.

Primers were designed using Geneious Pro software (Biomatters Inc) based on NCBI sequence data (Table 2.2). Primer specificity was checked using BLAST, gel electrophoresis and melt curve analysis. Primer efficiencies were calculated using serial dilutions of tissue cDNA: 100ng, 50ng, 25ng, 12.5ng, 6.25ng, and 3.125ng. The ABI 7000 SDS software (Applied Biosystems) was used to measure threshold cycle (Ct) values. Baseline levels were calculated between cycles 3-14 and the threshold level was set to 0.3. Each sample was run in triplicate, allowing calculation of an average Ct value. These values were exported for analysis in Microsoft Excel, and they were plotted against log(dilution) and the efficiency of the reaction was calculated using the following equation: $10^{(-1/slope)}$ [231]. A value of 2 indicated that the reaction was optimal. All primers used in experiments in this thesis had efficiency of 1.9-2.1 (Table 2.2) as deviation from 2 indicates that there are factors interfering with the reaction (e.g. off-target PCR products). Efficiency values were used in the calculations of relative quantities of experimental samples.

The geNorm applet for Microsoft Excel was used to determine the most stable genes from a selection of candidate reference genes [232]. ACTB, HPRT1 and HSPA8 were identified as being the most stably expressed candidate reference genes and were thus used as reference genes for RT-qPCR (Table 2.2).

2.2.4. Data analysis and relative expression calculations

The Pfaffl method was used to transform Ct values into relative quantities [231]. Relative quantities were calculated per primer pair (i.e. if primers A, B, C were used for samples 1, 2, 3, the relative quantities were calculated for A[1, 2, 3], B[1, 2, 3], C [1, 2, 3]). The Ct value of the most abundant sample for each primer pair was set to 1 and the following equation was used:

$$\text{Relative quantity} = \text{efficiency}^{(\text{ct value most abundant} - \text{ct value sample})}$$

Relative quantities of all samples for a given primer pair ranged from 0 to 1. The geNorm applet for Microsoft Excel was used on the reference genes to calculate normalization factors (the geometric mean) for each tissue [232]. The normalization factor was then applied to the genes of interest to calculate the relative expression levels. geNorm analysis was carried out on complete sets of tissue samples. From these analyses the mean relative quantity was calculated for each tissue and this was used for statistical analysis.

Table 2.2: RT-qPCR primer information

Short Name	*Accession number*	*Sequence (5' to 3')*	*Amplicon (bp)*	*Efficiency*
ACTB	NM_007393	fwd: GCAGCTCCTTCGTTGCCGGT rev: TACAGCCCGGGGAGCATCGT	132	2.1
HPRT1	NM_013556	fwd: CCGGCAGCGTTTCTGAGCCA rev: GCTCGCGGCAAAAAGCGGTC	123	2.0
HSPA8	NM_031165	fwd: CAGCGCAGCTGGGCCTACAC rev: TAGCTTGGCGTGGTGCGGTT	152	1.9
Kir6.2	NM_010602	fwd: CGGGCGCATGGTGACAGAGG rev: CGATGGGCCTGGGCCGTTTT	126	2.1
SUR1	NM_011510	fwd: ACAGCCTTCGCAGACCGCAC rev: GCCCGAGCCAGGCAGAACAG	106	1.9
GFP	U73901.1	fwd: CGGCGACGTAAACGGCCACA rev: CAGCTTGCCGGTGGTGCAGA	103	2.0

2.3. Subcutaneous sulphonylurea therapy

For implantation of subcutaneous glibenclamide or placebo pellets, animals were anaesthetized with 2% isoflurane and a small area of the back was shaved. A 1cm transversal incision was made between the scapulae and animals were implanted with a 21-day slow-release subcutaneous pellet containing either placebo or glibenclamide (Innovative Research of America). Details of the sizes of the glibenclamide pellets used are given in each chapter. The incision was closed by means of coated Vicryl sutures (Ethicon) and Vetbond (3M), and the animal was placed on a heating pad during recovering from anaesthesia. A recovery period of one week was allowed between the surgery and any subsequent experiments; mice were monitored daily during the recovery period. Surgery was carried out on the same day for all littermates. All experiments were performed blinded to genotype of the animal and treatment given.

2.3.1. Blood glucose monitoring

Blood glucose monitoring was carried out 3 days before, and up to 7 days after, implantation with subcutaneous pellets. The mouse's tail was anaesthetised using lidocaine EMLA topical cream (AstraZeneca), and blood was obtained via tail vein puncture. Measurements were carried out between

14.00 and 15.00 as previous experience showed us this was the time when the blood glucose levels were most stable (K. Shimomura, *unpublished*). A Freestyle Lite handheld glucose meter (Abbott) was used for determining the glucose concentration.

2.4. Sensitivity to inhaled general anaesthetics

nV59M mice and control littermates were tested for sensitivity to isoflurane or halothane. Ubi-ROSA, Ubi-ROSA-CAGS and Ubi-ROSA-DN mice and control littermates were also tested for sensitivity to isoflurane. Mice were individually placed in a closed acrylic chamber (dimensions: 30 cm x18cm x17.5cm; Vet-tech Solutions), which had been previously equilibrated with 2% isoflurane (Abbott Laboratories) or 2% halothane (Merial) mixed with 100% oxygen. This gas mixture was continuously perfused at a rate of 1L/min throughout the experiment.

The time taken for a mouse to lose its righting reflex (LORR) was measured as follows. The time the mouse stopped moving after entering the chamber was recorded. To determine if this corresponded to the LORR, the chamber was tilted to turn the mouse upside down. If it remained with at least three paws in the air for more than 30s, its righting reflex was considered to be lost and the LORR was taken as the time to stop moving. However, if the mouse moved when tilted, the time continued to be recorded until it no longer moved

when inverted.

The time taken to lose the hindpaw withdrawal reflex (LOWR) was also measured: thirty seconds after the LORR (i.e. the mouse had stopped moving), the interdigital pads of one of the hindpaws were firmly pinched for up to 5s between the thumb and index finger. This procedure was repeated every 30s, alternating paws, until the withdrawal reflex was lost. The time taken for this to occur was recorded. Any purposeful movement was considered a positive response.

The concentration of isoflurane required to maintain general anaesthesia was also estimated. Following LOWR, the mouse was taken out of the induction chamber and an anaesthetic mask (Vet-Tech Solutions size 1) was placed over its face. The volume of isoflurane delivered was reduced from 2% to 1.5% and the animal was kept at this concentration for 5min, after which time the LOWR was re-assessed. If LOWR had been maintained, a volume of 1.5% isoflurane was deemed adequate for maintenance of general anaesthesia. If the withdrawal reflex was present, the volume of isoflurane was increased to 2%, and LOWR was re-assessed after 5min at this volume.

2.5. Chronic intracranioventricular delivery of glibenclamide

2.5.1. Surgical procedure for ICV delivery in mice

Mice were anaesthetised with 2% isoflurane and were then administered buprenorphine (30µg/ml; Vetergesic, Reckitt Benckiser Healthcare) pre-operatively as an analgesic. Once anaesthesia had been confirmed, an area covering the top of the head and the scapular area of the mice was shaved and cleaned. Bupivacaine (0.25%; Marcain, AstraZeneca) was then administered subcutaneously at the incision area. A 2.5cm incision was made from just above the eyes to the scapulae. A small subcutaneous pocket was made in the back of the animal and a pre-filled osmotic mini-pump (Model 2004, 28-day infusion, 0.25µl/h flow rate; Alzet, Durect Corporation) was implanted.

The mini-pumps had been previously filled following the manufacturer's instructions with either 280µM glibenclamide (Sigma; initial stock of 28mM in 100% DMSO) in phosphate-buffered artificial cerebrospinal fluid (aCSF; in mM: 143 NaCl, 1.2 $CaCl_2$, 2.7 KCl, 1 $MgCl_2$, 0.26 NaH_2PO_4, 1.74 Na_2HPO_4, pH 7.4; 1mg/ml bovine serum albumin) or aCSF (with 0.1% DMSO). These pumps had been incubated in sterile saline for a minimum of 48 hours at 37°C prior to implantation.

After implanting the osmotic mini-pumps, mice were placed on a Stoelting stereotaxic frame to insert the drug delivery cannula into the lateral ventricle. The Brain Infusion Kit III cannula (Alzet, Durect Corporation) was implanted at coordinates 0.1mm caudal to bregma, 0.9mm lateral from bregma and 3mm below the surface of the skull. After locating the coordinates, a small hole was drilled into the skull using a micro-drill with a 0.6mm burr (Ideal, Stoelting). The cannula was then placed into the hole and attached to the skull using super-glue (Loctite) and dental cement (Kemdent).

Once the cement had dried, the cannula was connected to the osmotic mini-pump using the polyethelene tubing provided with the kit. The incision was then closed by means of coated Vicryl sutures (Ethicon) and Vetbond (3M), and the animal was placed in a heated chamber during recovery from anaesthesia.

Mice were given subcutaneous physiological saline and glucose (10% glucose in 0.9% saline) throughout the procedure to prevent dehydration and hypoglycaemia. They were also kept on a heating pad to prevent hypothermia. Mice were allowed to recover for one week before any experiments were carried out; they were monitored daily during the recovery period.

2.5.2. Surgical procedure for ICV delivery in rats

Male adult Lister hooded rats were anaesthetised with 2-3% isoflurane and were administered buprenorphine (30µg/ml; Vetergesic, Reckitt Benckiser Healthcare) pre-operatively as an analgesic. Once anaesthesia had been confirmed, an area covering the top of the head and the scapular area of the rats was shaved and cleaned. Lidocaine (10mg Xylocaine spray, AstraZeneca) was then administered locally at the incision area. A 4cm incision was made from just above the eyes to the back of the neck. A small subcutaneous pocket was made in the back of the animal and a pre-filled osmotic mini-pump (Model 2ML4, 28-day infusion, 2.5µl/h flow rate; Alzet, Durect Corporation) was implanted.

The mini-pumps had been previously filled following manufacturer's instructions with either 110µM glibenclamide (Sigma; initial stock of 11mM in 100% DMSO) in phosphate-buffered artificial cerebrospinal fluid (aCSF; in mM: 143 NaCl, 1.2 $CaCl_2$, 2.7 KCl, 1 $MgCl_2$, 0.26 NaH_2PO_4, 1.74 Na_2HPO_4, pH 7.4; 1mg/ml bovine serum albumin) or vehicle (aCSF with 0.1% DMSO). After filling, the mini-pumps were incubated in sterile saline for a minimum of 48 hours at 37°C prior to implantation.

After implanting the osmotic mini-pumps, rats were placed on a Stoelting stereotaxic frame to insert the drug delivery cannula into the right lateral

ventricle. The Brain Infusion Kit II cannula (Alzet, Durect Corporation) was implanted at coordinates 0.9mm caudal to bregma, 1.3mm lateral from bregma and 4.5mm below the surface of the skull. After locating the coordinates, a small hole was drilled into the skull using a micro-drill with a 0.6mm burr (Ideal model, Stoelting). The cannula was then placed into the hole and attached to the skull using super-glue (Loctite) and dental cement (Kemdent). Two small bone screws were also placed on the skull and covered with the cement to stabilise the cannula. Once the cement had dried, the cannula was connected to the osmotic mini-pump using the polyethelene tubing provided with the kit.

The incision was closed by means of coated Vicryl sutures (Ethicon) and Vetbond (3M), and the animal was placed in a heated chamber during recovery from anaesthesia. Rats were given subcutaneous physiological saline and glucose (10% glucose in 0.9% saline) throughout the procedure to prevent dehydration and hypoglycaemia, and they were kept on a heating pad during the surgery to prevent hypothermia. Rats were left to recover for 7-10 days, after which they were sacrificed for plasma and cerebrospinal fluid collection. The experimenter was blinded to the drug treatment.

2.5.3. Histology for confirmation of cannula placement

ICV implanted animals were sacrificed with an overdose of Euthatal (sodium pentobarbital; Merial) injected intraperitoneally. They were then quickly decapitated and their brains removed and fixed in 4% paraformaldehyde in 0.1M phosphate buffer (PB; in mM: 19 NaH_2PO_4, 81 Na_2HPO_4) at pH7.4 and kept at 4°C until further processing.

Fixed brains were cryoprotected in 30% sucrose in 0.1M PB overnight before being cut into 30µm thick sections on a freezing microtome. They were subsequently washed in 0.1M PB, mounted on gelatine-coated slides and dried overnight. Dried sections were de-fattened by placing in xylene, rehydrated using a gradient of ethanol solutions (100%, 96%, 70%, 50% and distilled water) and stained with cresyl violet. The sections were then placed in 70% acidified ethanol, dehydrated using a gradient of ethanol solutions (70%, 96%, 100%), placed in xylene and coverslipped in DePeX. Images were acquired with a Leica light microscope connected to a Nikon digital camera.

2.6. Statistical analysis and Figures

Figures were made with Prism 5 (Graphpad Software) and Microsoft Excel. Statistical analyses were performed with Prism 5 (Graphpad Software) and

SPSS (IBM). The details of the particular tests used are provided in each chapter. Details of statistically significant results (degrees of freedom, F-values, etc) are given in the Appendices. Data sets were tested to see if their distributions satisfied the assumptions required by specific statistical tests. These assumptions are described below.

2.6.1. General assumptions for parametric statistical tests

The skewness and kurtosis of each data set was assessed using the D'Agostino-Pearson omnibus and Shapiro-Wilk normality tests to ensure the data sets were normally distributed. If data were significantly skewed, they were deemed unsuitable for parametric analysis. The homogeneity of variances of each data set was assessed using Bartlett's test for equal variances.

2.6.2. Corrections for multiple comparisons

Where multiple comparisons were made within the same data set, a Bonferroni correction was used to prevent type I errors. Results were considered significant if the *P* value was less than 0.05 divided by the number of comparisons made.

Chapter 3: Cognitive function of iDEND mouse model

3.1. Summary

1. ROSA and Nestin-cre mice were crossed to produce nV59M mice, which selectively express Kir6.2-V59M in neurones. A series of short-term working memory and anxiety tests were carried out to determine if they were adequate for evaluating the effect of sulphonylurea drugs on neurological function. Nes-cre, ROSA and wild-type littermates were used as controls.

2. nV59M mice were not significantly impaired on the spontaneous alternation and spatial novelty preference tasks, which assess short-term working memory. These tests are thus not adequate for assessing sulphonylurea therapy.

3. The dark/light box, successive alleys and elevated plus maze tasks revealed that nV59M mice are less anxious than control littermates. This could be related to impulsivity and inattention, which has been observed in human iDEND/DEND patients.

3.2. Introduction

K_{ATP} channels are expressed in many areas of the brain, including the hypothalamus, cerebellum, basal ganglia and hippocampus [26,68,83]. Although we have some understanding of the function of neuronal K_{ATP} channels, particularly in the hypothalamus and substantia nigra, the specific physiological role of the K_{ATP} channel in all brain regions has not been fully elucidated.

Overall, experimental evidence supports two main roles of the neuronal K_{ATP} channel, as discussed in Chapter 1. In glucose-responsive neurones, like those of the hypothalamus, the neuronal K_{ATP} channel is a key player in the regulation of energy metabolism and glucose homeostasis [86-89]. In non-glucose-responsive neurones, such as those in the substantia nigra, the K_{ATP} channel appears to have a protective role in ischemia and seizure development, acting as a metabolic sensor to raise the threshold for seizures [82,91-94,97,98].

In addition to these functions, recent experimental and clinical evidence indicate that the neuronal K_{ATP} channel in the hippocampus may be involved in memory and learning.

3.2.1. The hippocampal K_{ATP} channel

The hippocampal K_{ATP} channel was first discovered by pharmacological and electrophysiological studies [77,233-235]. *In situ* hybridization studies later confirmed that these K_{ATP} channels are mainly composed of Kir6.2 associated with SUR1 [26]. Glibenclamide binding studies have shown abundant expression of SUR1 in the granular layer of the dentate gyrus and the CA3 region of the hippocampus [68]. Furthermore, immunohistochemistry experiments have demonstrated high expression of Kir6.2 in pyramidal neurones, interneurones and glial cells from CA1, CA3, and dentate gyrus [236].

Although K_{ATP} currents have been recorded from CA1 pyramidal neurones and interneurones, real-time quantitative PCR studies suggest the highest density of Kir6.2/SUR1 is found in interneurones [73]. This is supported by the fact that larger outward currents, which respond to diazoxide and tolbutamide, are observed in interneurones than in CA1 pyramidal neurones when hippocampal slices are exposed to energy depletion [237].

Even though we have extensive knowledge on the location of the hippocampal K_{ATP} channel, our knowledge of the physiological function of these channels has lagged behind. It has been shown that closing of hippocampal K_{ATP} channels by glibenclamide increases the release of glutamate from CA3 mossy fibres in rat hippocampal slices [235]. Furthermore, diazoxide, an opener of the K_{ATP} channel, reduces glutamate release in

mossy fibre synaptosomes [92]. Modulation of neurotransmitter release by the K_{ATP} channel has been also shown in other areas of the brain, including the striatum, where it modulates the release of dopamine, acetylcholine and glutamate [238-240], and the substantia nigra, where it is involved in GABA release [241,242].

This modulation of neurotransmitter release supports the role of the hippocampal K_{ATP} in neuroprotection, particularly as it has been shown that mice overexpressing SUR1 in the forebrain (including the hippocampus) display a reduced sensitivity to kainic-acid induced seizures [99]. Conversely, Kir6.2 knockout mice are more prone to neuronal damage after ischemic insult, both at the *in vivo* and *in vitro* level (studied on hippocampal slices) [236].

However, various *in vitro* experiments suggest the hippocampal K_{ATP} channel may also play a role in memory and learning. It has been shown that zinc activation of presynaptic K_{ATP} channels in mossy fibres can inhibit long-term potentiation in hippocampal slices by reducing presynaptic calcium entry and thus zinc and glutamate release [92,243,244].

In vivo pharmacological studies have provided further evidence for a putative role of the K_{ATP} channel in learning and memory. Direct infusion of diazoxide, a K_{ATP} channel opener, into the CA3 region of the hippocampus strongly impairs contextual memory acquisition and/or consolidation as assessed by a contextual fear-conditioning task [245]. This effect was impaired by co-infusing

tolbutamide, a selective K_{ATP} channel blocker. Furthermore, it has been shown that intraseptal injection of glibenclamide enhances spontaneous alternation performance (a measure of working memory) in the rat [246]. Similar effects were observed after direct intrahippocampal administration of glibenclamide [247]. It thus appears that opening of the K_{ATP} channel impairs learning in rodents, while its closure enhances memory formation.

3.2.2. Cognitive function of K_{ATP} channel knockout mice

Knockout mouse models are useful tools for understanding the functional roles of K_{ATP} channels under physiological conditions. Deacon *et al.* (2006) [248] showed that working memory was impaired in Kir6.2 knockout (Kir6.2$^{-/-}$) mice, as assessed by performance in the T-maze spontaneous alternation task. However, the Kir6.2$^{-/-}$ mice took longer to make an arm choice and also ran slower than control wild-type mice, which the authors suggest may partially explain the alternation deficit observed [248]. In addition, Kir6.2$^{-/-}$ mice appeared to have an increased anxiety phenotype, as tested on the dark-light box and successive alleys tasks, which may have affected their performance on the spontaneous alternation test [248].

Interestingly, when a separate cohort of Kir6.2$^{-/-}$ mice were tested in the 4-arm radial maze for spontaneous alternation, a significant reduction in the number of successful alternations was observed when compared to wild-type controls

[249]. However, this result may also be affected by the motor and anxiety phenotypes reported by Deacon and colleagues[248].

It has also been reported that Kir6.2$^{-/-}$ mice are impaired in a contextual fear-conditioning task, which relies on the formation of contextual memory [245]. Their performance on the Morris water maze, a test of hippocampus-dependent spatial learning and memory, was also slightly impaired. Kir6.2$^{-/-}$ took longer than controls to find a hidden platform and also performed slightly worse than control mice in the probe test 24 hours after testing, which indicated their long-term spatial memory was impaired. However, the authors indicated the slight impairment in the Morris water maze task might be due to a higher emotional reaction to the stressful pool environment. The increased anxiety phenotype of the Kir6.2$^{-/-}$ described by Deacon and colleagues supports this argument.

The pharmacological studies as well as the experiments with the Kir6.2$^{-/-}$ mice support a role for the hippocampal K_{ATP} channel in memory and learning. However, the Kir6.2$^{-/-}$ behaviour contradicts the results obtained on the pharmacological *in vivo* studies. Thus, the exact involvement of the hippocampal K_{ATP} channel in memory and learning under physiological condition is currently not fully understood.

3.2.3. Cognitive function of iDEND and DEND patients

Patients with activating K_{ATP} channel mutations associated with iDEND and DEND syndromes present with muscle hypotonia, balance and coordination problems, and developmental delay in addition to neonatal diabetes [4,5,136]. It has been previously demonstrated that the motor symptoms (muscle hypotonia and balance and coordination problems) associated with gain-of-function K_{ATP} channel mutations are neuronal in origin [62].

In addition to the motor symptoms, iDEND and DEND patients suffer from cognitive developmental delay, taking longer to learn to walk and talk when compared to other children of similar age [5]. Furthermore, low scores on the Bayley Scales of Infant Development as well as on the Wechsler Preschool and Primary Scale of Intelligence have been reported for some of these patients [188,189,226]. Many of them also display learning difficulties at school [188,189,226,250].

Although it is currently not known whether these learning difficulties are directly caused by neuronal expression of the mutant K_{ATP} channel or whether they are indirectly caused by the neonatal diabetes and/or insulin-induced hypoglycaemia, the latter is highly unlikely as neurological dysfunction is not a common feature in other types of neonatal or Type 1 diabetes mellitus [251].

Furthermore, the pattern of neurological defect differs from that caused by severe hypoglycaemia [252].

3.2.4. Sulphonylurea therapy for iDEND/DEND cognitive function

After the discovery that activating K_{ATP} channel mutations are responsible for up to 50% of all neonatal diabetes cases, it became apparent that sulphonylureas could be a suitable treatment for these patients. Indeed, over 90% of ND patients have been successfully transitioned from insulin to sulphonylureas to manage their diabetes [6,218]. This has resulted in a considerable improvement in glycaemic control as well as quality of life [218]. In iDEND/DEND patients, it was hoped that sulphonylureas might also improve motor and cognitive functions. However, mixed results have been obtained, particularly in terms of cognition.

For many DEND patients, transition to sulphonylureas has been unsuccessful in ameliorating either their diabetes or neurological problems [6,157,227,253,254]. In most of these cases, the inability to become insulin-independent correlates with the extent to which a maximal concentration of tolbutamide (a sulphonylurea drug) blocks the whole-cell current through heterologously expressed K_{ATP} channels carrying the same mutation [6,164]. Thus, when the block is less than 65%, patients fail to respond to sulphonylureas, whereas when the block is greater than 75%, most patients respond.

Nonetheless, various patients with neurological symptoms, particularly those with iDEND syndrome, have been able to successfully switch to sulphonylurea therapy [6,188,189,221,222,224-226,255]. In some of these patients, moderate improvements in neurological function have been noted. For example, Shimomura *et al.* [221] showed a considerable improvement in motor function and social behaviour in a DEND patient (I167L-Kir6.2 mutation) after transfer to sulphonylureas. Similar improvements have been observed with iDEND patients after transitioning to sulphonylureas [151,188,189,225]. In terms of cognitive function, a moderate improvement in verbal performance on neuropsychological tests (such as the Bayles Scales of Infant Development) has been noted [188,222] as well as a moderate increase in intelligence quotient (IQ) [189,226].

Although these examples indicate that sulphonylureas may be beneficial for the neurological deficits associated with iDEND and DEND syndromes, the cognitive abilities of these patients are still considerably impaired. Even when treated, the IQ scores of some of these patients are still below average [189,222,226] and many of them have a functional age equivalent to that of a 3-5 year-old, even though they are chronologically older [188,189,224]. Furthermore, there are various examples of patients successfully transferring to sulphonylureas (measured in terms of glycaemic control) who show little to no improvement in terms of cognitive function [224,250,255].

It is thus clear that more work is needed to determine the extent to which sulphonylureas are able to reverse the learning and memory deficits seen in iDEND and DEND patients.

3.2.5. Cognitive function of iDEND mouse model

Although ideally a thorough clinical study should be conducted to assess the extent to which sulphonylureas ameliorate DEND syndrome, this is not a trivial task. First of all, this disease is quite rare, with an estimated incidence of 1 in 100-200,000 live births [113]. Second, there are few patients with the same mutation and they all have different ages. Finally, all iDEND and DEND patients who respond to sulphonylureas are already on treatment (for the management of their diabetes), and the drug doses differ considerably between individuals.

I have thus decided to use mice with selective neuronal expression of the Kir6.2-V59M mutation (nV59M mice) for assessing the effect of sulphonylurea therapy on cognitive function. These mice have been previously shown to recapitulate many of the neurological symptoms seen in iDEND patients [62].

The aim of this chapter is to determine whether short-term memory behaviour tests, such as the spontaneous alternation and spatial novelty preference tasks, are adequate for studying the effect of glibenclamide therapy on the

cognitive function of nV59M mice. In addition to this, various anxiety tests were carried out to determine whether nV59M mice, like the Kir6.2$^{-/-}$ mice, had an anxiety phenotype as this could significantly affect performance on short-term memory tests.

3.3. Methods

3.3.1. Generation of mice

Mice with selective neuronal expression of the Kir6.2-V59M mutation under the control of the ROSA promoter were used for the experiments outlined below. Details of the transgenic mice (breeding strategy, etc) are given in Chapter 2.

3.3.2. Behavioural tests

Cognitive function was assessed in adult (11-20 week old) nV59M and control mice. Spatial working memory was studied using the T-maze spontaneous alternation (discrete trial) and the Y-maze spatial novelty preference tests. Anxiety was also assessed using the dark/light box, successive alleys and plus-maze tasks. These tests are based on the well-documented tendencies of mice to avoid brightly lit or exposed places. All experiments were performed

blinded with respect to genotype of the mice and control littermates (ROSA$^{+/-}$, Nes-cre^{+}, wild-type) were used in all tests. All tests were performed during the animals' light phase.

3.3.2.1. Spontaneous alternation

The apparatus consisted of a wooden T-shaped maze made up of black arms (30cm x 10cm x 29cm) with a removable central partition extending 7cm from the back wall into the start arm (Fig. 3.1A). This divided the choice area into two and allowed access to only one goal arm at a time. The entrances to the choice arms had sliding guillotine doors, and the floor of the maze was covered with a thin layer of bedding to facilitate running.

The test consisted of two parts. For the first part, the guillotine doors were raised and the central partition was in place. The test started by placing a mouse at the end of the start arm facing away from the choice arms. Once the mouse had made a choice and entered one of the goal arms (the tail has to have cleared the entrance), the guillotine door was closed and the mouse was confined in the arm for 30s. In the second part of the test, the central partition was removed and the mouse was returned to the end of the start arm with both guillotine doors open. It was then allowed to make a choice. A correct alternation (the entire mouse entered the opposite arm to that initially

sampled) was given a score of 1. An incorrect alternation (mouse entered the same arm as initially sampled) was given a score of 0.

Mice were tested in batches of 20, all mice being tested before one mouse began a new trial. Each animal received two daily trials over a period of five days. A percent alternation score was calculated for all mice: (number of correct alternations)/(total number of trials).

3.3.2.2. Spatial novelty preference

The apparatus consisted of an enclosed Perspex Y-maze with arms of 30cm x 8cm x 20cm placed in a room with a variety of extra-maze cues. A thin layer of wood chips covered the floor. This layer was re-distributed between phases for individual animals and also between mice to eliminate intra-maze cues.

Mice were assigned two arms (the 'start' and the 'other' arm) to which they were exposed during the initial phase, the exposure phase, for five minutes (Fig. 3.1B). The selection of arms was counterbalanced with respect to genotype, and access to the third arm (the 'novel' arm) was blocked by means of a guillotine door.

The mouse was initially placed at the end of the start arm facing away from the entrance to the arm. After five minutes, the mouse was returned to its

home cage for a 1-minute interval between the exposure and test phases. During the test phase, the mouse was initially placed at the end of the start arm facing away from the entrance, and allowed to explore all three arms for two minutes. The time spent in each arm and the number of entries into each arm were recorded. An entry was defined by a mouse placing all four paws inside of an arm. A novelty preference ratio was calculated as: (time in novel arm)/(time in novel arm + time in other arm).

3.3.2.3. Dark-Light box

The dark-light box is an anxiogenic task, which tests the tendency of a mouse to explore new environments versus the aversiveness of a brightly lit area [256]. The equipment consisted of an open white compartment (30cm x 20cm x 20cm) joined to a black compartment with a lid (15cm x 20cm x 20cm) by a 3cm x 3cm door (Fig. 3.2A). One side of the light compartment was a transparent acrylic panel to facilitate observation of the mouse. The aversive nature of the white compartment was increased by providing additional illumination with a 60W lamp placed 45cm above the centre of the compartment. The test lasted 5 minutes and was started by placing the mouse in the middle of the light side, facing away from the door. The latency to cross with all four paws to the dark side, the amount of time spent in the dark side, and the number of transitions between the two compartments were

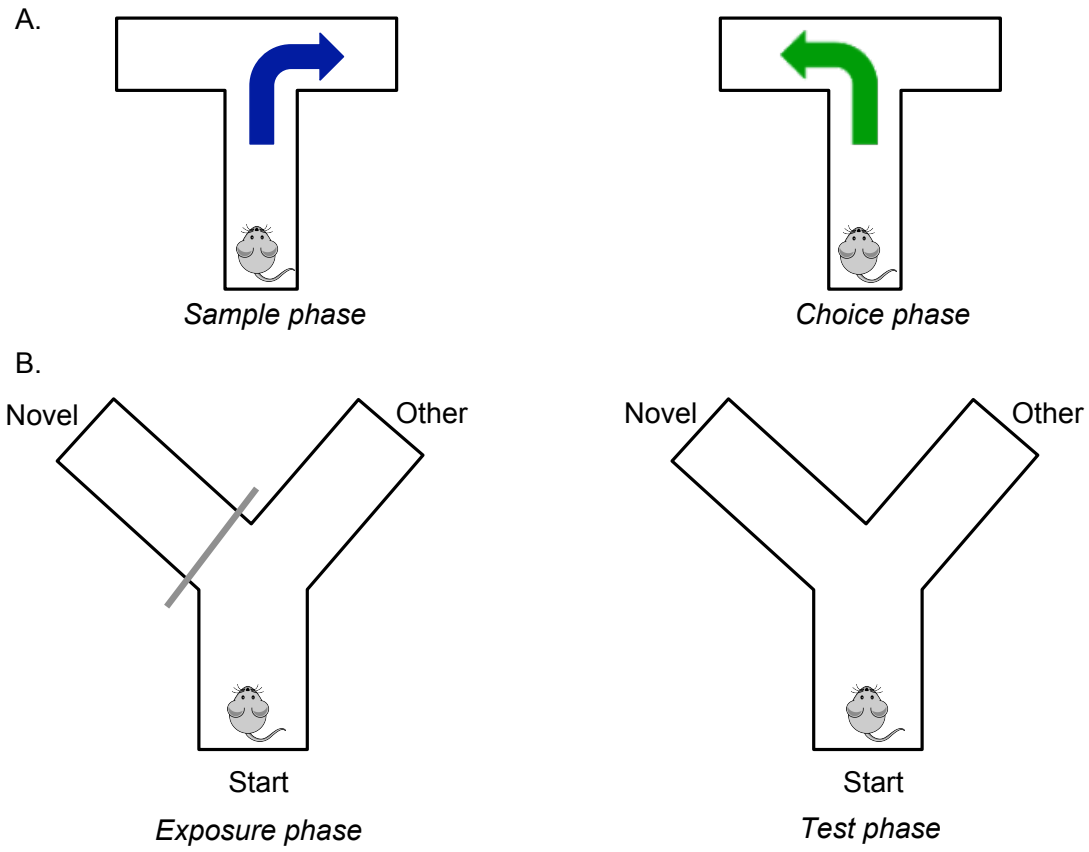

Figure 3.1: Spatial working memory tests

(**A**) The spontaneous alternation task consists of an initial sample phase where mice are allowed a free choice of two arms of the T-maze to explore. During the choice phase mice are required to select the previously unexplored arm to score a correct alternation. (**B**) In the spatial novelty preference task, mice are initially allowed to explore the 'start' and 'other' arms of the Y-maze for 5min (exposure phase). In the test phase, they are allowed to explore all three arms of the maze for 2min. A novelty preference ratio: (time in novel arm)/(time in novel arm + time in other arm) is then calculated. This gives an indication of the mouse's ability to remember having explored the known arms.

measured. The apparatus was cleaned between trials with a damp and then a dry tissue.

3.3.2.4. Successive alleys

The apparatus consists of four linearly connected wooden alleys of increasing anxiogenic character [257]. All sections are the same length (25cm), but have different widths and colour (Fig. 3.2B). Alley 1 is 8.5cm wide, painted black and has 25cm high walls. This is separated by a 0.5cm step from Alley 2, which is 8.5cm wide, painted grey and has 1.3cm high walls. Alley 3 is 1cm step down, 3.5cm wide, painted white and has 0.2cm high walls. The last section (Alley 4) is 1.2cm wide, painted white and has 0.2cm high walls. The apparatus was elevated 50cm above the floor and padding was provided underneath to cushion any falls. At the beginning of the test, each mouse was placed at the back of Alley 1 (facing away from the open end) and observed for 5 minutes. The latency to enter each alley (with all four paws), the number of entries into each alley, and the time spent on each section were recorded. The equipment was cleaned between trials with a damp and then a dry tissue.

3.3.2.5. Elevated plus maze

The plus maze consists of four arms (35cm x 6cm) arranged in a cross formation: two non-anxiogenic closed arms with 20cm-high walls and two anxiogenic open arms without walls (Fig. 3.2C) [258]. The apparatus was elevated 70cm above the ground and was placed in a brightly lit room with a digital video camera mounted overhead on the ceiling. Individual mice were placed at the junction of the open and closed arms (6cm x 6cm centre square), facing the open arm opposite the entrance to the testing room, and their movements were recorded for 5 minutes. An automated tracking system (Any-maze, Stoelting) was used to record the time spent in each region, the number of entries to each region, the latency to enter an open arm, and the total distance covered.

3.3.3. Molecular biology

Details of the protocols used for semi-quantitative and real-time quantitative PCR (primer sequences, reaction settings, etc) are given in Chapter 2.

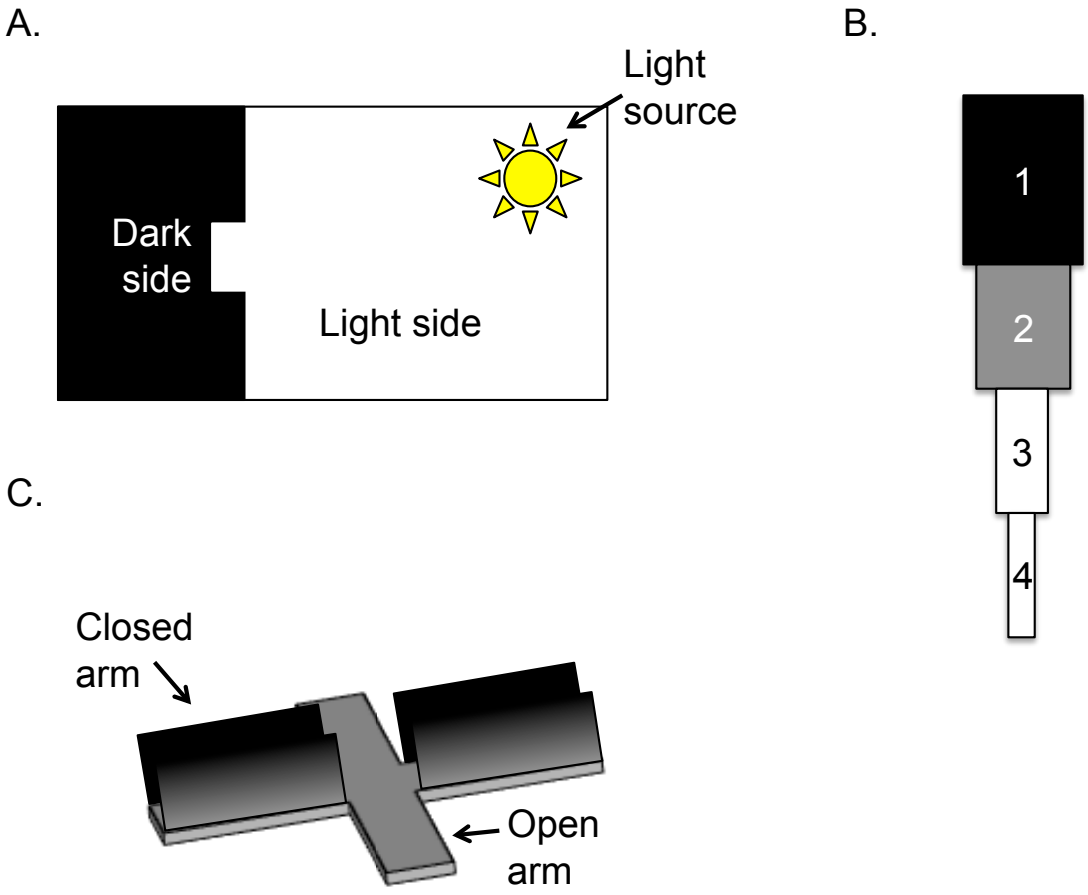

Figure 3.2: Anxiety tests

Diagrams of equipment for (**A**) dark-light box test, (**B**) successive alleys test, and (**C**) plus maze test.

3.3.4. Data analysis

Statistical analysis of data from male and female mice indicated no significant differences, so these data were pooled. Due to the low n-numbers for wild-type mice (n=1), the data for this mouse was pooled with the $ROSA^{+/-}$ data. Furthermore, analysis of data from $ROSA^{+/-}$ and Nes-cre^{+} indicated no significant differences, so these data were pooled. When the data distribution permitted (i.e. fulfilled the criteria of normality and equality of variance), a Student's t-test or a One-Way ANOVA was performed. Otherwise, data were analysed using a non-parametric test, the Mann-Whitney U-test or the Kruskal-Wallis One-Way ANOVA on Ranks. $P<0.05$ was considered statistically significant.

3.4. Results

3.4.1. nV59M mice show reduced anxiety in the dark-light box

The dark-light box task examines the conflict between the tendency of mice to explore novel environments versus the aversive properties of a brightly lit area. In this test, nV59M mice took significantly longer to cross into the dark compartment than control littermates (Table 3.1; Fig. 3.3A). However, once they crossed into the dark compartment, they transitioned significantly less

between the two compartments than control mice (Table 3.1; Fig. 3.3C), and they spent most of their time in the dark compartment (Table 3.1; Fig. 3.3B). Furthermore, there appears to be a trend towards a reduction in the number of rears performed by nV59M mice in the light side (Table 3.1), although statistical significance was not reached (Table 3.1; Fig. 3.3D). The number of rears performed was taken as an indication of increased exploratory behaviour.

Table 3.1: Behaviour of nV59M and control mice in the dark-light box

Measure	*Control*	*nV59M*	*P*
Latency to dark side (s)	8.5 [6-13]	19 [11.5-30]	0.0015
Time in dark side (s)	256 [235-274.5]	262 [246.5-276]	0.5537
Transitions	12 [3-17]	6 [1-8.5]	0.0046
Rears in light side	7 [1-11.75]	3 [2-7]	0.2793

Values are medians and interquartile ranges [IQR] for non-parametric data

3.4.2. nV59M mice are less anxious in the successive alleys task

The successive alleys task was performed to explore further the differences in anxiety observed in the dark-light box. This test consists of four connected wooden alleys of increasing anxiogenic character.

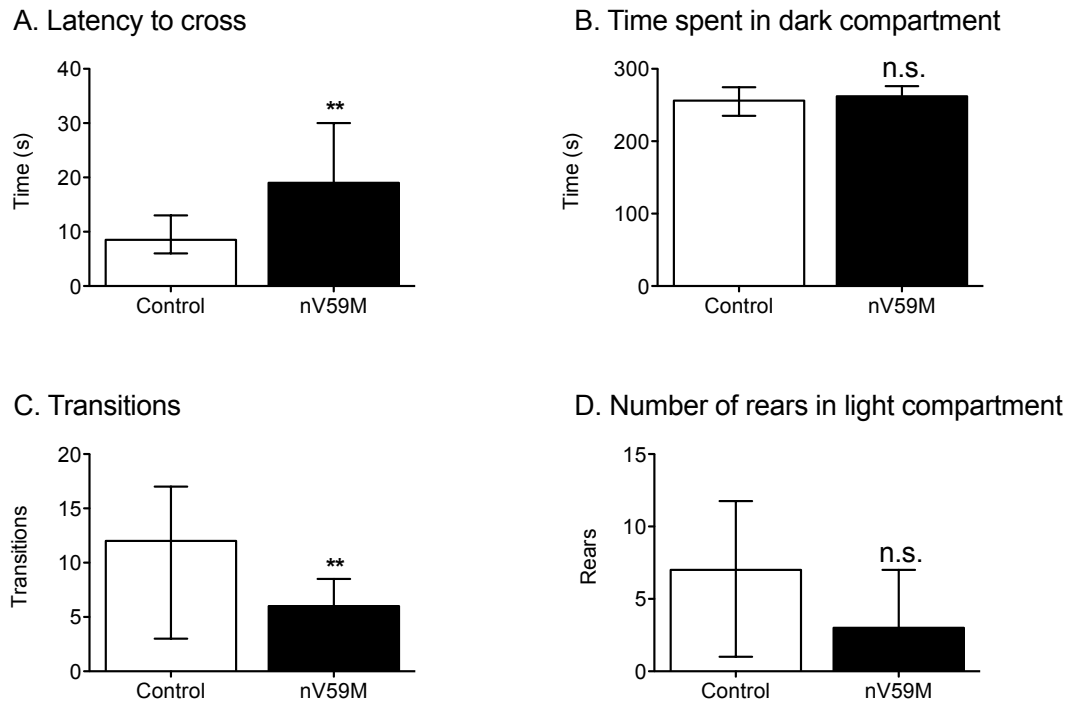

Figure 3.3: Dark-light box test

(**A**) Latency to cross to the dark side of the dark-light box, (**B**) amount of time spent in the dark compartment of the dark-light box, (**C**) number of transitions between the light and dark compartments, and (**D**) number of rears in light compartment for adult (11-20 week-old) control (wild-type: n=1; ROSA$^{+/-}$: n=12; Nes-Cre^{+}: n=13) and nV59M (n=14) littermates over a 300s period. Data are median and interquartile range. ** P<0.01; n.s. not significant [Mann-Whitney U-test].

nV59M mice spent significantly less time than control littermates in Alley 1 (Table 3.2; Fig. 3.4A). They also took less time transitioning into Alley 2, although statistical significance was not reached (Table 3.2; Fig. 3.4C). Furthermore, nV59M mice spent significantly more time than control littermates in Alleys 2-3, which is also reflected by the increased number of transitions between Alleys 1 and 2 (Table 3.2; Fig. 3.4D). Although most nV59M and control mice did not venture into Alleys 3 and 4, two nV59M entered Alley 3 while only one control mouse entered this alley (Table 3.2).

Table 3.2: Behaviour of nV59M and control mice in the successive alleys task

Measure	*Control*	*nV59M*	*P*
Time in alley 1 (s)	292 [275-300]	250 [201.3-300]	0.0032
Time spent in alleys 2 and 3 (s)	8 [0-25]	50 [24.5-98.75]	0.0032
Latency to enter alley 2 (s)	187 [46-300]	37 [31-235.8]	0.0806
Entries alley 2	1 [0-2]	4 [1.75-5.5]	0.0050
Entries alley 3	1	2	-
Entries alley 4	0	0	-

Values are medians and interquartile ranges [IQR] for non-parametric data

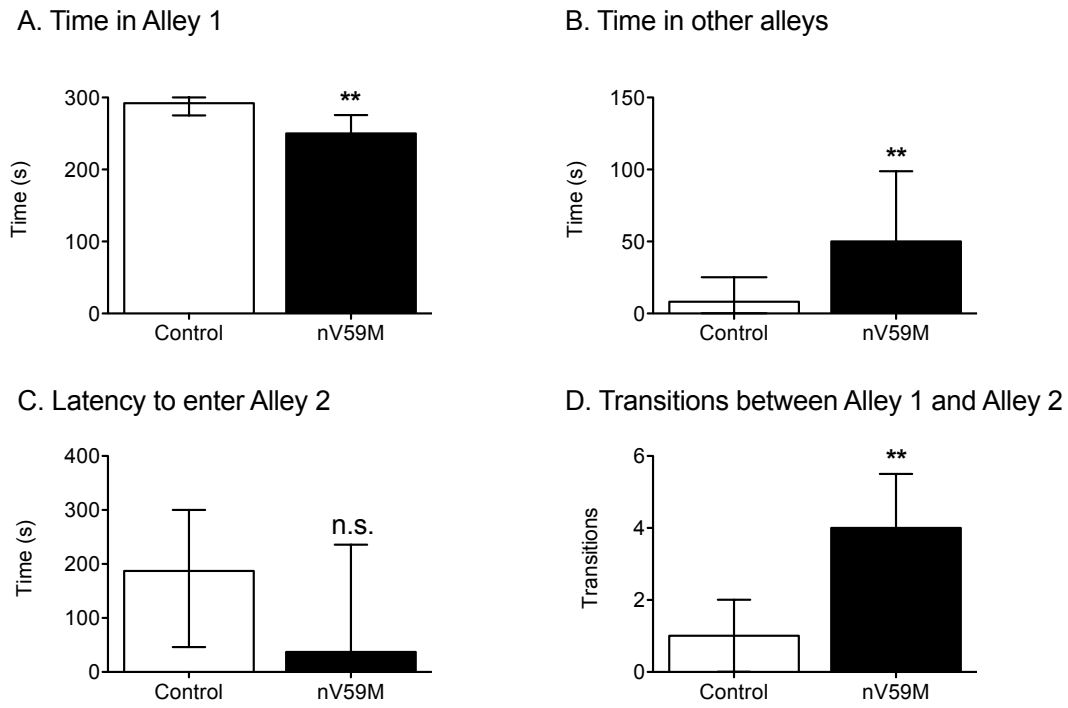

Figure 3.4: Successive alleys test

(**A**) Amount of time spent in the first alley, (**B**) amount of time spent in the second, third and fourth alleys, (**C**) latency to enter the second alley, and (**D**) number of transitions between the first and second alleys for adult (11-20 week-old) control (wild-type: n=1; ROSA$^{+/-}$: n=12; Nes-Cre^{+}: n=13) and nV59M (n=14) littermates over a 300s period. Data are median and interquartile range ** P<0.01; n.s. not statistically significant [Mann-Whitney U-test].

3.4.3. nV59M mice show less anxiety in the plus maze task

The plus maze is an anxiety task that measures the tendency of mice to remain in closed, protected spaces (such as the closed arms of the maze). nV59M mice spent significantly longer than control mice exploring the open arms of the maze (Table 3.3; Fig. 3.5B), which is also reflected by an increased number of entries into the open arms (Table 3.3; Fig. 3.5E). There was also a tendency for nV59M mice to take less time exiting the closed arms, however statistical significance was not reached (Table 3.3; Fig. 3.5C). No difference in the number of entries into the closed arms was observed, indicating the overall activity levels were similar for control and nV59M mice (Fig. 3.5F). Similarly, no difference in the number of entries into the centre square or the time spent in the centre square was observed (Appendix 1).

Table 3.3: Behaviour of nV59M and control littermates (both sexes) on the plus-maze task

Measure	*Control*	*nV59M*	*P*
Time spent in closed arms (s)	228.1 [211.5-272.1]	185.7 [162.6-264.2]	0.0251
Time spent in open arms (s)	10.9 [1.7-30.4]	44.5 [2.7-65]	0.0080
Latency first entry open arms (s)	80.9 [21.5-131.7]	51.2 [30.2-104.4]	0.5286
Entries open arms	2 [1-4.5]	5.5 [1.75-9.5]	0.0222

Values are medians and interquartile ranges [IQR] for non-parametric data

3.4.4. Spontaneous alternation is normal in nV59M mice

The T-maze spontaneous alternation is a commonly used test for assessing spatial working memory and cognition. It relies on the innate tendency of mice to explore their environment in a systematic fashion; they remember and avoid places they have recently visited. In this test, this results in mice normally entering the opposite arm than the one initially chosen when they get placed into the maze for a second time.

There appears to be greater variability in performance between trials for nV59M mice than for control littermates (Fig. 3.6A). Furthermore, there is a tendency for nV59M mice to perform worse than control mice (Fig. 3.6B). However, this difference is minimal (79.3±3.2% for nV59M versus 86±2.6% for control; mean ± SEM) and not statistically significant.

3.4.5. nV59M mice are not impaired in the spatial novelty preference task

The spatial novelty preference task is similar to the spontaneous alternation test; it assesses rapidly acquired, short-term spatial memory. It relies on the fact that mice prefer to explore novel rather than familiar spatial environments.

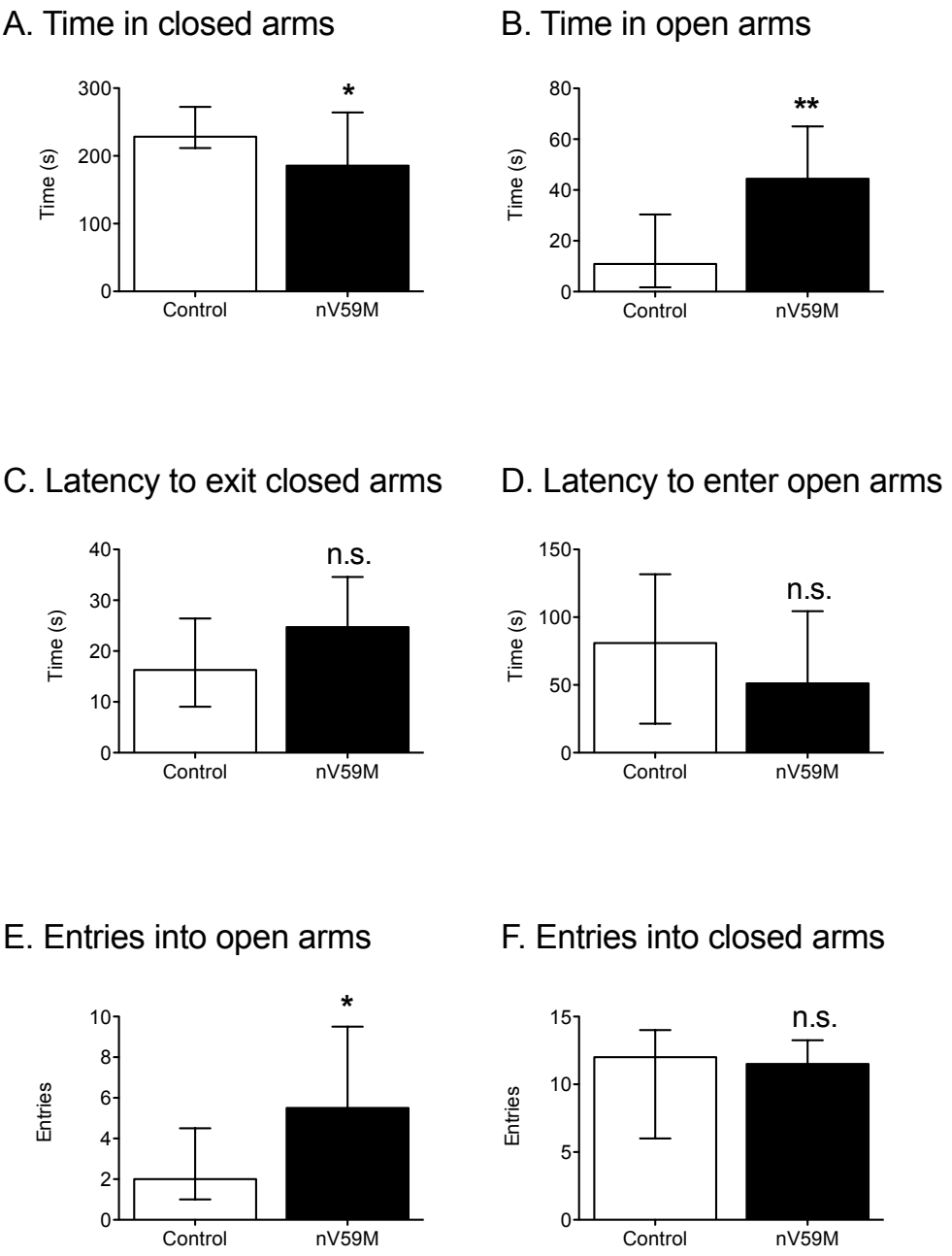

Figure 3.5: Plus maze test

(**A**) Amount of time spent in the closed arms, (**B**) amount of time spent in the open arms (**C**) latency to exit the closed arms, (**D**) latency to enter the open arms, (**E**) number of entries into the open arms, and (**F**) number of entries into the closed arms for adult (11-20 week-old) control (wild-type: n=1; $ROSA^{+/-}$: n=12; $Nes\text{-}Cre^{+}$: n=13) and nV59M (n=14) littermates over a 300s period. Data are median and interquartile range. * $P<0.05$; ** $P<0.01$; n.s. not statistically significant [Mann-Whitney U-test].

Thus, mice are expected to have an innate preference for the unvisited 'novel' arm during the test phase, but this relies on the ability to remember which arms have previously been visited.

There was no difference in the novelty preference ratio of nV59M and control mice (0.76±0.02 versus 0.74±0.02, respectively; Fig. 3.7A). Both groups of mice spent approximately 70% of time outside of the 'start' arm exploring the 'novel' arm. There was also no difference in the amount of time the two groups of mice spent exploring the three different arms, with both groups spending the majority of their time exploring the 'novel' arm (Fig. 3.7C). It appears nV59M mice spent slightly longer than control littermates in the 'start' arm, but statistical significance was not reached (Fig. 3.7C). Finally, there was no difference between the two groups in the number of entries into the 'novel' arm (Fig. 3.7B).

No differences were observed in the performance of control and nV59M during the exposure phase and the test phase (Appendix 2).

3.4.6. Expression pattern of Kir6.2 in nV59M mice

The expression pattern of wild-type and V59M Kir6.2 mRNA was determined in control and nV59M mice using semi-quantitative PCR. RNA was extracted from brain tissue of control and nV59M mice and reverse transcribed into

cDNA. Kir6.2 transcripts were amplified by PCR, digested with BtsCI and viewed on an agarose gel.

Introduction of the V59M mutation removes a unique BtsCI restriction site, which prevents cleavage of Kir6.2 cDNA. Hence, the presence of two bands indicates the presence of WT-Kir6.2 mRNA only while three bands indicates the presence of both WT and V59M Kir6.2 mRNA. As Figure 3.8B shows, V59M mRNA was expressed in brain tissue from nV59M and not control mice.

Real-time quantitative PCR was carried out to determine the amount of Kir6.2, GFP and SUR1 mRNA expression extracted from control and nV59M brains and reverse transcribed into cDNA. The amount of Kir6.2, GFP and SUR1 transcript was determined relative to a panel of house-keeping genes: HPRT1, HSPA8 and ACTB. As with semi-quantitative PCR, an aliquot of RNA was processed in tandem, but no reverse transcriptase was included in the reaction.

As Figure 3.9A shows, Kir6.2 expression was two-fold higher in brains of nV59M mice compared to control mice. This increase in Kir6.2 expression correlates with the amount of GFP expression (Fig. 3.9B) and hence to Kir6.2-V59M expression. The Kir6.2-V59M transcript contains a downstream IRES followed by a GFP sequence so the level of GFP expression is expected to be approximately equal to the amount of Kir6.2-V59M expression. As expected, SUR1 mRNA expression was unchanged in brains of nV59M mice (Fig. 3.9C).

A. Percentage of correct alternations

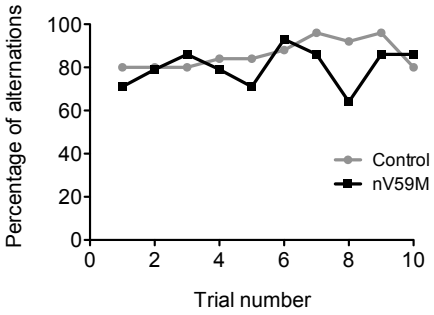

B. Overall percentage of correct alternations

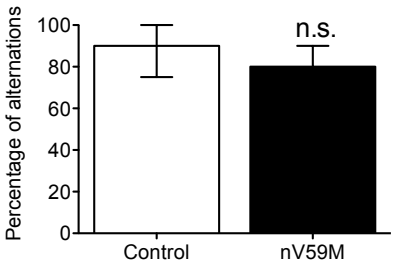

Figure 3.6: Spontaneous alternation test

(**A**) Percentage of correct alternations on each trial, and (**B**) overall percentage of correct alterations for adult (11-20 week-old) control (wild-type: n=1; ROSA$^{+/-}$: n=12; Nes-Cre^{+}: n=13) and nV59M (n=14) littermates in the spontaneous alternation task. Data are median and interquartile range. n.s. not statistically significant [Mann-Whitney U-test].

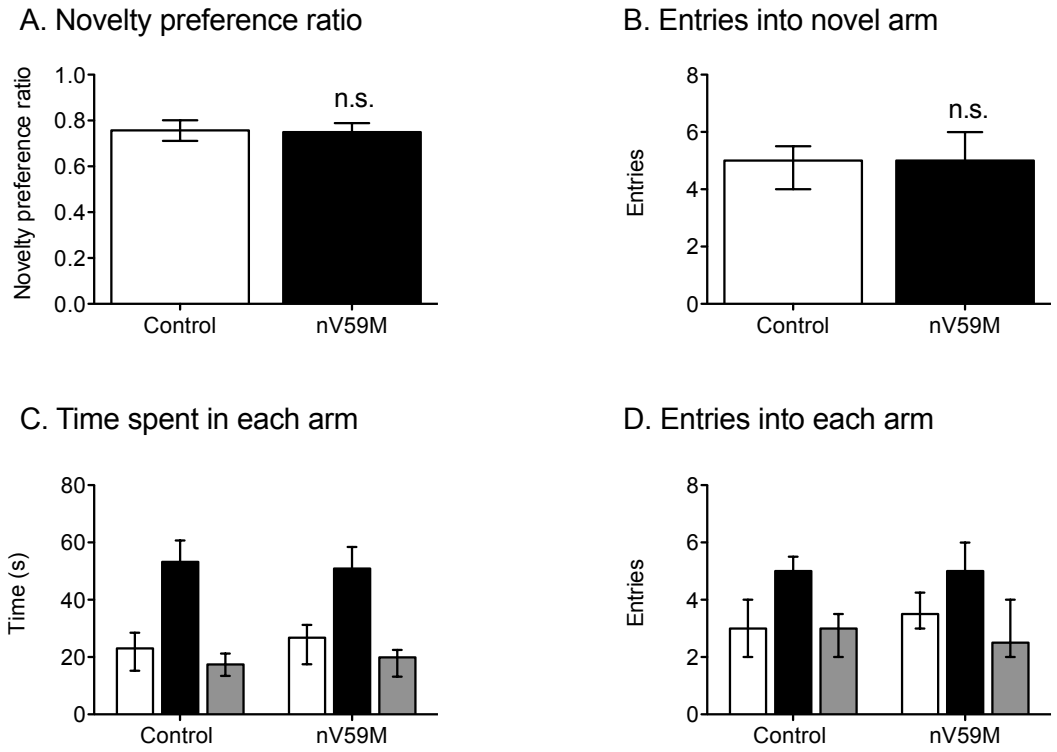

Figure 3.7: Spatial novelty preference test

(**A**) Novelty preference ratio, (**B**) number of entries, (**C**) amount of time spent, and (**D**) number of entries into the start (white bars), novel (black bars), and other (grey bars) arms in the spatial novelty preference test for adult (11-20 week-old) control (wild-type: n=1; $ROSA^{+/-}$: n=12; $Nes\text{-}Cre^{+}$: n=13) and nV59M (n=14) littermates. Data are median and interquartile range. n.s. not statistically significant [Mann-Whitney U-test (**A,B**); Kruskal-Wallis One Way ANOVA on Ranks (**C, D**)].

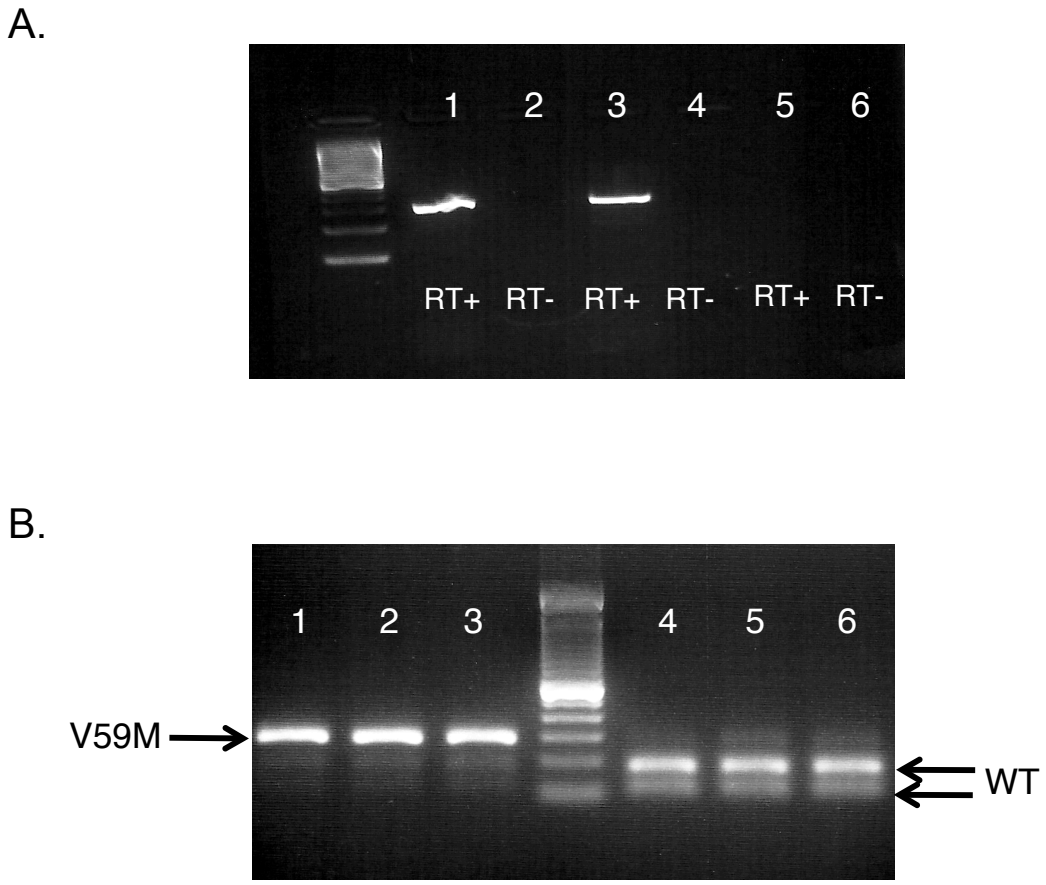

Figure 3.8: Kir6.2 expression in adult nV59M mice

(**A**) Identical RNA aliquots for brain tissue from control (lanes 1-2) or nV59M (lanes 3-4) mice were processed in a reverse transcription reaction with reverse transcriptase included (RT+) or omitted (RT-). Amplification of the Kir6.2 transcript was only seen in RT+ samples, indicating there was little genomic DNA contaminating the RNA samples. Lanes 5-6 are nuclease-free water controls. (**B**) Kir6.2 RNA expression in brain tissue isolated from nV59M (lanes 1-3) or control (lanes 4-6) mice. Wild-type (WT), but not mutant (V59M), Kir6.2 cDNA is digested by restriction enzyme BtsCI, hence two bands indicates the presence of WT Kir6.2 only while three bands indicates both WT and V59M mutant Kir6.2 are present. Data are representative of experiments on 5 control and 5 nV59M mice.

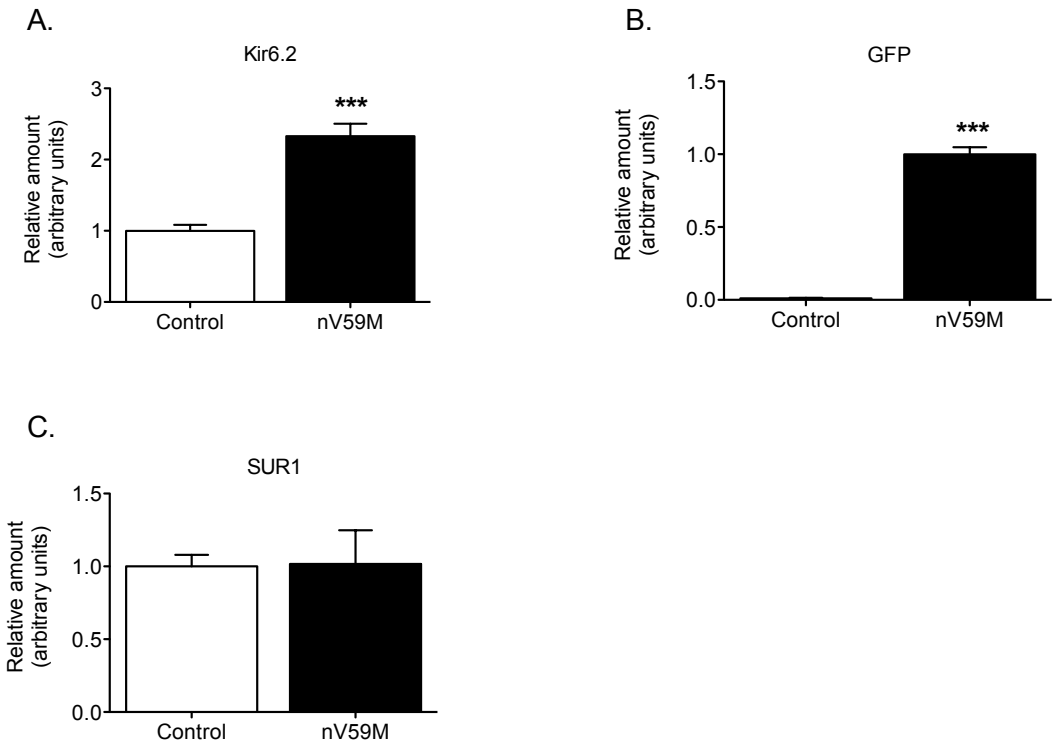

Figure 3.9: Relative expression of Kir6.2, GFP and SUR in brain

Quantitative PCR showing expression of (**A**) Kir6.2, (**B**) GFP, and (**C**) SUR1 in brain of control (n=8) and nV59M mice (n=7), relative to a panel of house-keeping genes. Data are mean ± SEM. *** $P<0.0001$ [Unpaired Student's t-test].

3.5. Discussion

iDEND and DEND syndromes are characterized by neonatal diabetes accompanied by muscle hypotonia, motor coordination deficits and developmental delay [5]. In many neonatal diabetes patients with activating mutations in the K_{ATP} channel, transfer from insulin to sulphonylurea therapy has resulted in improved glycaemic control [6,218]. As the neurological symptoms associated with iDEND/DEND syndrome are caused by the expression of the activating K_{ATP} channel mutation in neuronal tissue [62], it was hoped that sulphonylureas might also restore neurological function.

In some of the iDEND/DEND patients who have successfully switched to sulphonylurea therapy, moderate improvements in neurological function have been noted, particularly in terms of motor function [188,189,221,222,225,226]. Furthermore, improved cognition has been reported in a few patients. Nevertheless, their cognitive abilities are still considerably impaired [188,189,222,226]. It is thus not clear the extent to which sulphonylureas reverse the learning and memory deficits associated with these syndromes.

Due to the inherent difficulties in thoroughly examining this in human patients (rarity of the disease, differences in ages, differences in drug doses), I decided to use a mouse model with selective neuronal expression of the Kir6.2-V59M mutation for assessing the effect of sulphonylurea therapy on

neurological function. However, it was first necessary to determine whether short-term memory behaviour tests, such as the spontaneous alternation and spatial novelty preference tasks, are adequate for studying the effect of glibenclamide therapy on the cognitive function of nV59M mice.

3.5.1. Short-term working memory is not impaired in nV59M mice

The spontaneous alternation task is commonly used for assessing short-term working memory in transgenic mice [248,257]. In this task, wild-type mice consistently alternate at a rate of approximately 90% [248,257]. When assessed on the spontaneous alternation task, nV59M mice alternated at a lower rate (~79%) than previously reported wild-type mice (~91%) [248]. They also alternated at a slightly lower rate than control littermates (~86%), however, these differences were not statistically significant.

To further explore the slight differences seen in the spontaneous alternation task, nV59M mice and control littermates were assessed on the spatial novelty preference task. This test assesses rapidly acquired, short-term spatial memory. There was no difference in the nV59M mice's novelty preference ratio when compared to control littermates. Both groups spent the majority of the time exploring the novel arm. There was also no difference between the two groups in the number of entries into the novel arm of the maze.

The results obtained for the spontaneous alternation and spatial novelty preference tasks indicate that these tests are not adequate for assessing the effect of glibenclamide on the cognitive function of nV59M mice. Although nV59M mice performed slightly worse than control mice in the spontaneous alternation task, the difference observed was not statistically significant. Furthermore, it is possible that the slight difference observed was caused by nV59M mice taking longer to make an arm choice or being more inattentive than control mice. The former may be the case as no differences were observed in the spatial preference task, both in terms of time spent in each arm as well as number of entries into the different arms.

Interestingly, our group has previously observed a significant deficit in the performance of nV59M mice in both the spontaneous alternation and spatial novelty preference tasks (R.H. Clark, *unpublished*). In the spontaneous alternation task, nV59M mice previously alternated at a rate of approximately 70% while control littermates alternated at a rate of approximately 95%. In the spatial novelty preference task, nV59M mice spent the same amount of time exploring the 'novel' and the 'other' arm while control littermates spent most of their time exploring the novel arm. Furthermore, nV59M mice showed enhanced exploratory behaviour during the task, entering each arm more times than control littermates. This was not the case when I conducted the same test with a second cohort of nV59M mice (Fig. 3.7D).

The exact reason why we observed differences in the short-term working memory deficits between the two nV59M cohorts is not clear. It is possible that expression of the mutant Kir6.2-V59M may have decreased in the nV59M mice; however, I observed comparable Kir6.2 and GFP mRNA levels in the brains of nV59M mice to those previously reported [62]. Thus, the expression pattern of the mutation does not seem to have changed between the two nV59M cohorts.

Another possible explanation could be changes in the genetic background of the ROSA-Kir6.2-V59M line used to generate the nV59M colony. This line was initially developed using V6.5 embryonic stem cells, which are 50% C57Bl/6 and 50% 129/sv, injected into CB20 blastocysts [181]. The mice have been continually backcrossed to a C57Bl/6 genetic background. Thus, the initial cohort used by Clark may have had a more mixed 129/sv-C57Bl/6 background than the cohort I used for these experiments (by the time I conducted these experiments, the line had already been backcrossed 6 generations). It is known that these two inbred strains perform differently in behavioural tests, including the spontaneous alternation on the T-maze task [257]. In this task, 129/sv mice have been reported to alternate at a rate of ~70% while C57Bl/6 mice alternate at a rate of ~86% [257].

3.5.2. Decreased anxiety in nV59M mice

In addition to the short-term working memory tasks, I also conducted a battery of tests to determine whether the nV59M mice had an anxiety phenotype, as this could significantly affect performance on short-term memory tests. The dark-light box, successive alleys, and plus maze tasks are based on the well-documented tendencies of mice to avoid brightly exposed places and their fear of heights [257].

On all three tasks, nV59M mice were found to be less anxious than control littermates. nV59M mice took significantly longer to cross into the dark compartment in the dark-light box task. However, they spent spent a greater amount of time than control mice in the dark compartment and transitioned less between the two compartments, which does not fit with a phenotype of reduced anxiety.

It is possible that the increased latency to exit the light compartment was caused by increased freezing behaviour, an indication of increased anxiety: however, the results obtained with the successive alleys and plus maze tasks argue against this. In the successive alleys test, nV59M mice spent significantly longer exploring the more anxiogenic alleys (2-3) and transitioned more between the alleys. In the plus maze task, nV59M mice spent significantly longer than control mice exploring the more anxiogenic arms of

the maze. Overall, these results argue for a decreased anxiety phenotype being associated with neuronal expression of a gain-of-function K_{ATP} channel mutation.

It has been previously reported that nV59M mice display hyperactivity [62], which can be a confounding factor when assessing anxiety phenotypes. However, I did not observe any differences in the number of entries to the closed arms and centre square in the plus maze, which give an indication of the overall activity levels. Nonetheless, further assessment of the hyperactivity phenotype (presented in Chapter 4) showed that nV59M mice displayed significantly higher levels of activity than control littermates when placed in spontaneous activity threshold monitors, although no differences were observed in the non-anxiogenic open field or free-running wheels. It thus appears unlikely that locomotor differences between nV59M mice and control littermates may have affected their performance in the anxiety tests.

These findings, in combination with previous studies on Kir6.2$^{-/-}$ mice, argue for a role of the neuronal K_{ATP} channel in the regulation of emotion. Knockout of the Kir6.2 subunit results in increased anxiety as evaluated by the dark-light box, successive alleys and elevated plus maze tests [248]. Hence, loss of K_{ATP} channel activity leads to increased anxiety levels while increase K_{ATP} channel activity results in decreased anxiety levels.

This reduced anxiety phenotype in combination with the previously reported hyperactivity of nV59M mice [62] appears to correlate with the increased impulsivity and inattentiveness reported in iDEND/DEND patients [188,189,226,250].

3.6. Conclusion

The spontaneous alternation and spatial novelty preference tasks are not adequate for assessing the effects of sulphonylurea therapy on the cognitive function of nV59M mice. Although differences in performance were previously observed in the nV59M mice when compared to control littermates, the differences in performance in these two tests are currently not large enough to adequately assess therapeutic effects. Other behavioural tests, including assessment of locomotor function, may be better suited for examining the effect of sulphonylureas on neurological function.

Chapter 4: Effect of sulphonylureas on motor function

4.1. Summary

1. A series of locomotor function tests were carried out before and after implanting nV59M mice with subcutaneous slow-release glibenclamide or placebo pellets to determine if sulphonylurea therapy significantly ameliorates previously reported deficits in locomotor function in these mice. Nes-cre^{+}, ROSA$^{+/-}$ and wild-type littermates were used as controls.

2. As glibenclamide is a hypoglycaemic agent, blood glucose monitoring was carried out to ensure the implanted mice did not undergo hypoglycaemia. Treatment with a 2.5mg glibenclamide pellet did not significantly affect blood glucose concentrations in nV59M mice or control littermates.

3. It was not possible to assess the effect of glibenclamide therapy on muscle strength or balance and coordination as nV59M mice were not significantly impaired in the tasks used.

4. nV59M mice were significantly hyperactive as assessed by spontaneous activity on threshold monitors. However, it was not possible to determine the effect of glibenclamide, as changes in the performance of placebo- and glibenclamide-implanted nV59M mice and control littermates were observed.

4.2. Introduction

In addition to developmental delay and learning difficulties, iDEND and DEND patients suffer from muscle weakness as well as balance and coordination problems [5]. Our group previously showed that selective neuronal expression of the Kir6.2-V59M mutation in mice replicates the locomotor impairments observed in human iDEND patients [62]. I was thus interested in assessing this locomotor dysfunction in order to examine the effects of sulphonylureas on neurological function in nV59M mice.

4.2.1. Activating K_{ATP} channel mutations cause locomotor deficits

Approximately 25% of patients with gain-of-function K_{ATP} channel mutations present with marked delay in motor milestones and muscle weakness as well as neonatal diabetes [4,5,136]. Furthermore, balance and coordination problems have also been reported for many of these patients [189,225,226].

In terms of motor milestones, iDEND and DEND patients are reported to lag significantly behind children their age [251]. Most of these patients are unable to roll over or sit unaided by 12-13 months of age (both tasks normally achieved by 6-8 months of age) [151,221,227]. Furthermore, few patients have started walking independently before 24 months of age (normally achieved by 12-16 months of age) [250] and some patients have been reported to be unable to

walk at all [6,253]. Delays in development of grasping reflexes have been observed, with one patient showing no grasping reflex by the age of 3.5 years (normally present from birth) [221] and another patient only developing the pincer grasp by the age of 5 years (normally developed between 9-12 months of age) [188].

Upon neurological examination, it becomes apparent that most of these patients suffer from severe muscle weakness and hypotonia, particularly in the lower limbs [151,157,189,218,227]. This may partially explain their delay in achieving some motor milestones (i.e. rolling over, sitting unaided and walking) as they have significantly reduced muscle strength [221]. Furthermore, for patients with the most severe mutations, this has resulted in them being confined to wheelchairs as they are unable to walk unaided [253]. Interestingly, sensation and reflexes (other than grasping reflexes) do not seem to be affected in iDEND/DEND syndrome patients [151,189].

In addition to muscle weakness and hypotonia, iDEND and DEND patients also suffer from balance and coordination problems [5]. Several of the patients are reported to suffer from mild ataxia and have difficulties running as well as a higher tendency to fall over [189,225]. They also score poorly on tests assessing their fine motor skills and visual-motor integration, which considerably impairs their ability to complete every day tasks such as dressing alone [188,226,250]. Furthermore, iDEND patients have impaired hand-eye coordination when assessed using visual tracking tasks [259].

These motor deficits are thought to be directly caused by gain-of-function K_{ATP} channel mutations as they are not normally observed in other types of diabetes [5]. However, for a while it was not clear whether these symptoms were caused by the expression of the mutation in myocytes or neurones as both tissues are known to express the K_{ATP} channel [5].

4.2.2. The nV59M mouse model recapitulates the locomotor symptoms of iDEND syndrome

The majority of mutations associated with iDEND and DEND syndromes are found in the Kir6.2 subunit [113], which forms the potassium-selective pore of the K_{ATP} channel in most tissues including both skeletal muscle and the central and peripheral nervous systems [65]. It was thus not clear if the motor deficits associated with these syndromes originated from reduced muscle excitability, due to expression of the mutation in myocytes, or impaired neuronal regulation of muscle contraction, caused by the expression of the mutation in neurones.

Using a Cre-lox approach in combination with the muscle creatine kinase promoter or the nestin promoter, Clark *et al*. (2010) [62] generated mice with selective muscle or neuron expression of the Kir6.2-V59M mutation, which is the most common cause of iDEND syndrome in humans, and assessed their locomotor function using a variety of behavioural tests.

Muscle-specific expression of the Kir6.2-V59M mutation did not impair muscle strength or balance and coordination. By contrast, mice with selective neuronal expression of this mutation (nV59M mice) performed significantly worse than control littermates in all tests used to examine muscle strength, balance and motor coordination. Furthermore, the nV59M mice displayed hyperactivity, which some iDEND patients are reported to demonstrate once they learn to walk [187-189].

Clark and colleagues also showed that the motor impairments of nV59M mice were not caused by reduced neurotransmitter release at the neuromuscular junction as no differences were observed in miniature endplate potentials, evoked endplate potentials, and muscle resting potentials between nerve-muscle preparations isolated from control and nV59M mice [62]. This suggests the motor deficits originate in the central nervous system (CNS). This was supported by electrophysiological studies conducted on acute cerebellar slices from control and nV59M mice [62]. K_{ATP} channels are highly expressed in the cerebellum [26,68], which is heavily involved in motor control. Cell-attached and whole-cell recordings from cerebellar Purkinje cells from nV59M mice revealed significantly reduced action potential firing rate as well as significantly hyperpolarized resting membrane potential. Both of these parameters were restored to control levels by application of tolbutamide, a sulphonylurea [62].

Thus, it appears that the motor symptoms associated with iDEND syndrome are caused by impairment of neuronal, rather than muscle, function. This is further confirmed by the description of iDEND patients with gain-of-function mutations in SUR1 [166,224,260], which is the sulphonylurea receptor subtype expressed in neurones and not in myocytes (SUR2A expressed instead) [14].

4.2.3. Sulphonylurea treatment for iDEND/DEND locomotor symptoms

After the discovery that activating K_{ATP} channel mutations are responsible for up to 50% of all neonatal diabetes cases, it became apparent that sulphonylureas, which act by blocking the K_{ATP} channel, could be a suitable treatment for these patients. Indeed, over 90% of ND patients have been successfully transitioned from insulin to sulphonylureas to manage their diabetes [6,218]. This has resulted in a considerable improvement in glycaemic control as well as quality of life [218]. In iDEND/DEND patients, sulphonylureas were expected to also improve motor and cognitive functions.

For many DEND patients, transition to sulphonylureas has been unsuccessful [6,157,227,253,254]. In most of these cases, the inability to become insulin-independent correlates with the extent to which a maximal concentration of tolbutamide blocks the whole-cell current through heterologously expressed K_{ATP} channels carrying the same mutation [6,164].

Nonetheless, various patients with neurological symptoms, particularly those with iDEND syndrome, have been able to achieve good glycaemic control with sulphonylurea therapy [6,188,189,221,224-226,255]. In some of these patients, improvements in motor function have also been noted. For example, Shimomura *et al.* (2007) [221] observed a considerable improvement in motor function in a DEND patient (Kir6.2-I167L mutation) after transfer to sulphonylureas. Prior to transfer, the patient suffered from marked hypotonia and muscle weakness, being unable to roll over or sit without support, and displayed no grasping reflex at a chronological age of 3.5 years. After initiation of sulphonylurea therapy, the patient started being able to roll over, sit unaided, adopt a quadruped stance, and display grasping reflexes [221].

Similar results have been observed with other iDEND patients after transfer to sulphonylureas. Of note, a 2-year-old patient with the Kir6.2-V59M mutation was reported to start walking independently for the first time after transferring to sulphonylureas [151]. Prior to transfer, the patient was only able to do abdominal crawling and could not stand unsupported. Furthermore, neurological examination showed absence of hypotonia as well as improved muscle power after initiation of sulphonylurea therapy [151].

In addition to the improvements in muscle strength, improvements in balance and coordination have also been reported. Koster *et al.* (2008) described a patient with the Kir6.2-G53D mutation who displayed mild ataxia, slow gait, and poor coordination prior to sulphonylurea therapy. Treatment with

glibenclamide resulted in increased muscle tone as well as improved coordination and gait[225]. Similar improvements were observed by Mlynarski *et al.* (2007) with a Kir6.2-V59M patient who had difficulties running and fine motor control deficits [189].

Although these examples indicate that sulphonylureas may be beneficial for the motor deficits associated with iDEND and DEND syndromes, the locomotor performance of many of these patients is still considerably impaired [151,188,189,221,226] and many of them have a functional age equivalent to that of a 3-5 year-old, even though they are chronologically older [188,189,224,250]. For example, even on therapy, the Kir6.2-V59M patient described by Slingerland and colleagues had a maximum functional age of 4 years despite being chronologically 12 years of age [188]. Similarly, the Kir6.2-I167L patient described by Shimomura *et al.* (2007) was still unable to crawl or walk by the age of 4 years despite being on a high dose of sulphonylureas [221]. Moreover, there are various examples of patients successfully transferring to sulphonylureas (measured in terms of glycaemic control) who show little to no improvement in terms of locomotor function [224,250,255].

It is thus clear that more work is needed to determine the extent to which sulphonylureas are able to restore locomotor function in iDEND and DEND patients.

4.2.4. Effects of sulphonylureas on locomotion of iDEND mouse model

Although ideally a thorough clinical study should be conducted to assess the extent to which sulphonylureas ameliorate DEND syndrome, this is not a trivial task, particularly as all iDEND and DEND who respond to sulphonylureas are already on treatment (for the management of their diabetes), and the drug doses differ considerably between different patients.

I have thus decided to use the nV59M mice for assessing the effect of sulphonylurea therapy on locomotor function, particularly as these mice have previously been shown to recapitulate the motor deficits seen in iDEND patients [62].

The aim of this chapter was to determine if high-dose glibenclamide therapy (~5mg/kg/day) can significantly improve locomotor function in nV59M mice. These mice were tested with the same tasks previously used by Clark *et al.* (2010) [62] to assess their locomotor function (muscle strength, balance and coordination and hyperactivity) before and after implanting them with a 2.5mg slow-release subcutaneous glibenclamide or placebo pellet. In addition to this, blood glucose and body weight monitoring was carried out before and after pellet implantation to establish whether high-dose glibenclamide therapy triggers hypoglycaemia in non-diabetic animals.

4.3. Methods

4.3.1. Generation of mice

Mice with selective neuronal expression of the Kir6.2-V59M mutation under the control of the ROSA promoter (nV59M mice) were used for the experiments outlined below. Details of the transgenic mice (breeding strategy, etc) are given in Chapter 2.

4.3.2. Sulphonylurea therapy and behavioural phenotype

nV59M mice were tested for muscle strength, motor coordination and locomotion before and after implantation with a 21-day slow-release subcutaneous 2.5mg glibenclamide or placebo pellet (Innovative Research of America; dose: ~4.8mg/kg/day) at 11-14 weeks of age. A recovery period of one week was allowed between the surgery and the subsequent testing.

Muscle strength was assessed by the weight lifting and horizontal bar tests (forelimbs) and the inverted screen test (all four limbs). Motor coordination was assessed using the multiple static rods and the accelerating rotarod tests. Locomotion was assessed using free-running wheels, non-anxiogenic open field and threshold activity monitors. All experiments were performed blinded to genotype of the animal and treatment given. Control littermates ($ROSA^{+/-}$,

Nes-cre^{+}, wild-type) were used in all tests. All tests were performed during the animals' light phase and testing was carried out on the same day for all littermates.

4.3.2.1. Inverted screen test (muscle strength)

Mice were placed in the centre of a wire mesh grid, which was then inverted and placed 40-50 cm above a padded surface. The time taken for the mouse to fall was recorded and was given a score: 1 (110s or less), 2 (110-250s), 3 (251-599s) or 4 (600s or more). Mice were removed from the screen when the criterion time of 600s was reached.

4.3.2.2. Weight lifting test (muscle strength)

Six weights were used for this test. Each weight consisted of a ball of tangled fine gauge stainless steel wire (i.e. a kettle limescale collector) attached to a series of steel chain links. The number of links ranged from one to six (each link weighed approximately 13g). The mouse was held by the middle of the tail and lowered to grasp the first weight, which was lying on the laboratory bench. Once it had grasped the scale collector, the mouse was raised again

until the link was clear of the bench. The score was calculated as the number of chain links held for 3s multiplied by the time for which it was held.

4.3.2.3. Horizontal bar test (muscle strength and coordination)

This test measures forelimb strength and motor coordination. A 38cm long, 2mm thick brass bar was held 49cm above a padded bench surface by two supporting columns. The mouse was held from its tail and allowed to grasp the bar at the central point with its forepaws only. It was left holding the bar for up to 30s or removed if it reached one of the supporting columns. In these cases, a maximum score of 5 was awarded. For falls at earlier times, a graded scoring was used: 1 (5s or less), 2 (6-10s), 3 (11-20s), and 4 (21-29s).

4.3.2.4. Accelerating rotarod (motor coordination)

An accelerating rotarod (Ugo Basile, Italy, model 7650) with a start speed of 2.5 RPM and an acceleration rate of 20 RPM/min was used. The mouse was held by its tail and placed on the rotating rod, facing the direction of rotation. At 10s after placing the mouse, the acceleration was initiated. The time from

the start of acceleration until the mouse fell was recorded. An end-point of 120s was used (time at which the rotarod reached its maximum speed).

4.3.2.5. Static rods (motor coordination)

Three wooden rods of varying thickness (35, 22 and 9 mm diameter) each 60cm long were fixed at one end to a bench 40cm above a padded surface. Each mouse was placed approximately 20mm from the exposed end, facing away from the bench. The time taken to orientate 180° whilst remaining upright as well as the time taken to reach the end of the rod were recorded. A cut-off of 180s was used for both of these measurements. If a mouse fell before orientating or reaching the end of the rod, it was assigned a time of 180s for both measurements. The testing was repeated with all three rods (starting with the thickest one).

4.3.2.6. Free-running wheels

Mice were kept for 23h in a cage containing a running wheel: the duration of the time they spent on the free-running wheel, the average speed of running, and the distance travelled were measured electronically.

4.3.2.7. Threshold activity monitors

To measure their spontaneous locomotor activity, the mice were placed in activity monitors. The amount of time that each mouse was active for over a 23h period was monitored using a Home Cage Threshold Activity System monitor (Med Associates, St Albans VT).

4.3.2.8. Open field

A dark grey, open plastic box (50cm x 30cm x 18cm) with its floor divided into squares of 10cm (delimited by thin white borders) was used for this test. The test started by placing a mouse in a corner square of the open field apparatus and observing it for 5min. The number of squares crossed with all four paws, the latency to first rear, and the total number of rears (both front paws off the ground and not as part of grooming) were recorded. Between each trial, the floor and walls were cleaned with a damp and a dry tissue.

4.3.2.9. Glibenclamide therapy

Mice were implanted with a 21-day slow-release subcutaneous 2.5mg glibenclamide or placebo pellet (Innovative Research of America). For a mouse with an average weight of 25g, a 2.5mg pellet with a release duration

of 21 days corresponds to a dose of ~4.8mg/kg/day, which is ~10 times higher than the average dose given to a neonatal diabetes patient (0.45mg/kg/day) [6]. Details of the surgical procedure for subcutaneous implantation of slow-release pellets are given in Chapter 2.

4.3.3. Data analysis

Statistical analysis of data from male and female mice indicated no significant differences, so these data were pooled. Similarly, analysis of data from the three groups of control mice ($ROSA^{+/-}$, $Nes\text{-}cre^{+}$ and wild-type) indicated no significant differences, so these data were also pooled. When the data distribution permitted (i.e. fulfilled the criteria of normality and equality of variance), a Student's t-test or a One-Way ANOVA was performed. Otherwise, data were analysed using a non-parametric test, the Mann-Whitney U-test or the Kruskal-Wallis One-Way ANOVA on Ranks. $P<0.05$ was considered statistically significant.

4.4. Results

4.4.1. Subcutaneous glibenclamide therapy does not affect blood glucose or body weight in nV59M mice or control littermates

Prior to implantation with the glibenclamide pellet, free-fed blood glucose was measured daily over a period of 5 days to obtain a baseline measurement. As expected, there was no significant difference in blood glucose levels between control and nV59M mice (Figure 4.1A). As glibenclamide is a hypoglycaemic agent, daily blood glucose monitoring was carried out to ensure the implanted mice did not undergo hypoglycaemia (i.e. blood glucose levels of <2mM). As Figure 4.1A shows, treatment with a 2.5mg glibenclamide pellet did not significantly affect blood glucose concentrations in nV59M or control littermates.

Additionally, body weight was monitored daily over a period of 5 days prior to pellet implantation and up to 7 days after implantation to determine whether glibenclamide therapy affected the body weight of nV59M and control mice. However, as Figure 4.1B shows, there was no significant difference in the body weight of glibenclamide or placebo treated mice.

4.4.2. Muscle strength in nV59M mice

In order to determine whether high doses of glibenclamide significantly improve muscle strength in nV59M mice, their performance in the weight lifting, horizontal bar and inverted screen tasks was assessed a week before and a week after implantation with a 21-day slow-release pellet (either placebo or 2.5mg glibenclamide).

Prior to pellet implantation, nV59M mice performed slightly worse than control littermates in all three tasks, although statistical significance was not reached (Fig. 4.2). In the weight lifting task, nV59M mice received slightly lower scores than control mice (9.9±1.8 versus 10.9±2, respectively; mean ± SEM). Furthermore, a larger number of nV59M mice received scores in the lower score brackets (6-9), while a greater number of control mice received scores in the highest score brackets (14-17) (Fig. 4.2A). Similar results were obtained with the horizontal bar task, with nV59M mice scoring slightly lower than control mice (4.7±0.8 versus 4.9±0.5, respectively; mean ± SEM; Fig. 4.2B), as well as with the inverted screen test (3.8±0.5 versus 3.7±0.7, respectively; mean ± SEM; Fig. 4.2C). However, these differences were not statistically significant.

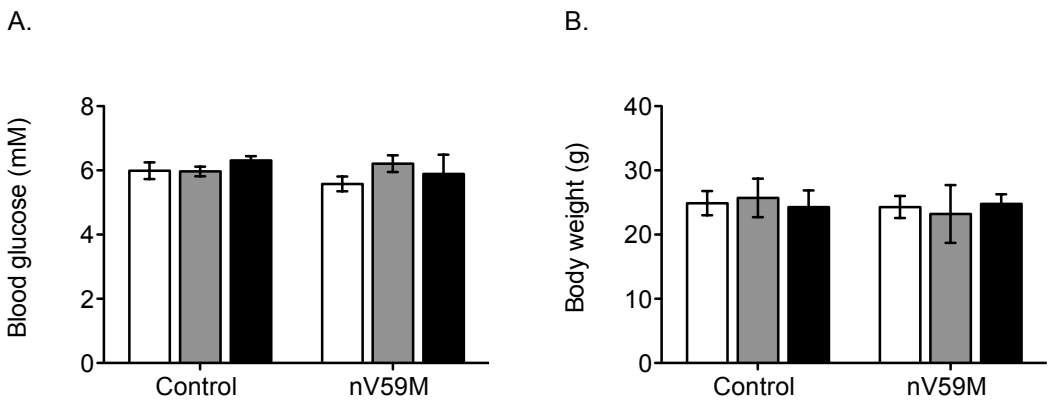

Figure 4.1: Effect of glibenclamide on blood glucose and body weight

(**A**) Free-fed blood glucose concentration and (**B**) body weight for 11-14 week-old control ($ROSA^{+/-}$: n=5; $Nes\text{-}Cre^{+}$: n=4) and nV59M (n=6) mice before (white bars) and after implanting with a 2.5mg placebo (grey bars) or glibenclamide (black bars) slow-release subcutaneous pellet. Half of the control and half of the nV59M mice were allocated to each treatment group. Data are mean ± SEM. The mean blood glucose and body weight for each mouse was averaged over a period of 5 days before and up to 7 days after pellet implantation. [Two-way ANOVA: treatment x genotype].

As the difference in performance between control and nV59M mice in the absence of therapy was not significantly different, it was not possible to assess the effect of glibenclamide on muscle strength using these tasks. Furthermore, in the weight lifting task performance seemed to be affected by previous exposure to the test as changes in the performance of both placebo-implanted control and nV59M mice were observed (Fig. 4.2A).

4.4.3. Balance and coordination in nV59M mice

In addition to impaired muscle strength, nV59M mice have been previously shown to have motor coordination and balance deficits [62]. I was hence interested in establishing whether high doses of glibenclamide could significantly ameliorate these deficits.

The performance of nV59M mice on the static rods and accelerating rotarod tasks was assessed a week before and a week after implantation with a 21-day slow-release pellet (either placebo or 2.5mg glibenclamide). However, as Figure 4.3 shows, I was unable to determine whether glibenclamide improved motor coordination in either of these tasks. For both of these tests, the difference between nV59M mice and control littermates in the absence of therapy was not significantly different.

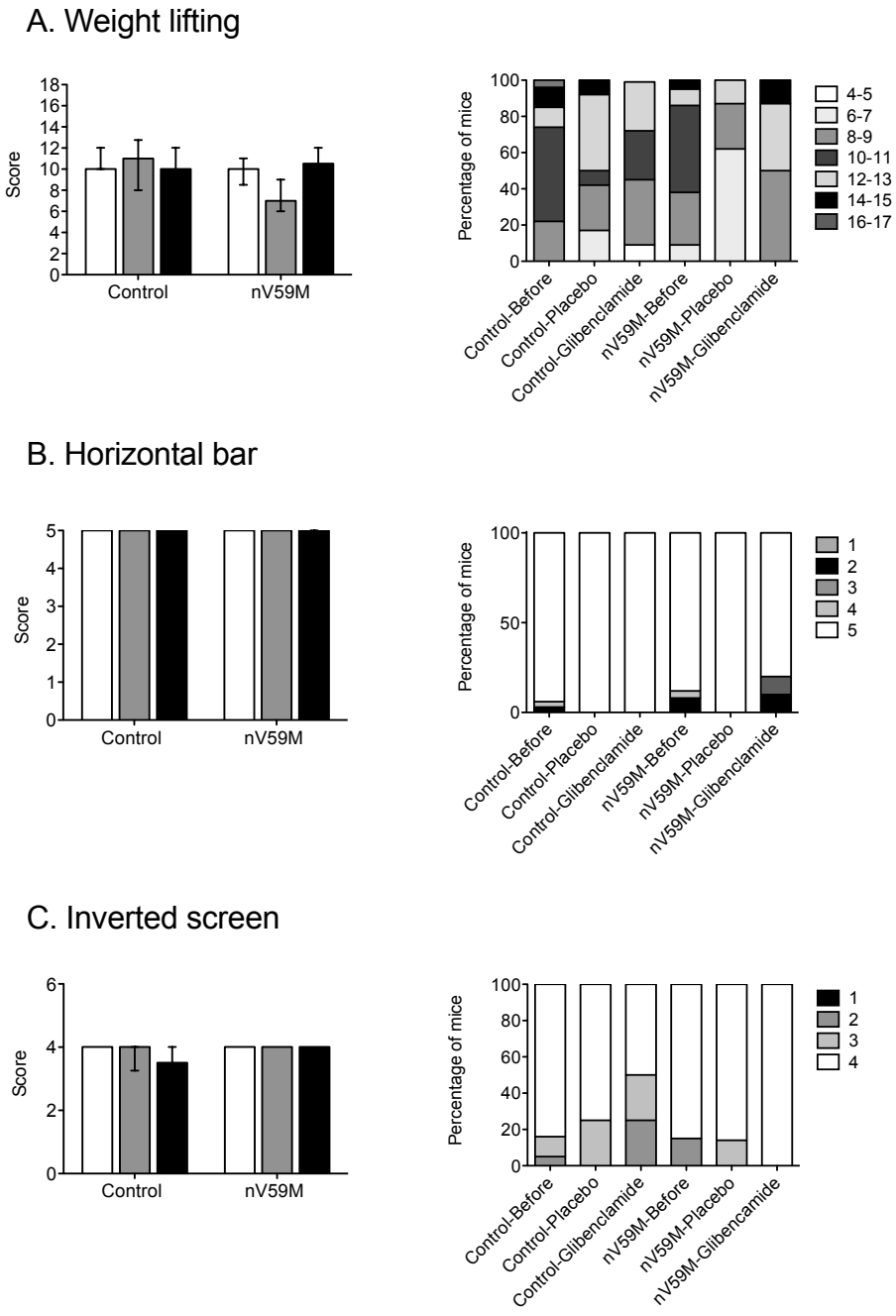

Figure 4.2: Effect of glibenclamide on muscle strength

(**A**) Weight lifting, (**B**) horizontal bar and (**C**) inverted screen tests carried out on 11-14 week-old control (WT: n=4; ROSA$^{+/-}$: n=21; Nes-Cre^{+}: n=6) and nV59M (n=21) mice before (white bars) and after implanting with a 2.5mg placebo (grey bars) or glibenclamide (black bars) slow-release subcutaneous pellet. Half of the control and half of the nV59M mice were allocated to each treatment group. Data are median and interquartile range. On the right the

percentage of mice achieving the indicated score is shown. [Kruskal-Wallis One-Way ANOVA on Ranks].

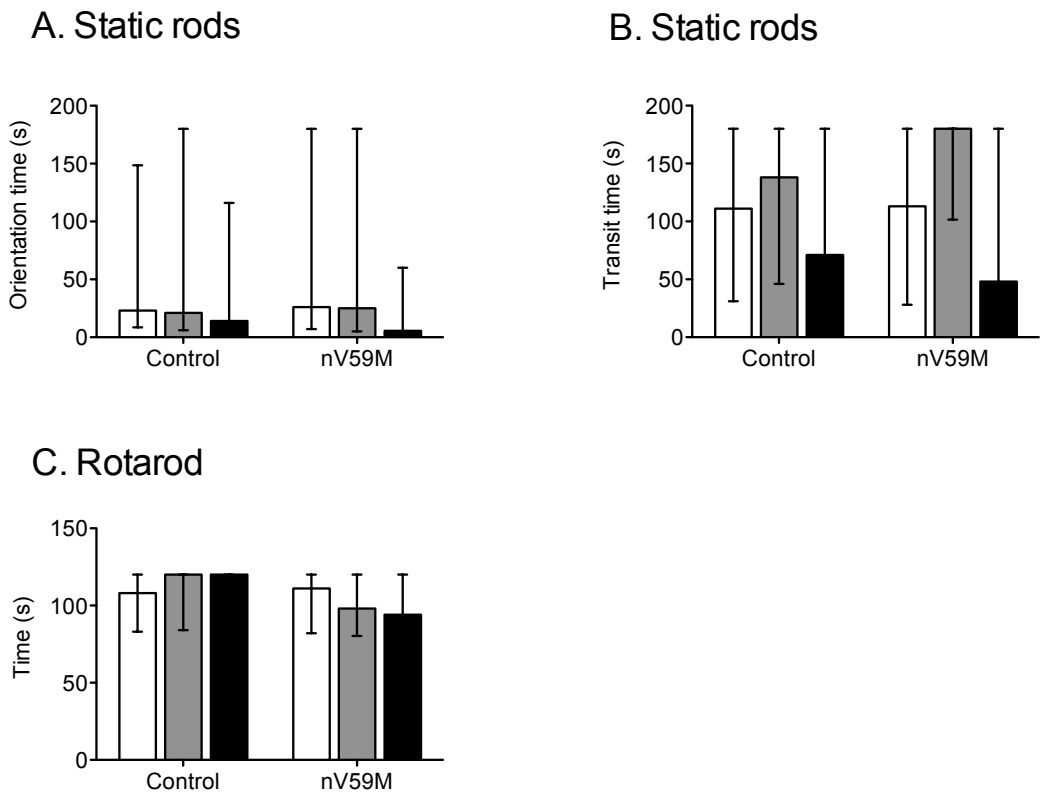

Figure 4.3: Effect of glibenclamide on balance and coordination

(**A, B**) Static rods (orientation and transit times on the thinnest rod, respectively) and (**C**) rotarod tests carried out on 11-14 week-old control (WT: n=4; ROSA$^{+/-}$: n=21; Nes-Cre^{+}: n=6) and nV59M (n=21) mice before (white bars) and after implanting with a 2.5mg placebo (grey bars) or glibenclamide (black bars) slow-release subcutaneous pellet. Half of the control and half of the nV59M mice were allocated to each treatment group. Data are median and interquartile range. [Kruskal-Wallis One-Way ANOVA on Ranks].

In the rotarod task, nV59M mice remained on the rod for an average of 100±4 seconds while control littermates stayed on the rod for an average of 99±4 seconds. In the thinnest of the static rods (9mm), nV59M mice took on average 70±15 seconds to orientate and 106±14 seconds to transit the rod while control littermates took on average 64±13 seconds to orientate and 108±12 seconds to transit the rod. Furthermore, for the static rods test, performance seemed to be affected by previous exposure to the test as changes in the performance of both placebo-implanted control and nV59M mice were observed (Fig. 4.3A-B).

4.4.4. Hyperactivity in nV59M mice

I evaluated whether high doses of glibenclamide significantly ameliorated the hyperactivity previously observed in nV59M mice [62]. Their performance in the non-anxiogenic open field, spontaneous activity on the threshold monitors and free-running wheels was assessed a week before and a week after implantation with a 21-day slow-release pellet (either placebo or 2.5mg glibenclamide).

Contrary to what was previously observed, the nV59M cohort I tested did not display hyperactivity/increased exploratory drive compared to control littermates in the non-anxiogenic open field task in the absence of therapy (Fig. 4.4). Although nV59M mice crossed more squares than control mice

(Fig. 4.4A), statistical significance was not reached. Furthermore, no difference was observed in the number of rears performed by each group (Fig. 4.4B). Thus, it was not possible to assess any changes in performance in the presence of glibenclamide.

Prior to glibenclamide therapy, nV59M mice spent a longer amount of time than control littermates when given access to free-running wheels (330±39min versus 277±23min, respectively; mean ± SEM; Fig. 4.5A). They also covered a longer distance than control littermates over a 23-hour period (10.8±2.2 km versus 7.4±0.9km, respectively; Fig. 4.5B). However, these differences were not statistically significant, making it difficult to determine whether glibenclamide can ameliorate hyperactivity in nV59M mice. Additionally, in the free-running wheels test performance seems to be affected by previous exposure to the test as changes in the performance of both placebo-implanted control and nV59M mice were observed (Fig. 4.5).

In the absence of glibenclamide therapy, a significant difference was observed in the spontaneous activity levels of nV59M mice. Over a period of 23 hours, nV59M mice were active for 220±24.3min compared to control littermates, which were active for 171±10.2min (P=0.028; unpaired Student's t-test). Interestingly, nV59M mice remained active for considerably longer than control littermates when placed in the threshold monitors (Fig. 4.6A).

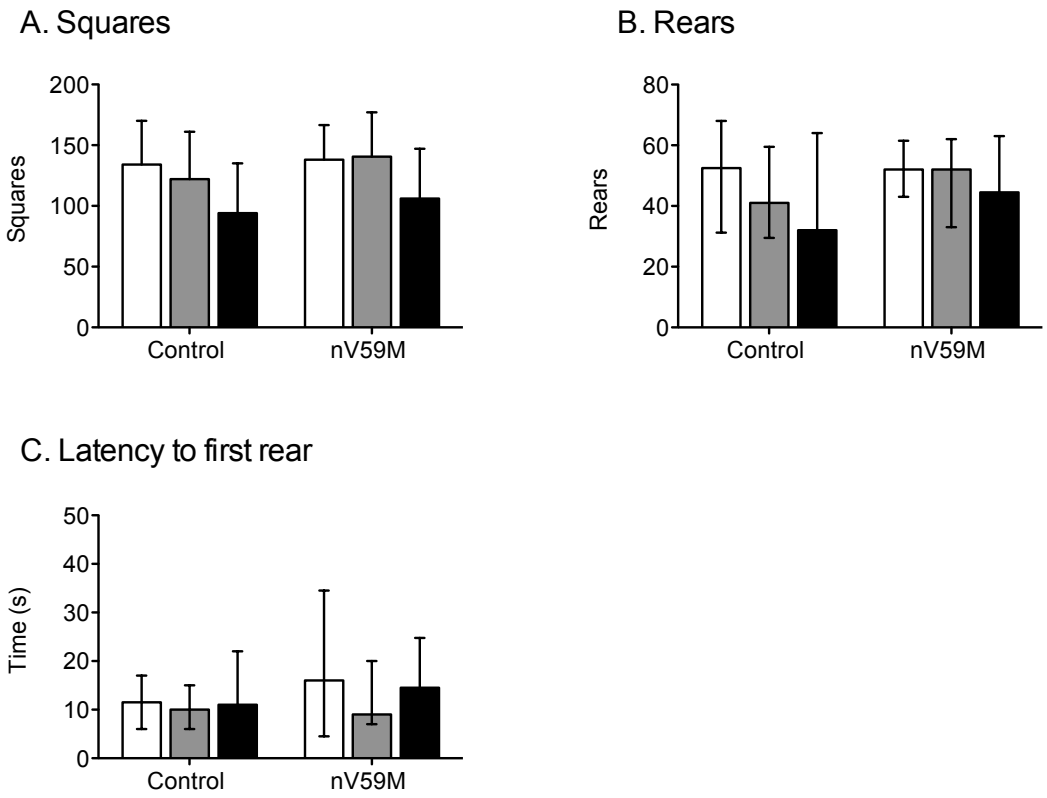

Figure 4.4: Effect of glibenclamide on non-anxiogenic open field test

(**A**) Total number of squares crossed, (**B**) total number of rears and (**C**) latency to first rear during a 5min period in the non-anxiogenic open field test for 11-14 week-old control (WT: n=8; ROSA$^{+/-}$: n=19; Nes-Cre^{+}: n=13) and nV59M (n=21) mice before (white bars) and after implanting with a 2.5mg placebo (grey bars) or glibenclamide (black bars) slow-release subcutaneous pellet. Half of the control and half of the nV59M mice were allocated to each treatment group. Data are median and interquartile range [Kruskal-Wallis One-Way ANOVA on Ranks].

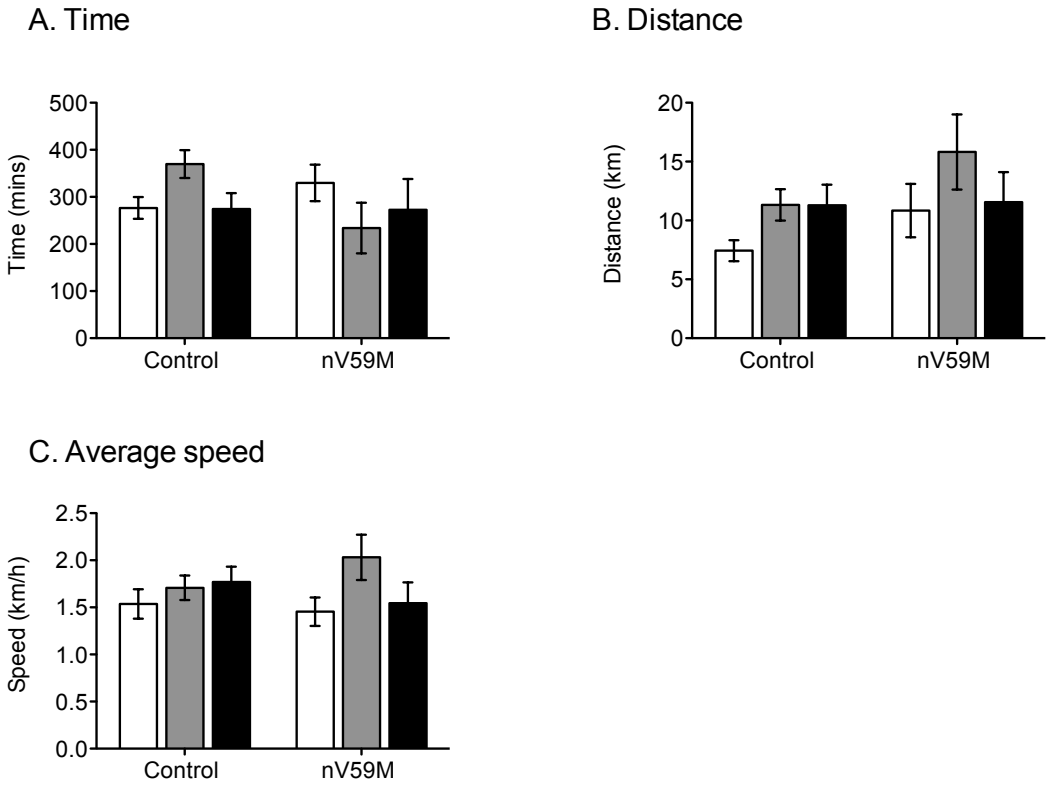

Figure 4.5: Effect of glibenclamide on free-running wheels test

(**A**) Duration of time, (**B**) distance ran and (**C**) average speed over a 23-hour period with free access to a running wheel for 11-14 week-old control (WT: n=8; ROSA$^{+/-}$: n=19; Nes-Cre^{+}: n=13) and nV59M (n=21) mice before (white bars) and after implanting with a 2.5mg placebo (grey bars) or glibenclamide (black bars) slow-release subcutaneous pellet. Half of the control and half of the nV59M mice were allocated to each treatment group. Data are mean ± SEM.

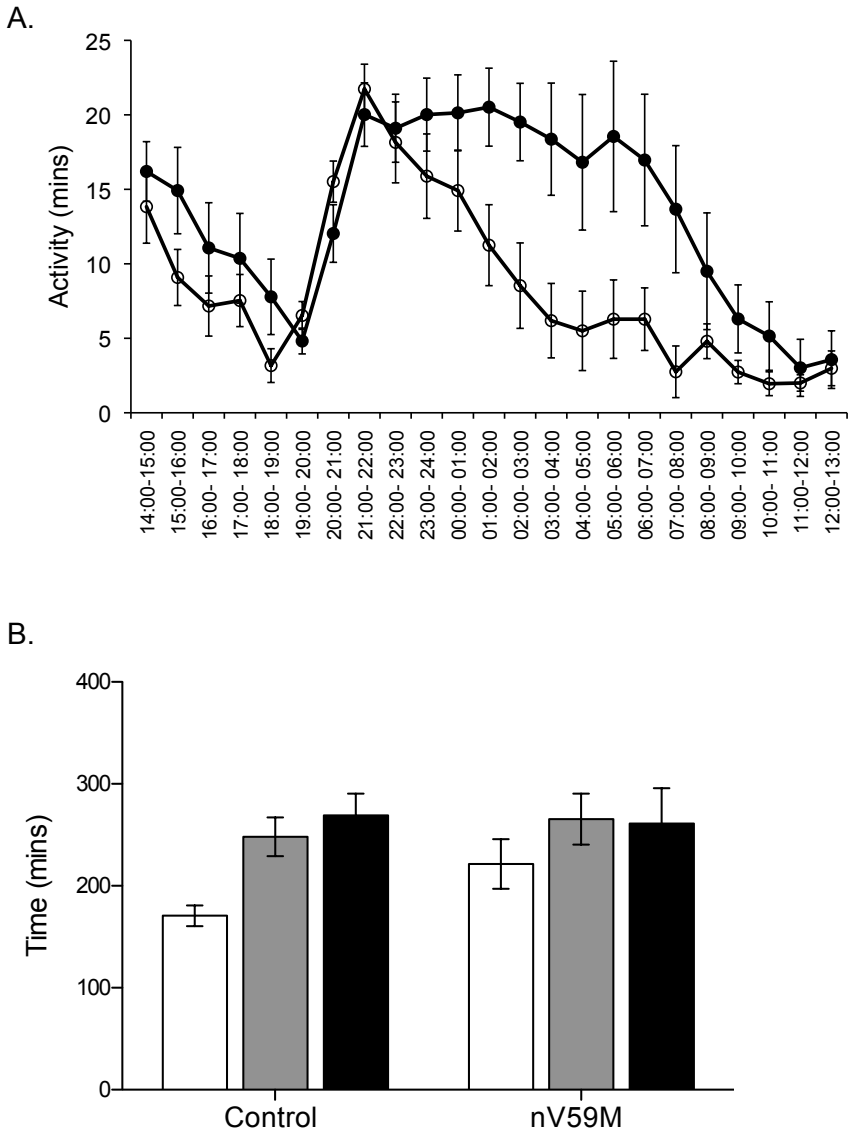

Figure 4.6: Spontaneous activity on threshold monitors

(**A**) Mean hourly spontaneous activity for nV59M mice (closed circles; n=21) and control littermates (open circles; WT: n=8; $ROSA^{+/-}$: n=19; $Nes\text{-}Cre^{+}$: n=13) over a 23-hour period. Lights were turned off at 19:00 and turned back on at 07:00. (**B**) Duration of time spent on spontaneous locomotor activity over a 23-hour period for 11-14 week-old control (WT: n=8; $ROSA^{+/-}$: n=19; $Nes\text{-}Cre^{+}$: n=13) and nV59M (n=21) mice before (white bars) and after implanting with a 2.5mg placebo (grey bars) or glibenclamide (black bars) slow-release subcutaneous pellet. Half of the control and half of the nV59M mice were allocated to each treatment group. Data are mean ± SEM.

However, as Figure 4.6B shows, it was not possible to assess whether glibenclamide ameliorated hyperactivity as an increase in the activity levels of all groups was observed after treatment.

4.5. Discussion

iDEND and DEND syndromes are characterized by neonatal diabetes accompanied by muscle hypotonia, motor coordination deficits, and developmental delay [5]. In many neonatal diabetes patients with activating mutations in the K_{ATP} channel, transfer from insulin to sulphonylurea therapy has resulted in improved glycaemic control [6,218]. As the extra-pancreatic symptoms associated with iDEND/DEND syndrome are caused by the expression of the activating K_{ATP} channel mutation in neuronal tissue [62], it was hoped that sulphonylureas would also restore neurological function.

In some of the iDEND/DEND patients who have successfully switched to sulphonylurea therapy, moderate improvements in neurological function have been noted [151,188,189,221,222,225,226]. However, the locomotor function of many of these patients is still considerably impaired [151,188,189,221,226], and various patients show little to no improvement in motor function when transferred to sulphonylureas despite improved glycaemic control [224,250,255]. It is thus not clear the extent to which sulphonylureas reverse the locomotor deficits associated with gain-of-function K_{ATP} channel mutations.

Due to the inherent difficulties in thoroughly examining this in human patients, I used a mouse model with selective neuronal expression of the Kir6.2-V59M mutation for assessing the effect of high dose glibenclamide therapy on locomotor function. These mice have been previously shown to replicate the locomotor impairments observed in human iDEND patients [62].

4.5.1. Subcutaneous glibenclamide therapy does not affect blood glucose or body weight in normoglycaemic mice

Sulphonylureas are mainly used for the management of non-insulin-dependent diabetes as they are effective hypoglycaemic agents, being able to directly stimulate insulin secretion from pancreatic β-cells [213,218]. As Clark and colleagues previously demonstrated that nV59M mice are normoglycaemic [62], I was concerned administration of high doses of sulphonylureas may trigger hypoglycaemia in these mice. Thus, I monitored the blood glucose concentrations of nV59M mice and control littermates prior to and after implantation with slow-release 2.5mg glibenclamide or placebo pellet. As expected, no differences were observed in the blood glucose levels between the two groups in the absence of therapy.

Interestingly, despite the mice being given a dose approximately 10 times higher than the average dose used to treat neonatal diabetes patients [6], none

of the mice suffered hypoglycaemia. Thus, treatment with a high dose of glibenclamide does not trigger hypoglycaemia in normoglycaemic mice.

It is possible that long-term treatment (the mice were only implanted for a maximum of one week) could alter glycaemic control in normoglycaemic mice. However, work by Michaela Iberl (*unpublished*) suggests that longer-term treatment (up to 4 weeks) does not trigger hypoglycaemia either. Intriguingly, she observed a significant increase in blood glucose levels of wild-type normoglycaemic mice after 4 weeks of treatment with slow-release 2.5mg glibenclamide pellets. Similar results have been obtained by Remedi & Nichols [261], who suggested that chronic glibenclamide treatment *in vivo* could cause loss of β-cell insulin secretory capacity due to excessive β-cell stimulation and hyperexcitability.

Additionally, body weight was monitored daily over a period of 5 days prior to pellet implantation and up to 7 days after implantation. Anecdotal evidence suggests that neonatal diabetes patients treated with glibenclamide experience a decrease in body weight. I was thus interested in determining whether glibenclamide therapy affected the body weight of nV59M and control mice. However, there was no significant difference in the body weight of glibenclamide or placebo-treated mice. It is possible that we did not see an effect on body weight as our experiment was relatively short term. However, work by other members of our group suggests that even after 4 weeks of

glibenclamide treatment, body weight does not change significantly (M. Iberl, *unpublished*).

Why mice and humans show differences in body weight changes in unclear, but it is perhaps pertinent that in our experiments placebo-treated animals were compared with sulphonylurea-treated animals whereas the body weight changes seen in patients with neonatal diabetes occur when they are transferred from insulin to sulphonylurea therapy.

4.5.2. Assessment of the effect of glibenclamide on muscle strength

It has been previously shown that nV59M mice have a significant muscle strength deficit [62]. Their performance on the inverted screen, horizontal bar and weight lifting tasks were significantly impaired. The inverted screen and weight lifting tasks measure muscle strength alone, as they require little balance. On the other hand, the horizontal bar task measures forearm strength, but also requires a degree of motor coordination.

In order to determine whether high doses of glibenclamide significantly improve muscle strength in nV59M mice, their performance on these three tasks was assessed a week before and a week after implantation with a slow-release glibenclamide or placebo pellet.

Prior to pellet implantation, nV59M mice performed slightly worse than control littermates in all three tasks, however statistical significance was not reached. It was thus not possible to assess the effect of glibenclamide on muscle strength using these tasks as the difference in performance between control and nV59M mice in the absence of therapy was not as marked as previously reported [62]. Furthermore, in the weight lifting task performance seemed to be affected by previous exposure to the test as changes in the performance of both placebo-implanted control and nV59M mice were observed.

4.5.3. Assessment of the effect of glibenclamide on balance and coordination

In addition to impaired muscle strength, nV59M mice have been previously shown to have motor coordination and balance deficits [62]. Their performance on the multiple static rods and the accelerating rotarod was significantly affected. These two tasks are commonly used to evaluate motor coordination; the multiple static rods assess the ability of a mouse to turn around and transverse a series of increasingly narrow wooden rods. For the accelerating rotarod task, mice are required to remain on a rotating rod as it accelerates over a period of 2 minutes.

In order to determine whether high doses of glibenclamide significantly improve motor coordination in nV59M mice, their performance on these two

tasks was assessed a week before and a week after implantation with a slow-release glibenclamide or placebo pellet.

However, I was unable to determine whether glibenclamide improved motor coordination in either of these tasks. For both tests, the difference between nV59M mice and control littermates in the absence of therapy was not as marked as previously reported [62], and did not reach statistical significance. Moreover, for the static rods test, performance seemed to be affected by previous exposure to the test as changes in the performance of both placebo-implanted control and nV59M mice were observed.

4.5.4. Assessment of the effect of glibenclamide on hyperactivity

Although hyperactivity was not initially recognised as a feature of iDEND syndrome, various iDEND children have been reported to exhibit symptoms of attention deficit hyperactivity disorder [188,189,226,250]. Furthermore, previous work by our group has shown that nV59M mice display hyperactivity as assessed by the non-anxiogenic open field task as well as threshold activity monitors and free-running wheels [62]. In the open field test, which assesses locomotion and exploratory behaviour [257], nV59M mice crossed a greater number of squares and reared more often than control littermates [62]. nV59M mice also displayed increased spontaneous activity when placed in threshold activity monitors as well as increased time spent in the free-running wheels [62].

I therefore decided to evaluate whether high doses of glibenclamide significantly ameliorated the hyperactivity observed in nV59M mice using the same tasks as Clark *et al.* (2010) [62].

Contrary to what was previously observed, the nV59M cohort I tested did not display hyperactivity/increased exploratory drive compared to control littermates in the non-anxiogenic open field task in the absence of therapy. By contrast, in the free-running wheels, nV59M mice spent a longer amount of time running and covered a longer distance than control littermates. However, these differences were not statistically significant. It was thus not possible to assess any changes in performance after introduction of glibenclamide therapy.

In the case of the threshold monitors, nV59M mice were significantly more active than control littermates prior to initiation of glibenclamide therapy. They also remained active for a considerably longer period of time. However, it was not possible to assess the effect of glibenclamide as an increase in the levels of spontaneous activity of all groups was observed after treatment. It therefore appears as if the level of spontaneous activity is affected by previous exposure to the threshold activity cages.

4.6. Conclusion

Despite using a variety of tests to assess the effect of sulphonylureas on locomotion, it was not possible to determine whether these drugs significantly affect neurological function. Surprisingly, for most of the tasks used, the difference between control and nV59M mice in the absence of therapy was not as marked as previously observed [62]. The exact reason why we observed differences in the locomotor deficits between the two nV59M cohorts is not clear.

A possible explanation could be changes in the genetic background of the ROSA-Kir6.2-V59M line used to generate the nV59M colony. This line was initially developed using V6.5 embryonic stem cells, which are 50% C57Bl/6 and 50% 129/sv, injected into CB20 blastocysts [181]. The mice have then been continually backcrossed to a C57Bl/6 genetic background. Thus, the initial cohort used by Clark may have had a more mixed 129/sv-C57Bl/6 background than the cohort I used for these experiments (by the time I conducted these experiments, the line had already been backcrossed 6 generations). It is known that these two inbred strains perform differently in behavioural tests, including the non-anxiogenic open field, the rotarod and the static rods tasks [257]. In these tasks, 129/sv mice were significantly less active and performed significantly worse than C57Bl/6 mice [257]. It is thus possible that the more homogeneous genetic background of the nV59M cohort I used

may have altered the phenotypic differences between the mutant mice and control littermates.

It is also possible that the additional stress of undergoing surgery under general anaesthesia may have affected performance on these tasks, particularly as changes in the performance of placebo-implanted control and nV59M mice were observed for some of the tasks (e.g. weight lifting, spontaneous activity). A longer period between the initial test battery and the post-surgery testing may have allowed the mice to recover better and could have reduced the effect of stress on test performance. However, previous experience has shown us that although the pellets are meant to last 21 days, their effect starts decreasing after 14 days (K. Shimomura, *unpublished*), which restricted the length of the period between testing sessions.

In addition to this, the changes in performance in the placebo-implanted mice could also be caused by previous exposure to the tasks (i.e. in the initial testing round). This could be addressed by performing a single set of experiments after treating half of the mice with glibenclamide and half with placebo. However, I was interested in the effect of the therapy on the performance of individual animals (i.e. does it significantly improve it?). Furthermore, mutant nV59M mice are not born with Mendelian frequency (R. H. Clark, *unpublished*), which significantly limits the number of mutant mice that can be used for testing.

Chapter 5: General anaesthetic sensitivity in iDEND

5.1. Summary

1. nV59M mice took significantly longer than control littermates to lose their righting and withdrawal reflexes when exposed to isoflurane or halothane anaesthesia.

2. Implantation of subcutaneous glibenclamide pellets did not restore the loss of righting reflex in nV59M mice, but partially restored the loss of withdrawal reflex produced by isoflurane. Subcutaneous glibenclamide had no effect on the righting or withdrawal reflexes of control mice.

3. Chronic intracranioventricular delivery of glibenclamide into the right lateral ventricle had no significant effect on the time taken for nV59M mice to lose their righting or withdrawal reflexes when exposed to isoflurane anaesthesia.

5.2. Introduction

General anaesthetics have been in clinical practice for close to 200 years, reducing the discomfort, trauma and pain associated with surgical procedures to bearable levels. Despite their common use in medicine, it is still not clear exactly where in the brain they exert their effects or the identity of the molecular targets that mediate their actions.

With the exception of its use for the treatment of status epilepticus, general anaesthesia is always used as an adjunct to another medical procedure [262]. The aim of general anaesthesia is to eliminate consciousness and pain and to prevent motor, autonomic and cardiovascular reflexes during a surgical procedure [263]. For a drug to be considered a general anaesthetic, its ability to mediate these effects must be reversible and produced without additional administration of muscle relaxants, sedatives or autonomic modulators [262].

The study of the underlying mechanisms of anaesthesia has focused on three main effects: loss of consciousness (hypnosis), immobility, and amnesia. As general anaesthetics are powerful drugs capable of virtually shutting down the central nervous system, it is clear they exert these effects by acting on different regions of the brain and spinal cord. In this chapter, I will focus on their role in hypnosis and immobility.

5.2.1. General anaesthesia: Hypnosis

In clinical medicine, hypnosis is defined as the impairment of perceptive awareness, and in human subjects it is identified by the loss of an appropriate response to specific spoken commands [262]. In laboratory animals, hypnosis is assessed by means of the loss of the righting reflex (LORR), which is defined as the inability to return to an upright position in response to a non-painful stimulus [262].

It has been suggested that the hypnotic/sedative actions of general anaesthetics are mediated by depression of regions involved in cognition, memory, learning, sleep and attentiveness, including the reticular-activating system, thalamus, amygdala, pons, and hippocampus [262,264-266]. In support of this idea, it has been shown that volatile general anaesthetics, such as isoflurane and halothane, selectively depress blood flow and glucose metabolism primarily in the thalamus and midbrain reticular formation in human subjects [267].

Moreover, neuroimaging studies (regional cerebral blood flow imaging with positron emission tomography) have shown that the first areas to reactivate upon re-entering consciousness in human subjects anaesthetized with dexmedetomidine or propofol were the thalamus, brainstem, hypothalamus, and the anterior cingulate cortex [268]. Additionally, in rats deeply anaesthetized with a volatile anaesthetic, evoked potentials travelling from the periphery to

the sensory cortex show increased latency and decreased amplitude. This signal degradation occurs at specific relay sites in the deep cortex and the thalamus [269].

Thus, the thalamus appears to be a central participant in the loss of consciousness induced by general anaesthetics. However, it is still not clear whether the thalamus is the main 'on-off switch' for consciousness (i.e. its inactivation *causes* the loss of consciousness) or whether it provides a 'read-out' of diminished activity elsewhere in the brain (i.e. its inactivation *is caused* by the loss of consciousness). Experimental evidence supporting both these two hypotheses exists, although the former appears to be favoured [262,268,270,271].

5.2.2. General anaesthesia: Immobility

One of the most important and desirable properties of general anaesthetics is their ability to induce ablation of movement in response to noxious stimuli [262]. In laboratory animals, immobility is assessed by means of the loss of the withdrawal reflex (LOWR), which is defined as the inability to rapidly move or withdraw a limb in response to the application of noxious pressure.

Unlike the hypnotic actions of general anaesthetics, the loss of mobility they induce is thought to be mainly mediated at the spinal cord level [262,272]. The

French physiologist Claude Bernard was the first to demonstrate that chloroform (the first general anaesthetic to be described) produced immobility in frogs by acting at the spinal cord [262]. More recently, it has been shown that cervical transection of the spinal cord in anaesthetized rats does not affect the minimal alveolar concentration (MAC) of an anaesthetic agent for immobility [273,274]. Furthermore, in goats, selective delivery of isoflurane to the body but not the brain did not alter the concentration required to inhibit hind-leg withdrawal in response to noxious stimulation [275].

Although there is strong evidence for the spinal cord as the main site of action of anaesthetic-induced immobility, experimental evidence also suggests that anaesthetic action in the brain has some influence on movement ablation [276]. For example, lesion of the medial septum in rats, which led to the loss of septohippocampal cholinergic afferents, decreases the amount of anaesthetic required to induce immobility [277]. It has also been suggested that pontine cholinergic networks are able to modulate nociceptive processing under general anaesthesia because injection of cholinomimetics into the pontine reticular nucleus alters LOWR in rats anaesthetized with halothane [278]. It thus appears that there is a subtle interplay between supra-spinal and spinal sites of anaesthetic action.

5.2.3. Volatile anaesthetic sensitivity of nV59M mice

During the subcutaneous surgical implantation of slow-release pellets (described in Chapter 4), it became apparent that nV59M mice had altered sensitivity to isoflurane anaesthesia. In this chapter, I discuss the effects of neuronal expression of the Kir6.2-V59M mutation on LORR and LOWR as well as the effect of glibenclamide therapy on these two measurements of general anaesthesia.

5.3. Methods

5.3.1. Generation of mice

Mice with selective neuronal expression of the Kir6.2-V59M mutation under the control of the ROSA promoter (nV59M mice) were used for the experiments outlined below. Details of the transgenic mice (breeding strategy, etc) are given in Chapter 2.

5.3.2. Subcutaneous sulphonylurea therapy and sensitivity to anaesthesia

nV59M mice and control littermates were tested for sensitivity to isoflurane anaesthesia before and after subcutaneous implantation of a 21-day slow-release 2.5mg glibenclamide or placebo pellet (Innovative Research of America) at 11-14 weeks of age. A recovery period of one week was allowed between the surgery and the subsequent testing. All experiments were performed blinded to genotype of the animal and treatment given. Testing was carried out on the same day for all littermates.

5.3.2.1. Sensitivity to isoflurane sensitivity

During induction of anaesthesia for implanting the slow-release pellets, mice were tested for sensitivity to isoflurane. Details of the method used for assessment of sensitivity to isoflurane anaesthesia are given in Chapter 2.

5.3.2.2. Glibenclamide therapy

Mice were implanted with a 21-day slow-release subcutaneous 2.5mg glibenclamide or placebo pellet (Innovative Research of America; dose:

~4.8mg/kg/day). Details of the surgical procedure for subcutaneous implantation of slow-release pellets are given in Chapter 2.

5.3.3. ICV sulphonylurea therapy and sensitivity to anaesthesia

11-14 week-old nV59M mice and control littermates were tested for sensitivity to isoflurane anaesthesia before and after implantation with a subcutaneous osmotic mini-pump (Model 2004, 28-day infusion, 0.25µl/h flow rate; Alzet, Durect Corporation) filled with either 280µM glibenclamide in artificial cerebrospinal fluid (aCSF; composition given in Chapter 2) or vehicle (aCSF with 0.1% DMSO) connected to a cannula implanted into the right lateral ventricle of the brain. Details of the surgery are given in Chapter 2. A recovery period of one week was allowed between the surgery and the subsequent testing. All experiments were performed blinded to genotype of the animal and treatment given.

Cannula placement was confirmed histologically for all animals used; only mice with adequate placement were included for analysis. Details of the procedure for histological confirmation are given in Chapter 2.

5.3.4. Data analysis

Statistical analysis of data from male and female nV59M mice indicated no significant differences, so these data were pooled. Similarly, analysis of data from the three groups of control mice ($ROSA^{+/-}$, $Nes\text{-}cre^{+}$ and wild-type) indicated no significant differences, so these data were also pooled. When the data distribution permitted (i.e. fulfilled the criteria of normality and equality of variance), a One-Way ANOVA was performed. For multiple comparisons, a Bonferroni multiple comparison post-test was used. $P<0.05$ was considered statistically significant.

The data for isoflurane sensitivity pre- and post-glibenclamide treatment was analysed by means of a repeated-measures Two-way ANOVA with post-hoc Bonferroni multiple comparisons. Pre- and post-treatment time taken to lose the reflexes was treated as a within-subjects factor while the genotype (control versus nV59M) and the drug treatment (vehicle versus glibenclamide) were treated as between-subjects factors.

5.4. Results

5.4.1. nV59M mice have reduce sensitivity to halothane and isoflurane anaesthesia

When exposed to isoflurane anaesthesia, nV59M mice take ~30% longer than control littermates to lose their righting reflex (LORR, Fig. 5.1A), which is an indication of sedation. Furthermore, they take ~30% longer than control littermates to lose their hindpaw withdrawal reflex (LOWR, Fig. 5.1B), which is a sign of pain awareness. As an additional control, mice selectively expressing the Kir6.2-V59M mutation in myocytes (mV59M) were exposed to isoflurane anaesthesia. No difference was found between mV59M mice and control littermates for either LORR or LOWR (Fig. 5.1). Moreover, no differences were found between nV59M control littermates and mV59M mice (Fig. 5.1).

Interestingly, nV59M mice also required a higher volume of isoflurane to maintain anaesthesia; only 3 out of 16 nV59M mice (~19%) remained asleep during a 10-minute period when isoflurane was reduced to 1.5%. By contrast, 22 out of 24 (~92%) control littermates remained asleep under the same conditions (P<0.0001; Fisher's exact test, two-sided).

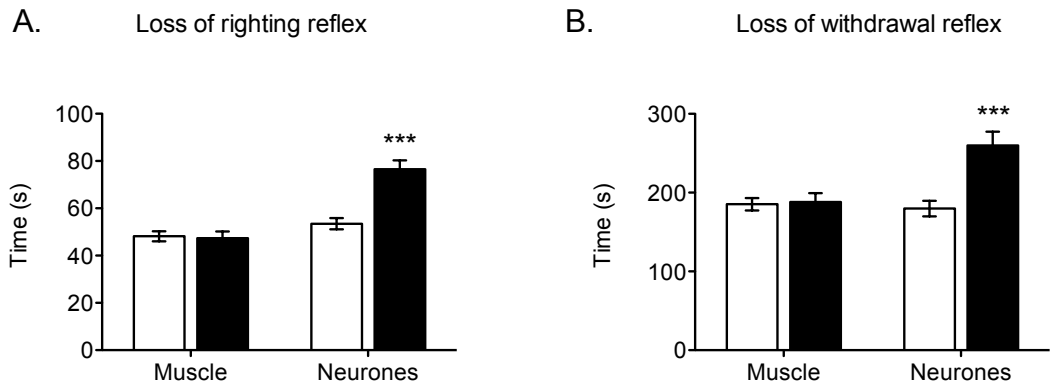

Figure 5.1: Sensitivity to isoflurane anaesthesia

Loss of (**A**) righting and (**B**) withdrawal reflexes in response to 2% isoflurane in 11-14 week-old mice. Mice selectively expressing the Kir6.2-V59M mutation (black bars) in either myocytes (mV59M; n=19) or neurones (nV59M; n=41) and control littermates (white bars) were used. For mV59M, control mice were a combination of Mck-Cre^{+} (n=11), wild-type (n=19), and ROSA$^{+/-}$ (n=21). For nV59M, control mice were a combination of Nes-cre^{+} (n= 18), wild-type (n=10), and ROSA$^{+/-}$ (n=27). All data are mean ± SEM. *** P<0.0001 [One-way ANOVA followed by Bonferroni multiple comparison post-test; test details given in Appendices 3 and 4].

In addition to isoflurane anaesthesia, nV59M mice were also exposed to halothane, another volatile anaesthetic. As Fig. 5.2 shows, nV59M mice also display impaired sensitivity to halothane. These mice took ~20% longer to lose their righting reflex (Fig. 5.2A) and ~35% longer to lose their withdrawal reflex (Fig. 5.2B) when compared to control mice.

5.4.2. Effect of subcutaneous glibenclamide therapy on isoflurane sensitivity

Although impaired sensitivity to general anaesthetics has not been described in human patients with activating K_{ATP} channel mutations so far, I was interested in determining whether this phenotype could be used to assess the effect of glibenclamide therapy on neurological function. I thus examined the response to isoflurane anaesthesia before and a week after implanting nV59M and control mice with either a placebo or a slow-release 2.5mg glibenclamide pellet.

There was no effect of either placebo or glibenclamide treatment on the LORR of control mice. In contrast, a significant decrease in the time taken to LORR was observed between pre- and post-treatment nV59M mice (Fig. 5.3A; P=0.036). However, no difference was observed between the two treatment groups (placebo and glibenclamide; Fig. 5.3A; P= 0.910), suggesting

subcutaneous glibenclamide therapy does not restore the impaired LORR in nV59M mice.

By contrast, a significant effect of glibenclamide treatment on the LOWR of nV59M mice was observed (P=0.018; Fig. 5.3B). Hence, subcutaneous glibenclamide therapy partially restored the altered LOWR in nV59M mice when compared to placebo-treated mice. Interestingly, there appears to be a slight decrease in the time taken to LOWR in glibenclamide-treated control mice: however, statistical significance was not reached (Fig. 5.3B).

5.4.3. Effect of intracranioventricular delivery of glibenclamide therapy on isoflurane sensitivity

In order to examine whether the failure of subcutaneous glibenclamide to restore LORR in nV59M mice was caused by an inability of the drug to cross the blood-brain barrier, mice were chronically treated with either 280μM glibenclamide or vehicle delivered into the right lateral ventricle via an intracranioventricular (ICV) cannula attached to an osmotic mini-pump. The response to isoflurane anaesthesia was examined before and a week after implanting nV59M and control mice with the ICV cannula and osmotic mini-pump.

As with the subcutaneous pellets, a significant decrease in the time taken to LORR was observed between pre- and post-ICV treatment nV59M mice (Fig. 5.4A; *P*= 0.025). However, no difference was observed between the two treatment groups (vehicle and glibenclamide; Fig. 5.4A; *P*= 0.536). No change in the time taken to LORR was observed for control mice (Fig. 5.4A).

Contrary to what was observed with subcutaneous glibenclamide therapy, ICV glibenclamide had no effect on LOWR in nV59M mice (Fig. 5.4B). There was also no difference in the time taken to LOWR in control mice.

5.5. Discussion

Despite their widespread use in clinical practice, the identity of the molecular targets of general anaesthetics has not been discovered yet. The proteins considered to be their most likely targets are ion channels as they are crucial for the regulation of synaptic transmission and membrane potentials in key regions of the central nervous system [262,279].

In this chapter, I have demonstrated that nV59M mice have impaired sensitivity to two common volatile anaesthetics, halothane and isoflurane, taking significantly longer than control littermates to lose their righting (LORR) and withdrawal (LOWR) reflexes when exposed to these compounds.

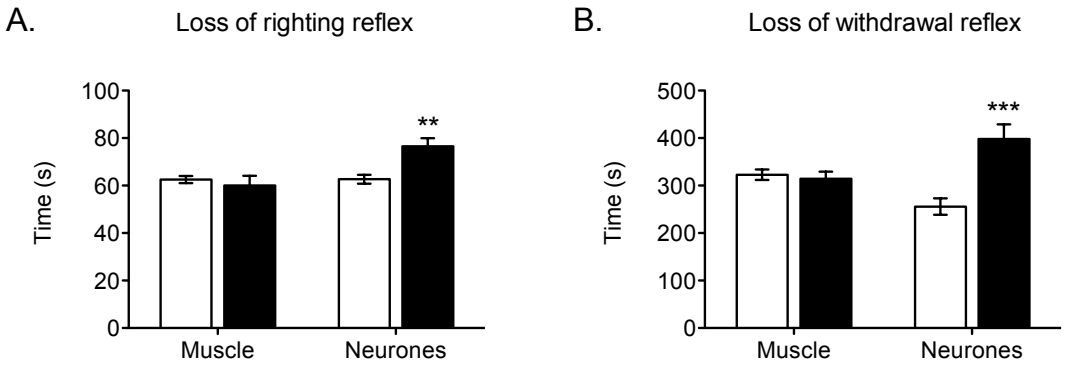

Figure 5.2: Sensitivity to halothane anaesthesia

Loss of (**A**) righting and (**B**) withdrawal reflexes in response to 2% halothane in 11-14 week-old mice. Mice selectively expressing the Kir6.2-V59M mutation (black bars) in either myocytes (mV59M; n=10) or neurones (nV59M; n=9) and control littermates (white bars) were used. For mV59M, control mice were a combination of Mck-Cre^{+} (n=9), wild-type (n=7), and ROSA$^{+/-}$ (n=6). For nV59M, control mice were a combination of Nes-cre^{+} (n=5), wild-type (n=2), and ROSA$^{+/-}$ (n=7). All data are mean ± SEM. ** P<0.001; *** P<0.0001 [One-way ANOVA followed by Bonferroni multiple comparison post-test; test details given in Appendices 5 and 6].

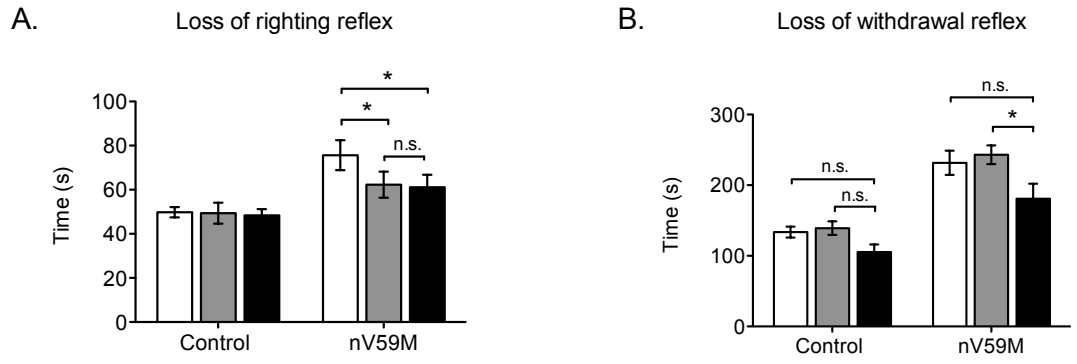

Figure 5.3: Effect of subcutaneous glibenclamide therapy on isoflurane anaesthesia

Subcutaneous implantation with a 2.5mg slow-release glibenclamide pellet does not restore impaired LORR in response to 2% isoflurane in nV59M mice (**A**), but it partially reverses impaired LOWR (**B**). Response to isoflurane anaesthesia was assessed before (white bars) and a week after implanting nV59M mice (n=24) and control littermates (wild-type, n=7; Nes-cre^{+}, n=5; ROSA$^{+/-}$, n=10) with either a placebo (grey bars) or 2.5mg glibenclamide (black bars) subcutaneous pellet. Half of the mice from each group were implanted with a placebo pellet and the other half with glibenclamide. All data are mean ± SEM. * P<0.05 [Repeated-measures Two-way ANOVA followed by Bonferroni multiple comparison post-test; test details given in Appendices 7 and 8].

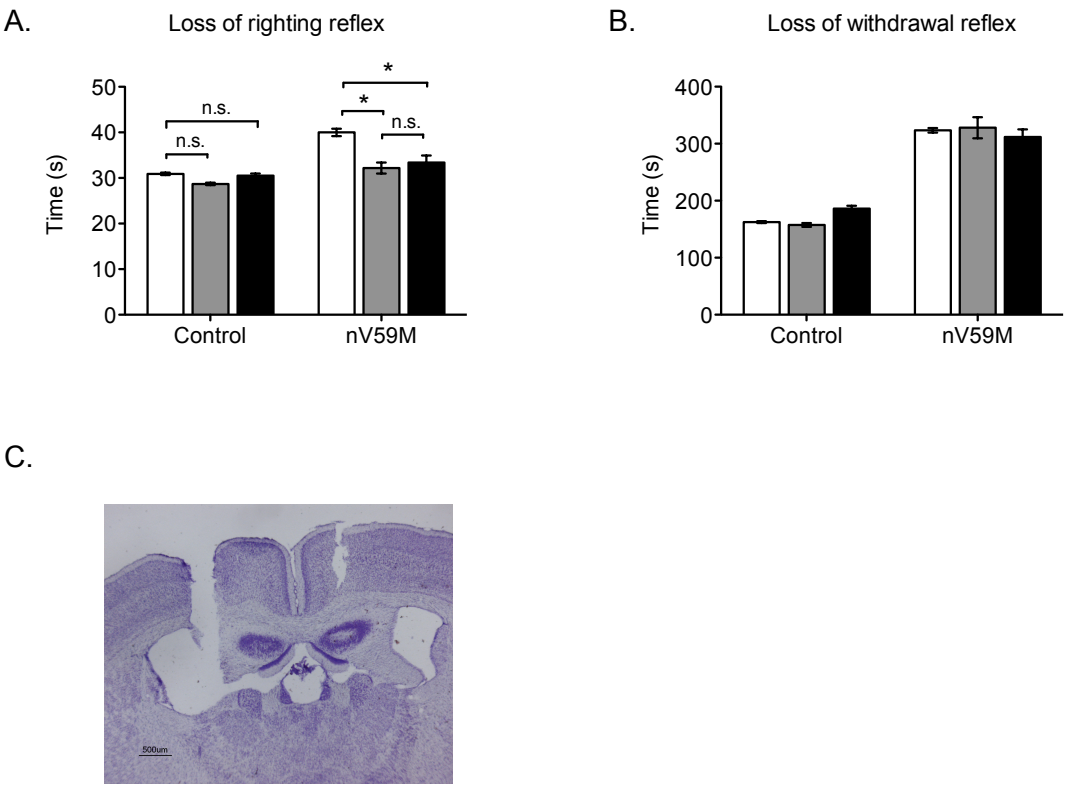

Figure 5.4: Effect of intracranioventricular glibenclamide on sensitivity to isoflurane anaesthesia

Intracranioventricular (ICV) delivery of 280µM glibenclamide does not restore impaired LORR (**A**) or LOWR (**B**) in response to 2% isoflurane in nV59M mice. Response to isoflurane anaesthesia was assessed before (white bars) and a week after implanting nV59M mice (n=12) and control littermates (wild-type, n=8; Nes-cre^{+}, n=8; ROSA$^{+/-}$, n=11) with an osmotic mini-pump and ICV cannula filled with either vehicle (artificial cerebrospinal fluid, aCSF; grey bars) or 280µM glibenclamide in aCSF (black bars). Half of the mice from each group were given vehicle and the other half glibenclamide. All data are mean ± SEM. n.s. not significant; * P<0.05 [Repeated Measures Two-way ANOVA followed by Bonferroni multiple comparison post-test; test details given in Appendix 9]. (**C**) Representative photo of Nissl stained coronal section from an ICV implanted mouse. Appropriate placement of the cannula into the right lateral ventricle was confirmed in all mice included for analysis.

5.5.1. nV59M mice take longer to lose their righting reflex in response to isoflurane and halothane anaesthesia

When exposed to 2% isoflurane, nV59M mice took approximately 30% longer than control mice to lose their righting reflex. Qualitatively similar results were obtained with halothane. In laboratory animals, this reflex is used as an indication of hypnosis or unconsciousness.

Although it is still not clear the specific brain region(s) that mediate anaesthesia-induced unconsciousness, most evidence points towards the deep brain structures, particularly the thalamus, hypothalamus, and pons [262,279]. These areas are known to be important in the regulation of arousal states and sleep [270]. Attention has focused on these areas as sleep states and general-anaesthesia states share electroencephalographic and behavioural features [262,270]. Furthermore, neuroimaging studies in anaesthetized human subjects have shown these regions are the first to reactivate upon returning consciousness [268]. Additionally, direct stimulation of these structures can reverse anaesthesia-induced unconsciousness in rats [280].

Interestingly, both the Kir6.2 and SUR1 subunits appear to be highly expressed in the thalamus and the pons [26], suggesting alteration of K_{ATP} channel function may affect the physiological functions of these brain regions.

Indeed, when the nV59M mice were placed in spontaneous activity threshold monitors for a period of 23 hours, not only were they active for considerably longer than control littermates, particularly in the dark phase, but unlike control mice, who returned to pre-lights-off activity levels approximately 3 hours prior to lights-on, nV59M mice did not return to pre-lights-off activity levels until 2-3 hours *after* lights were turned back on (Fig. 5.5). This suggests that nV59M mice may also have altered sleep regulation.

Based on these observations, it is tempting to suggest that expression of an activating K_{ATP} channel mutation in thalamic/pontine nuclei may affect initiation of sleep- and anaesthesia-induced unconsciousness.

5.5.2. nV59M mice take longer to lose their withdrawal reflex in response to isoflurane and halothane anaesthesia

In addition to the altered LORR, nV59M mice took approximately 30% longer to lose their withdrawal reflex when exposed to isoflurane and halothane anaesthesia. In laboratory animals, this reflex is used to assess anaesthesia-induce immobility in response to a noxious stimulus.

Anaesthesia-induced immobility is thought to be mediated at the spinal cord level, with a small degree of modulation by supraspinal regions [276]. Although little is known about the role of the K_{ATP} channel in spinal cord function,

experimental evidence has shown that K_{ATP} channels are expressed in the somata and axons of dorsal root ganglion neurones isolated from rats [281]. These channels are thought to be of the Kir6.2/SUR1 subtype and have been suggested to play a role in the physiological regulation of the resting membrane potential of primary afferent neurones [281].

However, the site of action for anaesthesia-mediated immobility is thought to be on the ventral portion of the spinal cord as pre-motor interneurones, ventral cord central pattern generator neurones and motoneurones are considerably more sensitive to volatile anaesthetic-induced depression than sensory neurones [282]. Furthermore, K_{ATP} channel expression has not yet been demonstrated in ventral horn neurones or motoneurones. Hence, it appears that impaired anaesthesia-induced immobility in nV59M mice is indirectly mediated by altered primary afferent function rather than by direct modulation at the putative site of general anaesthetic action.

Various studies of Kir6.2 knockout mice have suggested that K_{ATP} channels in peripheral sensory neurones play a role in nociception, hyperalgesia, and the development of neuropathic pain [281,283-286]. It is thus possible that nV59M mice have altered nociception rather than altered anaesthesia-induced immobility *per se*. However, experimental evidence suggests closing of the K_{ATP} channel is antinociceptive while my experimental data seems to indicate that activation of the K_{ATP} channel enhances nociception. Thus, further experiments are required to elucidate the effect of gain-of-function K_{ATP} channel mutations on

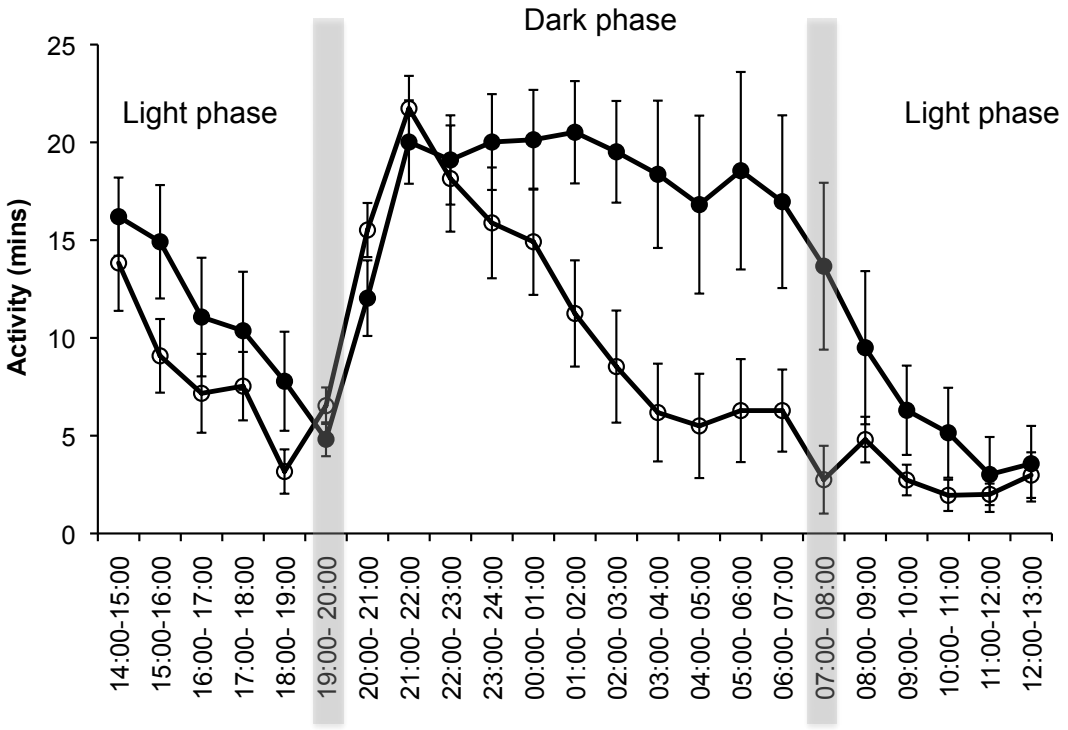

Figure 5.5: Spontaneous activity of nV59M mice and control littermates over a 23h period

Mean hourly spontaneous activity for nV59M mice (closed circles; n=21) and control littermates (open circles; WT: n=8; ROSA$^{+/-}$: n=19; Nes-Cre^{+}: n=13) over a 23-hour period. Lights were turned off at 19:00 and turned back on at 07:00 (indicated by the grey bars). Data are mean ± SEM.

nociception, particularly as the Kir6.2$^{-/-}$ mouse is a global knockout so contribution of deletion of the protein in other tissues cannot be discarded.

5.5.3. Subcutaneous glibenclamide therapy did not reverse the LORR deficit in nV59M mice, but it partially restored LOWR

Even though altered sensitivity to volatile anaesthetics has not been described in human iDEND/DEND syndrome patients so far, I wanted to establish whether this phenotype could be used to assess the effect of glibenclamide therapy on neurological function.

nV59M mice treated with glibenclamide delivered systemically (via subcutaneous slow-release pellets) took just as long as placebo-treated nV59M mice to lose their righting reflex. Interestingly, in both treatment groups, a decrease in the time taken to LORR was observed. It is possible that previous exposure to anaesthesia or surgery-induced stress may have affected the time taken to LORR. However, no changes were observed in the time taken to LORR for control littermates, which were exposed to the same procedure as the nV59M mice. Although it is not clear why the time taken to LORR decreased in nV59M mice after pellet implantation, the data seem to indicate that systemic glibenclamide therapy did not restore the deficit in LORR in nV59M mice as there was no difference in time taken to LORR between placebo- and glibenclamide-treated nV59M mice.

One possible explanation for the inability of glibenclamide therapy to restore LORR in nV59M mice is that the constitutive expression of the Kir6.2-V59M in nervous tissue triggers developmental adaptation leading to permanent (and irreversible) changes in the neuronal circuitry. This has been previously described for other neuronal mouse models where behavioural phenotypes reflected altered gene expression induced at a prior developmental stage, rather than at the period of interest [287,288]. This possibility will be further explored in Chapter 6.

It is also possible that systemically delivered glibenclamide was unable to restore LORR in nV59M mice because of an inability of the drug to cross the blood-brain barrier (BBB). This has been previously demonstrated with tolbutamide, another sulphonylurea [289]. This possibility will be further explored in Chapter 7.

In the case of LOWR, subcutaneous glibenclamide significantly reduced the time taken to lose the withdrawal reflex in nV59M mice. It did not fully restore the LOWR, as this still remained higher than in control mice. These results suggest that the K_{ATP} channel is involved in either anaesthetic-induced immobility or nociception. As was mentioned in Section 5.5.2, the latter option is more plausible as previous work by various research groups support the role of the K_{ATP} channel in pain perception. Further work is required to elucidate the effect of gain-of-function K_{ATP} channel mutations on nociception,

particularly as this may be of clinical importance for human patients with K_{ATP} channel mutations.

The fact that systemic glibenclamide therapy partially restored the LOWR in nV59M mice further supports the involvement of K_{ATP} channels expressed in primary afferent neurones as these lie outside of the BBB (unlike the putative spinal K_{ATP} channel). If, like tolbutamide, glibenclamide were unable to cross the blood-brain barrier, it would be unable to inhibit any putative spinal K_{ATP} channels. Data presented in Chapter 7 suggests that the drug does not cross the BBB in measureable amounts when given subcutaneously, providing some evidence in favour of a role for the K_{ATP} channel in peripheral neurones in nociception.

5.5.4. Intracranioventricular glibenclamide delivery had no effect on impaired anaesthesia sensitivity in nV59M mice

In order to address the possibility that glibenclamide was unable to restore LORR in nV59M mice because it could not cross the BBB, I used intracranioventricular cannulae connected to osmotic mini-pumps to deliver glibenclamide (or vehicle) directly into the right lateral ventricle, effectively bypassing the BBB.

Surprisingly, ICV glibenclamide was also unable to restore LORR in nV59M mice, as it took the same length of time for vehicle- and glibenclamide-treated nV59M mice to lose their righting reflex. As with systemically delivered glibenclamide, a reduction in the time taken to LORR was observed in both vehicle- and glibenclamide-treated nV59M mice. It is not clear why this is the case, particularly as time to LORR remained unchanged in control mice post-surgery. Overall, these results support the possibility that the altered LORR in nV59M mice is developmental in origin. However, I cannot exclude the possibility that the glibenclamide concentration used was insufficient to fully close mutant K_{ATP} channels.

In contrast to systemically delivered glibenclamide, ICV delivery did not reduce the time taken to LOWR in nV59M mice. This supports the involvement of peripheral sensory neuron K_{ATP} channels in the altered LOWR, as glibenclamide delivered directly into the brain would be unable to reach these peripheral targets.

A further explanation for the inability of ICV delivered glibenclamide to restore LORR in nV59M is that the drug may be actively transported out of the BBB, as is the case with tolbutamide [289]. If this were the case, the efflux rate could be faster than the rate at which the solution is pumped into the brain, making it difficult for glibenclamide to reach a high enough concentration at the site of action, both in terms of the altered LORR and LOWR (if it were mediated by spinal K_{ATP} channels).

If glibenclamide were to be actively transported out of the brain and into the periphery, one may expect a reduction in LOWR. However, this was not the case, most likely because the concentration of glibenclamide reaching the periphery would not be high enough to inhibit its target. Although the concentration of glibenclamide being pumped into the lateral ventricle is significantly high (~280μM), the volume being injected is rather low (~0.25μl per hour). Thus, once it is redistributed in the plasma, the circulating glibenclamide concentration would be negligible. This will be further addressed in Chapter 7.

5.5.5. The K_{ATP} channel: target for volatile anaesthetics?

The most likely molecular targets for general anaesthetics are ion channels. A plethora of knockout and transgenic mice for different ion channels have been generated in an attempt to identify *the* molecular target for anaesthetics [262,290-292]. Although many interesting anaesthetic phenotypes have been observed in these mice, it has not been possible to identify specific ion channels that render mice fully resistant to anaesthesia. Furthermore, it has become apparent that anaesthetic agents can modulate the function of many ion channels to different degrees and that no two anaesthetic agents have the same effect on the same target [262,279].

The results presented in this chapter open the door to the possibility that the K_{ATP} channel may be a target for volatile anaesthetics. Indeed, it has previously been shown that volatile anaesthetics impair insulin secretion by activating the pancreatic β-cell K_{ATP} channel [293,294]. However, a study by Ishiwa and colleagues showed that isoflurane had no significant effects on K_{ATP} currents recorded from principal neurones in substantia nigra pars compacta [295]. This would suggest that the altered sensitivity to volatile anaesthetics in nV59M mice are caused by changes in the neuro-circuitry of the pathways targeted by general anaesthesia rather than by an impairment in a putative direct interaction between volatile anaesthetics and the K_{ATP} channels.

Chapter 6: Inducible global mouse model of iDEND

6.1. Summary

1. The Ubiquitin-Cre-ER line was crossed with ROSA mice to generate an inducible global mouse model of iDEND syndrome (Ubi-ROSA mice).

2. Surprisingly, Ubi-ROSA mice failed to develop diabetes upon administration of tamoxifen to induce Kir6.2-V59M gene expression.

3. Kir6.2-V59M mRNA was found in brain and pancreatic tissue of Ubi-ROSA mice. However, expression levels seemed to be much higher in brain tissue than pancreatic tissue.

4. Ubi-ROSA mice exhibited impaired LOWR, but not LORR, when exposed to isoflurane anaesthesia following gene induction.

5. Ubi-ROSA-DN mice, which have a different activating K_{ATP} channel mutation, also exhibited impaired LOWR, but not LORR, in response to isoflurane anaesthesia. The altered LOWR appeared to be partially restored by systemic administration of glibenclamide.

6.2. Introduction

Gain-of-function mutations in the genes encoding either of the subunits of the K_{ATP} channel result in neonatal diabetes [4,5,136]. In approximately 25% of cases, the diabetes is accompanied by neurological symptoms including developmental delay, muscle hypotonia, balance and coordination problems, and in some cases, epilepsy [5,128]. The discovery that activating K_{ATP} channel mutations cause ND led to a paradigm shift in the management of the disease, with sulphonylurea drugs becoming the treatment of choice for patients with these mutations [6]. This change in treatment has resulted in significantly improved glycaemic control and a better quality of life when compared to insulin therapy [6,217,218].

As the composition of the principal neuronal K_{ATP} channel is thought to be the same as that found in pancreatic β-cells (Kir6.2-SUR1) [23,296], it was hoped that sulphonylurea therapy would also be able to improve the neurological symptoms of iDEND/DEND patients [6,217]. However, this has not been the case. In some patients, limited improvement of neurological function is observed after transition to glibenclamide therapy [151,189,221,225,226], but function has not been fully restored in any patients. It is not known if this failure is caused by an inability of glibenclamide (the sulphonylurea of choice for ND) to reach high enough levels in the brain or if excess K_{ATP} channel activity during

development causes permanent alterations in brain circuitry. The latter possibility will be investigated in this chapter.

6.2.1. Mouse models: constitutive versus inducible expression

Mouse models with constitutive expression of a mutation have been extremely useful for studying the physiological function of many proteins, with the K_{ATP} channel being no exception. However, many of these models are not physiological, as expression of the mutated protein is determined by an exogenous promoter rather than the endogenous promoter of the protein of interest [288,297]. This can result in activation of compensatory mechanisms that are not present in wild-type animals, particularly if the endogenous promoter and the promoter used to drive expression are activated at different stages of development. Indeed, this has been previously described for other mouse models, particularly those with neuronal expression of a mutation, where behavioural phenotypes may reflect altered gene expression induced at an earlier developmental stage than at the period of interest [287,288].

In Chapter 5, I demonstrated that mice with selective neuronal expression of the Kir6.2-V59M mutation have an altered loss of righting reflex (LORR) when exposed to isoflurane anaesthesia. It was hoped that administration of glibenclamide would restore LORR in nV59M mice, however this was not the case. One possible explanation for this finding is that constitutive expression

of the Kir6.2-V59M mutation in nervous tissue triggers developmental adaptations that lead to permanent and irreversible changes in neuronal circuitry.

This possibility can be addressed using mouse lines with inducible Cre-promoters that grant spatial and temporal control over the expression of specific mutations. One of the most widely used inducible systems is based on a modified Cre-recombinase, which remains non-functional until a pharmacological agent is administered [297]. In this system, Cre-recombinase is fused to a mutated nuclear oestrogen receptor (ER), which is insensitive to endogenous oestrogen. As a consequence, the fusion protein is sequestrated in the cytoplasm, preventing Cre activity (Fig.6.1A) [298,299]. Upon administration of tamoxifen, a synthetic oestrogen agonist, the Cre-ER fusion complex migrates into the nucleus, enabling Cre to ablate its target (Fig.6.1B).

Use of an inducible Cre-promoter line should enable me to determine whether the altered LORR observed in nV59M mice is due to developmental compensation (for the presence of the Kir6.2-V59M mutation). Furthermore, it could help address whether the neurological symptoms observed in human iDEND/DEND patients are caused by a direct effect of the mutation on neuronal function *per se* or if they are partially caused by alterations in brain circuitry due to excess K_{ATP} channel activity during development.

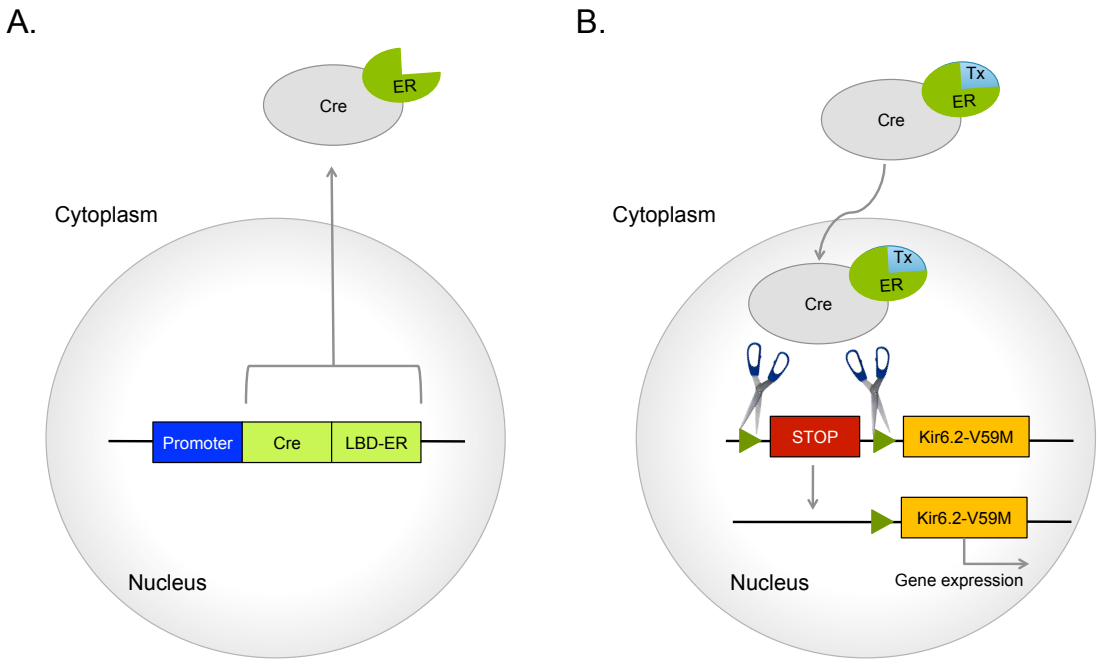

Figure 6.1: The Cre-ER-loxP system

(**A**) In the absence of tamoxifen, the Cre-LBD-ER fusion complex (LBD-ER: ligand-binding domain of the oestrogen receptor), is inactivated and confined to the cytoplasm. (**B**) Upon binding of tamoxifen to the LBD-ER, the Cre-ER fusion protein is translocated into the nucleus, where the loxP-flanked STOP sequence is excised by the Cre-recombinase, allowing expression of the Kir6.2-V59M mutation.

6.2.2. An inducible mouse model with global expression of the Kir6.2-V59M mutation

In order to assess the effect of developmental expression of the Kir6.2-V59M mutation, I activated the mutant Kir6.2 gene in adult life. I used a tamoxifen-inducible Cre-recombinase line, under the control of the human ubiquitin-C promoter (Ubi-Cre-ER mice)[230]: because ubiquitin is believed to show global expression I anticipated the mutant gene would be expressed in all tissues, so generating an inducible model of iDEND syndrome (Ubi-ROSA line). Our group has previously used a pancreatic β-cell specific tamoxifen-inducible Cre-line to successfully express the Kir6.2-V59M mutation during adulthood (K. Shimomura, *unpublished*). This resulted in overt diabetes (free-fed blood glucose >20mM) within 2 days of tamoxifen injection.

Use of the ubiquitin-Cre-ER mouse line was expected to allow temporally controlled expression of the mutation in a wide range of tissues including brain, pancreas, muscle, intestine, and liver [230]. Using a promoter with global expression should allow targeting of all neurones (in a similar way to the nestin promoter), with the added advantage that it permits tracking of recombination/expression of the mutation by the development of diabetes (as the mutation is expected to be expressed in pancreatic β-cells).

In this chapter, I used the Ubiquitin-ROSA line to determine if the altered loss of righting reflex associated with neuronal expression of the Kir6.2-V59M mutation is developmental in origin. I also assessed the feasibility of using this line as an inducible global mouse model of iDEND syndrome.

6.3. Methods

6.3.1. Generation of mice

Mice heterozygous for the Kir6.2-V59M mutation were used in these studies. Details of these mice are given in Chapter 2. In addition, I used a second mouse line in which the Kir6.2-V59M mutation was expressed under the control of the CAG (chicken beta-actin promoter with cytomegalovirus enhancer) promoter. Details of these mice, which are referred to as ROSA-CAGS in this chapter, are given in Chapter 2.

Mice heterozygous for the Kir6.2-[K185Q, ΔN30] mutation were also used for these studies. Details of these mice, which are referred to as ROSA-DN in this chapter, are given in Chapter 2.

The ROSA, ROSA-CAGS and ROSA-DN mice were crossed with mice expressing a modified Cre-recombinase fused to a mutant oestrogen receptor (ER) ligand-binding domain under the control of the human ubiquitin C

promoter (Ubi-cre-ER, stock name B6.Cg-Tg(UBC-cre/ERT2)1Ejb/J #008085; Jackson Laboratory) [230]. The Cre-ER fusion protein is selectively activated only in the presence of tamoxifen, but not oestrogen [230,300]. Use of the Ubi-cre-ER mice was predicted to produce global expression of the mutation as well as allowing temporal control over expression [230].

The ROSA-V59M, ROSA-CAGS, ROSA-DN and Ubi-cre-ER lines were all on a pure C57Bl6/J line. Details of the genotyping protocols and primers used for all lines are given in Chapter 2. Control littermates (Ubi-Cre-ER, ROSA, ROSA-DN or ROSA-CAGS, and WT) were used in all experiments.

6.3.2. Transgene induction

Kir6.2-V59M or Kir6.2-[K185Q, ΔN30] expression was induced at 12 weeks by a single subcutaneous injection of 0.4ml tamoxifen (20mg/ml; Sigma) dissolved in corn oil (Sigma). Both mutant and control littermates were injected with the tamoxifen.

6.3.3. Blood glucose and body weight monitoring

Mouse body weight was measured daily on scales calibrated to 0.01g. Free-fed plasma glucose levels were monitored daily, using the FreeStyle Lite

Blood Glucose Monitoring System (Abbott). Measurements were made on Ubi-ROSA, Ubi-ROSA-CAGS and Ubi-ROSA-DN mice as well as control littermates for up to 4 days before and up to 10 days after gene induction. For mice administered glibenclamide (subcutaneously or intracranioventricularly), measurements were also made up to 5 days after the surgical procedure.

6.3.4. Molecular biology

Details of the protocols used for semi-quantitative and real-time quantitative PCR (primer sequences, reaction settings, etc) are given in Chapter 2.

6.3.5. Sensitivity to isoflurane anaesthesia

Details of the method used for assessment of sensitivity to isoflurane anaesthesia are given in Chapter 2. Sensitivity was tested on Ubi-ROSA and Ubi-ROSA-DN mice a day before and 7 days after transgene induction by administration of tamoxifen.

6.3.6. Implantation of subcutaneous glibenclamide pellets

Ubi-ROSA and Ubi-ROSA-DN mice and their control littermates were tested for sensitivity to isoflurane anaesthesia before and after implantation with a 21-day slow-release subcutaneous 2.5mg glibenclamide or placebo pellet (Innovative Research of America; dose: ~4.8mg/kg/day) at 11-14 weeks of age. Details of the surgical procedure are given in Chapter 2. A recovery period of one week was allowed between the surgery and the subsequent testing. All experiments were performed blinded to genotype of the animal and treatment given.

6.3.7. Intracranioventricular delivery of glibenclamide

11-14 week-old Ubi-ROSA-DN mice and control littermates were tested for sensitivity to isoflurane anaesthesia before and after implantation with a subcutaneous osmotic mini-pump (Alzet, Durect Corporation; model 2004, 28-day infusion, 0.25µl/h flow rate) filled with either 280µM glibenclamide in artificial cerebrospinal fluid (aCSF; composition given in Chapter 2) or vehicle (aCSF with 0.1% DMSO) connected to a cannula implanted into the right lateral ventricle of the brain. Details of the surgical procedure are given in Chapter 2. A recovery period of one week was allowed between the surgery

and the subsequent testing. All experiments were performed blinded to genotype of the animal and treatment given.

Cannula placement was confirmed histologically for all animals used; only mice with adequate placement were included for analysis. Details of the procedure for histological confirmation are given in Chapter 2.

6.3.8. Data analysis

Statistical analysis of data from male and female mice indicated no significant differences, so these data were pooled. Similarly, analysis of data from the three groups of control mice ($ROSA^{+/-}$, Ubi-cre-ER^{+} and wild-type) indicated no significant differences, so these data were also pooled. When the data distribution permitted (i.e. fulfilled the criteria of normality and equality of variance), a Student's t-test or a One-Way ANOVA were performed. Otherwise, data were analysed using a non-parametric test, the Mann-Whitney U-test or the Kruskal-Wallis One-Way ANOVA on Ranks. For multiple comparisons, a Bonferroni multiple comparison post-test was used. $P<0.05$ was considered statistically significant.

The data for isoflurane sensitivity pre- and post-tamoxifen treatment was analysed by means of a repeated-measures ANOVA. Pre- and post-treatment time taken to lose the reflexes was treated as a within-subjects factor while

genotype (control versus Ubi-ROSA or Ubi-ROSA-DN) was treated as a between-subjects factor.

Similarly, the data for isoflurane sensitivity pre- and post-glibenclamide treatment was analysed by means of a repeated-measures Two-way ANOVA with post-hoc Bonferroni multiple comparisons. Pre- and post-treatment time taken to lose the reflexes was treated as a within-subjects factor while the genotype (control versus Ubi-ROSA or Ubi-ROSA-DN) and the drug treatment (vehicle versus glibenclamide) were treated as between-subjects factors.

6.4. Results

6.4.1. Ubi-ROSA mice did not develop diabetes

Prior to gene induction by tamoxifen, the blood glucose levels of Ubi-ROSA mice and control littermates were monitored daily over a 4-day period to establish their free-fed blood glucose baseline. As Fig. 6.2 shows, Ubi-ROSA and control littermates had similar free-fed blood glucose levels (7.9±0.1mM, n=10; and 7.4±0.1mM, n=14; respectively) before tamoxifen injection.

The tamoxifen injection was expected to activate the Cre-recombinase, which would delete the upstream stop codon and lead to expression of the Kir6.2-V59M mutation in pancreatic β-cells. This would induce diabetes, which is

defined as a mouse having a blood glucose level higher than 20mM, in Ubi-ROSA mice but not control littermates. Daily blood glucose monitoring was conducted over a 4-day period after tamoxifen injection: as Fig. 6.2A shows, the blood glucose levels of Ubi-ROSA mice did not go above 10mM despite receiving a tamoxifen dose sufficient to induce diabetes (i.e. blood glucose level higher than 20mM) in an inducible pancreatic β-cell specific ROSA-V59M mouse within 2 days of tamoxifen injection (K. Shimomura & M. Iberl, *unpublished*).

A second ROSA-V59M line (ROSA-CAGS mice), which has a CAG promoter to drive overexpression, was crossed with the Ubi-Cre-ER line in an attempt to determine why the Ubi-ROSA mice failed to express diabetes. However, as Fig. 6.3B shows, Ubi-ROSA-CAGS mice did not become diabetic either. These mice were injected up to 4 times with tamoxifen in case a higher amount of drug was needed for adequate recombination. Nonetheless, as Fig. 6.3A shows, repetitive tamoxifen injection did not trigger diabetes in Ubi-ROSA-CAGS mice.

I also crossed a third ROSA line with the Ubi-Cre-ER. These mice, Ubi-ROSA-DN, express a stronger mutation (Kir6.2-[K185QΔN30]) under the control of the CAG promoter. Despite this, the mice failed to express diabetes after tamoxifen injection (Fig. 6.3C).

Administration of tamoxifen had no effect on the body weight of Ubi-ROSA, Ubi-ROSA-CAGS, Ubi-ROSA-DN mice or their respective control littermates (Fig. 6.4).

6.4.2. Kir6.2 and GFP expression in brain and pancreas

The expression pattern of wild-type and V59M Kir6.2 mRNA was determined in control (wild-type, $ROSA^{+/-}$ and Ubi-cre-ER^{+}) and Ubi-ROSA mice using semi-quantitative PCR. RNA was extracted from pancreatic and brain tissue of control and Ubi-ROSA mice and reverse transcribed into cDNA. A second aliquot of RNA was processed simultaneously, but no reverse transcriptase was added, to confirm absence of genomic DNA contamination (Fig. 6.5A). Kir6.2 transcripts were amplified by PCR, digested with BtsCI and viewed on an agarose gel.

Introduction of the V59M mutation removes a unique BtsCI restriction site, which prevents cleavage of Kir6.2 cDNA. Hence, the presence of two bands on the agarose gel indicates the presence of WT-Kir6.2 mRNA alone while three bands indicates the presence of both WT and mutant Kir6.2 mRNA. As Figure 6.5B shows, Kir6.2-V59M mRNA is expressed in brain tissue from Ubi-ROSA and not control mice. Kir6.2-V59M mRNA also appears to be expressed in pancreatic tissue from Ubi-ROSA and not control mice, as the top band (i.e. undigested PCR product) was only present in the Ubi-ROSA

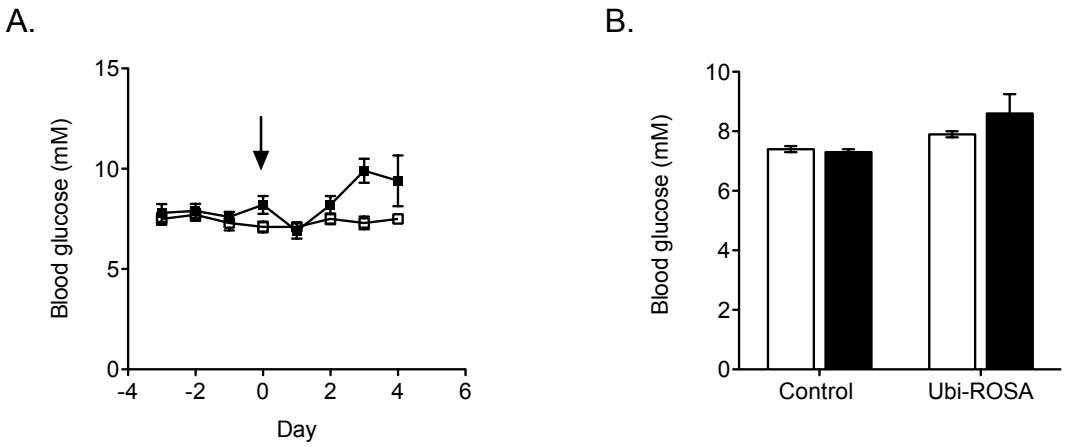

Figure 6.2: Blood glucose monitoring Ubi-ROSA mice

(**A**) Mean ± SEM daily free-fed blood glucose for Ubi-ROSA (closed squares; n=10) and control littermates (open squares; WT: n=7, Ubi-cre-ER^{+}: n=3, ROSA$^{+/-}$: n=4) prior to (days -3 to 0) and after (days 1 to 4) subcutaneous injection with tamoxifen (indicated by the arrow; day 0) to induce transgene expression. (**B**) Mean ± SEM blood glucose for Ubi-ROSA (n=10) and control littermates (n=14) over a 4 day period before (white bars) and a 4 day period after (black bars) tamoxifen injection.

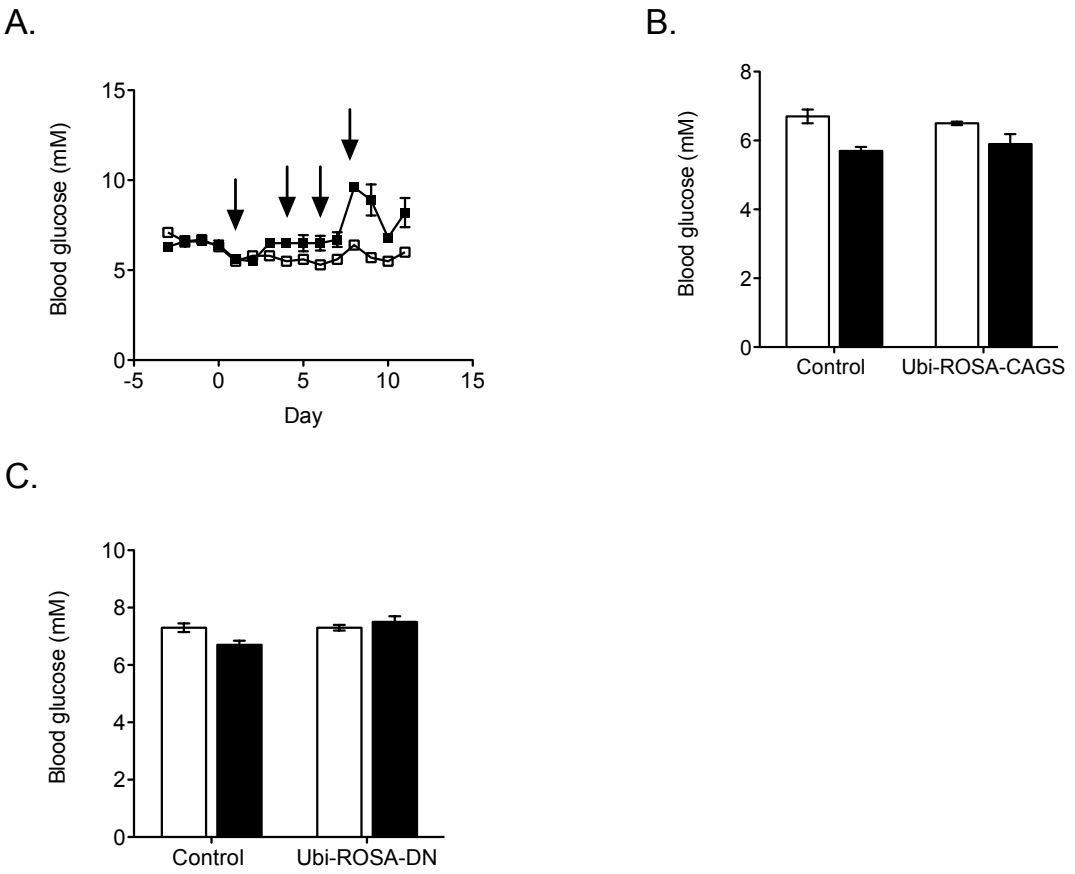

Figure 6.3: Blood glucose monitoring Ubi-ROSA-CAGS and Ubi-ROSA-DN mice

(**A**) Mean ± SEM daily blood glucose for Ubi-ROSA-CAGS (closed squares; n=6) and control littermates (open squares; n=14; WT: n=4; Ubi-cre-ER^{+}: n=5; ROSA-CAGS$^{+/-}$: n=7) prior to (days -3 to 0) and after repetitive subcutaneous injection with tamoxifen (indicated by the arrows; days 0, 3, 5 and 7) to induce transgene expression. (**B**) Mean ± SEM blood glucose for Ubi-ROSA-CAGS (n=6) and control littermates (n=16) over a 4 day period before (white bars) and a 4 day period after (black bars) tamoxifen injection. (**C**) Mean ± SEM blood glucose for Ubi-ROSA-DN (n=20) and control littermates (WT: n=9; Ubi-cre-ER^{+}: n=12; ROSA-DN$^{+/-}$: n=14) over a 4 day period before (white bars) and a 4 day period after (black bars) tamoxifen injection.

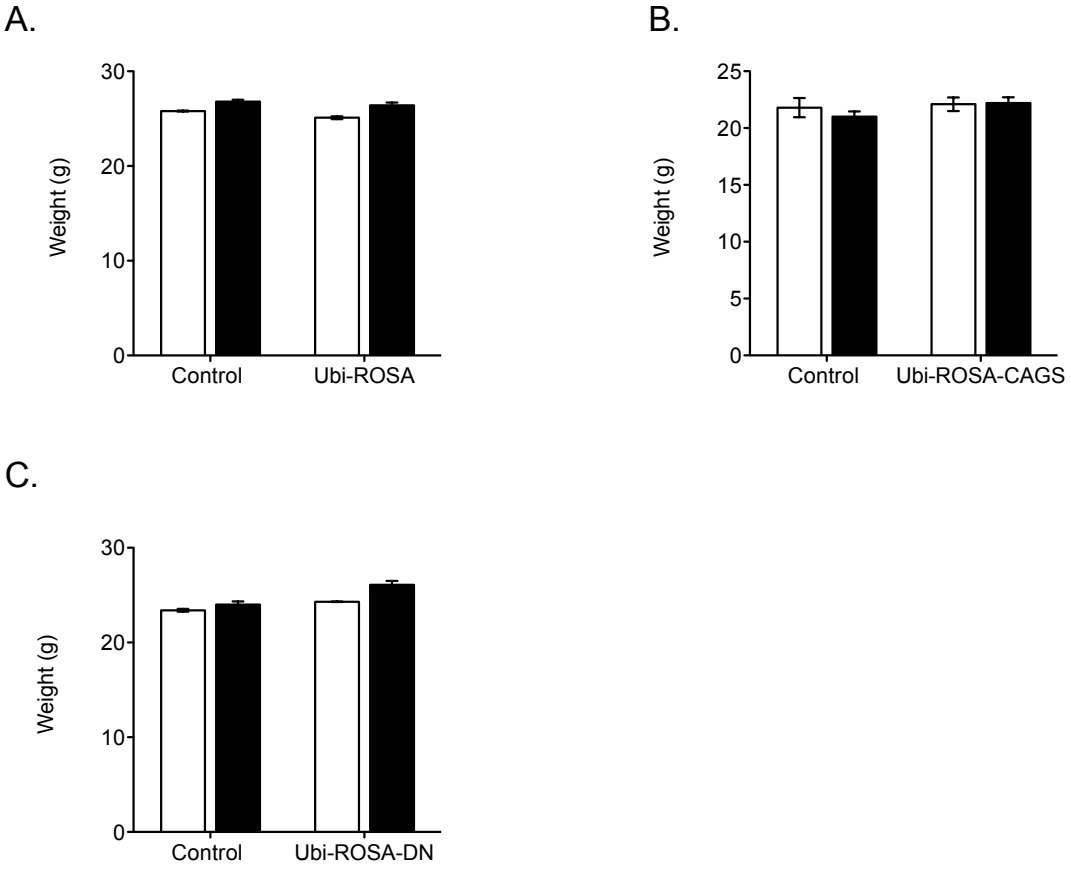

Figure 6.4: Body weight monitoring Ubi-ROSA, Ubi-ROSA-CAGS and Ubi-ROSA-DN mice

(**A**) Mean ± SEM body weight for Ubi-ROSA (n=10) and control littermates (n=16; WT: n=7, Ubi-cre-ER^{+}: n=3, ROSA$^{+/-}$: n=4) over a 4 day period before (white bars) and a 4 day period after (black bars) tamoxifen injection. (**B**) Mean ± SEM body weight for Ubi-ROSA-CAGS (n=6) and control littermates (WT: n=4; Ubi-cre-ER^{+}: n=5; ROSA-CAGS$^{+/-}$: n=7) over a 4 day period before (white bars) and a 4 day period after (black bars) tamoxifen injection. (**C**) Mean ± SEM body weight for Ubi-ROSA-DN (n=20) and control littermates (n=35; WT: n=9; Ubi-cre-ER^{+}: n=12; ROSA-DN$^{+/-}$: n=14) over a 4 day period before (white bars) and a 4 day period after (black bars) tamoxifen injection.

samples. The mRNA isolated from pancreas from Ubi-ROSA and control mice was degraded (as assessed by the Agilent Bioanalyser), which may explain the faintness of the WT bands in the agarose gel.

Quantitative PCR was carried out to determine the relative amounts of Kir6.2, GFP and SUR1 mRNA expression in pancreatic and brain tissue extracted from control and Ubi-ROSA mice. The amount of Kir6.2, GFP and SUR1 transcript was determined relative to a panel of house-keeping genes: HPRT1, HSPA8 and ACTB.

As Figure 6.6A shows, Kir6.2 expression was two-fold higher in brains of Ubi-ROSA mice compared to control mice. By contrast, no difference was observed for Kir6.2 expression in pancreatic tissue.

GFP expression was also quantified as the Kir6.2-V59M transcript contains a downstream IRES followed by GFP so that the level of GFP expression gives an indication of the amount of Kir6.2-V59M expression. As Figure 6.6B shows, GFP was highly expressed in the brains of Ubi-ROSA mice. There also was a significantly greater amount of GFP in pancreatic tissue of Ubi-ROSA mice than WT mice. However, the increase was very modest when compared to the differences observed with brain tissue (Fig. 6.6B).

SUR1 mRNA expression was unchanged in pancreatic and brain tissue of Ubi-ROSA mice (Fig. 6.6C). There was a slight increase in the SUR1

expression in brain tissue of Ubi-ROSA mice, but this was not statistically significant.

6.4.3. Isoflurane sensitivity of Ubi-ROSA and Ubi-ROSA-DN mice

The sensitivity to isoflurane anaesthesia was tested in Ubi-ROSA and Ubi-ROSA-DN mice a day before and 4 days after gene induction. As Fig. 6.7A shows, there was no difference in the time taken for loss of the righting reflex (LORR) between Ubi-ROSA and control mice prior to tamoxifen injection. There was also no difference in LORR between these two groups after gene induction. Interestingly, an increase in the time taken to LORR was observed for both groups after injection with tamoxifen (Appendix 10).

As with the LORR, no difference in the time taken for loss of the withdrawal reflex (LOWR) was observed between control and Ubi-ROSA mice prior to tamoxifen injection (Fig. 6.7B). However, a significant increase in time taken to LOWR was observed for the Ubi-ROSA mice following gene induction (Appendix 10). No difference was seen in control mice after tamoxifen injection.

Similar results, both in terms of LORR and LOWR, were obtained with the Ubi-ROSA-DN mice (Fig. 6.7C-D; Appendix 11).

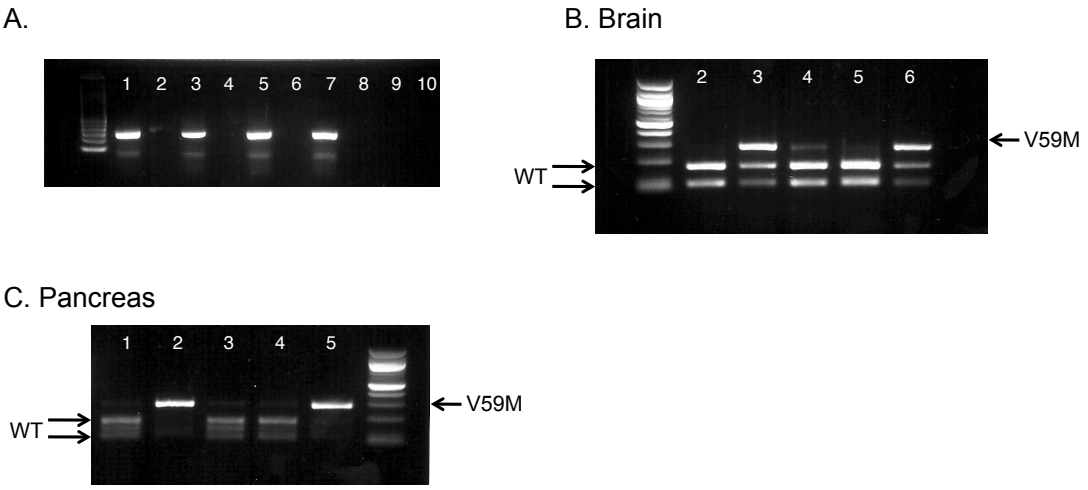

Figure 6.5: Kir6.2 expression in adult Ubi-ROSA mice

(**A**) Identical RNA aliquots from pancreatic tissue (lanes 1-4) and brain tissue (lanes 5-8) from control (lanes 1-2 and 5-6) or Ubi-ROSA (lanes 3-4 and 7-8) mice were processed in a reverse transcription reaction with reverse transcriptase included (RT+; lanes 1, 3, 5, 7, 9) or omitted (RT-; lanes 2, 4, 6, 8, 10). Amplification of the Kir6.2 transcript was only seen in RT+ samples, indicating there was little genomic DNA contaminating the RNA samples. Lanes 9-10 are nuclease-free water controls. (**B**) Kir6.2 RNA expression in brain tissue isolated from Ubi-ROSA (lanes 3 and 6) or control (lanes 2, 4 and 5) mice. Wild-type (WT), but not mutant (V59M), Kir6.2 cDNA is digested by restriction enzyme BtsCI, hence two bands indicates the presence of WT Kir6.2 only while three bands indicates both WT and V59M mutant Kir6.2 are present. (**C**) Kir6.2 RNA expression in pancreatic tissue isolated from Ubi-ROSA (lanes 2 and 5) or control (lanes 1, 3 and 4) mice. Wild-type (WT), but not mutant (V59M), Kir6.2 cDNA is digested by restriction enzyme BtsCI, hence two bands indicates the presence of WT Kir6.2 only while three bands indicates both WT and V59M mutant Kir6.2 are present. Data are representative of experiments on 5 control and 5 Ubi-ROSA mice.

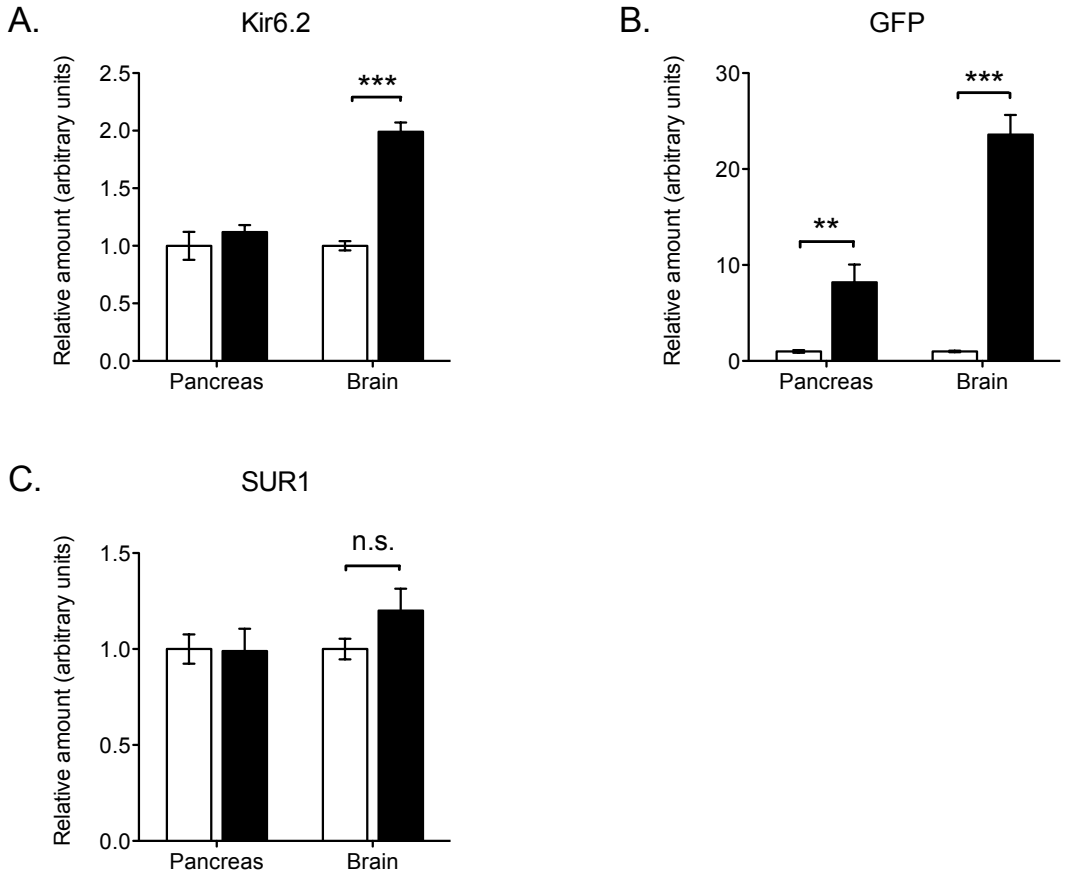

Figure 6.6: Relative expression of Kir6.2, GFP and SUR in pancreas and brain

Quantitative PCR showing expression of (**A**) Kir6.2, (**B**) GFP, and (**C**) SUR1 in pancreas and brain of control (n=5) and Ubi-ROSA mice (n=5), relative to a panel of house-keeping genes. Data are mean ± SEM. n.s. not significant; ** $P<0.01$; *** $P<0.0001$ [Unpaired Student's t-test].

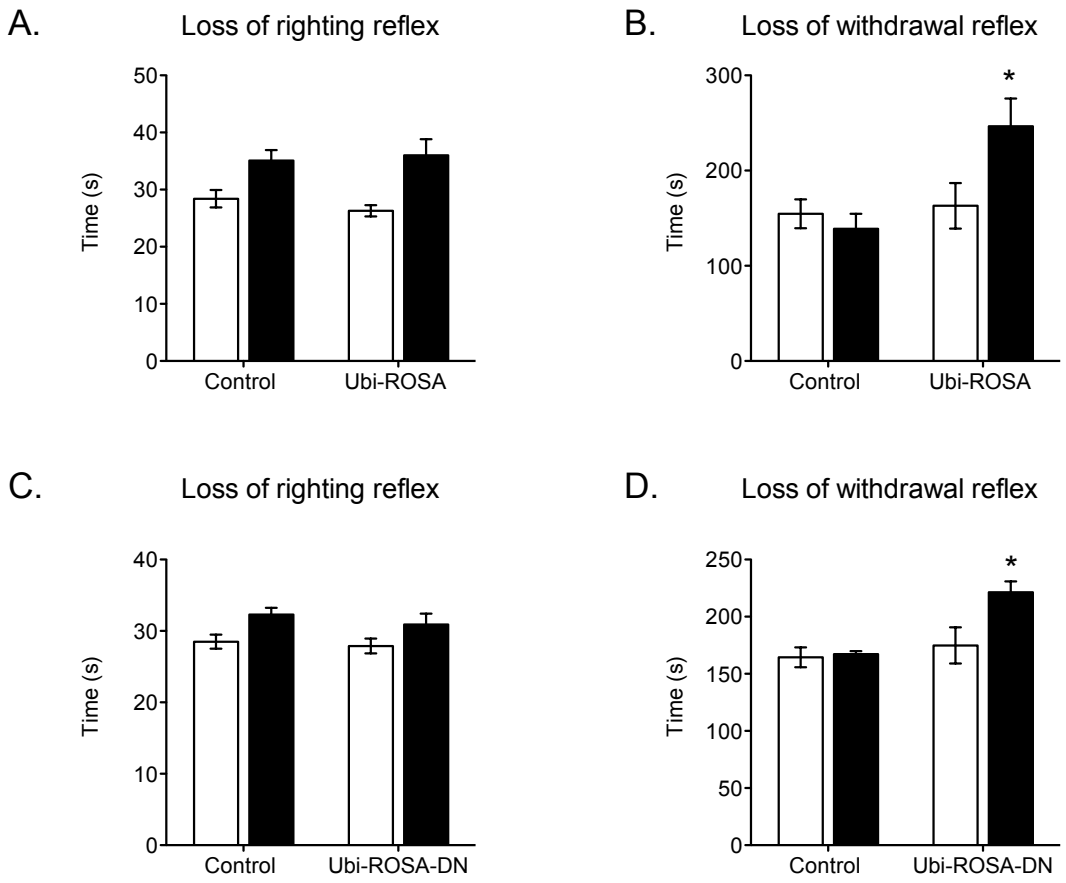

Figure 6.7: Sensitivity to isoflurane anaesthesia

(**A, B**) Loss of (**A**) righting and (**B**) withdrawal reflexes in response to 2% isoflurane in 11-14 week-old Ubi-ROSA mice (n=10) and control littermates (n=14; WT: n=7, Ubi-cre-ER^{+}: n=3, ROSA$^{+/-}$: n=4) before (white bars) and 4 days after (black bars) Kir6.2-V59M transgene induction by tamoxifen injection. (**C, D**) Loss of (**C**) righting and (**D**) withdrawal reflexes in response to 2% isoflurane in 11-14 week-old Ubi-ROSA-DN mice (n=20) and control littermates (n=35; WT: n=9; Ubi-cre-ER^{+}: n=12; ROSA-DN$^{+/-}$: n=14) before (white bars) and 4 days after (black bars) Kir6.2-[K185Q,ΔN30] transgene induction by tamoxifen injection. All data are mean ± SEM. * P<0.05 [Repeated-measures ANOVA- within-subjects factor: time (before and after tamoxifen); between-subjects factor: genotype; test details given in Appendices 10-11].

6.4.4. Subcutaneous glibenclamide therapy

The effect of subcutaneous glibenclamide therapy on the sensitivity of Ubi-ROSA-DN mice to isoflurane anaesthesia was tested. As expected, the drug had no effect on the LORR, as the phenotype observed in the nV59M mice (Chapter 5) was absent from the Ubi-ROSA-DN mice (Fig. 6.8A).

Glibenclamide-treated Ubi-ROSA-DN mice appeared to take a shorter time than placebo-treated mice to lose their withdrawal reflex (Fig. 6.8B): indeed the time to LOWR was similar to that of their control littermates. However, statistical significance was not reached (Appendix 12).

6.4.5. Intracranioventricular glibenclamide therapy

The effect of intracranioventricular glibenclamide therapy on the Ubi-ROSA-DN mice sensitivity to isoflurane anaesthesia was tested. As expected, the drug had no effect on time taken to LORR as the phenotype observed in the nV59M mice (Chapter 5) was absent from the Ubi-ROSA-DN mice (Fig. 6.9A).

As with the nV59M mice treated with ICV glibenclamide, no effect of drug treatment on time taken to LOWR was observed (Fig. 6.9B).

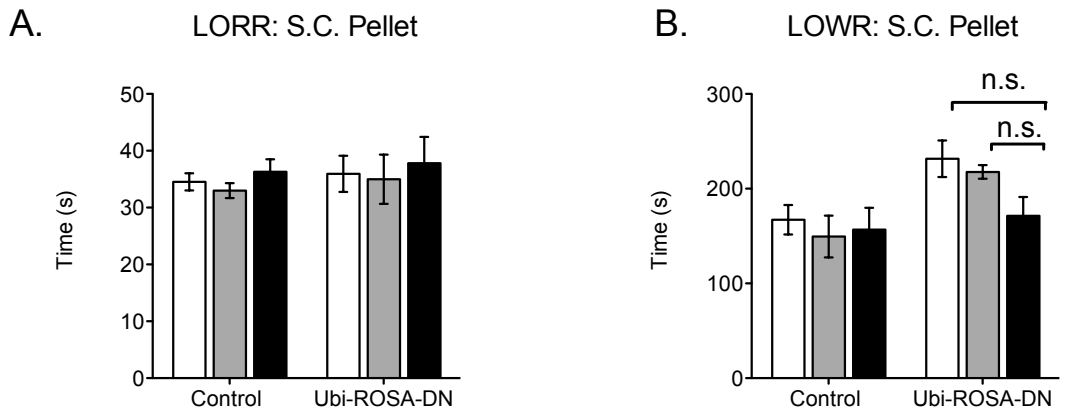

Figure 6.8: Effect of subcutaneous glibenclamide therapy on isoflurane anaesthesia sensitivity

(A) LORR in response to 2% isoflurane in Ubi-ROSA-DN mice or control littermates before (white bars) and after treatment with placebo (grey bars) or 2.5mg glibenclamide (black bars) subcutaneous pellets. (**B**) LOWR in response to 2% isoflurane in Ubi-ROSA-DN mice or control littermates before (white bars) and after treatment with placebo (grey bars) or 2.5mg glibenclamide (black bars) subcutaneous pellets. Response to isoflurane anaesthesia was assessed before and a week after implanting Ubi-ROSA-DN mice (n=7) and control littermates (n=15; WT: n=5; ROSA-DN$^{+/-}$: n=3; Ubi-cre-ER^{+}: n=7). Half of the mice from each group were implanted with a placebo pellet and the other half with glibenclamide. All data are mean ± SEM. n.s. not significant [Repeated-Measures Two-way ANOVA followed by Bonferroni multiple comparison post-test; test details given in Appendix 12].

(B)

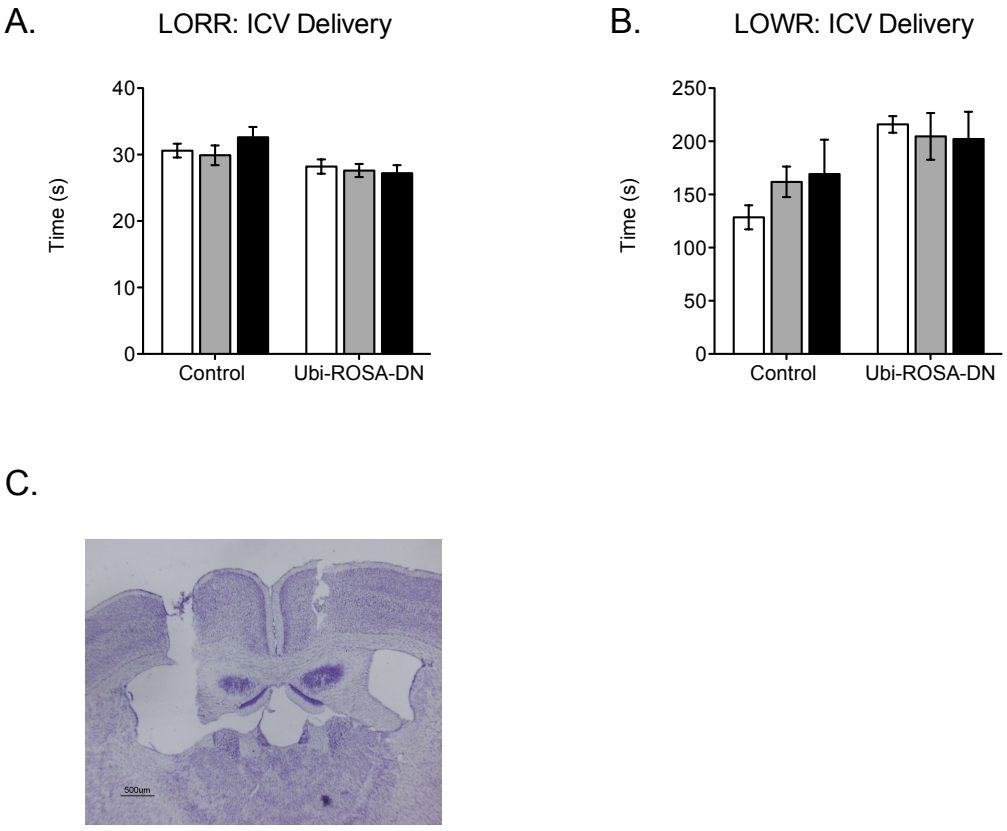

Figure 6.9: Effect of intracranioventricular glibenclamide therapy on isoflurane anaesthesia sensitivity

(**A**) LORR in response to 2% isoflurane in Ubi-ROSA-DN mice or control littermates before (white bars) and after treatment with vehicle (grey bars) or 280µM glibenclamide (black bars) delivered into the right lateral ventricle. (**B**) LOWR in response to 2% isoflurane in Ubi-ROSA-DN mice or control littermates before (white bars) and after treatment with vehicle (grey bars) or 280µM glibenclamide (black bars) delivered into the right lateral ventricle. Response to isoflurane anaesthesia was assessed before and a week after the surgical procedure; Ubi-ROSA-DN mice (n=13) and control littermates (n=20;WT: n=4; ROSA-DN$^{+/-}$: n=11; Ubi-cre-ER^{+}: n=5). Half of the mice from each group were given vehicle and the other half glibenclamide. All data are mean ± SEM. [Repeated-Measures Two-way ANOVA]. (**C**) Representative photo of Nissl stained coronal section from an ICV implanted mouse. Appropriate placement of the cannula into the right lateral ventricle was confirmed for all mice included for analysis.

An increase in the time taken to LOWR was observed in placebo- and glibenclamide-treated control mice. It is not clear why this occurred, particularly as changes were not observed in nV59M control littermates after ICV surgery. However, the changes observed were not statistically significant. Appropriate placement of the delivery cannulae was confirmed histologically (Fig. 6.9C).

6.5. Discussion

Mouse models are one of the most important tools we have available for studying the physiological role of different proteins at the whole organism level. However, there are various drawbacks associated with their use. One of these is the effect of constitutively expressed mutations during embryonic development, as activation of the mutation at a stage prior to the period of interest can result in unexpected behavioural phenotypes that may confound the results of a study [287,288,301]. One possible way of addressing this is by using mouse models with inducible Cre-recombinase, as this grants the researcher control over when the mutation is expressed [301].

In order to evaluate if developmental compensation is responsible for the inability of glibenclamide to reverse the impaired loss of righting reflex observed in the nV59M mice, I used the Ubiquitin-Cre-ER line in an attempt to generate an inducible global mouse model of the Kir6.2-V59M mutation.

6.5.1. Tamoxifen administration did not result in diabetes in a global mouse model of iDEND syndrome

Unexpectedly, the Ubi-ROSA mice did not develop diabetes after tamoxifen administration, despite receiving a dose that invariably induces diabetes in the Rip-Cre-ER-ROSA mouse (pancreatic β-cell specific inducible Kir6.2-V59M line; K. Shimomura & M. Iberl, *unpublished*). I also generated another mouse line using a ROSA-Kir6.2-V59M with a stronger promoter (CAG promoter; Ubi-ROSA-CAGS line) to determine if the lack of diabetes in the Ubi-ROSA mouse was due to weak expression of the mutation. However, these mice also failed to develop diabetes, even after being administered tamoxifen repetitively. A third mouse line, which had a stronger mutation (Kir6.2-[K185QΔn30]) [180] did not develop diabetes either.

I carried out semi-quantitative and quantitative PCR on RNA isolated from brain and pancreatic tissue samples from Ubi-ROSA mice and control littermates to determine whether the Kir6.2-V59M mutation was expressed in these tissues at the mRNA level. Interestingly, semi-quantitative PCR results appeared to indicate there was expression of the mutation in both the pancreas and the brain of Ubi-ROSA mice.

The quantitative PCR results confirmed adequate expression of the Kir6.2-V59M mRNA in the brain of Ubi-ROSA mice, both in terms of increased Kir6.2 mRNA and the presence of an intense GFP signal. However, in the pancreas there was no difference in the amount of Kir6.2 mRNA between Ubi-ROSA and control mice. Surprisingly in view of the lack of an increase in Kir6.2 expression, there was a greater amount of GFP in the pancreas of Ubi-ROSA mice when compared to control littermates, although the difference was not as marked as that observed in the brain. Due to the degradation of the pancreatic RNA samples, it was not possible to directly compare Kir6.2 and GFP amounts between the brain and pancreas of Ubi-ROSA mice. Nonetheless, these results suggest that the Kir6.2-V59M mutation is expressed in the pancreas of Ubi-ROSA mice, although not at levels high enough to trigger diabetes.

Interestingly, in the original paper in which the Ubi-Cre-ER mice were described, the authors reported >70% recombination in the pancreas of their mice following tamoxifen treatment [230]. They assessed recombination at the DNA level by Southern hybridization so post-transcription modifications may underlie the differences between what they reported and what I observed in the Ubi-ROSA mice. Furthermore, assessment of Cre-recombination sites in the Ubi-Cre-ER mice carried out by the Jackson Laboratory using a β-galactosidase (β-gal) reporter line indicated that β-gal expression in pancreatic islets was mosaic (http://cre.jax.org/UBC-creERT/UBC-creERT.html)[302]. It thus seems likely that recombination in the pancreatic β-

cells of the Ubi-ROSA mice did not produce not sufficient expression of Kir6.2-V59M to induce diabetes.

6.5.2. Sensitivity to isoflurane anaesthesia in an inducible global mouse model of iDEND syndrome

As the Kir6.2-V59M mRNA levels appear to be high in the brains of Ubi-ROSA mice, I assessed their sensitivity to isoflurane anaesthesia. As expected, prior to tamoxifen administration, no differences were observed between uninduced Ubi-ROSA mice and control littermates in terms of the loss of righting and withdrawal reflexes. Following tamoxifen injection, there was no difference in the time taken to LORR between Ubi-ROSA and control littermates, although there was an increase in the time taken to LORR for both the Ubi-ROSA and control littermates when compared to before tamoxifen administration. Why this was the case is not clear, particularly as I had previously not observed any changes in the time taken to LORR for control mice upon re-exposure to isoflurane (Chapter 5). It is thus possible that tamoxifen administration or the stress associated with the injection may have an effect on LORR.

In terms of LOWR, a significant increase in the time taken to lose the reflex was observed for Ubi-ROSA after tamoxifen administration when compared to control littermates as well as prior to gene induction. This result indicates that

the impaired LOWR observed in nV59M mice is most likely directly caused by the expression of the mutation in neuronal tissue.

I also assessed the sensitivity of Ubi-ROSA-DN mice to isoflurane anaesthesia as I was interested in determining whether the phenotype observed in nV59M and Ubi-ROSA mice was mutation-specific. The Ubi-ROSA-DN carry a different gain-of-function mutation, Kir6.2-[K185QΔN30], which results in a greater decrease in ATP sensitivity (~30-fold less sensitive versus ~3-fold less sensitive for the Kir6.2-V59M mutation) [156,178,180,225].

As was the case with the Ubi-ROSA mice, no differences in LORR or LOWR were observed prior to tamoxifen treatment. However, following gene induction a significant increase in the time taken to LOWR was observed for Ubi-ROSA-DN mice when compared to control littermates as well as before tamoxifen administration. As with the Ubi-ROSA mice, no differences were observed in the time taken to LORR in Ubi-ROSA-DN after tamoxifen administration.

The fact that the LORR phenotype was not observed in Ubi-ROSA or Ubi-ROSA-DN despite tamoxifen treatment may indicate that the altered response observed in nV59M mice is developmental in origin. However, it is also possible that Cre-mediated recombination was not homogeneous throughout the brain. Indeed, assessment of Cre-recombination sites in the Ubi-Cre-ER mice carried out by the Jackson Laboratory using a β-galactosidase reporter

line indicated that β-gal expression in some areas of the brain, including the medulla and the pons, was mosaic (http://cre.jax.org/UBC-creERT/UBC-creERT.html)[302]. This mosaic brain-specific expression has been previously reported for other mouse lines [303]. It is thus not possible to conclude whether the lack of a LORR phenotype was due to poor recombination in this inducible mouse model or due to a developmental effect of the mutation. Further work with neuronal-specific inducible mouse lines, such as the Nestin-Cre-ER [304], is required to address this.

6.5.3. Effect of glibenclamide therapy on Ubi-ROSA-DN isoflurane sensitivity

To determine if it was possible to reverse the impaired LOWR in Ubi-ROSA-DN mice, I implanted mice with slow-release subcutaneous glibenclamide pellets and assessed their isoflurane sensitivity a week after implantation (2 weeks after gene induction by tamoxifen). The treatment had no effect on the time taken to LORR, which was expected, as these mice do not exhibit the impaired LORR phenotype observed in nV59M mice.

In the case of LOWR, glibenclamide treatment appears to reduce the time taken to lose the reflex in Ubi-ROSA-DN mice. However, statistical significance was not reached, most likely due to the small sample size (n=3 for placebo-treated Ubi-ROSA-DN and n=4 for glibenclamide-treated ones). A

larger sample size is required for adequate statistical analysis, but these results suggest that subcutaneous glibenclamide therapy may partially restore the impaired LOWR in Ubi-ROSA-DN mice; in the same way it restores it in nV59M mice.

I also assessed the effect of direct brain delivery of glibenclamide, via intracranioventricular cannulae, on the isoflurane sensitivity or Ubi-ROSA-DN mice. As with the nV59M mice, no difference was observed in time taken to LORR or LOWR after ICV glibenclamide treatment. As was mentioned in Chapter 5, the inability of ICV glibenclamide to restore LOWR could be due to the drug being transported out of the brain and becoming too diluted upon entering systemic circulation to act on its targets (if, for example, peripheral sensory neuron K_{ATP} channels are involved in the altered LOWR). This will be further addressed in Chapter 7.

6.6. Conclusion

The use of the Ubiquitin-Cre-ER line to generate an inducible global model of iDEND syndrome was not successful as recombination in pancreatic islets does not seem to be sufficient to induce diabetes, a key feature of iDEND syndrome. Furthermore, it was not possible to use this model to determine if the altered LORR observed in nV59M mice is developmental in origin as there also appears to be mosaic recombination in certain brain areas, particularly

the pons and medulla, which are thought to play an important role in arousal/sleep/anaesthesia regulation. Interestingly, the altered LOWR observed in nV59M mice was also present in Ubi-ROSA and Ubi-ROSA-DN mice, indicating this phenotype is directly caused by the presence of an activating K_{ATP} channel mutation.

Chapter 7: Quantification of glibenclamide in rodent plasma, cerebrospinal fluid and brain

7.1. Summary

1. A liquid chromatography-tandem mass spectrometry method was used to quantify the glibenclamide concentration in rodent plasma, brain and cerebrospinal fluid.

2. When implanted with subcutaneous glibenclamide pellets, significantly higher glibenclamide concentrations were measured in the plasma of female mice when compared to male mice.

3. Glibenclamide was not detected in the cerebrospinal fluid of rats implanted with subcutaneous glibenclamide pellets despite high drug concentrations being found in the plasma.

4. Glibenclamide was detected in the cerebrospinal fluid, plasma and brain of rats after acute intracranioventricular injection into the right lateral ventricle.

5. The inability of glibenclamide to enter the brain appears to be partially mediated by P-glycoprotein.

7.2. Introduction

Sulphonylurea drugs have been used in clinical practice for the management of non-insulin dependent diabetes for close to 60 years [191]. With the discovery that more that 50% of all cases of neonatal diabetes are caused by activating mutations in the K_{ATP} channel, sulphonylureas became the treatment of choice for this disease [6]. Nearly 25% of patients with activating K_{ATP} channel mutations present with neurological symptoms in addition to neonatal diabetes [4,5,128].

The main K_{ATP} channel subtype found in the brain is thought to be the same as that found in the pancreatic β-cell (Kir6.2-SUR1)[26,83]. It was therefore hoped that sulphonylurea therapy would be as successful at improving the neurological symptoms as it is at managing the diabetes [6,217]. However, this has not proved to be the case, with sulphonylureas being ineffective at substantially improving neurological function for many of the patients, even if they have adequate glycaemic control [157,220,222,224,227].

One of the possible explanations for the drugs' inability to fully restore neurological function could be due to sulphonylureas being unable to penetrate the blood-brain barrier (BBB) and reach a high enough concentration in the cerebrospinal fluid (CSF) and brain tissue to modulate neuronal function. This possibility will be examined in this chapter.

7.2.1. The blood-brain barrier

For appropriate neuronal network function, it is crucial to maintain a stable microenvironment. The BBB is believed to play a key role in ensuring the stability of this environment, by tightly regulating the movement of solutes and substrates into and out of the CNS [305]. The BBB is formed by the endothelium of blood micro-vessels, which form tight junctions between adjacent cells to prevent the flux of molecules via the paracellular pathway. In addition to this physical barrier, endothelial cells also express enzymes that metabolise molecules in transit, as well as specific transporters that mediate active solute flux [305]. Thus, the BBB protects the neural milieu by a combination of physical, enzymatic, and transport barriers.

Due to the presence of tight junctions between endothelial cells, which effectively convert the BBB into a continuous cell membrane, most polar and water-soluble compounds are virtually incapable of entering the brain, except via specific solute-carriers [305,306]. By contrast, lipid soluble molecules can passively diffuse across the BBB and enter the brain [307].

There appears to be a correlation between a compound's lipid solubility and the rate at which it enters the CNS [308]. Hence, increasing the lipophilicity of a drug has been used as a strategy to make it more brain permeant. However, in many cases this has been counter-productive, resulting in a considerably lower rate of entry into the CNS than expected [305]. This is because many

highly-lipid soluble compounds are actively transported from the brain and capillary endothelium by ABC (ATP-binding cassette) transporters [309].

7.2.2. ABC transporters at the blood-brain barrier

ABC transporters utilize the energy of ATP hydrolysis to transport substrates against their concentration gradient [309,310]. There are 49 members of the human ABC transporter superfamily, which are grouped into sub-families on the basis of structural homology [310,311]. Several of these proteins have been shown to be involved in absorption and distribution of many drugs as well as playing a role in the development of drug-resistance [310,312]. Of these, P-glycoprotein (P-gp; ABCB1), the Multidrug Resistance-associated Proteins (MRPs; ABCC1, 2, 4, 5 and possibly 3 and 6), and Breast Cancer Resistance Protein (BRCP; ABCG2) are thought to be key players in the efflux of drugs across the BBB [305,310].

P-gp and BRCP are expressed at the luminal membrane of the BBB, where they transport substrates from the endothelium to the blood [309,313]. BRCP recognises a great variety of molecules, ranging from chemotherapeutic agents to vitamin B_2, while P-gp tends to preferentially transport hydrophobic and cationic molecules [312,314]. Interestingly, these two transporters have been reported to work cooperatively in the efflux of compounds from the BBB [315].

By contrast, MRPs are expressed at the abluminal and luminal membranes of the BBB, and they tend to favour water-soluble conjugates as substrates [305,316].

7.2.3. Sulphonylureas and the blood-brain barrier

It has been previously shown that tolbutamide, a sulphonylurea drug, accumulates poorly in the rat brain [289]. Using cultured brain capillary endothelial cells as an *in vitro* model of the BBB, Takanaga and colleagues[289] demonstrated that tolbutamide was transported from the abluminal to the luminal membrane via a transcellular mechanism, which became saturated at high concentrations. They also showed that the mechanism was not P-gp-dependent, as inhibitors of this protein had no effect on the movement of tolbutamide. These results suggest that the poor accumulation of tolbutamide in the brain is caused by the unidirectional transport of the drug from the brain to the blood.

In the case of glibenclamide, which is the most widely used sulphonylurea for the management of ND and iDEND/DEND syndromes [6], *in vitro* experiments have indicated that this drug is able to inhibit P-gp and may also be a substrate for this transporter [317,318]. Furthermore, *in silico* modelling of P-gp and SUR has been used to identify potential binding sites on both proteins for glibenclamide [318].

These results suggest glibenclamide and other sulphonylureas may be actively transported out of the brain. Whether this is the case *in vivo* is not entirely clear. In this chapter, I used a liquid chromatography-tandem mass spectrometry (LC-MS) method to quantify the glibenclamide concentration in plasma, cerebrospinal fluid (CSF) and brain of rodents after drug administration in an attempt to assess whether sulphonylureas are able to cross the BBB.

7.3. Methods

7.3.1. Animal care

Male and female adult C57Bl6/J mice (11-14 weeks) and male adult Lister hooded rats (250-300 grams) were used in these experiments. Animals were housed in same-sex littermate groups of 2-8 mice or 2-5 rats, in a temperature and humidity controlled room on a 12h light-dark cycle (lights on at 7 am). They had *ad libitum* access to regular chow food and water at all times.

7.3.2. Subcutaneous pellet implantation

Details of the surgical procedure for subcutaneous implantation of slow-release pellets are given in Chapter 2. For these experiments, different size pellets were used, with mice receiving 0.25mg, 2.5mg or 25mg pellets and rats receiving 25mg or 200mg pellets. Animals were left to recover for 7-10 days, after which they were sacrificed for plasma and cerebrospinal fluid (rats only) collection. The experimenter was blinded to the drug treatment.

7.3.3. Intracranioventricular (ICV) delivery of glibenclamide

7.3.3.1. Chronic ICV administration of glibenclamide

Adult male Lister-hooded rats were implanted with a subcutaneous osmotic mini-pump (Model 2ML4, 28-day infusion, 2.5µl/h flow rate; Alzet, Durect Corporation) filled with either 110µM glibenclamide (Sigma; initial stock: 11mM in 100% DMSO) in artificial cerebrospinal fluid (aCSF; composition given in Chapter 2) or vehicle (aCSF; 0.1% DMSO) connected to a cannula implanted into the right lateral ventricle of the brain. Details of the surgical procedure are given in Chapter 2.

A recovery period of one week was allowed between the surgery and the subsequent testing. All experiments were performed blinded to treatment given. Adequate cannula placement was confirmed histologically for all animals used. Details of the procedure for histological confirmation are given in Chapter 2.

7.3.3.2. Acute ICV administration of glibenclamide

Rats were anaesthetised with isoflurane and were administered buprenorphine (30µg/ml; Vetergesic, Reckitt Benckiser Healthcare) pre-operatively as an analgesic. Once anaesthesia had been confirmed, an area covering the top of the head and the scapular area of the rats was shaved and cleaned. Lidocaine (10mg Xylocaine spray, AstraZeneca) was then administered locally at the incision area.

A 4cm incision was made from just above the eyes to the back of the neck, the skull surface was exposed, and a small hole drilled at the coordinates of the right lateral ventricle (coordinates: 0.9mm caudal to bregma, 1.3mm lateral from bregma and 4.5mm below the surface of the skull). Rats were then administered a 5µl injection of glibenclamide dissolved in 100% DMSO (25mg/ml solution; Sigma) or vehicle (100% DMSO; Sigma) into the right lateral ventricle using a Hamilton 10µl syringe.

One hour after administration of glibenclamide, animals were sacrificed for plasma, cerebrospinal fluid, and brain collection. Rats were kept anaesthetised with 2-3% isoflurane for the duration of the experiment. The experimenter was blinded to the drug treatment.

7.3.4. Intraperitoneal (IP) administration of the P-glycoprotein inhibitor elacridar

7.3.4.1. IP administration of elacridar and glibenclamide

Rats were administered an intraperitoneal injection of either 10 mg/kg elacridar dissolved in 100% DMSO (6 mg/ml solution; Tocris) or an equal volume of 100% DMSO (Sigma) at time 0. An hour after the first intraperitoneal injection, rats were administered a second intraperitoneal injection of 50 mg/kg glibenclamide dissolved in 100% DMSO (20 mg/ml solution; Sigma). Four hours after administration of glibenclamide, animals were sacrificed for plasma and cerebrospinal fluid collection. The experimenter was blinded to the drug treatment.

7.3.4.2. IP administration of elacridar and ICV glibenclamide

Rats were administered an intraperitoneal injection of either 10 mg/kg elacridar dissolved in 100% DMSO (6 mg/ml solution; Tocris) or an equal volume of 100% DMSO (Sigma) at time 0. In order to administer glibenclamide directly into the lateral ventricle, rats were anaesthetised with 2-3% isoflurane following the intraperitoneal injection. Once anaesthesia had been confirmed, an area covering the top of the head and the scapular area of the rats was shaved and cleaned. Lidocaine (10mg Xylocaine spray, AstraZeneca) was then administered locally at the incision area and the rat placed on a Stoelting stereotaxic frame.

A 4cm incision was made from just above the eyes to the back of the neck, the skull surface was exposed, and a small hole drilled at the coordinates of the right lateral ventricle (coordinates: 0.9mm caudal to bregma, 1.3mm lateral from bregma and 4.5mm below the surface of the skull). An hour after the first intraperitoneal injection, rats were administered a 5µl injection of glibenclamide dissolved in 100% DMSO (25mg/ml solution; Sigma) into the right lateral ventricle using a Hamilton 10µl syringe.

One hour after administration of glibenclamide, animals were sacrificed for plasma, cerebrospinal fluid, and brain collection. Rats were kept

anaesthetised with 2-3% isoflurane for the duration of the experiment. The experimenter was blinded to the drug treatment.

7.3.5. Plasma and cerebrospinal fluid sample collection

Animals were killed with an overdose of sodium pentobarbital (Euthatal, Merial). After confirmation of loss of withdrawal reflex, the abdominal cavity was exposed and blood was collected from the posterior vena cava into a heparinised syringe. The blood was then placed into a heparinised Eppendorf tube and centrifuged at 1000xg for 20min at 4°C. Following centrifugation, the supernatant was collected and kept at -20°C until further processing.

Cerebrospinal fluid was collected from the cisterna magna. After confirmation of death (by exsanguination for blood collection), a sagittal incision was made between the ears and the back of the neck. The subcutaneous tissue and muscles were separated to expose the dura matter of the cisterna magna (cerebromedullary cistern). The animal's head was placed at a 90° angle with respect to the body and the dura matter of the cisterna magna was pierced with the tip of a 0.3ml insulin syringe (BD Micro-Fine+, BD Diabetes). CSF was allowed to flow into the syringe, and if needed, a small amount of negative pressure was applied. The CSF was placed in an Eppendorf tube and stored at -20°C until further processing.

7.3.6. Plasma and cerebrospinal fluid sample preparation

7.3.6.1. Calibration standards

For preparation of the plasma calibration standards a stock solution of glibenclamide (Santa Cruz Biological) was made in methanol (1.0 mg/ml). Blank mouse plasma (Lampire Biological Laboratories) was spiked with the stock glibenclamide solution at a concentration of 10µg/ml, and a range of standard concentrations was prepared by individual dilutions at the following concentrations (ng/ml): 4000, 3000, 2000, 1000, 500, 200, 100, 50, 20, 5, 1 and no drug. The same standard concentrations were used for the cerebrospinal fluid and brain homogenate calibration curves. Phosphate-buffered artificial cerebrospinal fluid (composition given in Chapter 2) was used to dilute the CSF calibration standards. In the case of the brain calibration curve, brains obtained from drug-naïve rats were homogenised and diluted 2:1 (v/w) with phosphate-buffered saline (PBS; Sigma). This homogenate was used to dilute the calibration standards.

A separate calibration curve was run for each set of experimental samples, and each set of samples was analysed in triplicate LC-MS runs.

7.3.6.2. Preparation of brain samples

Brains were homogenised and diluted 2:1 (v/w) with PBS (Sigma). A 500µl aliquot of homogenate was used for further processing. The internal standard (16µl of 10µg/ml d_{11}-glibenclamide; Santa Cruz) was added to the brain sample and 4% *ortho*-phosphoric acid (85% w/w; Fluka) was added to a final volume of 766µl.

Prior to solid phase extraction, brain samples were prepared by liquid-liquid extraction. One volume of water-saturated ethyl acetate (Acros Organics) was added to each sample. These were mixed thoroughly by vortexing and centrifuged at 16,100xg for 2min. The upper solvent phase was then collected for further processing. This procedure was repeated twice, with an equal volume of ethyl acetate being added each time and the upper solvent phase being collected.

The samples were evaporated in a vacuum centrifuge at 35°C. The remaining residue was taken up in 10% methanol (100µl; Fisher Scientific) by sonication in an ultrasonic bath (10min). Samples were then prepared by reverse phase extraction.

7.3.6.3. Solid phase extraction

Prior to LC-MS analysis, samples were prepared by reverse phase C18 solid phase extraction (C18-SPE). In the case of the plasma and CSF samples, the internal standard (1µl of 10µg/ml d_{11}-glibenclamide; Santa Cruz) was added to 30µl of the plasma sample and 4% *ortho*-phosphoric acid (85% w/w; Fluka) was added to a final volume of 62µl.

All samples were further diluted with 600µl of wash buffer (94.9% water, 5% acetonitrile, Merck; 0.1% formic acid, Fluka) and applied to a pre-equilibrated 96-well reverse phase C18-SPE extraction plate (50mg C18 resin; Microlute Varian) attached to a Vac Master-96 vacuum manifold (Biotage). Wells were pre-equilibrated with 500µl elution buffer (80% acetonitrile, 19.9% water, 0.1% formic acid) followed by 1000µl of wash buffer. Following sample application, the wells were washed twice with 1000µl of wash buffer and eluted with elution buffer (2 x 200µl).

The eluates were transferred into silanized 1.5ml Eppendorf tubes and evaporated in a vacuum centrifuge at 35°C. The remaining residue was taken up in 20% methanol (30µl; Fisher Scientific) by sonication in an ultrasonic bath (10min). Samples were centrifuged (16,100xg at 4°C) for 15min and the supernatant was transferred to glass LC-MS sample vials (Kinesis).

7.3.7. Sample analysis

7.3.7.1. Liquid chromatography

Plasma, CSF and brain were separated by high-pressure liquid chromatography (HPLC) on an Ultimate 3000 HPLC system (Dionex). A 3µl aliquot was injected per LC-MS run. Separation was carried out at a flow rate of 250µl/min on an ACE Excel 2 C8 column (2.1x50mm, Advanced Chromatography Technologies) using buffer A (5% methanol, 0.5mM ammonium formate; Fluka), buffer B (95% methanol, 0.5mM ammonium formate) and the buffer gradient shown in Table 7.1.

Table 7.1: Buffer gradient for liquid chromatography

Minutes	*% Buffer B*
0	20
1	35
6	90
8	90
8.5	20
11	20

7.3.7.2. Mass Spectrometry

The HPLC system was coupled via the standard electrospray ionisation (ESI) interface to an amaZon ETD ion trap mass spectrometer (Bruker Daltonics) and a nitrogen generator (Dominick Hunter). The mass spectrometer was controlled by TrapControl software version 7.0 and the LC-MS system was controlled by HyStar software version 3.2.

Ionization was achieved with a capillary voltage of 4500V, a nitrogen gas flow of 15psi at 8 l/min and a temperature of 300°C. The ion trap was set to an ion charge control target of 250,000 and a maximum accumulation time of 200ms. The scan range observed was 250-850 m/z. The instrument was calibrated at least once a month using an ESI-T tuning mix (Agilent) by performing scan, isolation, and fragmentation calibrations (Bruker Daltonics).

Quantification experiments were conducted in Selected Reaction Monitoring (SRM) mode, observing two mass transitions in the Ion Trap: 494.1→369.0 for detection of glibenclamide and 505.1→369.0 for detection of d_{11}-glibenclamide. The isolation width was 2.0Da and the amplitude was 0.7V for fragmentation of both precursor ions.

7.3.8. Data analysis

Analysis was performed using Quantanalysis software version 2.0 (Bruker Daltonics) for chromatograms of mass transitions for glibenclamide and the internal standard (d_{11}-glibenclamide). A Gaussian smoothing algorithm (smoothing width 1s, 1 cycle) was applied to the chromatograms and automatic peak detection parameters for glibenclamide and d_{11}-glibenclamide were 6.6min for retention time and 0.3min for the retention time window.

For the calibration curves, peak area ratios of glibenclamide to d_{11}-glibenclamide were plotted against the concentrations. A linear regression analysis of the calibration standards was carried out using the least squares method with a $1/y^2$ weighting. Calibration and experimental samples were analysed by triplicate injection on the LC-MS/MS system and the determined value was taken as the arithmetic mean of the three measurements.

7.3.9. Statistical analysis

When the data distribution permitted (i.e. fulfilled the criteria of normality and equality of variance), a Student's t-test or a One-Way ANOVA were performed. Otherwise, data were analysed using a non-parametric test, the Mann-Whitney U-test or the Kruskal-Wallis One-Way ANOVA on Ranks.

Differences between groups were considered statistically significant at $P<0.05$. All analyses were performed using two-tailed tests.

7.4. Results

7.4.1. Method development

The glibenclamide quantification method was previously developed by Dr. Holger Kramer (Kramer et al., *in preparation*). The method uses selected reaction monitoring to monitor the mass transitions resulting from the fragmentation of glibenclamide (494.1→369.0) and deuterated glibenclamide (d_{11}-glibenclamide; internal standard; 505.1→369.0) (Fig. 7.1). D_{11}-glibenclamide was chosen as the internal standard (IS) as it offers the advantages of near co-elution and similar ionization properties to the analyte. The IS was added at a concentration of 333ng/ml into all samples.

SRM is a non-scanning mass spectrometry (MS) technique, which increases the specificity of detection compared to full scan MS acquisition, as each mass transition requires the parent ion and corresponding fragment ion to be detected.

The ratio of glibenclamide to d_{11}-glibenclamide peak area was linear over the concentration range 0-4000 ng/ml (0-8100 nM). The lower limit of quantitation

was 20ng/ml (40nM). The glibenclamide concentration calculated for calibration samples below this value deviated by more than 20% from their theoretical concentration.

7.4.2. Mouse and rat plasma samples

After validation of the method using glibenclamide-spiked blank mouse plasma samples, samples obtained from mice and rats previously treated with glibenclamide were analysed. The total glibenclamide concentration in mouse plasma, 7-10 days after implantation with a 2.5mg slow-release subcutaneous glibenclamide pellet was between 500 and 2100 nM (Fig. 7.2A).

As expected, no signal was detected in placebo-implanted mice (Fig. 7.2B).

To examine the effect of the pellet drug dose on the plasma glibenclamide concentration, male mice (Fig. 7.3A) and rats (Fig. 7.3B) were implanted with different sizes of slow-release pellets. Mice treated with a 0.25mg glibenclamide pellet had a mean plasma concentration of 236±55nM (n=5) while those implanted with a 25mg pellet had a mean concentration of 2200±783nM (n=5). In the case of the rats, a mean plasma concentration of 1750±514nM was obtained for those implanted with a 25mg pellet (n=5), and a mean concentration of 3914±977nM was measured in rats treated with

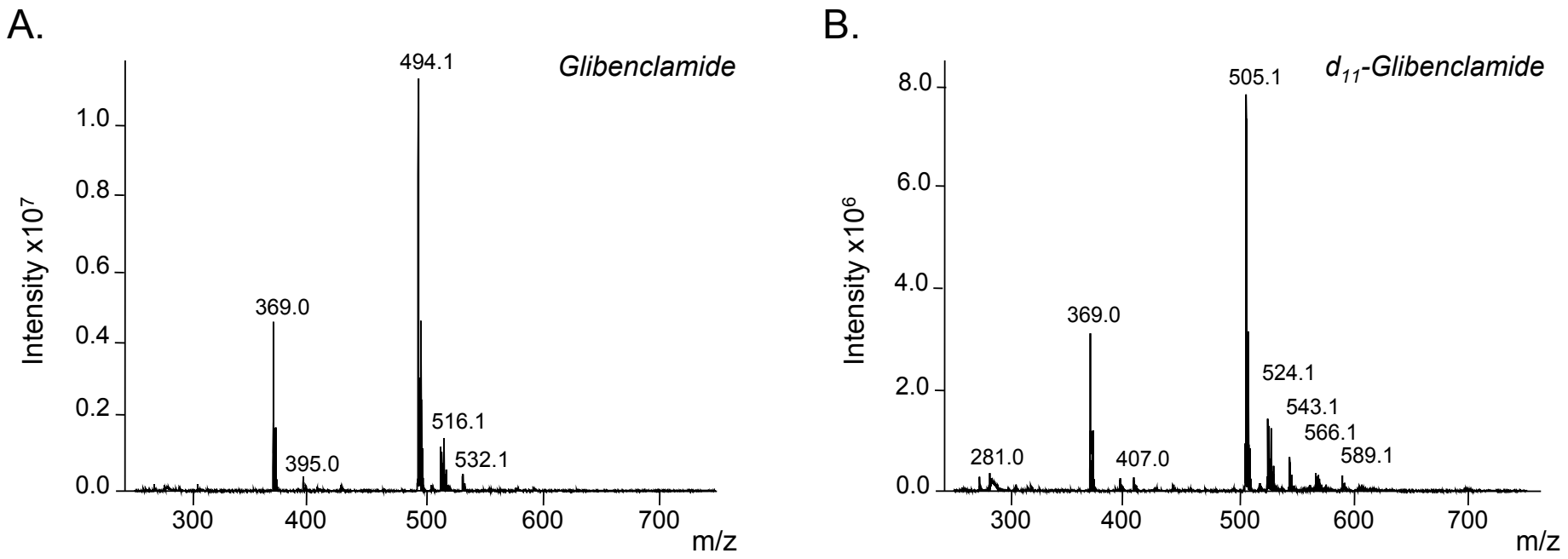

Figure 7.1: Mass spectra of glibenclamide and d11-glibenclamide

Mass spectra of glibenclamide (**A**) and d_{11}-glibenclamide (**B**) in positive ionization mode obtained by direct injection ion trap mass spectrometry. Protonated molecular ions [$M+H^+$] m/z (**A**) 494.1, (**B**) 505.1. Fragment ion m/z, (**A, B**) 369.0.

200mg glibenclamide pellets (n=5). Thus, there appears to be no linear correlation between the drug dose administered and the drug plasma concentration.

7.4.3. Gender differences in plasma glibenclamide concentrations

Interestingly, in the mice implanted with the 2.5mg pellets, a significant difference in the mean plasma glibenclamide concentration was observed between male and female mice (Fig. 7.2C). The drug concentration detected in plasma from female mice (n=4) was approximately twice that detected in male mice (n=7) (1545±424nM vs. 777.5±222nM, respectively; *P*=0.003; unpaired Student's t-test).

7.4.4. Plasma versus CSF concentrations in 200mg implanted rats

To establish whether systemically administered glibenclamide is able to cross the BBB, male adult rats were implanted with slow-release 200mg subcutaneous glibenclamide pellets and their plasma, CSF, and brains were collected 7 days after the surgical procedure. I chose this method of drug delivery as it is somewhat equivalent to daily oral administration in human

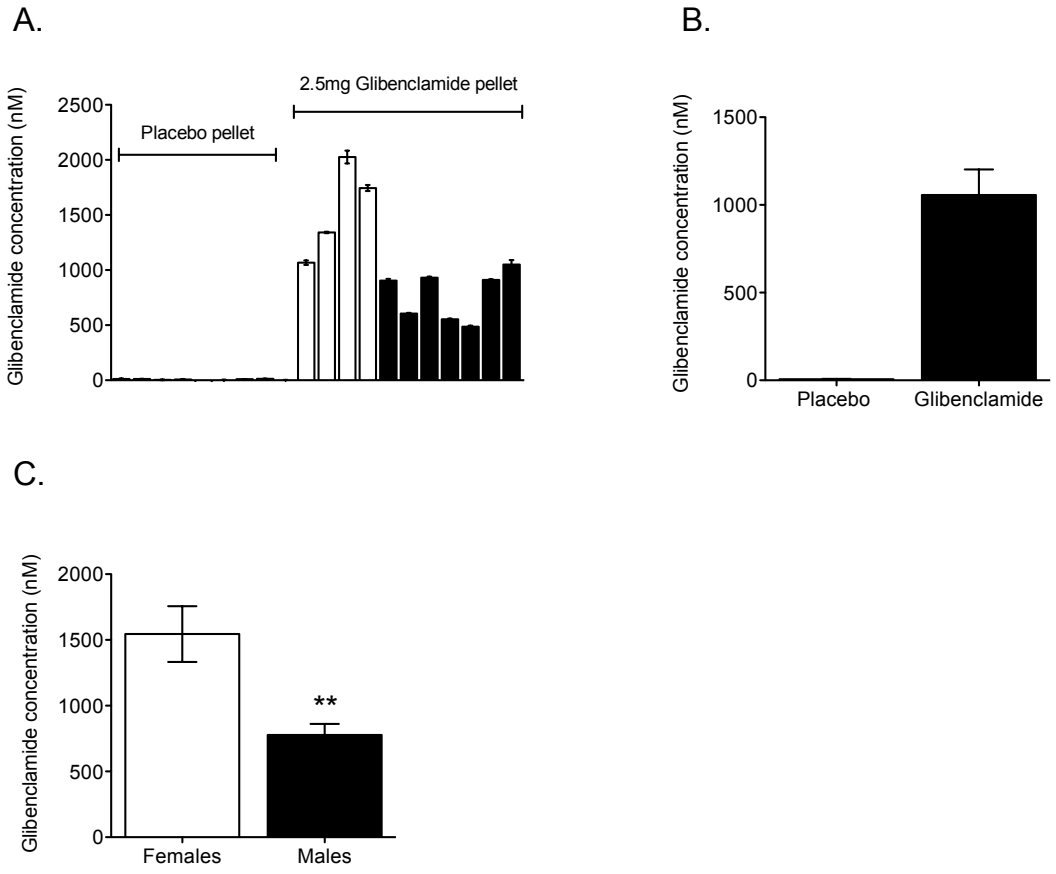

Figure 7.2: Plasma glibenclamide concentrations

(**A**) Glibenclamide concentration in plasma from individual female (white bars) and male (black bars) mice implanted with a 21-day slow release 2.5mg glibenclamide pellet or a placebo pellet. Data are mean ± SEM of triplicate measurements. (**B**) Mean ± SEM determined glibenclamide concentration in plasma from placebo (n=9 animals) or glibenclamide (n=11 animals) treated mice. (**C**) Mean ± SEM determined glibenclamide concentration in plasma from female (white bars) and male (black bars) mice implanted with placebo (n=4 and n=5 animals, respectively) or glibenclamide (n=4 and n=7 animals, respectively). ***P*<0.01 [Unpaired Student's t-test].

patients and allows for continuous drug administration for a period of up to 21 days. Rats were used for all experiments involving CSF collection as the volume of CSF that could be collected from mice (5-10µl) was below that needed for accurate quantification (minimum volume: 30µl).

The rats received a glibenclamide dose of approximately 50mg/kg/day for the duration of the experiment, which resulted in a mean plasma concentration of 2961±619nM (n=11; Fig. 7.4). By contrast, negligible concentrations of glibenclamide were detected in the CSF, with the values falling below the method's limit of detection (Fig. 7.4). As expected, glibenclamide was not detected in the samples taken from placebo-implanted rats.

Glibenclamide concentrations were also measured from brain homogenates obtained from the pellet-implanted rats in order to determine whether the drug had partitioned out of the CSF and into the brain tissue. However, glibenclamide concentrations in the brain samples were below the limit of quantitation of the method.

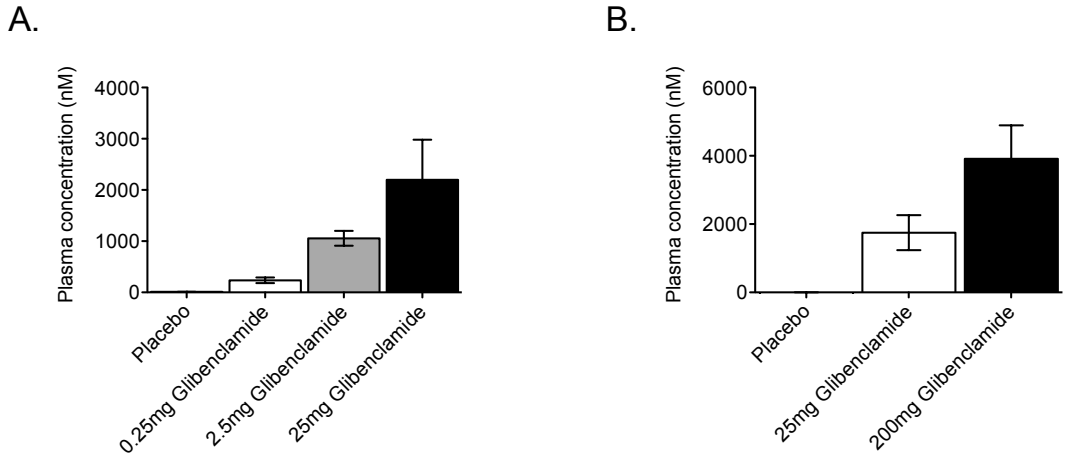

Figure 7.3: Effect of pellet drug dose on plasma glibenclamide concentration

(**A**) Mean ± SEM determined glibenclamide concentration in plasma from male mice implanted with a placebo (n=19 animals), a 0.25mg glibenclamide (n=5 animals), a 2.5mg glibenclamide (n=11 animals) or a 25mg glibenclamide pellet (n=5 animals). (**B**) Mean ± SEM glibenclamide concentration in plasma from male rats implanted with a placebo (n=10 animals), a 25mg glibenclamide (n=5 animals) or a 200mg glibenclamide pellet (n=5 animals).

7.4.5. Intracranioventricular delivery of glibenclamide

7.4.5.1. Chronic ICV delivery

In order to resolve why glibenclamide was not detected in the CSF or brain homogenate of pellet-implanted rats, I used osmotic mini-pumps pre-filled with 110µM glibenclamide or vehicle connected to intracranioventricular cannulae to deliver glibenclamide directly into the lateral ventricle. This would effectively bypass the BBB, allowing glibenclamide to enter the CSF circulation.

A week after implantation with the ICV cannulae, rats were sacrificed and their plasma and CSF was collected. Surprisingly, glibenclamide was not detected in either the plasma or the CSF of glibenclamide treated rats, even though the concentration of the solution collected from the mini-pumps the rats were implanted with was approximately 22µM (Fig. 7.5A).

To determine the concentration of drug excreted by the osmotic mini-pumps (i.e. the solution entering the CSF), I filled two 2ML4 pumps (rat model) and two 2004 pumps (mouse model) with 110µM and 280µM glibenclamide, respectively, kept them 37°C water bath and collected the solution excreted

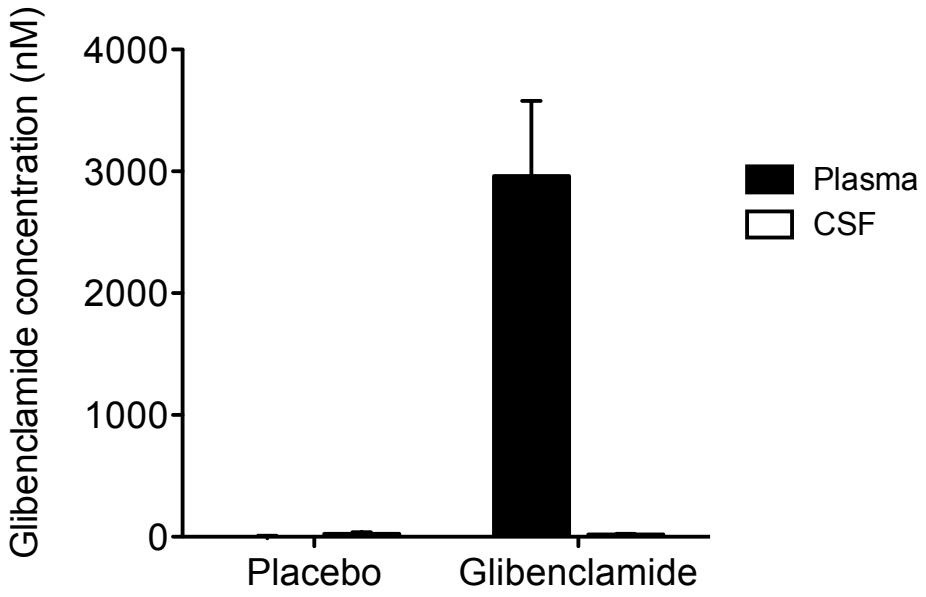

Figure 7.4: 200mg slow-release subcutaneous glibenclamide pellets

(**A**) Plasma and CSF glibenclamide concentrations from rats implanted with 200mg slow-release subcutaneous placebo (n=9) or glibenclamide pellets (n=11). Data are mean ± SEM.

over a 7 day period. As Figure 7.5B shows, for both the rat and mouse pumps, the glibenclamide concentration measured in the excreted solution is lower than that the pump was initially filled with (~3-fold lower for the rat pumps and ~5-fold lower for the mouse pumps). This suggests that despite the addition of bovine serum albumin (BSA) to the solution to reduce the binding of glibenclamide to the plastic tubing and pump, a considerable amount of the drug is still "sticking" to the plastic resulting in a reduction in the drug concentration being excreted. Nevertheless, the concentration found in the excreted solution (both for the rat and the mouse pumps) is still considerably high (~20μM for the rat and ~4μM for the mouse) and above that measured in the CSF.

Thus, the lack of glibenclamide detection in the plasma and CSF of rats implanted with ICV cannulae and osmotic mini-pumps was unlikely to have been caused by a lack of glibenclamide in the solution infused into the CSF.

The lack of drug detection was also not caused by a problem with the cannula placement as appropriate placement of the delivery cannulae was confirmed histologically for all animals used (Fig. 7.5C).

7.4.5.2. Acute ICV delivery

A possible explanation for the inability to detect glibenclamide in the CSF of the rats implanted with the osmotic mini-pumps is that glibenclamide exits the CSF at a rate faster than it enters. If this were the case, it might also not be possible to detect it in the plasma, as once it entered systemic circulation it would be diluted to a concentration below the limit of detection.

This hypothesis was tested by injecting rats with 5µl of either 25mg/ml glibenclamide or vehicle (100% DMSO) into the right lateral ventricle. Plasma, CSF, and brains were then collected an hour after injection. This concentration of glibenclamide, which is at the limit of DMSO solubility for the drug, was chosen as it would allow detection of the drug even if it were diluted upon entering systemic circulation.

As Figure 7.6A shows, glibenclamide was detected in both the CSF and the plasma of rats injected with the drug. Interestingly, the concentration in the plasma of glibenclamide-treated rats was considerably higher than in the CSF.

In the acute ICV injection rats, glibenclamide was also detected at a high concentration in the brain homogenate (Fig. 7.6B). Furthermore, as Fig. 7.6C shows, the glibenclamide concentration detected in the brain homogenate

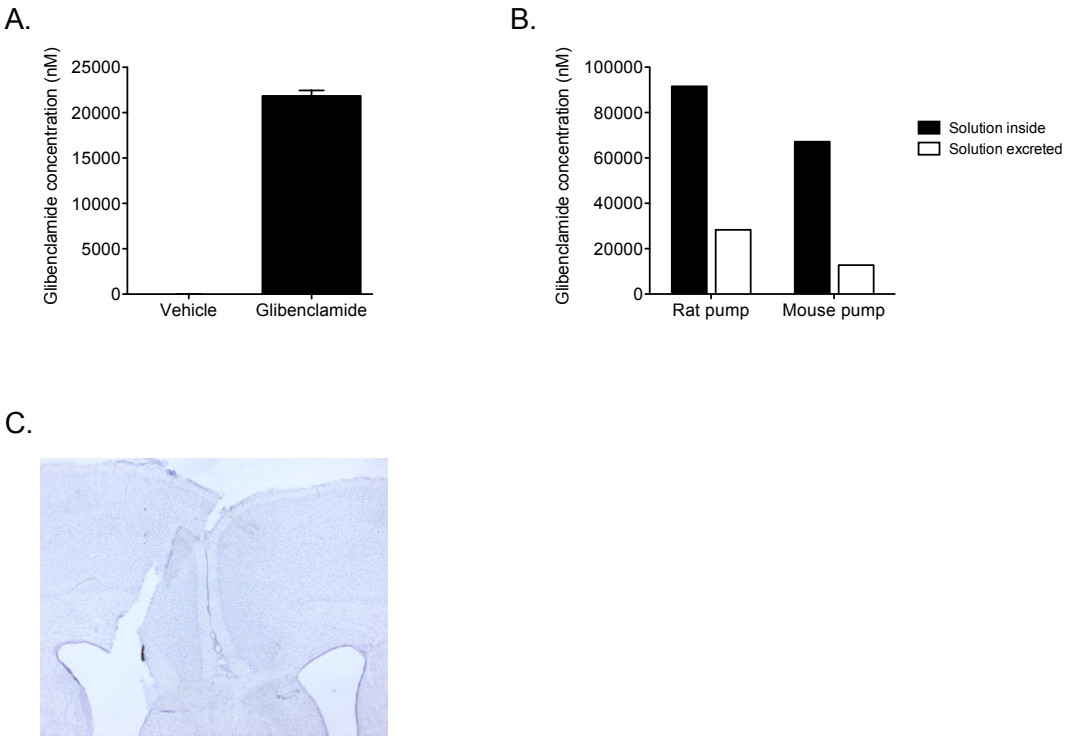

Figure 7.5: Chronic intracranial (ICV) delivery of glibenclamide

(**A**) Glibenclamide concentration from the osmotic mini-pump solutions (vehicle: n=4; glibenclamide: n=5). Data are mean ± SEM. (**B**) Glibenclamide concentrations from the solution inside and the solution excreted by rat and mouse osmotic mini-pumps filled with 110µM and 280µM glibenclamide, respectively. Pumps were left running in a water bath at 37°C for 7 days. (**C**) Representative photo of Nissl stained coronal section from an ICV implanted rat. Appropriate placement of the cannula into the right lateral ventricle was confirmed in all rats included for analysis.

from acute ICV injection rats is around 1000-fold higher than that detected in the brain homogenate from pellet-implanted rats, despite the fact that their plasma glibenclamide concentrations were relatively similar (~1000nM for ICV versus ~2000nM for pellet implantation).

7.4.6. P-glycoprotein inhibition

To test whether P-glycoprotein plays a role in the transport of glibenclamide across the BBB *in vivo*, rats were administered glibenclamide as an intraperitoneal bolus in the presence of elacridar, a selective P-glycoprotein inhibitor [319,320].

As Figure 7.7A shows, elacridar did not affect the plasma glibenclamide concentration, as the drug levels were relatively similar in rats treated with glibenclamide in the presence and absence of elacridar (~130µM versus ~110µM, respectively). However, rats treated with elacridar appeared to have higher glibenclamide concentrations in the CSF (Fig. 7.7B), although statistical significance was not reached (P=0.3421; unpaired Student's t-test). Interestingly, glibenclamide was detected in the CSF of rats administered glibenclamide by intraperitoneal bolus, even in the absence of elacridar.

A separate batch of rats was administered glibenclamide (5µl of 25mg/ml) into the right lateral ventricle in the presence of elacridar to examine whether P-gp

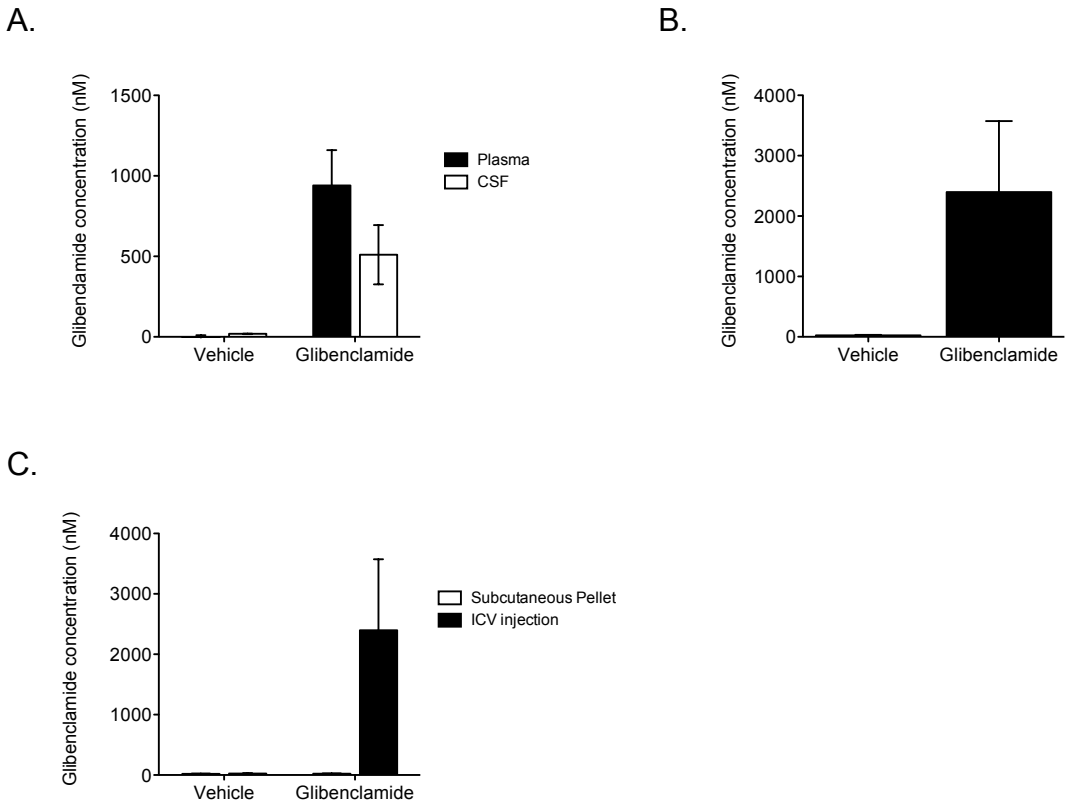

Figure 7.6: Acute intracranioventricular (ICV) delivery of glibenclamide

(**A**) Plasma and CSF glibenclamide concentrations from rats injected with 5µl of DMSO (vehicle; n=4) or glibenclamide (25mg/ml in 100% DMSO; n=6) into the right lateral ventricle. (**B**) Brain homogenate glibenclamide concentrations from rats injected with 5µl of DMSO (vehicle; n=4) or glibenclamide (25mg/ml in 100% DMSO; n=6) into the right lateral ventricle. (**C**) Brain homogenate glibenclamide concentrations in rats given vehicle (S.C: 200mg placebo pellet, n=3; ICV: 5µl 100% DMSO; n=4) or glibenclamide (S.C: 200mg glibenclamide pellet, n=6; ICV: 5µl of 25mg/ml in 100% DMSO) either subcutaneously or by ICV injection into the right lateral ventricle. All data are mean ± SEM.

actively pumps the drug out of the brain. As Fig. 7.8A shows, there was no difference in the CSF glibenclamide concentrations between rats that received elacridar and those that did not. There was also no difference in the brain glibenclamide concentration between the two treatment groups (Fig. 7.8B). Unexpectedly, the mean plasma glibenclamide concentration in rats that were not treated with elacridar was considerably lower than in those that did (Fig. 7.8A).

7.5. Discussion

Sulphonylureas are the treatment of choice for the management of neonatal diabetes caused by activating K_{ATP} channel mutations [6,218]. They are also the treatment of choice for the neurological symptoms associated with these mutations, but the extent to which they are able to cross the BBB is not clear, particularly as experiments using *in vitro* models of the BBB suggest they are transported out of the brain [289,317].

In an attempt to determine whether glibenclamide is transported across the BBB *in vivo*, I measured the glibenclamide concentration in plasma, CSF, and brain from rats after administration of glibenclamide systemically or directly into the brain.

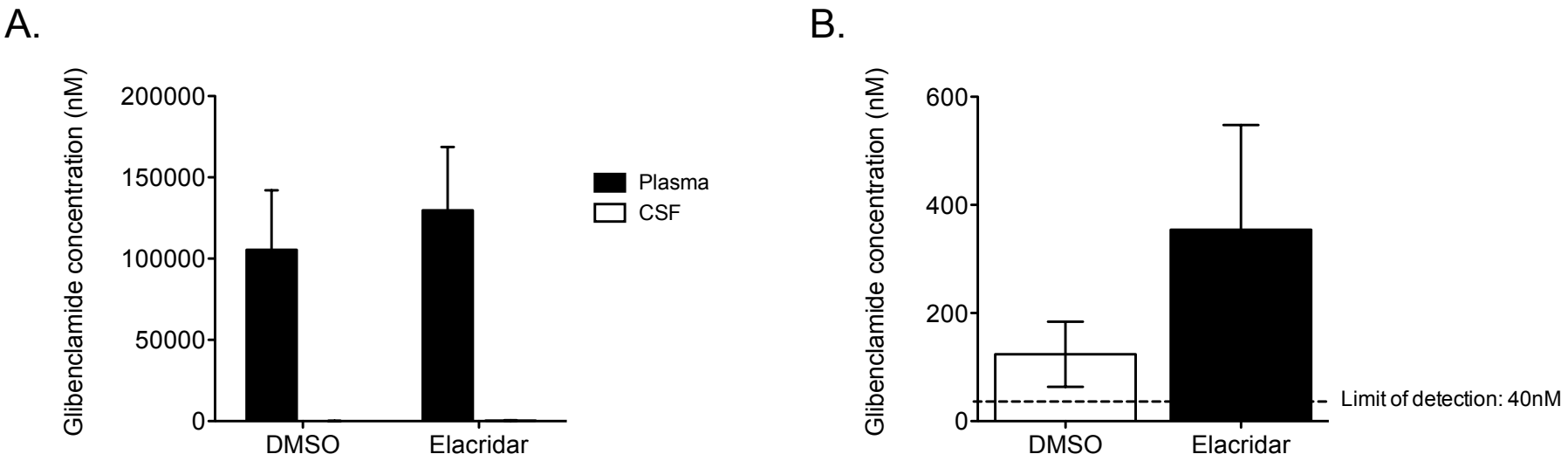

Figure 7.7: Systemic administration of glibenclamide in the presence of a P-glycoprotein inhibitor (elacridar)

(**A**) Plasma and cerebrospinal fluid glibenclamide concentrations from rats injected intraperitoneally with 50mg/kg glibenclamide in the presence of vehicle (100% DMSO; n=4) or elacridar (10mg/kg in 100% DMSO; n=5) (**B**) CSF glibenclamide concentrations from rats injected intraperitoneally with 50mg/kg glibenclamide in the presence of vehicle (100% DMSO; white bars; n=4) or elacridar (10mg/kg in 100% DMSO; black bars; n=5). The limit of detection of the assay (40nM) is shown in panel B. Data are mean ± SEM.

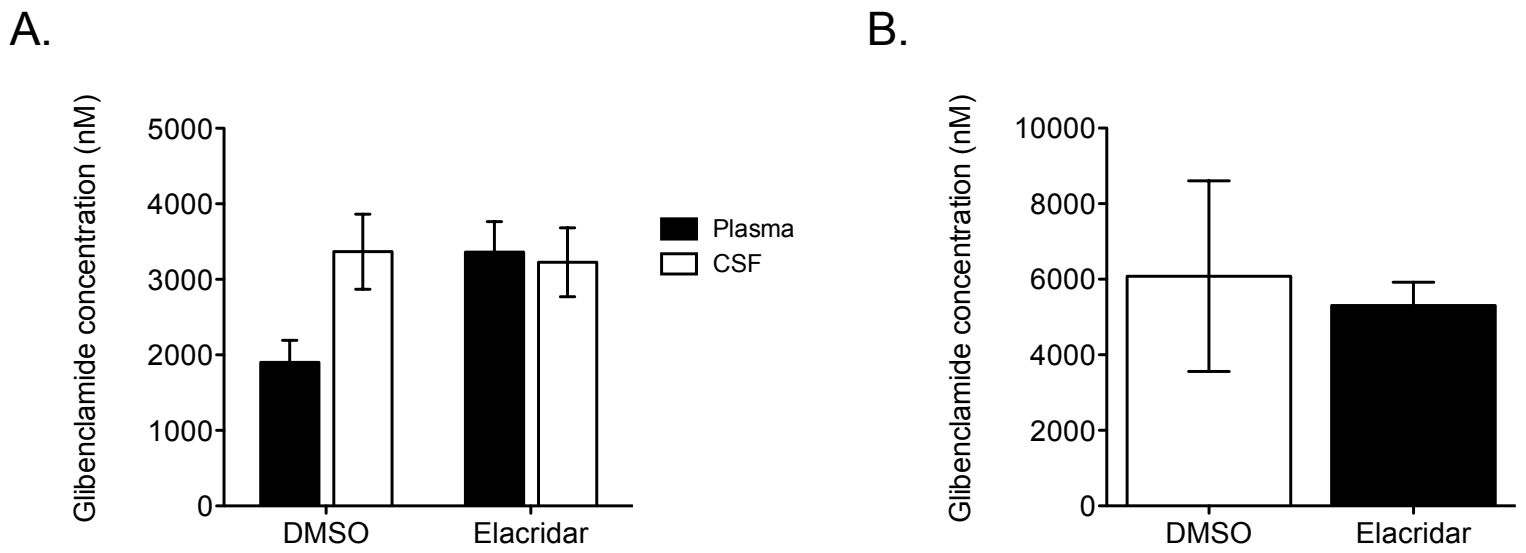

Figure 7.8: Intracranioventricular administration of glibenclamide in the presence of a P-gp inhibitor (elacridar)

(**A**) Plasma and cerebrospinal fluid glibenclamide concentrations from rats injected with 5µl of glibenclamide (25mg/ml in 100% DMSO; n=6) into the right lateral ventricle in the absence (100% DMSO alone; n=6) or presence of elacridar (10mg/kg in 100% DMSO; n=6). (**B**) Brain homogenate glibenclamide concentrations from rats injected with 5µl of glibenclamide (25mg/ml in 100% DMSO; n=6) into the right lateral ventricle in the absence (100% DMSO; white bars; n=6) or presence of elacridar (10mg/kg in 100% DMSO; black bars; n=6). Data are mean ± SEM.

7.5.1. Validation of the quantification method

As the method of quantification was developed using blank mouse plasma samples spiked with different concentrations of glibenclamide, I first implanted mice and rats with slow-release subcutaneous pellets to assess the feasibility of using this method for measuring glibenclamide in plasma after *in vivo* drug administration. For both mice and rats, I was able to quantify the drug concentration in the plasma of glibenclamide-treated animals, and as expected, no signal was detected in placebo-implanted animals.

When comparing the effect of different pellet drug doses on the plasma concentration, increasing the dose administered led to greater plasma concentrations, but no linear correlation was observed for either mice or rats. This is not unexpected as this pharmacokinetic behaviour is observed for drugs that conform to multi-compartmental models, as is the case for glibenclamide (two-compartment open model) [321,322].

Interestingly, in the initial cohort of mice used for the validation of the method (implanted with 2.5mg pellets), a significant difference in the plasma glibenclamide concentration of male and female mice was observed, with females having almost twice the plasma concentration of males. Sex differences in pharmacokinetics have been observed for a wide range of drugs [323,324]. They are thought to reflect differences in drug bioavailability,

distribution, metabolism, and excretion. The primary determinant of sex differences in pharmacokinetics is thought to be sex-associated differences in metabolism, particularly in terms of differences in the expression of hepatic P450 and other drug-metabolising enzymes [324]. It is important to determine whether gender-differences in plasma glibenclamide concentrations are also observed in human patients as this could have important clinical implications.

7.5.2. Subcutaneous therapy

Systemic administration of glibenclamide via subcutaneous slow-release pellets did not result in significant glibenclamide levels being detected in the CSF, despite high glibenclamide concentrations being found in the plasma. It is possible that glibenclamide was rapidly taken up into brain cells, thereby reducing the CSF concentration, particularly as the poor protein content of the CSF makes it an unfavourable environment for glibenclamide. However, this possibility seems unlikely as glibenclamide levels in homogenised brain samples from pellet-implanted rats were also below the limit of quantitation. These results suggest that glibenclamide is unable to cross the BBB despite being found at significant concentrations in the plasma.

7.5.3. Intracranioventricular delivery of glibenclamide

To determine if glibenclamide is effluxed across the BBB, I delivered the drug into the right lateral ventricle of rats using osmotic mini-pumps connected to intracranioventricular cannulae. This would allow sustained delivery of the drug directly into the CSF, effectively bypassing the BBB. Surprisingly, glibenclamide was not detected in the plasma or CSF of the drug-treated rats, despite the fact that it was detected in the osmotic mini-pump solution at high concentrations and that proper placement of the cannulae had been confirmed histologically.

A possible explanation for this finding is that the glibenclamide concentration in the solution excreted by the mini-pump is not high enough to be detected once it enters the CSF. Glibenclamide is a highly lipophilic drug and has a tendency to precipitate out of solution when dissolved in solutions with high salt content, as is the case with artificial CSF. However, I had included bovine serum albumin in the aCSF to reduce the likelihood of glibenclamide precipitating (in plasma it is known to be ~98% bound to proteins) [321,325] as well as decreasing its binding to the polyethelene tubing (previous experience in our group has shown that glibenclamide “sticks” to plastic rather strongly).

To confirm that glibenclamide is present in the solution that leaves the pump, I filled osmotic mini-pump, connected them to cannulae, and collected the

solution excreted over a 7-day period. Glibenclamide was detected in both the solution inside the mini-pump as well as the solution excreted. However, there was a considerable reduction in the glibenclamide concentration in the excreted solution, suggesting the drug may be “sticking” to the plastic tubing, as no clear signs of precipitation were observed. Nonetheless, the drug concentration in the excreted solution was still considerable, which suggests inability to detect glibenclamide in the CSF of rats given the drug by ICV infusion was not caused by an issue with the osmotic mini-pumps.

Another possible explanation for the lack of glibenclamide in the CSF of these rats is that the rate at which the drug exits the CSF is faster than the rate at which it is being pumped in. This, however, raises the question of why glibenclamide was not detected in the plasma if it is being quickly pumped out into the blood. Using the volume of distribution of a drug (0.155 l/kg for glibenclamide) [321], it is possible to calculate the expected plasma concentration when a given amount of drug is administered.

If the total amount of glibenclamide administered over the 7-day period the rats were left with the osmotic mini-pumps had been given as a bolus, the expected plasma concentration would be around 150nM. However, this calculation does not take into account the rate at which the drug is being metabolised and excreted and it assumes administration of the total amount as a bolus. Thus, the lack of glibenclamide detection in the plasma of rats administered glibenclamide by ICV infusion was probably due to it being

diluted to a concentration below the limit of detection upon entry to the systemic circulation. This would also explain why ICV delivery of glibenclamide did not affect the impaired response to anaesthesia exhibited by nV59M mice, as described in Chapter 5.

I tested this hypothesis by administering a highly concentrated dose of glibenclamide acutely into the right lateral ventricle. This should allow detection of the drug in the plasma if it were diluted upon entry to the systemic circulation. Interestingly, glibenclamide levels in the plasma were already higher than those in the CSF one hour after administration of the drug, suggesting glibenclamide is rapidly transported out of the CSF.

High levels of glibenclamide were also detected in the brain homogenate, as expected for a highly lipophilic drug (i.e. greater stability in tissue than in protein-poor CSF). Interestingly, the glibenclamide concentration detected in the brain of acute ICV-injected rats was around 1000-fold higher than that detected in the brains of pellet-implanted rats, despite the plasma concentrations being relatively similar for both groups. This suggests glibenclamide struggles to enter and remain in brain tissue unless it is directly administered into the CSF.

Overall, these results support the existence of a rapid, unidirectional transport mechanism for glibenclamide from the brain to the systemic circulation.

7.5.4. The effect of P-glycoprotein inhibition on plasma and CSF glibenclamide

Previous *in vitro* experiments have shown that glibenclamide is able to inhibit P-gp and may be also a substrate for this transporter [317,318]. P-gp is thought to be one of the most important ABC transporters at the BBB, mediating the efflux of a host of different pharmacological agents [305]. I thus tested the effect of inhibiting P-glycoprotein *in vivo* on the plasma and CSF glibenclamide concentrations in rats.

Elacridar, a P-gp inhibitor, did not affect the plasma glibenclamide concentrations produced by intraperitoneal administration of glibenclamide. By contrast, when elacridar was present, higher glibenclamide concentrations were detected in the CSF of rats administered glibenclamide, suggesting glibenclamide is a substrate for P-gp at the BBB. A larger sample size is required to determine if this effect is statistically significant.

Interestingly, glibenclamide was also detected in the CSF of rats given an intraperitoneal injection of glibenclamide in the absence of elacridar, albeit at a concentration more than 1000-fold lower than in plasma. As the plasma glibenclamide concentrations in these rats were approximately 100-fold higher than those of the pellet-implanted rats, despite receiving equivalent doses, it is possible that the higher circulating concentration led to an increase in the

CSF glibenclamide concentration. Takanaga *et al.* (1998) previously showed that the transcellular mechanism responsible for efflux of tolbutamide across an *in vitro* model of the BBB becomes saturated at high concentrations[289]. It is possible that a similar phenomenon occurs *in vivo* with the transport of glibenclamide across the BBB.

Interestingly, elacridar did not affect the movement of glibenclamide from the CSF to the blood after drug injection into the lateral ventricle. It is known that the BBB in the ventricular system is different from that of other brain areas as it is formed by the epithelia of the choroid plexuses (CP) rather than the capillary endothelium [313,326]. These epithelial cells form tight junctions between adjacent cells, preventing diffusion of blood-borne solutes into the CSF [313].

Like the BBB endothelium, CP epithelial cells express a variety of different ABC transporters. However, studies with KO mice have shown that the distribution and expression pattern of ABC transporters in CP epithelial cells is different from the BBB endothelium [327]. For example, P-gp appears to be expressed less at the CP than the BBB endothelium, while MRP4, another ABC transporter, is more highly expressed at the CP than at the BBB endothelium [328]. It is thus possible that a separate transport mechanism is responsible for the movement of glibenclamide from the CSF to the blood. Further work with specific inhibitors for other ABC transporters is required.

7.6. Conclusions

The results of this chapter suggest that glibenclamide is unable to cross the BBB and enter the brain in significant amounts. It is rapidly removed from the brain when injected directly into the lateral ventricle. This appears to be mediated by active transport across the BBB and may involve P-glycoprotein as well as potentially other members of the ABC transporter super-family.

Chapter 8: Discussion

In the last decade, the physiological importance of the K_{ATP} channel has been highlighted by the discovery that activating mutations in this channel are associated with a variety of metabolic syndromes, ranging from neonatal diabetes (ND) [4] to intermediate DEND (iDEND) and DEND syndromes [5].

Until as recently as 2004, ND patients were treated with insulin for the management of their diabetes. However, the discovery that they carried activating K_{ATP} channel mutations led to the suggestion that sulphonylureas could be used instead. These drugs act by blocking open K_{ATP} channels, leading to secretion of insulin from pancreatic β-cells. Electrophysiological studies had shown that ND mutations lead to a permanent opening of the channel regardless of the metabolic state of the cell. However, most mutant channels were found to be sulphonylurea sensitive, closing in the presence of the drug and so stimulating insulin release [4,5,212,219].

This work resulted in more than 90% of ND patients with K_{ATP} channel mutations being successfully transferred onto sulphonylurea therapy, which has resulted in a significant improvement in glycaemic control and quality of life when compared to insulin therapy [6,217].

In the case of iDEND and DEND syndromes, it was hoped that sulphonylureas would also restore neurological function in these patients, particularly as the composition of the principal neuronal K_{ATP} channel is thought to be the same as that found in pancreatic β-cells (Kir6.2-SUR1) [23,26]. However, this has not been the case. Nevertheless, in some patients, improvements have been observed, especially in terms of motor function [151,189,221,225,226].

Although these reports are encouraging, for many iDEND and most DEND patients, sulphonylureas have been ineffective at improving cognitive deficits, developmental delay or seizures, even when they successfully control the patient's diabetes [157,220,222,224,227]. Furthermore, even in the cases where improved neurological function has been observed, it was not restored to normal.

In this thesis, I used the nV59M iDEND mouse model to determine whether the lack of success of sulphonylureas at fully restoring neurological function was due to irreversible changes caused by the expression of the mutation during development or whether it was due to an inability of sulphonylurea drugs to penetrate the blood-brain barrier (BBB) and reach high enough concentrations in the brain. The results in this thesis argue that the latter is the main cause of the failure of sulphonylureas to fully restore neurological function in iDEND and DEND patients.

8.1. Behavioural assessment of the nV59M mice

Previous work by our group has shown that the nV59M mouse is a faithful model of iDEND syndrome, recapitulating many of the symptoms associated with this condition, including muscle weakness, balance deficits and coordination problems as well as hyperactivity [62]. I thus decided to assess the effect of sulphonylureas on the behaviour of these mice in attempt to determine if inhibition of the K_{ATP} channel *in vivo* restores the deficits associated with iDEND syndrome.

8.1.1. Cognitive function of nV59M mice

Some improvements have been observed in the neurological function of iDEND/DEND patients following transition to sulphonylurea therapy; however, these have mainly been restricted to improved motor function [189,221,225,226,329]. By contrast, very limited improvements in cognitive function have been observed [188,189,222,224,226].

Before testing the effect of sulphonylureas on cognitive function, I first explored if the spontaneous alternation and spatial novelty preference tasks were suitable for studying cognitive deficits in nV59M mice.

Unfortunately, I did not observe a short-term memory deficit in nV59M mice on either of these tasks, preventing any assessment of glibenclamide modulation of cognitive function. This was particularly surprising as our group had previously observed a significant deficit in the performance of nV59M mice on both of these tests (R.H. Clark, *unpublished*).

It is not clear why the phenotype of the nV59M has changed; particularly as the mRNA levels of Kir6.2-V59M in brain tissue from nV59M remain the same. It is possible that these discrepancies were caused by changes in the genetic background of the ROSA-Kir6.2-V59M line used to generate the nV59M colony. The initial ROSA line was on a mixed 129/v-C57Bl/6 background and has been continuously backcrossed to C57Bl/6. As the nV59M cohort I used was on a purer C57Bl/6 background than that used by Clark, it is possible that this may have affected the performance on the behavioural tasks, particularly as it is known that the performance of these two strains varies significantly on behavioural tests [257].

8.1.2. nV59M mice display a decreased anxiety phenotype

In addition to the cognitive tests performed, the nV59M cohort was put through a battery of anxiety tests to determine whether they had an anxiety phenotype.

Interestingly, nV59M mice displayed decreased anxiety as assessed by the dark-light box, successive alleys, and elevated plus maze tests. This is in contrast to mice with global knockout of the Kir6.2, which display increased anxiety [248]. Taken together, these findings argue for a role of the neuronal K_{ATP} channel in the regulation of emotion: loss of K_{ATP} activity leads to increased anxiety levels while enhanced K_{ATP} activity results in decreased anxiety.

Although it would have been interesting to assess whether sulphonylureas can modulate this anxiety phenotype, this would have been difficult to do on an individual basis (i.e. on the same mouse prior to and following treatment) as repeated exposure to these tasks has been shown to affect performance [330].

Nonetheless, the reduced anxiety phenotype in combination with the previously reported hyperactivity of nV59M mice [62] appears to correlate with the increased impulsivity and inattentiveness reported in iDEND/DEND patients [188,189,226,250].

8.1.3. The effect of glibenclamide on the motor function of nV59M mice

One of the hallmarks of iDEND/DEND syndromes is muscle weakness accompanied by balance and coordination problems [4,5]. Our group previously demonstrated these symptoms are caused by impaired neuronal function using the nV59M mouse [62].

In human patients, improvements in motor function have been observed shortly after transition onto sulphonylurea therapy, with various patients walking and talking for the first time [151,189,221,225,226]. However, the motor function of other patients has not improved at all, despite excellent glycaemic control following transfer to sulphonylureas [224,250,255]. Furthermore, even in those patients where improvements were observed, their locomotor performance was still impaired, particularly when their chronological age was taken into account [151,188,189,221,226].

I thus used the nV59M mouse, which has been previously shown to display many of the locomotor problems observed in iDEND/DEND patients [62], to assess whether modulation of the neuronal K_{ATP} channel by sulphonylurea drugs could be responsible for the improvements observed in these patients.

The performance of nV59M mice on a variety of tests used to examine muscle strength, balance and coordination, and spontaneous activity was assessed prior to and following treatment with glibenclamide. Surprisingly, in most of these tasks, the difference between nV59M mice and control littermates in the absence of therapy was not as marked as previously observed [62]. As with the cognitive function tests, it is possible that these variations in performance were caused by changes in the genetic background of the ROSA-Kir6.2-V59M line used to generate the nV59M colony. Because of the weak phenotype, it was not possible to determine whether modulation of the neuronal K_{ATP} channel by sulphonylurea drugs improved locomotor function using the nV59M mouse model.

Interestingly, our group previously described impaired hand-eye tracking in iDEND patients, which is thought to be partially caused by cerebellar dysfunction [259]. These deficits were observed in all iDEND patients examined despite the fact they were all being treated with sulphonylureas, suggesting these drugs are not capable of fully improving motor/neuronal function in human patients.

8.2. Sensitivity to volatile anaesthetics

During the surgical implantation of the slow-release subcutaneous pellets, it became apparent that nV59M mice had altered sensitivity to isoflurane

anaesthesia. They took significantly longer than control littermates to lose their righting and withdrawal reflexes (LORR and LOWR, respectively) when exposed to isoflurane and also when exposed to halothane anaesthesia.

8.2.1. Impaired loss of righting reflex

Although the exact mechanisms by which volatile anaesthetic agents exert their effects are not entirely clear, it is thought that their ability to induce unconsciousness results from their action on the thalamus and pons, which are involved in the regulation of arousal states and sleep [270,279]. Interestingly, these areas have been shown to highly express both Kir6.2 and SUR1 [26], and nV59M mice also appear to have altered sleep patterns, as shown in Chapter 5. Anecdotal evidence suggests children with iDEND/DEND syndrome also have sleep disturbances (http://www.babieswithdiabetes.com/)[331].

Taken together, these results point towards the involvement of the K_{ATP} channel in the regulation of arousal states and consciousness *in vivo*. Further work is required to determine how the K_{ATP} channel modulates the function of specific neuronal networks/areas to exert these effects and whether this modulation is important for normal physiological function.

8.2.2. Impaired withdrawal reflex

The withdrawal reflex is used to assess anaesthesia-induced immobility. This reflex appears to be primarily regulated at the spinal cord level, with particular involvement of ventral spinal cord neurones [276,282].

Little is known about the role of the K_{ATP} channel in the spinal cord, and the expression of these channels in ventral horn neurones has not been studied. However, it is known that K_{ATP} channels of the Kir6.2/SUR1 subtype are expressed in dorsal root ganglion neurones, and they have been shown to play a role in the physiological regulation of the electrical activity of primary afferent neurones [281]. Furthermore, it is thought that K_{ATP} channels in these neurones are involved in nociception and hyperalgesia [281,283-286]. Thus, it seems likely that the impaired LOWR observed in nV59M mice may be caused by altered nociception.

Interestingly, one iDEND patient with the Kir6.2-V59M mutation has been diagnosed with sensory integration dysfunction, which is characterised by impaired sensory processing resulting in behavioural alterations [332]. In the case of this patient, he displays over-responsivity to tactile stimuli: “For a child that is super sensitive to the sensations on his face, a haircut can feel like razor blades on the skin.” (Excerpt from: http://www.babieswithdiabetes.com/) [331]. Although this is anecdotal evidence from only one patient, when taken

together with the nV59M impaired LOWR, it suggests the K_{ATP} channel may be involved in the processing of noxious and non-noxious stimuli. Therefore, further work is required to elucidate the channel's role in sensory perception and primary afferent neuron function.

8.2.3. Glibenclamide therapy partially restores isoflurane sensitivity of nV59M mice

As the main aim of this thesis was to establish whether sulphonylurea drugs are capable of modulating neuronal function *in vivo*, I decided to test the effect of glibenclamide on the impaired sensitivity to volatile anaesthetics observed in nV59M mice.

Systemic delivery of glibenclamide had no effect on the impaired LORR of nV59M mice, but partially restored the LOWR. The disparity in the effect of the drug could be due to an inability of glibenclamide to enter the brain, particularly if the altered LOWR in nV59M mice is due to expression of the mutation in primary afferent neurones, as these lie outside of the BBB.

I therefore administered glibenclamide directly into the brain via a cannula implanted into the right lateral ventricle. Surprisingly, ICV-administered glibenclamide had no effect on the LORR or LOWR in nV59M mice. This suggests that either expression of the mutation during development may be

activating irreversible compensatory mechanisms or that the drug is actively excreted from the brain. To address the first possibility, I generated an inducible model of iDEND syndrome, in order to bypass the effect of the mutation on development. To test the second idea, I used an analytical chemistry method to quantify the concentration of glibenclamide in the plasma, cerebrospinal fluid and brain of rodents after administration of the drug.

8.3. The Ubi-ROSA mouse: An inducible global model of iDEND syndrome?

In mouse models with constitutive expression of a mutation, compensatory mechanisms that are not present in wild-type mice may be activated, particularly if the endogenous promoter and the exogenous promoter used to drive expression are activated at different stages of development [297]. In neuronal mouse models, this can result in behavioural phenotypes caused by altered gene expression induced at a prior developmental stage rather than at the period of interest [287,288].

To address any confounding effects of the mutation during development and to determine whether these are responsible for the impaired LORR in nV59M mice, I used the ubiquitin-Cre-ER line to generate the Ubi-ROSA line, which enabled me to activate the mutant gene at any specific stage of development.

The Ubi-ROSA line did not prove to be a good global model of iDEND syndrome, as the mice did not develop diabetes following activation of the gene. This appears to be due to poor recombination in pancreatic islets.

Interestingly, following gene induction, Ubi-ROSA mice did not display the impaired LORR phenotype observed in nV59M mice. This might indicate that this phenotype arose in nV59M mice because of some compensatory mechanism during development. However, ubiquitin-Cre-ER line appears to show mosaic expression of Cre recombinase in certain brain areas, including the pons and the medulla [333]. It was thus not possible to conclude that the altered LORR in nV59M mice is developmental in origin.

The Ubi-ROSA and Ubi-ROSA-DN mice displayed altered LOWR, which was reversed by systemic glibenclamide therapy. This validates the results obtained with the nV59M mice and indicates that the K_{ATP} channel is most likely involved in modulation of sensory input *in vivo*. It also indicates that ubiquitin and nestin must be expressed in the same neurones and demonstrates that the impaired LOWR is due to K_{ATP} channel activation *per se* and is not a secondary consequence of developmental changes resulting from K_{ATP} channel hyperactivity during brain development.

Although the Ubi-ROSA was not an adequate mouse model, due to the mosaic expression of ubiquitin, it would be of value to generate an inducible model of iDEND syndrome, particularly for the study of the neurological

symptoms. This could help address whether these problems are caused by a direct effect of the mutation on neuronal function or if they are partially caused by alterations to the brain circuitry due to excess K_{ATP} channel activity during development. Importantly, discrepancies have been observed in the responses to sulphonylurea therapy, with better clinical outcome being associated with early administration of sulphonylurea therapy [6,218,259]. It is not clear whether this is due to better glycaemic control from early age, particularly as marked blood glucose fluctuations can affect cognitive function [334], or due to irreversible changes in neuronal circuitry. An adequate inducible model might help to address these questions.

8.4. Sulphonylureas and the blood-brain barrier

Sulphonylureas are highly lipophilic drugs, which allows them to partition into the lipid bilayer and rapidly enter many tissues, including the brain. However, it has been previously shown that tolbutamide, a sulphonylurea, is actively extruded from the brain [289]. To determine whether this is also the case for glibenclamide, I measured drug concentrations in the plasma, cerebrospinal fluid and brain of rats after administration of glibenclamide.

Glibenclamide was not detected in the brain or CSF of rats after implantation of subcutaneous drug pellets (equivalent to oral therapy in patients). This was despite high drug concentrations being detected in the plasma of the same

animals, and the dose administered being more than 10-fold higher than that administered to iDEND/DEND patients (maximum ~3mg/kg/day; rats administered ~50mg/kg/day) [6]. It thus appears unlikely that glibenclamide will be detected in the CSF or brain of human patients after oral administration, even with high doses of the drug.

Interestingly, when a 50mg/kg bolus of glibenclamide was administered intraperitoneally to rats, the drug was detected in the CSF of the animals. However, the concentration measured was more than 1000-fold lower than that in plasma. Furthermore, the plasma concentration of these rats was 100-fold higher than that of pellet-implanted rats. This suggests that glibenclamide may be kept out of the brain and CSF by a mechanism that becomes saturated at very high drug concentrations, in a similar fashion to that previously described for tolbutamide [289].

Although this might suggests that increasing the glibenclamide dose administered to iDEND/DEND patients would allow the drug to accumulate in the CSF/brain, it is important to bear in mind that the dose administered to our rats was more than 10-fold higher than the maximum dose given to a human patient and that the plasma concentrations observed are in the supra-pharmacological range. This could lead to undesirable effects in the periphery, including hypoglycaemia and potential pharmacokinetic complications. Thus, it appears that such a drastic increase in the dose

administered would be clinically unfeasible, particularly as the concentrations detected in the CSF are relatively modest.

To explore how readily glibenclamide is removed from the brain, I administered the drug directly into the right lateral ventricle. This resulted in rapid excretion of glibenclamide from the CSF into the systemic circulation; within an hour of administering a high dose into the ventricle, the levels detected in the plasma were already higher than those in the CSF. This further supports the idea that the drug is rapidly transported across the BBB. Moreover, this result suggests intrathecal administration of glibenclamide to iDEND/DEND patients to increase the drug concentration in the CSF is unlikely to be clinically beneficial as the drug will most likely be rapidly effluxed across the BBB.

P-glycoprotein (P-gp) is one of the most important transporters at the BBB, mediating the efflux of many endogenous and exogenous agents from the brain [305]. As this transporter has been shown to pump glibenclamide *in vitro* [317,318], I assessed if it was responsible for the efflux of glibenclamide across the BBB *in vivo*. Interestingly, administration of elacridar, a P-gp inhibitor, appeared to increase the concentration of glibenclamide detected in the CSF of rats after intraperitoneal administration of the drug. However, P-gp inhibition did not alter the efflux of glibenclamide into the systemic circulation when the drug was administered directly into the lateral ventricle.

The BBB in the ventricular system is different from that in other brain areas and it is known to express different ABC transporters [309,313,327]. It is hence possible that a separate transport mechanism is responsible for the movement of glibenclamide from the CSF to the systemic circulation. It is also possible that elacridar was not able to reach its site of action at the ventricular BBB. Administration of both drugs directly into the lateral ventricle may be desirable to determine if P-gp is involved in this transportation.

Although the potential involvement of P-gp in glibenclamide efflux may open up the possibility of using P-gp inhibitors to increase drug concentrations in the brain of iDEND/DEND patients, this would be highly undesirable clinically as it may allow other pharmacological agents, normally transported across the BBB by P-gp, to enter the brain. Furthermore, P-gp is found in other tissues, particularly the kidney, where it is involved in the excretion of drugs. Inhibition of peripheral P-gp could therefore have adverse effects on the metabolism and excretion of other pharmacological agents as well as glibenclamide.

8.5. Future directions

The work presented in this thesis suggests that glibenclamide is unable to fully restore neurological function in iDEND/DEND patients because it fails to reach high enough concentrations in the brain. Glibenclamide is a highly lipophilic drug, which allows it to readily enter tissues by partitioning into the

lipid bilayer. Thus, the negligible concentrations of glibenclamide found in the CSF and brain, despite high doses being administered systemically, are most likely due to the drug being rapidly transported out of the brain by a saturable efflux system.

Despite my findings, some neurological improvement, particularly in terms of motor function, is observed in iDEND/DEND patients following transition to sulphonylurea therapy. Furthermore, imaging studies using single-photon emission computer tomography (SPECT) have shown increased cerebellar perfusion in iDEND, but not PNDM, patients following transition to sulphonylureas [335]. Taken together, these clinical results suggest that glibenclamide may be able to enter the human brain to some extent.

It is possible that the BBB of iDEND patients is slightly “leakier”, as has been reported in other neurological conditions including epilepsy, stroke, Alzheimer’s disease, and Parkinson’s disease [305]. However, this would not explain why improved perfusion is only observed in the cerebellum and why motor function is preferentially improved by sulphonylurea therapy. Further work is required to clarify this. One approach might be to perform SPECT imaging of nV59M mice prior to, and during, sulphonylurea therapy and following the subsequent removal of the drug. This might reveal if the changes in cerebellar perfusion seen in human patients are caused by the drug acting on the neuronal K_{ATP} channel.

Even though our assay can detect glibenclamide concentrations as low as ~40nM, it has been shown that concentrations lower than this can partially block K_{ATP} currents *in vitro* [336]. It is thus possible that the drug may be able to modulate neuronal function (resulting in improved cerebellar perfusion and motor function) in certain brain areas even at concentrations below those we can accurately quantify. The contribution of the K_{ATP} channel to the resting membrane potential may vary in different subtypes of neurones, which may explain why motor function is preferentially improved. Further work is required to obtain a lower limit of detection for our assay so as to accurately determine the maximum glibenclamide concentration that reaches the CSF/brain after systemic delivery.

Although the neurological effects of activating K_{ATP} channel mutations are well understood at the whole animal level, the cellular effects of the mutation still need to be elucidated. This could be addressed by using different Cre lines to selectively target different brain areas, as well as different neuronal subtypes. This would not only be useful in understanding how the different neurological symptoms arise, but may also help in finding adequate therapies for the treatment of iDEND/DEND patients. Furthermore, this could also help in elucidating the mechanisms involved in anaesthesia-mediated loss of consciousness.

My work suggests that glibenclamide accumulates rather poorly in the brain *in vivo*. However, it is possible that other sulphonylureas, such as gliclazide, or

other K_{ATP} channel blockers such as repaglinide, may be able to cross the BBB and accumulate in the brain more readily. It is thus necessary to assess the BBB permeability of other sulphonylureas because finding one that enters (and stays) in the brain could be useful for the management of iDEND/DEND patients. Unfortunately, this seems unlikely as not only are tolbutamide and glibenclamide both effluxed from the brain, but they all share a similar chemical structure, making it likely that they are all transported out of the brain by the same mechanism.

Interestingly, it has been recently shown that carbamazepine, an antiepileptic drug, can inhibit K_{ATP} currents *in vitro* [337]. As this drug can be assumed to readily cross the BBB (it is used in the management of epilepsy and other neurological conditions), it may be useful for the management of the neurological symptoms of iDEND/DEND patients. Further work needs to be conducted to determine the extent to which carbamazepine can block K_{ATP} channels with activating mutations and whether the concentrations at which it inhibits the channel are safe to use clinically.

Finally, my results demonstrate glibenclamide does not accumulate in the brain/CSF of rodents. However, this has not been directly assessed in humans. Differences in the transporters expressed in the BBB of rodents and humans have been reported [338], so it is possible that this may lead to differences in the drugs transported across the BBB in rodents versus humans. Nonetheless, it has been recently demonstrated using radiolabelled-

glibenclamide positron emission topography that glibenclamide does not readily accumulate in the brain of baboons and that P-gp is involved in limiting glibenclamide brain uptake in non-human primates [339]. This further supports my results and suggests that a similar mechanism may play a role in glibenclamide uptake across the BBB in humans. Assessing glibenclamide permeability across the human BBB will be difficult, although it may be possible to retrospectively measure glibenclamide concentrations in CSF samples from iDEND/DEND patients if they ever were to have a lumbar puncture.

In conclusion, the discrepancies between the ability of glibenclamide to improve the diabetes and the neurological symptoms in iDEND/DEND patients are most likely due to the inability of the drug to reach a high enough concentration in the brain.

References

1. Ashcroft, S. J. & Ashcroft, F. M. Properties and functions of ATP-sensitive K-channels. *Cell. Signal.* **2,** 197–214 (1990).
2. Seino, S. & Miki, T. Physiological and pathophysiological roles of ATP-sensitive K+ channels. *Prog. Biophys. Mol. Biol.* **81,** 133–176 (2003).
3. Nichols, C. G. KATP channels as molecular sensors of cellular metabolism. *Nature* **440,** 470–476 (2006).
4. Gloyn, A. L. *et al.* Activating mutations in the gene encoding the ATP-sensitive potassium-channel subunit Kir6.2 and permanent neonatal diabetes. *N. Engl. J. Med.* **350,** 1838–1849 (2004).
5. Hattersley, A. T. & Ashcroft, F. M. Activating mutations in Kir6.2 and neonatal diabetes: new clinical syndromes, new scientific insights, and new therapy. *Diabetes* **54,** 2503–2513 (2005).
6. Pearson, E. R. *et al.* Switching from insulin to oral sulfonylureas in patients with diabetes due to Kir6.2 mutations. *N. Engl. J. Med.* **355,** 467–477 (2006).
7. Noma, A. ATP-regulated K+ channels in cardiac muscle. *Nature* **305,** 147–148 (1983).
8. Cook, D. L. & Hales, C. N. Intracellular ATP directly blocks K+ channels in pancreatic B-cells. *Nature* **311,** 271–273 (1984).
9. Ashcroft, F. M., Harrison, D. E. & Ashcroft, S. J. Glucose induces closure of single potassium channels in isolated rat pancreatic beta-cells. *Nature* **312,** 446–448 (1984).
10. Rorsman, P. & Trube, G. Glucose dependent K+-channels in pancreatic beta-cells are regulated by intracellular ATP. *Pflugers Arch.* **405,** 305–309 (1985).
11. Spruce, A. E., Standen, N. B. & Stanfield, P. R. Voltage-dependent ATP-sensitive potassium channels of skeletal muscle membrane. *Nature* **316,** 736–738 (1985).
12. Standen, N. B. *et al.* Hyperpolarizing vasodilators activate ATP-sensitive K+ channels in arterial smooth muscle. *Science* **245,** 177–180 (1989).
13. Ashford, M. L., Boden, P. R. & Treherne, J. M. Tolbutamide excites rat glucoreceptive ventromedial hypothalamic neurones by indirect inhibition of ATP-K+ channels. *British Journal of Pharmacology* **101,** 531–540 (1990).
14. Sakura, H., Ammälä, C., Smith, P. A., Gribble, F. M. & Ashcroft, F. M. Cloning and functional expression of the cDNA encoding a novel ATP-sensitive potassium channel subunit expressed in pancreatic beta-cells, brain, heart and skeletal muscle. *FEBS Lett.* **377,** 338–344 (1995).
15. Clement, J. P. *et al.* Association and stoichiometry of K(ATP) channel

subunits. *Neuron* **18,** 827–838 (1997).
16. Shyng, S. & Nichols, C. G. Octameric stoichiometry of the KATP channel complex. *J. Gen. Physiol.* **110,** 655–664 (1997).
17. Mikhailov, M. V. *et al.* 3-D structural and functional characterization of the purified KATP channel complex Kir6.2-SUR1. *EMBO J.* **24,** 4166–4175 (2005).
18. Inagaki, N. *et al.* Reconstitution of IKATP: an inward rectifier subunit plus the sulfonylurea receptor. *Science* **270,** 1166–1170 (1995).
19. Matsuda, H., Saigusa, A. & Irisawa, H. Ohmic conductance through the inwardly rectifying K channel and blocking by internal Mg2+. *Nature* **325,** 156–159 (1987).
20. Lopatin, A. N., Makhina, E. N. & Nichols, C. G. Potassium channel block by cytoplasmic polyamines as the mechanism of intrinsic rectification. *Nature* **372,** 366–369 (1994).
21. Pegan, S. *et al.* Cytoplasmic domain structures of Kir2.1 and Kir3.1 show sites for modulating gating and rectification. *Nat Neurosci* **8,** 279–287 (2005).
22. Nichols, C. G. & Lopatin, A. N. Inward rectifier potassium channels. *Annu. Rev. Physiol.* **59,** 171–191 (1997).
23. Zhou, M. *et al.* Localization of the ATP-sensitive K(+) channel regulatory subunits SUR2A and SUR2B in the rat brain. *Neurosci. Res.* **74,** 91–105 (2012).
24. Aguilar-Bryan, L. *et al.* Cloning of the beta cell high-affinity sulfonylurea receptor: a regulator of insulin secretion. *Science* **268,** 423–426 (1995).
25. Aittoniemi, J. *et al.* Review. SUR1: a unique ATP-binding cassette protein that functions as an ion channel regulator. *Philos. Trans. R. Soc. Lond., B, Biol. Sci.* **364,** 257–267 (2009).
26. Karschin, C., Ecke, C., Ashcroft, F. M. & Karschin, A. Overlapping distribution of K(ATP) channel-forming Kir6.2 subunit and the sulfonylurea receptor SUR1 in rodent brain. *FEBS Lett.* **401,** 59–64 (1997).
27. Liss, B., Bruns, R. & Roeper, J. Alternative sulfonylurea receptor expression defines metabolic sensitivity of K-ATP channels in dopaminergic midbrain neurons. *EMBO J.* **18,** 833–846 (1999).
28. Flagg, T. P. *et al.* Differential structure of atrial and ventricular KATP: atrial KATP channels require SUR1. *Circ. Res.* **103,** 1458–1465 (2008).
29. Isomoto, S. *et al.* A novel sulfonylurea receptor forms with BIR (Kir6.2) a smooth muscle type ATP-sensitive K+ channel. *J. Biol. Chem.* **271,** 24321–24324 (1996).
30. Inagaki, N. *et al.* A family of sulfonylurea receptors determines the pharmacological properties of ATP-sensitive K+ channels. *Neuron* **16,** 1011–1017 (1996).
31. Zerangue, N., Schwappach, B., Jan, Y. N. & Jan, L. Y. A new ER trafficking signal regulates the subunit stoichiometry of plasma membrane K(ATP) channels. *Neuron* **22,** 537–548 (1999).
32. Mikhailov, M. V., Proks, P., Ashcroft, F. M. & Ashcroft, S. J.

Expression of functionally active ATP-sensitive K-channels in insect cells using baculovirus. *FEBS Lett.* **429,** 390–394 (1998).
33. Inanobe, A., Ito, H., Ito, M., Hosoya, Y. & Kurachi, Y. Immunological and physical characterization of the brain G protein-gated muscarinic potassium channel. *Biochem. Biophys. Res. Commun.* **217,** 1238–1244 (1995).
34. Nishida, M. & MacKinnon, R. Structural basis of inward rectification: cytoplasmic pore of the G protein-gated inward rectifier GIRK1 at 1.8 A resolution. *Cell* **111,** 957–965 (2002).
35. Kuo, A. *et al.* Crystal structure of the potassium channel KirBac1.1 in the closed state. *Science* **300,** 1922–1926 (2003).
36. Nishida, M., Cadene, M., Chait, B. T. & MacKinnon, R. Crystal structure of a Kir3.1-prokaryotic Kir channel chimera. *EMBO J.* **26,** 4005–4015 (2007).
37. Antcliff, J. F., Haider, S., Proks, P., Sansom, M. S. P. & Ashcroft, F. M. Functional analysis of a structural model of the ATP-binding site of the KATP channel Kir6.2 subunit. *EMBO J.* **24,** 229–239 (2005).
38. Stansfeld, P. J., Hopkinson, R., Ashcroft, F. M. & Sansom, M. S. P. PIP(2)-binding site in Kir channels: definition by multiscale biomolecular simulations. *Biochemistry* **48,** 10926–10933 (2009).
39. Mikhailov, M. V., Mikhailova, E. A. & Ashcroft, S. J. Molecular structure of the glibenclamide binding site of the beta-cell K(ATP) channel. *FEBS Lett.* **499,** 154–160 (2001).
40. Babenko, A. P. & Bryan, J. SUR-dependent modulation of KATP channels by an N-terminal KIR6.2 peptide. Defining intersubunit gating interactions. *J. Biol. Chem.* **277,** 43997–44004 (2002).
41. Chan, K. W., Zhang, H. & Logothetis, D. E. N-terminal transmembrane domain of the SUR controls trafficking and gating of Kir6 channel subunits. *EMBO J.* **22,** 3833–3843 (2003).
42. Higgins, C. F. & Linton, K. J. The ATP switch model for ABC transporters. *Nat. Struct. Mol. Biol.* **11,** 918–926 (2004).
43. Yamada, M. & Kurachi, Y. The nucleotide-binding domains of sulfonylurea receptor 2A and 2B play different functional roles in nicorandil-induced activation of ATP-sensitive K+ channels. *Mol. Pharmacol.* **65,** 1198–1207 (2004).
44. Campbell, J. D., Sansom, M. S. & Ashcroft, F. M. Potassium channel regulation. *EMBO Rep* **4,** 1038–1042 (2003).
45. Hollenstein, K., Dawson, R. J. P. & Locher, K. P. Structure and mechanism of ABC transporter proteins. *Curr. Opin. Struct. Biol.* **17,** 412–418 (2007).
46. Babenko, A. P. A novel ABCC8 (SUR1)-dependent mechanism of metabolism-excitation uncoupling. *J. Biol. Chem.* **283,** 8778–8782 (2008).
47. de Wet, H. *et al.* A mutation (R826W) in nucleotide-binding domain 1 of ABCC8 reduces ATPase activity and causes transient neonatal diabetes. *EMBO Rep* **9,** 648–654 (2008).
48. Locher, K. P., Lee, A. T. & Rees, D. C. The E. coli BtuCD structure: a framework for ABC transporter architecture and mechanism. *Science*

296, 1091–1098 (2002).
49. Ward, A., Reyes, C. L., Yu, J., Roth, C. B. & Chang, G. Flexibility in the ABC transporter MsbA: Alternating access with a twist. *PNAS* **104,** 19005–19010 (2007).
50. Dawson, R. J. P. & Locher, K. P. Structure of a bacterial multidrug ABC transporter. *Nature* **443,** 180–185 (2006).
51. Dawson, R. J. P. & Locher, K. P. Structure of the multidrug ABC transporter Sav1866 from Staphylococcus aureus in complex with AMP-PNP. *FEBS Lett.* **581,** 935–938 (2007).
52. Proks, P., Takano, M. & Ashcroft, F. M. Effects of intracellular pH on ATP-sensitive K+ channels in mouse pancreatic beta-cells. *J. Physiol. (Lond.)* **475,** 33–44 (1994).
53. Fan, Z. & Makielski, J. C. Anionic phospholipids activate ATP-sensitive potassium channels. *J. Biol. Chem.* **272,** 5388–5395 (1997).
54. Shyng, S. L. & Nichols, C. G. Membrane phospholipid control of nucleotide sensitivity of KATP channels. *Science* **282,** 1138–1141 (1998).
55. Larsson, O., Deeney, J. T., Bränström, R., Berggren, P. O. & Corkey, B. E. Activation of the ATP-sensitive K+ channel by long chain acyl-CoA. A role in modulation of pancreatic beta-cell glucose sensitivity. *J. Biol. Chem.* **271,** 10623–10626 (1996).
56. Gribble, F. M., Proks, P., Corkey, B. E. & Ashcroft, F. M. Mechanism of cloned ATP-sensitive potassium channel activation by oleoyl-CoA. *J. Biol. Chem.* **273,** 26383–26387 (1998).
57. Nichols, C. G. *et al.* Adenosine diphosphate as an intracellular regulator of insulin secretion. *Science* **272,** 1785–1787 (1996).
58. Tucker, S. J., Gribble, F. M., Zhao, C., Trapp, S. & Ashcroft, F. M. Truncation of Kir6.2 produces ATP-sensitive K+ channels in the absence of the sulphonylurea receptor. *Nature* **387,** 179–183 (1997).
59. Gribble, F. M., Tucker, S. J. & Ashcroft, F. M. The essential role of the Walker A motifs of SUR1 in K-ATP channel activation by Mg-ADP and diazoxide. *EMBO J.* **16,** 1145–1152 (1997).
60. Zingman, L. V. *et al.* Signaling in channel/enzyme multimers: ATPase transitions in SUR module gate ATP-sensitive K+ conductance. *Neuron* **31,** 233–245 (2001).
61. Baukrowitz, T. & Fakler, B. KATP channels gated by intracellular nucleotides and phospholipids. *Eur. J. Biochem.* **267,** 5842–5848 (2000).
62. Clark, R. H. *et al.* Muscle dysfunction caused by a KATP channel mutation in neonatal diabetes is neuronal in origin. *Science* **329,** 458–461 (2010).
63. Yamada, M. *et al.* Sulphonylurea receptor 2B and Kir6.1 form a sulphonylurea-sensitive but ATP-insensitive K+ channel. *J. Physiol. (Lond.)* **499 (Pt 3),** 715–720 (1997).
64. Ashcroft, F. M. & Rorsman, P. Electrophysiology of the pancreatic beta-cell. *Prog. Biophys. Mol. Biol.* **54,** 87–143 (1989).
65. Ashcroft, F. M. The Walter B. Cannon Physiology in Perspective Lecture, 2007. ATP-sensitive K+ channels and disease: from molecule

to malady. *Am. J. Physiol. Endocrinol. Metab.* **293,** E880–9 (2007).
66. Kang, G. *et al.* cAMP sensor Epac as a determinant of ATP-sensitive potassium channel activity in human pancreatic beta cells and rat INS-1 cells. *J. Physiol. (Lond.)* **573,** 595–609 (2006).
67. Zhang, C.-L. *et al.* The cAMP sensor Epac2 is a direct target of antidiabetic sulfonylurea drugs. *Science* **325,** 607–610 (2009).
68. Mourre, C., Widmann, C. & Lazdunski, M. Sulfonylurea binding sites associated with ATP-regulated K+ channels in the central nervous system: autoradiographic analysis of their distribution and ontogenesis, and of their localization in mutant mice cerebellum. *Brain Res.* **519,** 29–43 (1990).
69. Dunn-Meynell, A. A., Rawson, N. E. & Levin, B. E. Distribution and phenotype of neurons containing the ATP-sensitive K+ channel in rat brain. *Brain Res.* **814,** 41–54 (1998).
70. Zhou, M. *et al.* Localization of the ATP-sensitive potassium channel subunit (Kir6. 1/uK(ATP)-1) in rat brain. *Brain Res. Mol. Brain Res.* **74,** 15–25 (1999).
71. Grigg, J. J. & Anderson, E. G. Glucose and sulfonylureas modify different phases of the membrane potential change during hypoxia in rat hippocampal slices. *Brain Res.* **489,** 302–310 (1989).
72. Fujimura, N., Tanaka, E., Yamamoto, S., Shigemori, M. & Higashi, H. Contribution of ATP-sensitive potassium channels to hypoxic hyperpolarization in rat hippocampal CA1 neurons in vitro. *J. Neurophysiol.* **77,** 378–385 (1997).
73. Zawar, C., Plant, T. D., Schirra, C., Konnerth, A. & Neumcke, B. Cell-type specific expression of ATP-sensitive potassium channels in the rat hippocampus. *J. Physiol. (Lond.)* **514 (Pt 2),** 327–341 (1999).
74. Matsumoto, N., Komiyama, S. & Akaike, N. Pre- and postsynaptic ATP-sensitive potassium channels during metabolic inhibition of rat hippocampal CA1 neurons. *J. Physiol. (Lond.)* **541,** 511–520 (2002).
75. Spanswick, D., Smith, M. A., Groppi, V. E., Logan, S. D. & Ashford, M. L. Leptin inhibits hypothalamic neurons by activation of ATP-sensitive potassium channels. *Nature* **390,** 521–525 (1997).
76. Lee, K., Dixon, A. K., Richardson, P. J. & Pinnock, R. D. Glucose-receptive neurones in the rat ventromedial hypothalamus express KATP channels composed of Kir6.1 and SUR1 subunits. *J. Physiol. (Lond.)* **515 (Pt 2),** 439–452 (1999).
77. Schwanstecher, C. & Panten, U. Tolbutamide- and diazoxide-sensitive K+ channel in neurons of substantia nigra pars reticulata. *Naunyn-Schmiedeberg's Archives of Pharmacology* **348,** 113–117 (1993).
78. Roeper, J. & Pongs, O. Presynaptic potassium channels. *Curr. Opin. Neurobiol.* **6,** 338–341 (1996).
79. Guatteo, E. *et al.* Whole cell patch-clamp recordings of rat midbrain dopaminergic neurons isolate a sulphonylurea- and ATP-sensitive component of potassium currents activated by hypoxia. *J. Neurophysiol.* **79,** 1239–1245 (1998).
80. Ohno-Shosaku, T. & Yamamoto, C. Identification of an ATP-sensitive K+ channel in rat cultured cortical neurons. *Pflugers Arch.* **422,** 260–

266 (1992).
81. Dallaporta, M., Perrin, J. & Orsini, J. C. Involvement of adenosine triphosphate-sensitive K+ channels in glucose-sensing in the rat solitary tract nucleus. *Neurosci. Lett.* **278,** 77–80 (2000).
82. Liss, B. & Roeper, J. Molecular physiology of neuronal K-ATP channels (review). *Mol. Membr. Biol.* **18,** 117–127 (2001).
83. Zhou, M. *et al.* Localization of pore-forming subunit of the ATP-sensitive K(+)-channel, Kir6.2, in rat brain neurons and glial cells. *Brain Res. Mol. Brain Res.* **101,** 23–32 (2002).
84. Thomzig, A., Laube, G., Prüss, H. & Veh, R. W. Pore-forming subunits of K-ATP channels, Kir6.1 and Kir6.2, display prominent differences in regional and cellular distribution in the rat brain. *J. Comp. Neurol.* **484,** 313–330 (2005).
85. Thomzig, A. *et al.* Kir6.1 is the principal pore-forming subunit of astrocyte but not neuronal plasma membrane K-ATP channels. *Mol Cell Neurosci* **18,** 671–690 (2001).
86. Miki, T. *et al.* ATP-sensitive K+ channels in the hypothalamus are essential for the maintenance of glucose homeostasis. *Nat Neurosci* **4,** 507–512 (2001).
87. Steffens, A. B., Strubbe, J. H., Balkan, B. & Scheurink, J. W. Neuroendocrine mechanisms involved in regulation of body weight, food intake and metabolism. *Neurosci Biobehav Rev* **14,** 305–313 (1990).
88. Levin, B. E., Dunn-Meynell, A. A. & Routh, V. H. Brain glucose sensing and body energy homeostasis: role in obesity and diabetes. *Am. J. Physiol.* **276,** R1223–31 (1999).
89. Pocai, A. *et al.* Hypothalamic K(ATP) channels control hepatic glucose production. *Nature* **434,** 1026–1031 (2005).
90. Kishore, P. *et al.* Activation of K(ATP) channels suppresses glucose production in humans. *J. Clin. Invest.* **121,** 4916–4920 (2011).
91. Yamada, K. *et al.* Protective role of ATP-sensitive potassium channels in hypoxia-induced generalized seizure. *Science* **292,** 1543–1546 (2001).
92. Bancila, V., Nikonenko, I., Dunant, Y. & Bloc, A. Zinc inhibits glutamate release via activation of pre-synaptic K channels and reduces ischaemic damage in rat hippocampus. *J Neurochem* **90,** 1243–1250 (2004).
93. Tanner, G. R., Lutas, A., Martínez-François, J. R. & Yellen, G. Single K ATP channel opening in response to action potential firing in mouse dentate granule neurons. *Journal of Neuroscience* **31,** 8689–8696 (2011).
94. Giménez-Cassina, A. *et al.* BAD-dependent regulation of fuel metabolism and K(ATP) channel activity confers resistance to epileptic seizures. *Neuron* **74,** 719–730 (2012).
95. Cunningham, M. O. *et al.* Neuronal metabolism governs cortical network response state. *Proc. Natl. Acad. Sci. U.S.A.* **103,** 5597–5601 (2006).
96. Seutin, V., Shen, K. Z., North, R. A. & Johnson, S. W. Sulfonylurea-

sensitive potassium current evoked by sodium-loading in rat midbrain dopamine neurons. *Neuroscience* **71,** 709–719 (1996).
97. Miki, T. *et al.* Defective insulin secretion and enhanced insulin action in KATP channel-deficient mice. *Proc. Natl. Acad. Sci. U.S.A.* **95,** 10402–10406 (1998).
98. Muñoz, A. *et al.* Ischemic preconditioning in the hippocampus of a knockout mouse lacking SUR1-based K(ATP) channels. *Stroke* **34,** 164–170 (2003).
99. Hernández-Sánchez, C. *et al.* Mice transgenically overexpressing sulfonylurea receptor 1 in forebrain resist seizure induction and excitotoxic neuron death. *Proc. Natl. Acad. Sci. U.S.A.* **98,** 3549–3554 (2001).
100. Schiemann, J. *et al.* K-ATP channels in dopamine substantia nigra neurons control bursting and novelty-induced exploration. *Nat Neurosci* **15,** 1272–1280 (2012).
101. Aynsley-Green, A. *et al.* Nesidioblastosis of the pancreas: definition of the syndrome and the management of the severe neonatal hyperinsulinaemic hypoglycaemia. *Arch. Dis. Child.* **56,** 496–508 (1981).
102. Thomas, P. M. *et al.* Mutations in the sulfonylurea receptor gene in familial persistent hyperinsulinemic hypoglycemia of infancy. *Science* **268,** 426–429 (1995).
103. Dunne, M. J., Cosgrove, K. E., Shepherd, R. M., Aynsley-Green, A. & Lindley, K. J. Hyperinsulinism in infancy: from basic science to clinical disease. *Physiol. Rev.* **84,** 239–275 (2004).
104. Flanagan, S. E. *et al.* Dominantly acting ABCC8 mutations in patients with medically unresponsive hyperinsulinaemic hypoglycaemia. *Clin. Genet.* **79,** 582–587 (2011).
105. Thomas, P. M., Cote, G. J., Hallman, D. M. & Mathew, P. M. Homozygosity mapping, to chromosome 11p, of the gene for familial persistent hyperinsulinemic hypoglycemia of infancy. *Am. J. Hum. Genet.* **56,** 416–421 (1995).
106. Thomas, P., Ye, Y. & Lightner, E. Mutation of the pancreatic islet inward rectifier Kir6.2 also leads to familial persistent hyperinsulinemic hypoglycemia of infancy. *Hum. Mol. Genet.* **5,** 1809–1812 (1996).
107. Stanley, C. A. *et al.* Hyperinsulinism and hyperammonemia in infants with regulatory mutations of the glutamate dehydrogenase gene. *N. Engl. J. Med.* **338,** 1352–1357 (1998).
108. Glaser, B. *et al.* Familial hyperinsulinism caused by an activating glucokinase mutation. *N. Engl. J. Med.* **338,** 226–230 (1998).
109. Pearson, E. R. *et al.* Macrosomia and hyperinsulinaemic hypoglycaemia in patients with heterozygous mutations in the HNF4A gene. *PLoS Med.* **4,** e118 (2007).
110. Clayton, P. T. *et al.* Hyperinsulinism in short-chain L-3-hydroxyacyl-CoA dehydrogenase deficiency reveals the importance of beta-oxidation in insulin secretion. *J. Clin. Invest.* **108,** 457–465 (2001).
111. Otonkoski, T. *et al.* Physical exercise-induced hyperinsulinemic hypoglycemia is an autosomal-dominant trait characterized by

abnormal pyruvate-induced insulin release. *Diabetes* **52,** 199–204 (2003).
112. Otonkoski, T. *et al.* Physical exercise-induced hypoglycemia caused by failed silencing of monocarboxylate transporter 1 in pancreatic beta cells. *Am. J. Hum. Genet.* **81,** 467–474 (2007).
113. Flanagan, S. E. *et al.* Diazoxide-responsive hyperinsulinemic hypoglycemia caused by HNF4A gene mutations. *Eur. J. Endocrinol.* **162,** 987–992 (2010).
114. Kane, C. *et al.* Loss of functional KATP channels in pancreatic beta-cells causes persistent hyperinsulinemic hypoglycemia of infancy. *Nat. Med.* **2,** 1344–1347 (1996).
115. Pinney, S. E. *et al.* Clinical characteristics and biochemical mechanisms of congenital hyperinsulinism associated with dominant KATP channel mutations. *J. Clin. Invest.* **118,** 2877–2886 (2008).
116. Ashcroft, F. M. ATP-sensitive potassium channelopathies: focus on insulin secretion. *J. Clin. Invest.* **115,** 2047–2058 (2005).
117. Dunne, M. J. *et al.* Familial persistent hyperinsulinemic hypoglycemia of infancy and mutations in the sulfonylurea receptor. *N. Engl. J. Med.* **336,** 703–706 (1997).
118. Partridge, C. J., Beech, D. J. & Sivaprasadarao, A. Identification and pharmacological correction of a membrane trafficking defect associated with a mutation in the sulfonylurea receptor causing familial hyperinsulinism. *J. Biol. Chem.* **276,** 35947–35952 (2001).
119. Taschenberger, G. *et al.* Identification of a familial hyperinsulinism-causing mutation in the sulfonylurea receptor 1 that prevents normal trafficking and function of KATP channels. *J. Biol. Chem.* **277,** 17139–17146 (2002).
120. Shyng, S. L. *et al.* Functional analyses of novel mutations in the sulfonylurea receptor 1 associated with persistent hyperinsulinemic hypoglycemia of infancy. *Diabetes* **47,** 1145–1151 (1998).
121. Matsuo, M. *et al.* Functional analysis of a mutant sulfonylurea receptor, SUR1-R1420C, that is responsible for persistent hyperinsulinemic hypoglycemia of infancy. *J. Biol. Chem.* **275,** 41184–41191 (2000).
122. Huopio, H. *et al.* Dominantly inherited hyperinsulinism caused by a mutation in the sulfonylurea receptor type 1. *J. Clin. Invest.* **106,** 897–906 (2000).
123. Tanizawa, Y. *et al.* Genetic analysis of Japanese patients with persistent hyperinsulinemic hypoglycemia of infancy: nucleotide-binding fold-2 mutation impairs cooperative binding of adenine nucleotides to sulfonylurea receptor 1. *Diabetes* **49,** 114–120 (2000).
124. Magge, S. N. *et al.* Familial leucine-sensitive hypoglycemia of infancy due to a dominant mutation of the beta-cell sulfonylurea receptor. *J. Clin. Endocrinol. Metab.* **89,** 4450–4456 (2004).
125. Nestorowicz, A. *et al.* A nonsense mutation in the inward rectifier potassium channel gene, Kir6.2, is associated with familial hyperinsulinism. *Diabetes* **46,** 1743–1748 (1997).
126. Henwood, M. J. *et al.* Genotype-phenotype correlations in children

with congenital hyperinsulinism due to recessive mutations of the adenosine triphosphate-sensitive potassium channel genes. *J. Clin. Endocrinol. Metab.* **90,** 789–794 (2005).
127. Flanagan, S. E. *et al.* Update of mutations in the genes encoding the pancreatic beta-cell K(ATP) channel subunits Kir6.2 (KCNJ11) and sulfonylurea receptor 1 (ABCC8) in diabetes mellitus and hyperinsulinism. *Hum. Mutat.* **30,** 170–180 (2009).
128. Edghill, E. L., Flanagan, S. E. & Ellard, S. Permanent neonatal diabetes due to activating mutations in ABCC8 and KCNJ11. *Rev Endocr Metab Disord* **11,** 193–198 (2010).
129. Edghill, E. L. *et al.* Activating mutations in the KCNJ11 gene encoding the ATP-sensitive K+ channel subunit Kir6.2 are rare in clinically defined type 1 diabetes diagnosed before 2 years. *Diabetes* **53,** 2998–3001 (2004).
130. Polak, M. & Shield, J. Neonatal and very-early-onset diabetes mellitus. *Semin Neonatol* **9,** 59–65 (2004).
131. Shield, J. P. H. *et al.* An assessment of pancreatic endocrine function and insulin sensitivity in patients with transient neonatal diabetes in remission. *Arch. Dis. Child. Fetal Neonatal Ed.* **89,** F341–3 (2004).
132. Temple, I. K. *et al.* Transient neonatal diabetes: widening the understanding of the etiopathogenesis of diabetes. *Diabetes* **49,** 1359–1366 (2000).
133. Remedi, M. S. & Koster, J. C. K(ATP) channelopathies in the pancreas. *Pflugers Arch.* **460,** 307–320 (2010).
134. Gardner, R. J. *et al.* An imprinted locus associated with transient neonatal diabetes mellitus. *Hum. Mol. Genet.* **9,** 589–596 (2000).
135. Flanagan, S. E. *et al.* Mutations in ATP-sensitive K+ channel genes cause transient neonatal diabetes and permanent diabetes in childhood or adulthood. *Diabetes* **56,** 1930–1937 (2007).
136. Babenko, A. P. *et al.* Activating mutations in the ABCC8 gene in neonatal diabetes mellitus. *N. Engl. J. Med.* **355,** 456–466 (2006).
137. Ashcroft, F. M. & Rorsman, P. Diabetes mellitus and the β cell: the last ten years. *Cell* **148,** 1160–1171 (2012).
138. Craig, T. J. *et al.* An in-frame deletion in Kir6.2 (KCNJ11) causing neonatal diabetes reveals a site of interaction between Kir6.2 and SUR1. *J. Clin. Endocrinol. Metab.* **94,** 2551–2557 (2009).
139. Ellard, S. *et al.* Permanent neonatal diabetes caused by dominant, recessive, or compound heterozygous SUR1 mutations with opposite functional effects. *Am. J. Hum. Genet.* **81,** 375–382 (2007).
140. Stoffers, D. A., Zinkin, N. T., Stanojevic, V., Clarke, W. L. & Habener, J. F. Pancreatic agenesis attributable to a single nucleotide deletion in the human IPF1 gene coding sequence. *Nat. Genet.* **15,** 106–110 (1997).
141. Yoo, H.-W., Shin, Y.-L., Seo, E.-J. & Kim, G.-H. Identification of a novel mutation in the GLUT2 gene in a patient with Fanconi-Bickel syndrome presenting with neonatal diabetes mellitus and galactosaemia. *Eur. J. Pediatr.* **161,** 351–353 (2002).
142. Osbak, K. K. *et al.* Update on mutations in glucokinase (GCK), which

cause maturity-onset diabetes of the young, permanent neonatal diabetes, and hyperinsulinemic hypoglycemia. *Hum. Mutat.* **30,** 1512–1526 (2009).
143. Støy, J. *et al.* Clinical and molecular genetics of neonatal diabetes due to mutations in the insulin gene. *Rev Endocr Metab Disord* **11,** 205–215 (2010).
144. Catli, G. *et al.* Permanent neonatal diabetes caused by a novel mutation in the INS gene. *Diabetes Res. Clin. Pract.* **99,** e5–8 (2013).
145. Delépine, M. *et al.* EIF2AK3, encoding translation initiation factor 2-alpha kinase 3, is mutated in patients with Wolcott-Rallison syndrome. *Nat. Genet.* **25,** 406–409 (2000).
146. Sellick, G. S. *et al.* Mutations in PTF1A cause pancreatic and cerebellar agenesis. *Nat. Genet.* **36,** 1301–1305 (2004).
147. Bennett, C. L. *et al.* A rare polyadenylation signal mutation of the FOXP3 gene (AAUAAA-->AAUGAA) leads to the IPEX syndrome. *Immunogenetics* **53,** 435–439 (2001).
148. Smith, S. B. *et al.* Rfx6 directs islet formation and insulin production in mice and humans. *Nature* **463,** 775–780 (2010).
149. Senée, V. *et al.* Mutations in GLIS3 are responsible for a rare syndrome with neonatal diabetes mellitus and congenital hypothyroidism. *Nat. Genet.* **38,** 682–687 (2006).
150. Tonini, G. *et al.* Sulfonylurea treatment outweighs insulin therapy in short-term metabolic control of patients with permanent neonatal diabetes mellitus due to activating mutations of the KCNJ11 (KIR6.2) gene. *Diabetologia* **49,** 2210–2213 (2006).
151. Slingerland, A. S., Nuboer, R., Hadders-Algra, M., Hattersley, A. T. & Bruining, G. J. Improved motor development and good long-term glycaemic control with sulfonylurea treatment in a patient with the syndrome of intermediate developmental delay, early-onset generalised epilepsy and neonatal diabetes associated with the V59M mutation in the KCNJ11 gene. *Diabetologia* **49,** 2559–2563 (2006).
152. Jones, A. G. & Hattersley, A. T. Reevaluation of a case of type 1 diabetes mellitus diagnosed before 6 months of age. *Nat Rev Endocrinol* **6,** 347–351 (2010).
153. Pearl, P. L. *Inherited Metabolic Epilepsies*. (Demos Medical Publishing, 2012).
154. Proks, P. *et al.* Molecular basis of Kir6.2 mutations associated with neonatal diabetes or neonatal diabetes plus neurological features. *Proc. Natl. Acad. Sci. U.S.A.* **101,** 17539–17544 (2004).
155. Proks, P., Girard, C. & Ashcroft, F. M. Functional effects of KCNJ11 mutations causing neonatal diabetes: enhanced activation by MgATP. *Hum. Mol. Genet.* **14,** 2717–2726 (2005).
156. Koster, J. C., Remedi, M. S., Dao, C. & Nichols, C. G. ATP and sulfonylurea sensitivity of mutant ATP-sensitive K+ channels in neonatal diabetes: implications for pharmacogenomic therapy. *Diabetes* **54,** 2645–2654 (2005).
157. Masia, R. *et al.* An ATP-binding mutation (G334D) in KCNJ11 is associated with a sulfonylurea-insensitive form of developmental

delay, epilepsy, and neonatal diabetes. *Diabetes* **56,** 328–336 (2007).
158. Gloyn, A. L. *et al.* Relapsing diabetes can result from moderately activating mutations in KCNJ11. *Hum. Mol. Genet.* **14,** 925–934 (2005).
159. Drain, P., Li, L. & Wang, J. KATP channel inhibition by ATP requires distinct functional domains of the cytoplasmic C terminus of the pore-forming subunit. *Proc. Natl. Acad. Sci. U.S.A.* **95,** 13953–13958 (1998).
160. Tucker, S. J. *et al.* Molecular determinants of KATP channel inhibition by ATP. *EMBO J.* **17,** 3290–3296 (1998).
161. Girard, C. A. J. *et al.* Functional analysis of six Kir6.2 (KCNJ11) mutations causing neonatal diabetes. *Pflugers Arch.* **453,** 323–332 (2006).
162. Proks, P., Shimomura, K., Craig, T. J., Girard, C. A. J. & Ashcroft, F. M. Mechanism of action of a sulphonylurea receptor SUR1 mutation (F132L) that causes DEND syndrome. *Hum. Mol. Genet.* **16,** 2011–2019 (2007).
163. Tammaro, P. *et al.* A Kir6.2 mutation causing severe functional effects in vitro produces neonatal diabetes without the expected neurological complications. *Diabetologia* **51,** 802–810 (2008).
164. McTaggart, J. S., Clark, R. H. & Ashcroft, F. M. The role of the KATP channel in glucose homeostasis in health and disease: more than meets the islet. *J. Physiol. (Lond.)* **588,** 3201–3209 (2010).
165. Tammaro, P., Girard, C., Molnes, J., Njølstad, P. R. & Ashcroft, F. M. Kir6.2 mutations causing neonatal diabetes provide new insights into Kir6.2-SUR1 interactions. *EMBO J.* **24,** 2318–2330 (2005).
166. Proks, P. *et al.* A heterozygous activating mutation in the sulphonylurea receptor SUR1 (ABCC8) causes neonatal diabetes. *Hum. Mol. Genet.* **15,** 1793–1800 (2006).
167. de Wet, H. *et al.* Studies of the ATPase activity of the ABC protein SUR1. *FEBS J.* **274,** 3532–3544 (2007).
168. Yorifuji, T. *et al.* The C42R mutation in the Kir6.2 (KCNJ11) gene as a cause of transient neonatal diabetes, childhood diabetes, or later-onset, apparently type 2 diabetes mellitus. *J. Clin. Endocrinol. Metab.* **90,** 3174–3178 (2005).
169. Patch, A. M., Flanagan, S. E., Boustred, C., Hattersley, A. T. & Ellard, S. Mutations in the ABCC8 gene encoding the SUR1 subunit of the KATP channel cause transient neonatal diabetes, permanent neonatal diabetes or permanent diabetes diagnosed outside the neonatal period. *Diabetes, Obesity and Metabolism* **9 Suppl 2,** 28–39 (2007).
170. Miki, T. *et al.* Abnormalities of pancreatic islets by targeted expression of a dominant-negative KATP channel. *Proc. Natl. Acad. Sci. U.S.A.* **94,** 11969–11973 (1997).
171. Silverman, S. K., Kofuji, P., Dougherty, D. A., Davidson, N. & Lester, H. A. A regenerative link in the ionic fluxes through the weaver potassium channel underlies the pathophysiology of the mutation. *Proc. Natl. Acad. Sci. U.S.A.* **93,** 15429–15434 (1996).
172. Seghers, V., Nakazaki, M., DeMayo, F., Aguilar-Bryan, L. & Bryan, J.

Sur1 knockout mice. A model for K(ATP) channel-independent regulation of insulin secretion. *J. Biol. Chem.* **275,** 9270–9277 (2000).
173. Hugill, A., Shimomura, K., Ashcroft, F. M. & Cox, R. D. A mutation in KCNJ11 causing human hyperinsulinism (Y12X) results in a glucose-intolerant phenotype in the mouse. *Diabetologia* **53,** 2352–2356 (2010).
174. Koster, J. C. *et al.* Hyperinsulinism induced by targeted suppression of beta cell KATP channels. *Proc. Natl. Acad. Sci. U.S.A.* **99,** 16992–16997 (2002).
175. Grimberg, A. *et al.* Dysregulation of insulin secretion in children with congenital hyperinsulinism due to sulfonylurea receptor mutations. *Diabetes* **50,** 322–328 (2001).
176. Huopio, H. *et al.* A new subtype of autosomal dominant diabetes attributable to a mutation in the gene for sulfonylurea receptor 1. *Lancet* **361,** 301–307 (2003).
177. Kassem, S. A., Ariel, I., Thornton, P. S., Scheimberg, I. & Glaser, B. Beta-cell proliferation and apoptosis in the developing normal human pancreas and in hyperinsulinism of infancy. *Diabetes* **49,** 1325–1333 (2000).
178. Koster, J. C., Marshall, B. A., Ensor, N., Corbett, J. A. & Nichols, C. G. Targeted overactivity of beta cell K(ATP) channels induces profound neonatal diabetes. *Cell* **100,** 645–654 (2000).
179. Koster, J. C. *et al.* Expression of ATP-insensitive KATP channels in pancreatic beta-cells underlies a spectrum of diabetic phenotypes. *Diabetes* **55,** 2957–2964 (2006).
180. Remedi, M. S. *et al.* Secondary consequences of beta cell inexcitability: identification and prevention in a murine model of K(ATP)-induced neonatal diabetes mellitus. *Cell Metab.* **9,** 140–151 (2009).
181. Girard, C. A. *et al.* Expression of an activating mutation in the gene encoding the KATP channel subunit Kir6.2 in mouse pancreatic beta cells recapitulates neonatal diabetes. *J. Clin. Invest.* **119,** 80–90 (2009).
182. Koster, J. C., Sha, Q., Shyng, S. & Nichols, C. G. ATP inhibition of KATP channels: control of nucleotide sensitivity by the N-terminal domain of the Kir6.2 subunit. *J. Physiol. (Lond.)* **515 (Pt 1),** 19–30 (1999).
183. Allen, N. D., Keverne, E. B. & Surani, M. A. A position-dependent transgene reveals patterns of gene expression in the developing brain. *Brain Res. Dev. Brain Res.* **55,** 181–190 (1990).
184. Dobie, K. W. *et al.* Variegated transgene expression in mouse mammary gland is determined by the transgene integration locus. *Proc. Natl. Acad. Sci. U.S.A.* **93,** 6659–6664 (1996).
185. Herrera, P. L. Defining the cell lineages of the islets of Langerhans using transgenic mice. *Int. J. Dev. Biol.* **46,** 97–103 (2002).
186. Zhang, H., Fujitani, Y., Wright, C. V. E. & Gannon, M. Efficient recombination in pancreatic islets by a tamoxifen-inducible Cre-recombinase. *Genesis* **42,** 210–217 (2005).

187. Sagen, J. V. *et al.* Permanent neonatal diabetes due to mutations in KCNJ11 encoding Kir6.2: patient characteristics and initial response to sulfonylurea therapy. *Diabetes* **53,** 2713–2718 (2004).
188. Slingerland, A. S. *et al.* Sulphonylurea therapy improves cognition in a patient with the V59M KCNJ11 mutation. *Diabet. Med.* **25,** 277–281 (2008).
189. Mlynarski, W. *et al.* Sulfonylurea improves CNS function in a case of intermediate DEND syndrome caused by a mutation in KCNJ11. *Nat Clin Pract Neurol* **3,** 640–645 (2007).
190. Boyd, A. E., Aguilar-Bryan, L. & Nelson, D. A. Molecular mechanisms of action of glyburide on the beta cell. *Am. J. Med.* **89,** 3S–10S–discussion 51S–53S (1990).
191. Henquin, J. C. The fiftieth anniversary of hypoglycaemic sulphonamides. How did the mother compound work? *Diabetologia* **35,** 907–912 (1992).
192. LOUBATIERES, A. The mechanism of action of the hypoglycemic sulfonamides; a concept based on investigations in animals and in man. *Diabetes* **6,** 408–417 (1957).
193. MEHNERT, H., SCHAEFER, G., KALIAMPETSOS, G., STUHLFAUTH, K. & ENGELHARDT, W. [Insulin secretion of the pancreas in extracorporeal perfusion. II. Perfusions of the pancreas with periston, glucose, carbutamide and biguanides]. *Klin. Wochenschr.* **40,** 1146–1151 (1962).
194. Sussman, K. E., Vaughan, G. D. & Timmer, R. F. An in vitro method for studying insulin secretion in the perfused isolated rat pancreas. *Metab. Clin. Exp.* **15,** 466–476 (1966).
195. Malaisse, W. J., Malaisse-Lagae, F. & Wright, P. H. Insulin secretion in vitro by islets from insulin-deficient rats. *Proc. Soc. Exp. Biol. Med.* **126,** 474–476 (1967).
196. Sturgess, N. C., Ashford, M. L., Cook, D. L. & Hales, C. N. The sulphonylurea receptor may be an ATP-sensitive potassium channel. *Lancet* **2,** 474–475 (1985).
197. Trube, G., Rorsman, P. & Ohno-Shosaku, T. Opposite effects of tolbutamide and diazoxide on the ATP-dependent K+ channel in mouse pancreatic beta-cells. *Pflugers Arch.* **407,** 493–499 (1986).
198. Schmid-Antomarchi, H., de Weille, J., Fosset, M. & Lazdunski, M. The antidiabetic sulfonylurea glibenclamide is a potent blocker of the ATP-modulated K+ channel in insulin secreting cells. *Biochem. Biophys. Res. Commun.* **146,** 21–25 (1987).
199. Aguilar-Bryan, L., Nichols, C. G., Rajan, A. S., Parker, C. & Bryan, J. Co-expression of sulfonylurea receptors and KATP channels in hamster insulinoma tumor (HIT) cells. Evidence for direct association of the receptor with the channel. *J. Biol. Chem.* **267,** 14934–14940 (1992).
200. Khan, R. N., Hales, C. N., Ozanne, S. E., Adogu, A. A. & Ashford, M. L. Dissociation of KATP channel and sulphonylurea receptor in the rat clonal insulin-secreting cell line, CRI-D11. *Proc. Biol. Sci.* **253,** 225–231 (1993).

201. Nichols, C. G. Molecular biology of the KATP channel. Where's the clone? *Cardiovasc. Res.* **28,** 727–728 (1994).
202. Ammälä, C. *et al.* Promiscuous coupling between the sulphonylurea receptor and inwardly rectifying potassium channels. *Nature* **379,** 545–548 (1996).
203. Inagaki, N. *et al.* Cloning and functional characterization of a novel ATP-sensitive potassium channel ubiquitously expressed in rat tissues, including pancreatic islets, pituitary, skeletal muscle, and heart. *J. Biol. Chem.* **270,** 5691–5694 (1995).
204. Inagaki, N., Gonoi, T. & Seino, S. Subunit stoichiometry of the pancreatic beta-cell ATP-sensitive K+ channel. *FEBS Lett.* **409,** 232–236 (1997).
205. Lorenz, E. *et al.* Evidence for direct physical association between a K+ channel (Kir6.2) and an ATP-binding cassette protein (SUR1) which affects cellular distribution and kinetic behavior of an ATP-sensitive K+ channel. *Mol. Cell. Biol.* **18,** 1652–1659 (1998).
206. Gribble, F. M., Ashfield, R., Ammälä, C. & Ashcroft, F. M. Properties of cloned ATP-sensitive K+ currents expressed in Xenopus oocytes. *J. Physiol. (Lond.)* **498 (Pt 1),** 87–98 (1997).
207. Uhde, I., Toman, A., Gross, I., Schwanstecher, C. & Schwanstecher, M. Identification of the potassium channel opener site on sulfonylurea receptors. *J. Biol. Chem.* **274,** 28079–28082 (1999).
208. Gillis, K. D. *et al.* Effects of sulfonamides on a metabolite-regulated ATPi-sensitive K+ channel in rat pancreatic B-cells. *Am. J. Physiol.* **257,** C1119–27 (1989).
209. Barrett-Jolley, R. & Davies, N. W. Kinetic analysis of the inhibitory effect of glibenclamide on KATP channels of mammalian skeletal muscle. *J. Membr. Biol.* **155,** 257–262 (1997).
210. Koster, J. C., Sha, Q. & Nichols, C. G. Sulfonylurea and K(+)-channel opener sensitivity of K(ATP) channels. Functional coupling of Kir6.2 and SUR1 subunits. *J. Gen. Physiol.* **114,** 203–213 (1999).
211. Lawrence, C. L. *et al.* Gliclazide produces high-affinity block of KATP channels in mouse isolated pancreatic beta cells but not rat heart or arterial smooth muscle cells. *Diabetologia* **44,** 1019–1025 (2001).
212. Proks, P., Reimann, F., Green, N., Gribble, F. & Ashcroft, F. Sulfonylurea stimulation of insulin secretion. *Diabetes* **51 Suppl 3,** S368–76 (2002).
213. Gribble, F. M. & Reimann, F. Sulphonylurea action revisited: the post-cloning era. *Diabetologia* **46,** 875–891 (2003).
214. Proks, P. & Ashcroft, F. M. Modeling K(ATP) channel gating and its regulation. *Prog. Biophys. Mol. Biol.* **99,** 7–19 (2009).
215. Ashfield, R., Gribble, F. M., Ashcroft, S. J. & Ashcroft, F. M. Identification of the high-affinity tolbutamide site on the SUR1 subunit of the K(ATP) channel. *Diabetes* **48,** 1341–1347 (1999).
216. Hambrock, A., Löffler-Walz, C., Russ, U., Lange, U. & Quast, U. Characterization of a mutant sulfonylurea receptor SUR2B with high affinity for sulfonylureas and openers: differences in the coupling to Kir6.x subtypes. *Mol. Pharmacol.* **60,** 190–199 (2001).

217. Rafiq, M. *et al.* Effective treatment with oral sulfonylureas in patients with diabetes due to sulfonylurea receptor 1 (SUR1) mutations. *Diabetes Care* **31,** 204–209 (2008).
218. Ashcroft, F. M. New uses for old drugs: neonatal diabetes and sulphonylureas. *Cell Metab.* **11,** 179–181 (2010).
219. Proks, P. *et al.* A gating mutation at the internal mouth of the Kir6.2 pore is associated with DEND syndrome. *EMBO Rep* **6,** 470–475 (2005).
220. Shimomura, K. *et al.* Mutations at the same residue (R50) of Kir6.2 (KCNJ11) that cause neonatal diabetes produce different functional effects. *Diabetes* **55,** 1705–1712 (2006).
221. Shimomura, K. *et al.* A novel mutation causing DEND syndrome: a treatable channelopathy of pancreas and brain. *Neurology* **69,** 1342–1349 (2007).
222. Gurgel, L. C. *et al.* Sulfonylrea treatment in permanent neonatal diabetes due to G53D mutation in the KCNJ11 gene: improvement in glycemic control and neurological function. *Diabetes Care* **30,** e108 (2007).
223. Mannikko, R. *et al.* Interaction between mutations in the slide helix of Kir6.2 associated with neonatal diabetes and neurological symptoms. *Hum. Mol. Genet.* **19,** 963–972 (2010).
224. Zwaveling-Soonawala, N. *et al.* Successful transfer to sulfonylurea therapy in an infant with developmental delay, epilepsy and neonatal diabetes (DEND) syndrome and a novel ABCC8 gene mutation. *Diabetologia* **54,** 469–471 (2011).
225. Koster, J. C., Kurata, H. T., Enkvetchakul, D. & Nichols, C. G. DEND mutation in Kir6.2 (KCNJ11) reveals a flexible N-terminal region critical for ATP-sensing of the KATP channel. *Biophys. J.* **95,** 4689–4697 (2008).
226. Battaglia, D. *et al.* Glyburide ameliorates motor coordination and glucose homeostasis in a child with diabetes associated with the KCNJ11/S225T, del226-232 mutation. *Pediatr Diabetes* **13,** 656–660 (2012).
227. Manna, Della, T. *et al.* Glibenclamide unresponsiveness in a Brazilian child with permanent neonatal diabetes mellitus and DEND syndrome due to a C166Y mutation in KCNJ11 (Kir6.2) gene. *Arq Bras Endocrinol Metabol* **52,** 1350–1355 (2008).
228. Soriano, P. Generalized lacZ expression with the ROSA26 Cre reporter strain. *Nat. Genet.* **21,** 70–71 (1999).
229. Tronche, F. *et al.* Disruption of the glucocorticoid receptor gene in the nervous system results in reduced anxiety. *Nat. Genet.* **23,** 99–103 (1999).
230. Ruzankina, Y. *et al.* Deletion of the developmentally essential gene ATR in adult mice leads to age-related phenotypes and stem cell loss. *Cell Stem Cell* **1,** 113–126 (2007).
231. Pfaffl, M. W. A new mathematical model for relative quantification in real-time RT-PCR. *Nucleic Acids Res.* **29,** e45 (2001).
232. Vandesompele, J. *et al.* Accurate normalization of real-time

quantitative RT-PCR data by geometric averaging of multiple internal control genes. *Genome Biol.* **3,** RESEARCH0034 (2002).
233. Ben Ari, Y. Effect of glibenclamide, a selective blocker of an ATP-K+ channel, on the anoxic response of hippocampal neurones. *Pflugers Arch.* **414 Suppl 1,** S111–4 (1989).
234. Mourre, C., Ben Ari, Y., Bernardi, H., Fosset, M. & Lazdunski, M. Antidiabetic sulfonylureas: localization of binding sites in the brain and effects on the hyperpolarization induced by anoxia in hippocampal slices. *Brain Res.* **486,** 159–164 (1989).
235. Ben Ari, Y. Hippocampal potassium ATP channels and anoxia: presynaptic, postsynaptic or both? *Trends Neurosci.* **13,** 409–410 (1990).
236. Sun, H.-S., Feng, Z.-P., Miki, T., Seino, S. & French, R. J. Enhanced neuronal damage after ischemic insults in mice lacking Kir6.2-containing ATP-sensitive K+ channels. *J. Neurophysiol.* **95,** 2590–2601 (2006).
237. Zawar, C. & Neumcke, B. Differential activation of ATP-sensitive potassium channels during energy depletion in CA1 pyramidal cells and interneurones of rat hippocampus. *Pflügers Archiv* **439,** 256–262 (2000).
238. Amoroso, S., Schmid-Antomarchi, H., Fosset, M. & Lazdunski, M. Glucose, sulfonylureas, and neurotransmitter release: role of ATP-sensitive K+ channels. *Science* **247,** 852–854 (1990).
239. Lee, K., Brownhill, V. & Richardson, P. J. Antidiabetic sulphonylureas stimulate acetylcholine release from striatal cholinergic interneurones through inhibition of K(ATP) channel activity. *J Neurochem* **69,** 1774–1776 (1997).
240. Shi, X.-R. *et al.* Kir6.2 knockout alters neurotransmitter release in mouse striatum: an in vivo microdialysis study. *Neurosci. Lett.* **439,** 230–234 (2008).
241. Schmid-Antomarchi, H., Amoroso, S., Fosset, M. & Lazdunski, M. K+ channel openers activate brain sulfonylurea-sensitive K+ channels and block neurosecretion. *Proc. Natl. Acad. Sci. U.S.A.* **87,** 3489–3492 (1990).
242. During, M. J., Leone, P., Davis, K. E., Kerr, D. & Sherwin, R. S. Glucose modulates rat substantia nigra GABA release in vivo via ATP-sensitive potassium channels. *J. Clin. Invest.* **95,** 2403–2408 (1995).
243. Quinta-Ferreira, M. E. & Matias, C. M. Tetanically released zinc inhibits hippocampal mossy fiber calcium, zinc and synaptic responses. *Brain Res.* **1047,** 1–9 (2005).
244. Matias, C. M., Saggau, P. & Quinta-Ferreira, M. E. Blockade of presynaptic K ATP channels reduces the zinc-mediated posttetanic depression at hippocampal mossy fiber synapses. *Brain Res.* **1320,** 22–27 (2010).
245. Betourne, A. *et al.* Involvement of hippocampal CA3 K(ATP) channels in contextual memory. *Neuropharmacology* **56,** 615–625 (2009).
246. Stefani, M. R. & Gold, P. E. Intra-septal injections of glucose and glibenclamide attenuate galanin-induced spontaneous alternation

performance deficits in the rat. *Brain Res.* **813,** 50–56 (1998).
247. Stefani, M. R. & Gold, P. E. Intrahippocampal infusions of k-atp channel modulators influence spontaneous alternation performance: relationships to acetylcholine release in the hippocampus. *Journal of Neuroscience* **21,** 609–614 (2001).
248. Deacon, R. M. J. *et al.* Behavioral phenotyping of mice lacking the K ATP channel subunit Kir6.2. *Physiol. Behav.* **87,** 723–733 (2006).
249. Choeiri, C. *et al.* Cerebral glucose transporters expression and spatial learning in the K-ATP Kir6.2(-/-) knockout mice. *Behav. Brain Res.* **172,** 233–239 (2006).
250. Mohamadi, A. *et al.* Medical and developmental impact of transition from subcutaneous insulin to oral glyburide in a 15-yr-old boy with neonatal diabetes mellitus and intermediate DEND syndrome: extending the age of KCNJ11 mutation testing in neonatal DM. *Pediatr Diabetes* **11,** 203–207 (2010).
251. Slingerland, A. S. & Hattersley, A. T. Mutations in the Kir6.2 subunit of the KATP channel and permanent neonatal diabetes: new insights and new treatment. *Ann. Med.* **37,** 186–195 (2005).
252. Warren, R. E. & Frier, B. M. Hypoglycaemia and cognitive function. *Diabetes, Obesity and Metabolism* **7,** 493–503 (2005).
253. Sumnik, Z., Kolouskova, S., Wales, J. K. H., Komarek, V. & Cinek, O. Sulphonylurea treatment does not improve psychomotor development in children with KCNJ11 mutations causing permanent neonatal diabetes mellitus accompanied by developmental delay and epilepsy (DEND syndrome). *Diabet. Med.* **24,** 1176–1178 (2007).
254. Itoh, S. *et al.* DEND syndrome due to V59A mutation in KCNJ11 gene: unresponsive to sulfonylureas. *J. Pediatr. Endocrinol. Metab.* **26,** 143–146 (2013).
255. Dupont, J. *et al.* Permanent neonatal diabetes mellitus due to KCNJ11 mutation in a Portuguese family: transition from insulin to oral sulfonylureas. *J. Pediatr. Endocrinol. Metab.* **25,** 367–370 (2012).
256. Crawley, J. N. Exploratory behavior models of anxiety in mice. *Neurosci Biobehav Rev* **9,** 37–44 (1985).
257. Contet, C., Rawlins, J. N. & Deacon, R. M. A comparison of 129S2/SvHsd and C57BL/6JOlaHsd mice on a test battery assessing sensorimotor, affective and cognitive behaviours: implications for the study of genetically modified mice. *Behav. Brain Res.* **124,** 33–46 (2001).
258. Lister, R. G. The use of a plus-maze to measure anxiety in the mouse. *Psychopharmacology (Berl.)* **92,** 180–185 (1987).
259. McTaggart, J. S. *et al.* Gain-of-function mutations in the K(ATP) channel (KCNJ11) impair coordinated hand-eye tracking. *PLoS ONE* **8,** e62646 (2013).
260. Vaxillaire, M. *et al.* New ABCC8 mutations in relapsing neonatal diabetes and clinical features. *Diabetes* **56,** 1737–1741 (2007).
261. Remedi, M. S. & Nichols, C. G. Chronic antidiabetic sulfonylureas in vivo: reversible effects on mouse pancreatic beta-cells. *PLoS Med.* **5,** e206 (2008).

262. Campagna, J. A., Miller, K. W. & Forman, S. A. Mechanisms of actions of inhaled anesthetics. *N. Engl. J. Med.* **348,** 2110–2124 (2003).
263. Bischoff, P. & Rundshagen, I. Awareness under general anesthesia. *Dtsch Arztebl Int* **108,** 1–7 (2011).
264. Goodman, S. J. & Mann, P. E. Reticular and thalamic multiple unit activity during wakefulness, sleep and anesthesia. *Exp. Neurol.* **19,** 11–24 (1967).
265. Hobson, J. A., McCarley, R. W., Pivik, R. T. & Freedman, R. Selective firing by cat pontine brain stem neurons in desynchronized sleep. *J. Neurophysiol.* **37,** 497–511 (1974).
266. Kendig, J. J., MacIver, M. B. & Roth, S. H. Anesthetic actions in the hippocampal formation. *Ann. N. Y. Acad. Sci.* **625,** 37–53 (1991).
267. Alkire, M. T., Haier, R. J. & Fallon, J. H. Toward a unified theory of narcosis: brain imaging evidence for a thalamocortical switch as the neurophysiologic basis of anesthetic-induced unconsciousness. *Conscious Cogn* **9,** 370–386 (2000).
268. Långsjö, J. W. *et al.* Returning from oblivion: imaging the neural core of consciousness. *Journal of Neuroscience* **32,** 4935–4943 (2012).
269. Angel, A. Central neuronal pathways and the process of anaesthesia. *Br J Anaesth* **71,** 148–163 (1993).
270. Lydic, R. & Baghdoyan, H. A. Sleep, anesthesiology, and the neurobiology of arousal state control. *Anesthesiology* **103,** 1268–1295 (2005).
271. Mashour, G. A. & Alkire, M. T. Consciousness, anesthesia, and the thalamocortical system. *Anesthesiology* **118,** 13–15 (2013).
272. Eger, E. I., Koblin, D. D., Harris, R. A. & Kendig, J. J. Hypothesis: inhaled anesthetics produce immobility and amnesia by different mechanisms at different sites. *Anesthesia & …* (1997).
273. Rampil, I. J., Mason, P. & Singh, H. Anesthetic potency (MAC) is independent of forebrain structures in the rat. *Anesthesiology* (1993).
274. Rampil, I. J. Anesthetic potency is not altered after hypothermic spinal cord transection in rats. *Anesthesiology* **80,** 606–610 (1994).
275. Antognini, J. F. & Schwartz, K. Exaggerated anesthetic requirements in the preferentially anesthetized brain. *Anesthesiology* **79,** 1244–1249 (1993).
276. Antognini, J. F. Anesthetic action: the importance of the spinal cord to immobility. *Vet. J.* **187,** 151–152 (2011).
277. Leung, L. S., Ma, J., Shen, B., Nachim, I. & Luo, T. Medial septal lesion enhances general anesthesia response. *Exp. Neurol.* (2013). doi:10.1016/j.expneurol.2013.01.010
278. Ishizawa, Y., Ma, H. C., Dohi, S. & Shimonaka, H. Effects of cholinomimetic injection into the brain stem reticular formation on halothane anesthesia and antinociception in rats. *J. Pharmacol. Exp. Ther.* **293,** 845–851 (2000).
279. Alkire, M. T., Hudetz, A. G. & Tononi, G. Consciousness and anesthesia. *Science* **322,** 876–880 (2008).
280. Alkire, M. T., McReynolds, J. R., Hahn, E. L. & Trivedi, A. N. Thalamic microinjection of nicotine reverses sevoflurane-induced loss of righting

reflex in the rat. *Anesthesiology* **107,** 264–272 (2007).
281. Kawano, T. *et al.* ATP-sensitive potassium currents in rat primary afferent neurons: biophysical, pharmacological properties, and alterations by painful nerve injury. *Neuroscience* **162,** 431–443 (2009).
282. Kim, J. *et al.* Neurons in the ventral spinal cord are more depressed by isoflurane, halothane, and propofol than are neurons in the dorsal spinal cord. *Anesth. Analg.* **105,** 1020–6– table of contents (2007).
283. Sachs, D., Cunha, F. Q. & Ferreira, S. H. Peripheral analgesic blockade of hypernociception: activation of arginine/NO/cGMP/protein kinase G/ATP-sensitive K+ channel pathway. *Proc. Natl. Acad. Sci. U.S.A.* **101,** 3680–3685 (2004).
284. Chi, X. X., Jiang, X. & Nicol, G. D. ATP-sensitive potassium currents reduce the PGE2-mediated enhancement of excitability in adult rat sensory neurons. *Brain Res.* **1145,** 28–40 (2007).
285. Galdino, G. S., Cortes, S. F., Duarte, I. & Perez, A. C. Involvement of the nitric oxide/ C GMP/K ATP pathway in antinociception induced by exercise in rats. *Life Sci.* (2010).
286. Wu, X.-F. *et al.* Reopening of ATP-sensitive potassium channels reduces neuropathic pain and regulates astroglial gap junctions in the rat spinal cord. *Pain* **152,** 2605–2615 (2011).
287. Rios, M., Lambe, E. K., Liu, R., Teillon, S. & Liu, J. H. Severe deficits in 5-HT2A-mediated neurotransmission in BDNF conditional mutant mice. *Journal of …* (2006).
288. Fowler, C. D. & Kenny, P. J. Utility of genetically modified mice for understanding the neurobiology of substance use disorders. *Hum. Genet.* **131,** 941–957 (2012).
289. Takanaga, H. *et al.* Efflux transport of tolbutamide across the blood-brain barrier. *J. Pharm. Pharmacol.* **50,** 1027–1033 (1998).
290. Joo, D. T. *et al.* Blockade of AMPA receptors and volatile anesthetics: reduced anesthetic requirements in GluR2 null mutant mice for loss of the righting reflex and antinociception but not minimum alveolar concentration. *Anesthesiology* **94,** 478–488 (2001).
291. Nishikawa, K. & Harrison, N. L. The actions of sevoflurane and desflurane on the γ-aminobutyric acid receptor type A: Effects of TM2 mutations in the α and β subunits. *Anesthesiology* (2003).
292. Lee, S. N., Li, L. & Zuo, Z. Glutamate transporter type 3 knockout mice have a decreased isoflurane requirement to induce loss of righting reflex. *Neuroscience* **171,** 788–793 (2010).
293. Tanaka, K. *et al.* Mechanisms of impaired glucose tolerance and insulin secretion during isoflurane anesthesia. *Anesthesiology* **111,** 1044–1051 (2009).
294. Tanaka, K. *et al.* Differential effects of propofol and isoflurane on glucose utilization and insulin secretion. *Life Sci.* **88,** 96–103 (2011).
295. Ishiwa, D., Kamiya, Y., Itoh, H., Saito, Y. & Ohtsuka, T. Effects of isoflurane and ketamine on ATP-sensitive K channels in rat substantia nigra. *…* (2004).
296. Karschin, A., Brockhaus, J. & Ballanyi, K. KATP channel formation by the sulphonylurea receptors SUR1 with Kir6.2 subunits in rat dorsal

vagal neurons in situ. *J. Physiol. (Lond.)* **509 (Pt 2),** 339–346 (1998).
297. Gama Sosa, M. A., De Gasperi, R. & Elder, G. A. Animal transgenesis: an overview. *Brain Struct Funct* **214,** 91–109 (2010).
298. Metzger, D., Clifford, J., Chiba, H. & Chambon, P. Conditional site-specific recombination in mammalian cells using a ligand-dependent chimeric Cre recombinase. *Proc. Natl. Acad. Sci. U.S.A.* **92,** 6991–6995 (1995).
299. Zhang, Y. *et al.* Inducible site-directed recombination in mouse embryonic stem cells. *Nucleic Acids Res.* **24,** 543–548 (1996).
300. Feil, R., Wagner, J., Metzger, D. & Chambon, P. Regulation of Cre recombinase activity by mutated estrogen receptor ligand-binding domains. *Biochem. Biophys. Res. Commun.* **237,** 752–757 (1997).
301. Harno, E., Cottrell, E. C. & White, A. Metabolic pitfalls of CNS cre-based technology. *Cell Metab.* **18,** 21–28 (2013).
302. *Ubiquitin-cre-ER expression*. (Jackson Labs). at <http://cre.jax.org>
303. Kellendonk, C. *et al.* Inducible site-specific recombination in the brain. *J. Mol. Biol.* **285,** 175–182 (1999).
304. Burns, K. A. *et al.* Nestin-CreER mice reveal DNA synthesis by nonapoptotic neurons following cerebral ischemia hypoxia. *Cereb. Cortex* **17,** 2585–2592 (2007).
305. Abbott, N. J., Patabendige, A. A. K., Dolman, D. E. M., Yusof, S. R. & Begley, D. J. Structure and function of the blood-brain barrier. *Neurobiol. Dis.* **37,** 13–25 (2010).
306. Begley, D. J. & Brightman, M. W. Structural and functional aspects of the blood-brain barrier. *Prog Drug Res* **61,** 39–78 (2003).
307. Levin, V. A. Relationship of octanol/water partition coefficient and molecular weight to rat brain capillary permeability. *J. Med. Chem.* **23,** 682–684 (1980).
308. Clark, D. E. In silico prediction of blood-brain barrier permeation. *Drug Discov. Today* **8,** 927–933 (2003).
309. Begley, D. J. ABC transporters and the blood-brain barrier. *Curr. Pharm. Des.* **10,** 1295–1312 (2004).
310. Dallas, S., Miller, D. S. & Bendayan, R. Multidrug resistance-associated proteins: expression and function in the central nervous system. *Pharmacol. Rev.* **58,** 140–161 (2006).
311. Dean, M. & Allikmets, R. Complete characterization of the human ABC gene family. *J. Bioenerg. Biomembr.* **33,** 475–479 (2001).
312. International Transporter Consortium *et al.* Membrane transporters in drug development. *Nat Rev Drug Discov* **9,** 215–236 (2010).
313. Begley, D. J. Delivery of therapeutic agents to the central nervous system: the problems and the possibilities. *Pharmacol. Ther.* **104,** 29–45 (2004).
314. Robey, R. W. *et al.* ABCG2: a perspective. *Adv. Drug Deliv. Rev.* **61,** 3–13 (2009).
315. Polli, J. W. *et al.* An unexpected synergist role of P-glycoprotein and breast cancer resistance protein on the central nervous system penetration of the tyrosine kinase inhibitor lapatinib (N-{3-chloro-4-[(3-fluorobenzyl)oxy]phenyl}-6-[5-({[2-(methylsulfonyl)ethyl]amino}methyl)-

2-furyl]-4-quinazolinamine; GW572016). *Drug Metab. Dispos.* **37,** 439–442 (2009).
316. Roberts, L. M. *et al.* Subcellular localization of transporters along the rat blood-brain barrier and blood-cerebral-spinal fluid barrier by in vivo biotinylation. *Neuroscience* **155,** 423–438 (2008).
317. Golstein, P. E. *et al.* P-glycoprotein inhibition by glibenclamide and related compounds. *Pflugers Arch.* **437,** 652–660 (1999).
318. Bessadok, A. *et al.* Recognition of sulfonylurea receptor (ABCC8/9) ligands by the multidrug resistance transporter P-glycoprotein (ABCB1): functional similarities based on common structural features between two multispecific ABC proteins. *J. Biol. Chem.* **286,** 3552–3569 (2011).
319. Allen, J. D., Brinkhuis, R. F., Wijnholds, J. & Schinkel, A. H. The mouse Bcrp1/Mxr/Abcp gene: amplification and overexpression in cell lines selected for resistance to topotecan, mitoxantrone, or doxorubicin. *Cancer Res.* **59,** 4237–4241 (1999).
320. Ward, K. W. & Azzarano, L. M. Preclinical pharmacokinetic properties of the P-glycoprotein inhibitor GF120918A (HCl salt of GF120918, 9,10-dihydro-5-methoxy-9-oxo-N-[4-[2-(1,2,3,4-tetrahydro-6,7-dimethoxy-2-isoquinolinyl)ethyl]phenyl]-4-acridine-carboxamide) in the mouse, rat, dog, and monkey. *J. Pharmacol. Exp. Ther.* **310,** 703–709 (2004).
321. Rogers, H. J., Spector, R. G., Morrison, P. J. & Bradbrook, I. D. Pharmacokinetics of intravenous glibenclamide investigated by a high performance liquid chromatographic assay. *Diabetologia* **23,** 37–40 (1982).
322. Pearson, J. G. Pharmacokinetics of glyburide. *Am. J. Med.* **79,** 67–71 (1985).
323. Anderson, G. D. Sex and racial differences in pharmacological response: where is the evidence? Pharmacogenetics, pharmacokinetics, and pharmacodynamics. *J Womens Health (Larchmt)* **14,** 19–29 (2005).
324. Waxman, D. J. & Holloway, M. G. Sex differences in the expression of hepatic drug metabolizing enzymes. *Mol. Pharmacol.* **76,** 215–228 (2009).
325. Brown, K. F. & Crooks, M. J. Displacement of tolbutamide, glibencalmide and chlorpropamide from serum albumin by anionic drugs. *Biochem. Pharmacol.* **25,** 1175–1178 (1976).
326. Wolburg, H., Wolburg-Buchholz, K., Liebner, S. & Engelhardt, B. Claudin-1, claudin-2 and claudin-11 are present in tight junctions of choroid plexus epithelium of the mouse. *Neurosci. Lett.* **307,** 77–80 (2001).
327. Keep, R. F. & Smith, D. E. Choroid plexus transport: gene deletion studies. *Fluids Barriers CNS* **8,** 26 (2011).
328. Gazzin, S. *et al.* Differential expression of the multidrug resistance-related proteins ABCb1 and ABCc1 between blood-brain interfaces. *J. Comp. Neurol.* **510,** 497–507 (2008).
329. Slingerland, A. S. Monogenic diabetes in children and young adults:

Challenges for researcher, clinician and patient. *Rev Endocr Metab Disord* **7,** 171–185 (2006).
330. Buccafusco, J. J., Bailey, K. R. & Crawley, J. N. *Anxiety-Related Behaviors in Mice*. (CRC Press, 2009).
331. Vacchio, C. My 2 Sweet Babies. *babieswithdiabetes.com* at <http://www.babieswithdiabetes.com/>
332. Miller, L. J., Anzalone, M. E., Lane, S. J., Cermak, S. A. & Osten, E. T. Concept evolution in sensory integration: a proposed nosology for diagnosis. *Am J Occup Ther* **61,** 135–140 (2007).
333. Laboratories, J. UBC-cre/ERT2 Characterization by the GRS Cre Repository - The Jackson Laboratory. *Ubiquitin-cre-ER expression* at <http://cre.jax.org/UBC-creERT/UBC-creERT.html>
334. Cox, D., Gonder-Frederick, L., McCall, A., Kovatchev, B. & Clarke, W. The effects of glucose fluctuation on cognitive function and QOL: the functional costs of hypoglycaemia and hyperglycaemia among adults with type 1 or type 2 diabetes. *Int J Clin Pract Suppl* 20–26 (2002).
335. Fendler, W. *et al.* Switching to Sulphonylureas in Children With iDEND Syndrome Caused by KCNJ11 Mutations Results in Improved Cerebellar Perfusion. *Diabetes Care* **36,** 2311–2316 (2013).
336. Proks, P., de Wet, H. & Ashcroft, F. M. Molecular mechanism of sulphonylurea block of KATP channels carrying mutations that impair ATP inhibition and cause neonatal diabetes. *Diabetes* (2013). doi:10.2337/db13-0531
337. Chen, P.-C. *et al.* Carbamazepine as a Novel Small Molecule Corrector of Trafficking-impaired ATP-sensitive Potassium Channels Identified in Congenital Hyperinsulinism. *J. Biol. Chem.* **288,** 20942–20954 (2013).
338. Shawahna, R. *et al.* Transcriptomic and quantitative proteomic analysis of transporters and drug metabolizing enzymes in freshly isolated human brain microvessels. *Mol. Pharm.* **8,** 1332–1341 (2011).
339. Tournier, N. *et al.* Effects of Selected OATP and/or ABC Transporter Inhibitors on the Brain and Whole-Body Distribution of Glyburide. *AAPS J* (2013). doi:10.1208/s12248-013-9514-2

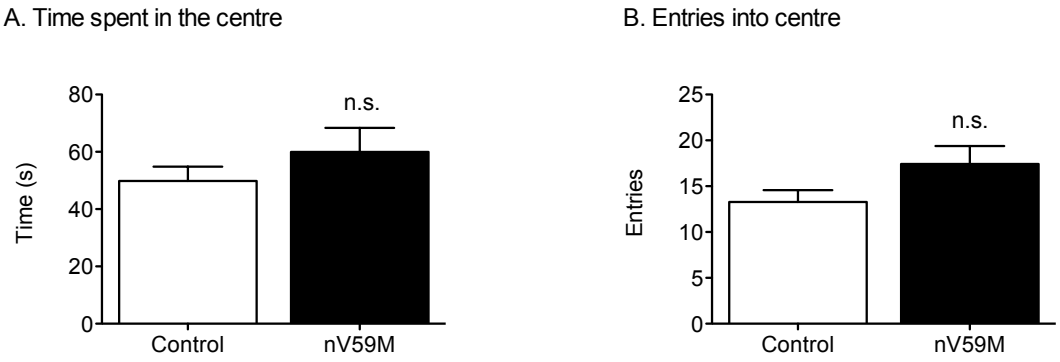

Appendix 1: Plus maze test- centre square

(**A**) Amount of time spent in the centre square and (**B**) number of entries into the centre square for adult (11-20 week-old) control (wild-type: n=1; ROSA$^{+/-}$: n=12; Nes-Cre^{+}: n=13) and nV59M (n=14) littermates over a 300s period. Data are mean ± SEM. n.s. not statistically significant [Mann-Whitney U-test].

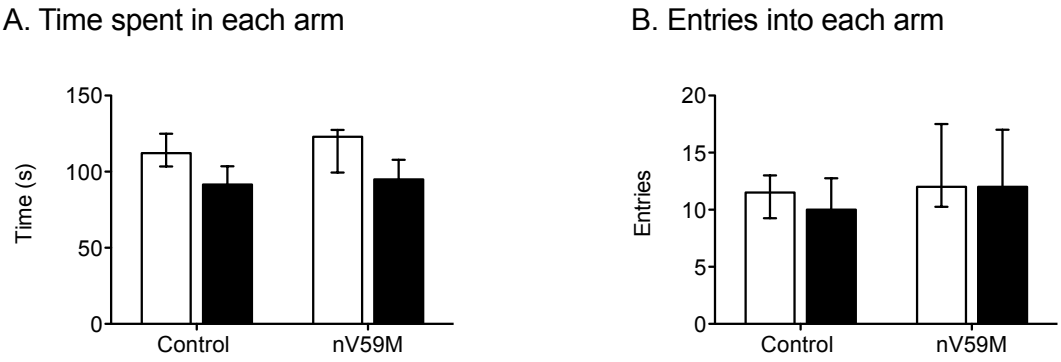

Appendix 2: Spatial novelty preference task- sample trial

(**A**) Time spent and (B) number of entries into the start arm (white bars) and other (black bars) arms for adult (11-20 week-old) control (wild-type: n=1; ROSA$^{+/-}$: n=12; Nes-Cre^{+}: n=13) and nV59M (n=14) littermates over a 120s period during the exposure phase. Data are median and interquartile range.

Appendix 3: Isoflurane LORR One-way ANOVA details (nV59M mice)

- Dependent factor: Time taken to LORR

	Degrees of Freedom	F-values	Significance
Between groups (Genotype)	3	22.088	<0.0001

- Bonferroni post-hoc multiple comparisons test

(I) Genotype	(J) Genotype	Mean Difference (I-J)	Std. Error	Sig.	95% Confidence Interval	
					Lower Bound	Upper Bound
Control muscle	mV59M	-.62745	4.99711	1.000	-13.9997	12.7448
	Control brain	-5.27614	3.88416	1.000	-15.6701	5.1178
	nV59M	-28.31612*	3.74275	.000	-38.3317	-18.3006
mV59M	Control muscle	.62745	4.99711	1.000	-12.7448	13.9997
	Control brain	-4.64869	5.25093	1.000	-18.7001	9.4027
	nV59M	-27.68867*	5.14720	.000	-41.4625	-13.9148
Control brain	Control muscle	5.27614	3.88416	1.000	-5.1178	15.6701
	mV59M	4.64869	5.25093	1.000	-9.4027	18.7001
	nV59M	-23.03997*	4.07545	.000	-33.9459	-12.1341
nV59M	Control muscle	28.31612*	3.74275	.000	18.3006	38.3317
	mV59M	27.68867*	5.14720	.000	13.9148	41.4625
	Control brain	23.03997*	4.07545	.000	12.1341	33.9459

Appendix 4: Isoflurane LOWR One-way ANOVA details (nV59M mice)

- Dependent factor: Time taken to LOWR

	Degrees of Freedom	F-values	Significance
Between groups (Genotype)	3	10.216	<0.0001

- Bonferroni post-hoc multiple comparisons test

(I) Genotype	(J) Genotype	Mean Difference (I-J)	Std. Error	Sig.	95% Confidence Interval	
					Lower Bound	Upper Bound
Control muscle	mV59M	-2.70455	18.82493	1.000	-53.0279	47.6188
	Control brain	5.58458	14.40454	1.000	-32.9220	44.0912
	nV59M	-74.62597*	15.58852	.000	-116.2976	-32.9543
mV59M	Control muscle	2.70455	18.82493	1.000	-47.6188	53.0279
	Control brain	8.28913	19.30977	1.000	-43.3303	59.9085
	nV59M	-71.92143*	20.20838	.003	-125.9430	-17.8998
Control brain	Control muscle	-5.58458	14.40454	1.000	-44.0912	32.9220
	mV59M	-8.28913	19.30977	1.000	-59.9085	43.3303
	nV59M	-80.21056*	16.17069	.000	-123.4385	-36.9826
nV59M	Control muscle	74.62597*	15.58852	.000	32.9543	116.2976
	mV59M	71.92143*	20.20838	.003	17.8998	125.9430
	Control brain	80.21056*	16.17069	.000	36.9826	123.4385

Appendix 5: Halothane LORR One-way ANOVA details (nV59M mice)

- Dependent factor: Time taken to LORR

	Degrees of Freedom	F-values	Significance
Between groups (Genotype)	3	6.892	0.001

- Bonferroni post-hoc multiple comparisons test

(I) Genotype	(J) Genotype	Mean Difference (I-J)	Std. Error	Sig.	95% Confidence Interval	
					Lower Bound	Upper Bound
Control muscle	mV59M	2.54545	3.39345	1.000	-6.7774	11.8683
	Control brain	-.14685	3.11264	1.000	-8.6982	8.4045
	nV59M	-14.01010*	3.52067	.001	-23.6824	-4.3378
mV59M	Control muscle	-2.54545	3.39345	1.000	-11.8683	6.7774
	Control brain	-2.69231	3.74257	1.000	-12.9743	7.5896
	nV59M	-16.55556*	4.08821	.001	-27.7871	-5.3240
Control brain	Control muscle	.14685	3.11264	1.000	-8.4045	8.6982
	mV59M	2.69231	3.74257	1.000	-7.5896	12.9743
	nV59M	-13.86325*	3.85830	.004	-24.4631	-3.2633
nV59M	Control muscle	14.01010*	3.52067	.001	4.3378	23.6824
	mV59M	16.55556*	4.08821	.001	5.3240	27.7871
	Control brain	13.86325*	3.85830	.004	3.2633	24.4631

Appendix 6: Halothane LOWR One-way ANOVA details (nV59M mice)

- Dependent factor: Time taken to LOWR

	Degrees of Freedom	F-values	Significance
Between groups (Genotype)	3	9.584	<0.0001

- Bonferroni post-hoc multiple comparisons test

(I) Genotype	(J) Genotype	Mean Difference (I-J)	Std. Error	Sig.	95% Confidence Interval	
					Lower Bound	Upper Bound
Control muscle	mV59M	8.06667	24.35154	1.000	-59.0748	75.2081
	Control brain	67.15000*	22.15303	.024	6.0702	128.2298
	nV59M	-75.93333*	24.35154	.019	-143.0748	-8.7919
mV59M	Control muscle	-8.06667	24.35154	1.000	-75.2081	59.0748
	Control brain	59.08333	26.75232	.193	-14.6775	132.8442
	nV59M	-84.00000*	28.59944	.031	-162.8536	-5.1464
Control brain	Control muscle	-67.15000*	22.15303	.024	-128.2298	-6.0702
	mV59M	-59.08333	26.75232	.193	-132.8442	14.6775
	nV59M	-143.08333*	26.75232	.000	-216.8442	-69.3225
nV59M	Control muscle	75.93333*	24.35154	.019	8.7919	143.0748
	mV59M	84.00000*	28.59944	.031	5.1464	162.8536
	Control brain	143.08333*	26.75232	.000	69.3225	216.8442

Appendix 7: Isoflurane LORR Pre- and Post-Pellet treatment Repeated Measures Two-way ANOVA (nV59M mice)

Factor	Degrees of Freedom	F-values	Significance
Within-subjects: pre- and post-treatment	1	5.040	0.029
Between-subjects: genotype (control versus nV59M)	1	14.988	<0.0001
Between-subjects: treatment (placebo versus glibenclamide)	1	0.120	0.731

Repeated Measures ANOVA for nV59M mice:

- Within-subjects: Pre- and Post-pellet treatment

Source	Time	Type III Sum of Squares	df	Mean Square	F	Sig.
Time	Pre vs. Post	4509.223	1	4509.223	5.042	.036
Time * Treatment	Pre vs. Post	126.614	1	126.614	.142	.710

- Between-subjects: Placebo versus glibenclamide

Source	Type III Sum of Squares	df	Mean Square	F	Sig.
Treatment	7.021	1	7.021	.013	.910

Appendix 8: Isoflurane LOWR Pre- and Post-Pellet treatment Repeated Measures Two-way ANOVA (nV59M mice)

Factor	Degrees of Freedom	F-values	Significance
Within-subjects: pre- and post-treatment	1	3.076	0.089
Between-subjects: genotype (control versus nV59M)	1	52.573	<0.0001
Between-subjects: treatment (placebo versus glibenclamide)	1	13.064	0.001

Repeated Measures ANOVA for control mice:

- Within-subjects: Pre- and Post-pellet treatment

Source	Time	Type III Sum of Squares	df	Mean Square	F	Sig.
Time	Pre vs. Post	776.095	1	776.095	.671	.422
Time * Treatment	Pre vs. Post	36.965	1	36.965	.032	.860

- Between-subjects: Placebo versus glibenclamide

Source	Type III Sum of Squares	df	Mean Square	F	Sig.
Treatment	2842.196	1	2842.196	3.056	.095

Repeated Measures ANOVA for nV59M mice:

- Within-subjects: Pre- and Post-pellet treatment

Source	Time	Type III Sum of Squares	df	Mean Square	F	Sig.
Time	Pre vs. Post	3729.540	1	3729.540	2.008	.184
Time * Treatment	Pre vs. Post	223.079	1	223.079	.120	.735

- Between subjects: Placebo versus glibenclamide

Source	Type III Sum of Squares	df	Mean Square	F	Sig.
Treatment	14271.927	1	14271.927	7.727	.018

Appendix 9: Isoflurane LORR Pre- and Post-ICV treatment Repeated Measures Two-way ANOVA (nV59M mice)

Factor	Degrees of Freedom	F-values	Significance
Within-subjects: pre- and post-treatment	1	10.378	0.003
Between-subjects: genotype (control versus nV59M)	1	7.073	0.012
Between-subjects: treatment (placebo versus glibenclamide)	1	1.070	0.308

Repeated Measures ANOVA for control mice:

- Within-subjects: Pre- and Post-ICV treatment

Source	Time	Type III Sum of Squares	df	Mean Square	F	Sig.
Time	Pre vs. Post	59.341	1	59.341	1.348	.257
Time * Treatment	Pre vs. Post	.081	1	.081	.002	.966

- Between-subjects: Vehicle versus glibenclamide

Source	Type III Sum of Squares	df	Mean Square	F	Sig.
Treatment	15.056	1	15.056	.510	.482

Repeated Measures ANOVA for nV59M mice:

- Within-subjects: Pre- and Post-ICV treatment

Source	Time	Type III Sum of Squares	df	Mean Square	F	Sig.
Time	Pre vs. Post	532.688	1	532.688	6.970	.025
Time * Treatment	Pre vs. Post	44.688	1	44.688	.585	.462

- Between-subjects: Vehicle versus glibenclamide

Source	Type III Sum of Squares	df	Mean Square	F	Sig.
Treatment	29.601	1	29.601	.411	.536

Appendix 10: Isoflurane sensitivity Pre- and Post-tamoxifen injection

Repeated Measures ANOVA (Ubi-ROSA mice)

- Within-subjects: Pre- and Post-tamoxifen treatment LORR

Source	Time	Type III Sum of Squares	df	Mean Square	F	Sig.
Time	Pre- vs. Post-tx.	1571.668	1	1571.668	35.105	.000
Time * Genotype	Pre- vs. Post-tx	52.001	1	52.001	1.161	.293

- Between-subjects: Genotype (Control versus Ubi-ROSA) LORR

Source	Type III Sum of Squares	df	Mean Square	F	Sig.
Group	2.357	1	2.357	.078	.782

- Within-subjects: Pre- and Post-tamoxifen treatment LOWR

Source	Time	Type III Sum of Squares	df	Mean Square	F	Sig.
Time	Pre- vs. Post-tx	26690.744	1	26690.744	6.987	.015
Time * Genotype	Pre- vs. Post-tx	57585.744	1	57585.744	15.075	.001

- Between-subjects: Genotype (Control versus Ubi-ROSA) LOWR

Source	Type III Sum of Squares	df	Mean Square	F	Sig.
Group	19599.174	1	19599.174	4.974	.036

Appendix 11: Isoflurane sensitivity Pre- and Post-tamoxifen injection

Repeated Measures ANOVA (Ubi-ROSA-DN mice)

- Within-subjects: Pre- and Post-tamoxifen treatment LORR

Source	Time	Type III Sum of Squares	df	Mean Square	F	Sig.
Time	Pre- vs. Post-tx	629.427	1	629.427	10.317	.002
Time * Genotype	Pre- vs. Post-tx	10.480	1	10.480	.172	.680

- Between-subjects: Genotype (Control versus Ubi-ROSA-DN) LORR

Source	Type III Sum of Squares	df	Mean Square	F	Sig.
Genotype	4.271	1	4.271	.247	.621

- Within-subjects: Pre- and Post-tamoxifen treatment LOWR

Source	Time	Type III Sum of Squares	df	Mean Square	F	Sig.
Time	Pre- vs. Post-tx	7376.618	1	7376.618	2.139	.149
Time * Genotype	Pre- vs. Post-tx	51671.145	1	51671.145	14.981	.000

- Between-subjects: Genotype (Control versus Ubi-ROSA-DN) LOWR

Source	Type III Sum of Squares	df	Mean Square	F	Sig.
Genotype	20126.080	1	20126.080	8.766	.005

Appendix 12: Isoflurane LOWR Pre- and Post-Pellet treatment Repeated Measures Two-way ANOVA (Ubi-ROSA-DN mice)

Factor	Degrees of Freedom	F-values	Significance
Within-subjects: pre- and post-treatment	1	3.217	0.090
Between-subjects: genotype (control versus Ubi-ROSA-DN)	1	12.990	0.001
Between-subjects: treatment (placebo versus glibenclamide)	1	0.007	0.0.935
Time*Genotype	1	4.284	0.047
Genotype*Treatment	1	0.004	0.950